frontiers | Research Topics

Recent advances on myocardium physiology, volume II

Edited by
Norio Fukuda, Henk Granzier, Shin'Ichi Ishiwata and Sachio Morimoto

Published in
Frontiers in Physiology

ISSN 1664-8714
ISBN 978-2-83252-017-8
DOI 10.3389/978-2-83252-017-8

About Frontiers

Frontiers is more than just an open access publisher of scholarly articles: it is a pioneering approach to the world of academia, radically improving the way scholarly research is managed. The grand vision of Frontiers is a world where all people have an equal opportunity to seek, share and generate knowledge. Frontiers provides immediate and permanent online open access to all its publications, but this alone is not enough to realize our grand goals.

Frontiers journal series

The Frontiers journal series is a multi-tier and interdisciplinary set of open-access, online journals, promising a paradigm shift from the current review, selection and dissemination processes in academic publishing. All Frontiers journals are driven by researchers for researchers; therefore, they constitute a service to the scholarly community. At the same time, the *Frontiers journal series* operates on a revolutionary invention, the tiered publishing system, initially addressing specific communities of scholars, and gradually climbing up to broader public understanding, thus serving the interests of the lay society, too.

Dedication to quality

Each Frontiers article is a landmark of the highest quality, thanks to genuinely collaborative interactions between authors and review editors, who include some of the world's best academicians. Research must be certified by peers before entering a stream of knowledge that may eventually reach the public - and shape society; therefore, Frontiers only applies the most rigorous and unbiased reviews. Frontiers revolutionizes research publishing by freely delivering the most outstanding research, evaluated with no bias from both the academic and social point of view. By applying the most advanced information technologies, Frontiers is catapulting scholarly publishing into a new generation.

What are Frontiers Research Topics?

Frontiers Research Topics are very popular trademarks of the *Frontiers journals series*: they are collections of at least ten articles, all centered on a particular subject. With their unique mix of varied contributions from Original Research to Review Articles, Frontiers Research Topics unify the most influential researchers, the latest key findings and historical advances in a hot research area.

Find out more on how to host your own Frontiers Research Topic or contribute to one as an author by contacting the Frontiers editorial office: frontiersin.org/about/contact

Recent advances on myocardium physiology, volume II

Topic editors

Norio Fukuda — Jikei University School of Medicine, Japan
Henk Granzier — University of Arizona, United States
Shin'Ichi Ishiwata — Waseda University, Japan
Sachio Morimoto — International University of Health and Welfare (IUHW), Japan

Citation

Fukuda, N., Granzier, H., Ishiwata, S., Morimoto, S., eds. (2023). *Recent advances on myocardium physiology, volume II*. Lausanne: Frontiers Media SA. doi: 10.3389/978-2-83252-017-8

Table of contents

frontiers | Frontiers in Physiology

TYPE Editorial
PUBLISHED 13 March 2023
DOI 10.3389/fphys.2023.1170396

OPEN ACCESS

EDITED AND REVIEWED BY
Paul M. L. Janssen,
The Ohio State University, United States

*CORRESPONDENCE
Norio Fukuda,
noriof@jikei.ac.jp

SPECIALTY SECTION
This article was submitted to Striated Muscle Physiology, a section of the journal Frontiers in Physiology

RECEIVED 20 February 2023
ACCEPTED 27 February 2023
PUBLISHED 13 March 2023

CITATION
Fukuda N, Granzier H, Ishiwata S and Morimoto S (2023), Editorial: Recent Advances on Myocardium Physiology, Volume II.
Front. Physiol. 14:1170396.
doi: 10.3389/fphys.2023.1170396

Editorial: Recent Advances on Myocardium Physiology, Volume II

Norio Fukuda[1]*, Henk Granzier[2], Shin'ichi Ishiwata[3] and Sachio Morimoto[4]

[1]Department of Cell Physiology, The Jikei University School of Medicine, Tokyo, Japan, [2]Department of Cellular and Molecular Medicine, University of Arizona, Tucson, AZ, United States, [3]Department of Physics, Faculty of Science and Engineering, Waseda University, Tokyo, Japan, [4]School of Health Sciences at Fukuoka, International University of Health and Welfare, Fukuoka, Japan

KEYWORDS

Ca^{2+}, cardiomyopathy, heart, muscle, myosin, sarcomere, titin, troponin

Editorial on the Research Topic
Recent Advances on Myocardium Physiology, Volume II

Myocardium has evolved to contract in a rhythmic fashion to provide blood from the heart to the body. The mechanical activities of myocardium originate in sarcomeres, composed of three filaments [i.e., thick and thin filaments, and the giant elastic protein titin (connectin)]. Cardiac researchers have developed and applied various new technologies to elucidate the in-depth mechanisms of sarcomeric functions in the heart (Fukuda et al., 2021 and related articles therein). It is now becoming clear that sarcomeres play critical roles in the processes regulating the dynamics, growth and remodeling of the heart. These exceptional technologies have provided new prospects to facilitate the development of novel drugs for intractable heart diseases. This Research Topic of *Frontiers in Physiology* is a collection of ten original research and review papers, showing the state-of-the-art research and future directions in the physiology and pathophysiology of myocardium.

Early on, contraction of cardiac myofilaments was thought to be regulated only *via* thin filament structural changes. Namely, under the relaxing condition, the troponin (Tn) and tropomyosin (Tm) complex blocks myosin binding to actin ("*off*" state). Following an increase in the intracellular Ca^{2+} concentration ($[Ca^{2+}]_i$), the binding of Ca^{2+} to TnC (one of the three subunits of Tn) causes displacement of Tm on thin filaments ("*on*" state), allowing myosin to interact with actin, and as a result, active force is generated (see Kobirumaki-Shimozawa et al., 2014 and references therein). Here, it is important that strongly bound cross-bridges, such as the actomyosin-ADP complex, desuppress the inhibition of Tn-Tm, synergistically with Ca^{2+}, and further activate thin filaments (Kobirumaki-Shimozawa et al., 2014 and references therein). In 2010, the group of Roger Cooke made a ground-breaking discovery showing that myosin molecules can be in a state with extremely low ATP turnover rate (Stewart et al., 2010). This novel relaxed state is widely known as the "*super-relaxed state*" (SRX) (e.g., Cooke, 2011; Irving, 2017; Craig and Padrón, 2022). SRX is in equilibrium with the "*disordered-relaxed state*" (DRX) in which myosin heads are in closer proximity to thin filaments, and can readily bind to actin (e.g., Cooke, 2011; Fusi et al., 2015). Decreasing

Abbreviations: $[Ca^{2+}]_i$, intracellular Ca^{2+} concentration; cryoEM, cryogenic electron microscopy; DCM, dilated cardiomyopathy; DRX, disordered-relaxed state; HCM, hypertrophied cardiomyopathy; HFrEF, heart failure with reduced ejection fraction; OM, omecamtive mecarbil; Pi, inorganic phosphate; SRX, super-relaxed state; STE, speckle tracking echocardiography; Tm, tropomyosin; Tn, troponin.

the number of myosin molecules in SRX results in an increase in the number of the heads available to produce active force (e.g., Schmid and Toepfer, 2021). It is considered that mechanical stress on thick filaments, such as myosin binding to thin filaments (Linari et al., 2015) or titin-based passive strain (Irving et al., 2011; Hessel et al., 2022), shifts the SRX-DRX equilibrium towards DRX. SRX is a biochemical and structural state, in which myosin heads interact with, and are folded back on, the thick filament backbone, thus unavailable for interacting with thin filaments. Currently, the thick filament-based regulation is the foremost Research Topic of myofilament research.

Hypertrophic cardiomyopathy (HCM) affects more than one in 500 people worldwide with high morbidity due mostly to arrhythmia, heart failure and sudden death. Kawana et al. reviewed HCM, from mutations to mechanisms and therapies. Based on rapid advances of biochemical and biophysical techniques, they have studied the molecular effects of HCM mutations on human β-cardiac myosin heavy chain, combining insights from clinical genetics and structural analyses of cardiac myosin. Accordingly, they concluded that HCM-causing mutations in sarcomere proteins cause hypercontractility, and that the increase in the number of myosin molecules available for interacting with actin is the primary driver. While β-blockers and Ca^{2+} channel blockers have been widely used to alleviate the heart's hyperdynamic contraction for decades, their effectiveness is often poorly tolerated in the clinical setting, especially for young patients. Recently, two small molecule cardiac myosin inhibitors that shift the SRX-DRX equilibrium to SRX have been developed. One of these, mavacamten, showed improvement in the composite endpoint of exercise capacity and symptom severity in the phase III study of HCM patients, and it has recently been approved by the US Food and Drug Administration. Mavacamten is the first compound that showed a benefit for HCM in a randomized controlled trial. The other small molecule cardiac myosin inhibitor is aficamten; it is currently under evaluation in a phase III trial, and the results are awaited.

On another front, omecamtive mecarbil (OM) was developed as a first-in-class myosin activator for the treatment of heart failure in patients with reduced ejection fraction (HFrEF). Several lines of evidence suggest that OM is effective in the treatment of HFrEF by improving cardiac function without increasing $[Ca^{2+}]_i$. This is a favorable property as an inotropic agent because an increase in $[Ca^{2+}]_i$ often causes arrhythmias due to membrane depolarization coupled with Na^+ entry *via* the Na^+/Ca^{2+} exchanger. Nakanishi et al. demonstrated by using skinned porcine venticular and atrial muscles that OM increases Ca^{2+} sensitivity in a concentration-dependent manner in a clinically relevant range (i.e., 0.5 and 1 μM), with the effect more pronounced in ventricular muscle. The Ca^{2+}-sensitizing effect of OM became less following thin filament reconstitution with fast skeletal Tn complex, and the ensuing decrease in the number of "*recruitable*" cross-bridges. Therefore, they concluded that OM's Ca^{2+} sensitizing effect results from the strongly bound cross-bridge-dependent allosteric activation of thin filaments. Also, as pointed out by Kampourakis et al. (2018), OM may modulate the thick filament structure and destabilize SRX, resulting in an increase in the number of myosin molecules that can readily bind to thin filaments and produce active force.

Yet further efforts are needed from various angles to fully uncover how the myosin state in SRX or DRX regulates contraction and relaxation of myocardium in living conditions, especially in the beating heart *in vivo*; myosin targeted drugs will open the door to new treatments for intractable heart diseases.

Three papers have added to the recent advances in the understanding of thin filament regulations. Accumulating evidence indicates that mutations in thin filament proteins cause genetic heart diseases such as HCM, dilated cardiomyopathy (DCM) and restictive cardiomyopathy (RCM) (e.g., Ohtsuki and Morimoto, 2008). Due to the lack of accurate information on the structural properties of proteins, our knowledge on the molecular mechanisms of thin filament regulation is still insufficient, especially in the presence of mutations. Just in the last decade, cryogenic electron microscopy (cryoEM) has emerged as the most powerful technique in biological sciences to reveal atomic structures, and this technology has been used in our research field as well. By taking advantage of computational analyses (i.e., structure prediction, protein-protein docking, molecular dynamics flexible fitting and molecular dynamics simulations), Rynkiewicz et al. analyzed the TnT domain spanning the head-to-tail overlap domain of tropomyosin, and refined the published cryoEM modeled structures. They also reinterpreted the interactions between Tm and TnI showing key features that hold Tm in its sterically blocking position at low $[Ca^{2+}]_i$. This refined understanding of thin filament structures will provide us with many opportunities such as designing molecular interventions for genetic heart diseases.

Chalovich et al. reviewed thin filament regulations with a focus on Tn mutants, in particular the HCM-causing mutation of Δ14 of TnT that is missing the last 14C-terminal residues of cardiac TnT. It is important that removal of the basic residues in this region eliminates the inactive Ca^{2+}-free state. Indeed, cardiac muscle fibers containing Δ14-TnT shows increased Ca^{2+} sensitivity by ~0.23 pCa units with no change in maximal Ca^{2+}-activated force (Nakaura et al., 1999), a finding that demonstrates that elimination of the inactive Ca^{2+}-free state results in increased basal activity. It is therefore likely that the C-terminal region of TnT limits Ca^{2+} activation in myocardium. As pointed out by Chalovich et al., systematic analyses of Tn mutants, occurring naturally or post-translationally, provide us with opportunities to fully elucidate details of actin-based regulations of myocardial contraction.

Mahmud et al. designed the novel small molecule Tn activator RPI-194 that targets Tn to increase Ca^{2+} sensitivity in myocardium. By using nuclear magnetic resonance, they determined that RPI-194 binds to cardiac Tn, and stabilizes the activated complex between TnC and the switch region of TnI. RPI-194 acts as a so-called "*Ca^{2+} sensitizer*" in that the compound at 100 μM shifts the mid-point of the force-pCa curve by ~0.28 and ~0.71 pCa units, respectively, in skinned rat cardiac trabeculae and slow skeletal muscle fibers. It shows cross-reactivity with skinned rat fast skeletal muscle fibers by shifting pCa_{50} by ~0.25 pCa units. It is to be noted that RPI-194 decreases the velocity of contraction in living unloaded cardiomyocytes from mice. RPI-194 represents a new class of non-specific Tn activators that could potentially be used either to enhance cardiac muscle contractility in the setting of systolic heart failure or to enhance skeletal muscle contraction in neuromuscular disorders.

Relaxation of myocardium is the key process for effective ventricular filling, and the duration of isovolumic relaxation depends on the rate of the transition from late-systole to early-

diastole. There are two important contributors to this transition; i.e., the fall of $[Ca^{2+}]_i$ and the detachment of cross-bridges. The increased rate of cross-bridge detachment leads to faster ventricular relaxation. Wakefield et al. investigated the effects of the hydrolytic product inorganic phosphate (Pi) on the myocardial relaxation rate when sarcomere lengthening (1%) was applied. Accordingly, they found that Pi enhanced the stretch-dependent increase in the cross-bridge detachment rate, with the magnitude becoming greater with faster stretching. Considering that Pi exists in the mM range in cardiomyocytes under physiological conditions, their finding will promote our understanding of the molecular mechanism of sarcomeric relaxation during the transition from late-systole to early-diastole.

Sarcomeres repeatedly shorten and lengthen in response to a change in $[Ca^{2+}]_i$ in myocytes under physiological conditions. In 2015, Shintani and colleagues found that when warmed to 37–43°C, sarcomeres exhibit rapid spontaneous sarcomeric auto-oscillations independent of $[Ca^{2+}]_i$ changes in neonatal rat cardiomyocytes (Shintani et al., 2015). They termed this phenomenon "*Hyperthermal Sarcomeric Oscillations* (HSOs)." HSOs are similar in characteristics to "*Spontaneous Oscillatory Contractions* (SPOCs)" that occur at partial activation of pCa ~6.0 in both neonatal and adult myocardium (e.g., Ishiwata et al., 2011; Shintani et al., 2014; Kagemoto et al., 2018); however, the frequency of HSOs is higher than that of SPOCs. Yet it is unknown whether or not HSOs (or SPOCs) occur under physiological conditions, Shintani provides a unique idea that sarcomeric spontaneous re-lengthening mechanisms may operate in the beating heart, allowing for rapid and effective relaxation of myocardium.

Haftbaradaran Esfahani et al. provide a novel hypothesis that dynamic changes in the geometry of cardiomyocytes play a role in their plasticity and signaling, with the magnitude of the effects being greater with increased beating frequency. This hypothesis was tested experimentally by fluorescence resonance energy transfer-based imaging of the activity of Src kinase and mathematically by assuming the constant volume behavior of cardiomyocyte contraction, i.e., the length shortening is compensated by Z-disk myofilament lattice expansion and dynamic deformation of the membrane between two adjacent Z-disks. Their experiments demonstrated higher concentrations of phospho-Src at higher beat frequencies. Yet future studies need to be systematically performed; their concept of locality of the surface-to-volume ratio may advance our understanding of the membrane-mediated signaling and plasticity of myocardium in response to biomechanical stress in the heart.

Kötter and Krüger review the roles of the giant elastic protein titin, with an emphasis on the relationship between the molecule and protein quality control. Titin, the largest molecule in biology, is well known for its multiple functions such as serving as a molecular spring in the sarcomere and a molecular ruler during embryonic development (e.g., Granzier and Labeit, 2004; Fukuda et al., 2008). In myocardium, titin is involved in length-dependent activation by decreasing the distance between the thick and thin filaments *via* its passive force, thereby forming the basis of the Frank-Starling law of the heart (e.g., Granzier and Labeit, 2004; Fukuda et al., 2008). Aside from these traditional roles, recent evidence indicates that titin plays a critical role in cellular signaling (e.g., Krüger and Linke, 2011; Linke and Hamdani, 2014; van der Pijl et al., 2018). In this review article, they discuss how proteasome, autophagy, heat shock proteins and proteases are involved in the protection and degradation of titin in myocardium, as well as in skeletal muscle. Although future studies are needed to fully uncover the fine-tuned sarcomere turnover processes, the comprehensive work by Kötter and Krüger will be useful for researchers in the field to understand the physiological roles of titin, and various muscular disease states due to the imbalance of the quality control of protein.

One paper introduces a technological advancement of the non-invasive analysis of *in vivo* cardiac function. In some areas of cardiac research, clinical approaches have surpassed research methods, allowing for in-depth analysis of the various tiers of heart function. Sturgill et al. reviewed the clinical usefulness of speckle tracking echocardiography (STE) for the quantification of cardiac function. STE uses B-mode imaging which records a video clip of the entire heart wall. Therefore, as an average measurement, STE provides data points along the entire heart wall rather than merely two from M-mode imaging. STE allows us to obtain displacement, velocity, strain and strain rate in radial, longitudinal and circumferential axes of the heart. STE is useful in basic research; in particular, further improvement of spatial and temporal resolutions will allow for more accurate analyses of the *in vivo* assessment of all tiers of cardiovascular performance in small rodents like mice, including left ventricular systolic and diastolic function and contractility.

In summary, this Research Topic highlights the considerable advancements cardiac researchers have made since the turn of the 21st century. We must move forward to further elucidate the physiology and pathophysiology of myocardium not only by taking advantage of the current technologies but also by developing newer advanced technologies. In doing so, all the contributions made by the authors in the Research Topic will be integrated for the prevention, diagnosis and treatment of disorders of the heart.

Author contributions

All authors listed have made a substantial, direct and intellectual contribution to the work and approved it for publication.

Funding

This work is supported in part by JSPS KAKENHI—Grant Nos. 20H03421 and 21K19929 (to NF).

Acknowledgments

We would like to thank all the authors who have submitted manuscripts to this Research Topic.

Conflict of interest

The authors declare that the research was conducted in the absence of any commercial or financial relationships that could be construed as a potential conflict of interest.

Publisher's note

References

Cooke, R. (2011). The role of the myosin ATPase activity in adaptive thermogenesis by skeletal muscle. *Biophys. Rev.* 3, 33–45. doi:10.1007/s12551-011-0044-9

Craig, R., and Padrón, R. (2022). Structural basis of the super- and hyperrelaxed states of myosin II. *J. Gen. Physiol.* 154, e202113012. doi:10.1085/jgp.202113012

Fukuda, N., Granzier, H., Ishiwata, S., and Morimoto, S. (2021). Editorial: Recent advances on myocardium physiology. *Front. Physiol.* 12, 697852. doi:10.3389/fphys.2021.697852

Fukuda, N., Granzier, H. L., Ishiwata, S., and Kurihara, S. (2008). Physiological functions of the giant elastic protein titin in mammalian striated muscle. *J. Physiol. Sci.* 58, 151–159. doi:10.2170/physiolsci.RV005408

Fusi, L., Huang, Z., and Irving, M. (2015). The conformation of myosin heads in relaxed skeletal muscle: Implications for myosin-based regulation. *Biophys. J.* 109, 783–792. doi:10.1016/j.bpj.2015.06.038

Granzier, H. L., and Labeit, S. (2004). The giant protein titin: A major player in myocardial mechanics, signaling, and disease. *Circ. Res.* 94, 284–295. doi:10.1161/01.RES.0000117769.88862.F8

Hessel, A. L., Ma, W., Mazara, N., Rice, P. E., Nissen, D., Gong, H., et al. (2022). Titin force in muscle cells alters lattice order, thick and thin filament protein formation. *Proc. Natl. Acad. Sci. U. S. A.* 119, e2209441119. doi:10.1073/pnas.2209441119

Irving, M. (2017). Regulation of contraction by the thick filaments in skeletal muscle. *Biophys. J.* 113, 2579–2594. doi:10.1016/j.bpj.2017.09.037

Irving, T., Wu, Y., Bekyarova, T., Farman, G. P., Fukuda, N., and Granzier, H. (2011). Thick-filament strain and interfilament spacing in passive muscle: Effect of titin-based passive tension. *Biophys. J.* 100, 1499–1508. doi:10.1016/j.bpj.2011.01.059

Ishiwata, S., Shimamoto, Y., and Fukuda, N. (2011). Contractile system of muscle as an auto-oscillator. *Prog. Biophys. Mol. Biol.* 105, 187–198. doi:10.1016/j.pbiomolbio.2010.11.009

Kagemoto, T., Oyama, K., Yamane, M., Tsukamoto, S., Kobirumaki-Shimozawa, F., Li, A., et al. (2018). Sarcomeric auto-oscillations in single myofibrils from the heart of patients with dilated cardiomyopathy. *Circ. Heart Fail.* 11, e004333. doi:10.1161/CIRCHEARTFAILURE.117.004333

Kampourakis, T., Zhang, X., Sun, Y. B., and Irving, M. (2018). Omecamtiv mercabil and blebbistatin modulate cardiac contractility by perturbing the regulatory state of the myosin filament. *J. Physiol.* 596, 31–46. doi:10.1113/JP275050

Kobirumaki-Shimozawa, F., Inoue, T., Shintani, S. A., Oyama, K., Terui, T., Minamisawa, S., et al. (2014). Cardiac thin filament regulation and the Frank-Starling mechanism. *J. Physiol. Sci.* 64, 221–232. doi:10.1007/s12576-014-0314-y

Krüger, M., and Linke, W. A. (2011). The giant protein titin: A regulatory node that integrates myocyte signaling pathways. *J. Biol. Chem.* 286, 9905–9912. doi:10.1074/jbc.R110.173260

Linari, M., Brunello, E., Reconditi, M., Fusi, L., Caremani, M., Narayanan, T., et al. (2015). Force generation by skeletal muscle is controlled by mechanosensing in myosin filaments. *Nature* 528, 276–279. doi:10.1038/nature15727

Linke, W. A., and Hamdani, N. (2014). Gigantic business: Titin properties and function through thick and thin. *Circ. Res.* 114, 1052–1068. doi:10.1161/CIRCRESAHA.114.301286

Nakaura, H., Morimoto, S., Yanaga, F., Nakata, M., Nishi, H., Imaizumi, T., et al. (1999). Functional changes in troponin T by a splice donor site mutation that causes hypertrophic cardiomyopathy. *Am. J. Physiol.* 277, C225–C232. doi:10.1152/ajpcell.1999.277.2.C225

Ohtsuki, I., and Morimoto, S. (2008). Troponin: Regulatory function and disorders. *Biochem. Biophys. Res. Commun.* 369, 62–73. doi:10.1016/j.bbrc.2007.11.187

Schmid, M., and Toepfer, C. N. (2021). Cardiac myosin super relaxation (SRX): A perspective on fundamental biology, human disease and therapeutics. *Biol. Open* 10, bio057646. doi:10.1242/bio.057646

Shintani, S. A., Oyama, K., Fukuda, N., and Ishiwata, S. (2015). High-frequency sarcomeric auto-oscillations induced by heating in living neonatal cardiomyocytes of the rat. *Biochem. Biophys. Res. Commun.* 457, 165–170. doi:10.1016/j.bbrc.2014.12.077

Shintani, S. A., Oyama, K., Kobirumaki-Shimozawa, F., Ohki, T., Ishiwata, S., and Fukuda, N. (2014). Sarcomere length nanometry in rat neonatal cardiomyocytes expressed with α-actinin-AcGFP in Z discs. *J. Gen. Physiol.* 143, 513–524. doi:10.1085/jgp.201311118

Stewart, M. A., Franks-Skiba, K., Chen, S., and Cooke, R. (2010). Myosin ATP turnover rate is a mechanism involved in thermogenesis in resting skeletal muscle fibers. *Proc. Natl. Acad. Sci. U. S. A.* 107, 430–435. doi:10.1073/pnas.0909468107

van der Pijl, R., Strom, J., Conijn, S., Lindqvist, J., Labeit, S., Granzier, H., et al. (2018). Titin-based mechanosensing modulates muscle hypertrophy. *J. Cachexia Sarcopenia Muscle.* 9, 947–961. doi:10.1002/jcsm.12319

frontiers in Physiology

OPINION
published: 28 March 2022
doi: 10.3389/fphys.2022.846206

Does the Hyperthermal Sarcomeric Oscillations Manifested by Body Temperature Support the Periodic Ventricular Dilation With Each Heartbeat?

Seine A. Shintani *

Department of Biomedical Sciences, College of Life and Health Sciences, Chubu University, Kasugai, Japan

Keywords: hyperthermal sarcomeric oscillations, contraction rhythm homeostasis, robustness of heartbeat, cardiac physiology, sarcomere

OPEN ACCESS

Edited by:
Henk Granzier,
University of Arizona, United States

Reviewed by:
Eng Kuan Moo,
University of Calgary, Canada
Bertrand C. W. Tanner,
Washington State University, United States

***Correspondence:**
Seine A. Shintani
shintani@isc.chubu.ac.jp
orcid.org/0000-0002-1084-2549

Specialty section:
This article was submitted to Striated Muscle Physiology, a section of the journal Frontiers in Physiology

Received: *30 December 2021*
Accepted: *14 March 2022*
Published: *28 March 2022*

Citation:
Shintani SA (2022) Does the Hyperthermal Sarcomeric Oscillations Manifested by Body Temperature Support the Periodic Ventricular Dilation With Each Heartbeat? Front. Physiol. 13:846206. doi: 10.3389/fphys.2022.846206

The heart transforms the chemical-mechanical reaction of myosin molecules, which move only stochastically by itself, into a robust heartbeat rhythm by its hierarchical structure (**Figure 1A**, Ishiwata et al., 2017). Myocardial pulsation is thought to be regulated by changes in calcium concentration in cardiomyocytes triggered by electrical excitement from cardiac pacemaker cells (Eisner et al., 2017). However, on the other hand, it has also been found that the heartbeat frequency is too high to sufficiently reduce the calcium concentration in cardiomyocytes that has increased due to muscle contraction (Eisner et al., 2017). The myocardium is known to be contracted when the intracellular calcium concentration is high (Eisner et al., 2017). So why can the heart relax quickly in the early diastole of each heartbeat, even though the calcium concentration in cardiomyocytes is high and the left ventricular pressure is low? Since the left ventricular pressure is low, there is little force to pull and lengthen the sarcomere. And since the calcium concentration in cardiomyocytes is still high, sarcomere generates force. Despite this, the reason why rapid relaxation to fill the ventricle with blood throughout diastole is possible may be that sarcomere has the property of periodically and rapidly relaxing and dilating even if the calcium concentration is still high.

In recent years, we have discovered that sarcomere in cardiomyocytes warmed to body temperature becomes an oscillation state that repeats contraction and relaxation (**Figure 1B**, Shintani et al., 2015). We named the sarcomere oscillations manifested by the heat of this body temperature HSOs (Hyperthermal Sarcomeric Oscillations). We believe that HSOs are the key to answering the previous question. Experiments with isolated cardiomyocytes have shown that HSOs enable rapid lengthening of sarcomere even at high intracellular calcium concentrations, and that the HSOs cycle is close to the heartbeat cycle (**Figure 1C**, Shintani et al., 2020). Given the rapid lengthening seen in HSOs during diastole of the heart, it explains the rapid lengthening of the heart despite high cardiomyocyte calcium levels and low left ventricular pressure.

HSOs are observed at 37°C–43°C in cardiomyocytes where calcium concentration fluctuates at about 1 Hz (Shintani et al., 2015; Shintani et al., 2020). Inhibiting calcium concentration fluctuations narrowed the temperature at which HSOs can be observed to 38°C–43°C (Shintani et al., 2015). To put it very simply, this may be due to a decrease in base calcium concentration. Conversely, when calcium concentration fluctuations higher than 1 Hz, such as heartbeat, occur, the base calcium concentration increases (Eisner et al., 2017), and the minimum temperature required to induce HSOs is likely to be lower than 37°C. The core body temperature of the working heart is higher than other parts of the body. Since even a mere core body temperature is measured at 37–38°C (Yoda et al., 2000), it is highly possible that the HSOs characteristics of sarcomere are manifested at the core body temperature of the working heart, which is considered to be higher.

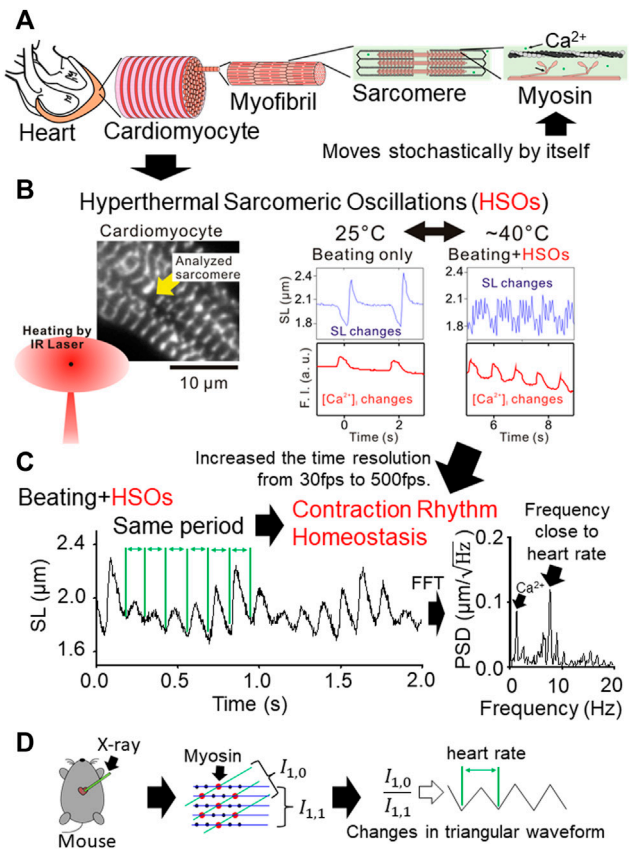

FIGURE 1 | (A) Schematic diagram of the hierarchical structure from the myosin molecule, which can move only stochastically by itself, to the heart, which has a strong heartbeat. **(B)** Schematic diagram of the features of HSOs revealed in 2015 (Shintani et al., 2015). Fluorescence microscope image of cardiomyocytes that expresses α-actinin-AcGFP fusion protein in Z-line and enables measurement of sarcomere length (left panel). The cardiomyocytes were reversibly warmed by irradiating the vicinity of the cardiomyocytes with infrared rays having a wavelength that water absorbs well (left panel). Time-series changes in sarcomere length and intracellular calcium concentration before and after heating (right panel). By warming, HSOs with a higher frequency than the change in calcium concentration were discovered (right panel). **(C)** Schematic diagram of the characteristics of HSOs revealed in 2020 (Shintani et al., 2020). When the time resolution of sarcomere length measurement was improved from 30 fps to 500 fps, it became clear that the period of a sarcomeric oscillation cycle was kept constant even though the waveform of the sarcomeric oscillation changed significantly with the change in calcium concentration (left panel). The frequency of HSOs was close to the heart rate (right panel). **(D)** Schematic diagram of a non-invasive real-time measurement of the movement of myocardial contractile protein molecules from the beating heart by synchrotron radiation X-ray diffraction (Pearson et al., 2007). When the sarcomere contracts, the $I_{0,1}/I_{1,1}$ value decreases, and when the sarcomere relaxes, the $I_{0,1}/I_{1,1}$ value increases.

It has been reported that sarcomere becomes an oscillation state that repeats contraction and relaxation under a solution with intermediate conditions between contraction and relaxation (Fabiato and Fabiato, 1978; Okamura and Ishiwata, 1988; Linke et al., 1993; Sasaki et al., 2006; Shintani et al., 2014; Shintani, 2021). Details are given in the cited paper, but "intermediate conditions between contraction and relaxation" are solution conditions in which sarcomere can exert a contractile force of about half of the maximum contractile force. In previous studies of sarcomeric oscillations, sarcomere was observed in a solution with a fixed calcium concentration (Ishiwata et al., 2017). The discovery of HSOs revealed that by warming cardiomyocyte sarcomere, it responds to changes in calcium concentration and at the same time performs sarcomeric oscillations with a cycle different from that of changes in calcium concentration (Shintani et al., 2015; Shintani et al., 2020). Moreover, sarcomere in the HSOs state has a CRH (Contraction Rhythm Homeostasis) that keeps the period constant, although the amplitude and waveform of the sarcomeric oscillation change significantly with changes in calcium concentration (Shintani et al., 2020). We named CRH the property of the contractile rhythm of HSOs that keeps the period constant even though the waveform changes in response to changes in calcium concentration. As mentioned above, sarcomere in the HSOs state, which repeats contraction and relaxation in a cycle close to the heartbeat, has a calcium concentration change responsiveness (Shintani et al., 2015; Shintani et al., 2020). Therefore, it is thought to synchronize in response to changes in calcium concentration in the heart cycle derived from the periodic excitement of cardiac pacemaker cells. We suspect that this synchronization of calcium concentration changes and mechanical sarcomeric oscillations is the basic state of the myocardial contractile system that supports the heartbeat.

In fact, in a mathematical model that reproduces HSOs, both sarcomere elongation and cardiac diastolic elongation of HSOs were movements based on the chained reversal stroke of myosin within the sarcomere (Washio et al., 2017; Washio et al., 2019; Shintani et al., 2020; Yoneda et al., 2021). It was a mathematical model-predicted expectation that myosin's chained reversal strokes would cause sarcomeric oscillations (Washio et al., 2017). However, after that, it was experimentally confirmed that the reverse swing motion of myosin II existed (Fujita et al., 2019; Hwang et al., 2021).

Synchrotron radiation X-ray diffraction is a method that can measure the movement of myocardial contractile protein molecules from the beating heart in real time non-invasively (Pearson et al., 2007). In the measurement results by this synchrotron radiation X-ray diffraction method, it has been confirmed that the degree to which the myosin head moves and binds to actin with the heartbeat changes in a triangular waveform (**Figure 1D**, Pearson et al., 2007). Previously known sarcomeric oscillations at constant calcium concentrations were saw waveforms with slow contraction and rapid extension, but HSOs can also be oscillated in triangular waveforms with similar contraction and extension (**Figure 1C**, Shintani et al., 2020). The degree to which the myosin head migrates and binds to actin correlates with changes in sarcomere length. Therefore, the measurement results of the synchrotron radiation X-ray diffraction method suggest that the sarcomere in the heart continuously contracts and relaxes in a triangular waveform. Since HSOs can also continuously contract and relax with a triangular waveform of the same cycle, it is highly possible that the heartbeat utilizes the HSOs characteristics (**Figures 1C,D**).

From the above experimental facts, we believe that the beating heart uses HSOs to enable rapid relaxation to fill the ventricle with blood throughout diastole with each beating. And I think that the synchronization of HSOs with CRH and calcium fluctuation supports the robustness of the heartbeat.

AUTHOR CONTRIBUTIONS

SS: Article writing and final approval of the published version.

FUNDING

This work was supported in part by Grants-in-Aid for Scientific Research from Japan (SS, JP17K15102 and JP20K15762), by the Strategic Information and Communications R&D Promotion Programme (SCOPE) of the Ministry of Internal Affairs and Communications of Japan, by the Chubu University production technology development center research fund (SS, Project (6)), and by the Chubu University special research fund (SS, 21M01CP).

REFERENCES

Eisner, D. A., Caldwell, J. L., Kistamás, K., and Trafford, A. W. (2017). Calcium and Excitation-Contraction Coupling in the Heart. *Circ. Res.* 121, 181–195. doi:10.1161/CIRCRESAHA.117.310230

Fabiato, A., and Fabiato, F. (1978). Myofilament-generated Tension Oscillations during Partial Calcium Activation and Activation Dependence of the Sarcomere Length-Tension Relation of Skinned Cardiac Cells. *J. Gen. Physiol.* 72, 667–699. doi:10.1085/jgp.72.5.667

Fujita, K., Ohmachi, M., Ikezaki, K., Yanagida, T., and Iwaki, M. (2019). Direct Visualization of Human Myosin II Force Generation Using DNA Origami-Based Thick Filaments. *Commun. Biol.* 2, 437. doi:10.1038/s42003-019-0683-0

Hwang, Y., Washio, T., Hisada, T., Higuchi, H., and Kaya, M. (2021). A Reverse Stroke Characterizes the Force Generation of Cardiac Myofilaments, Leading to an Understanding of Heart Function. *Proc. Natl. Acad. Sci. U.S.A.* 118, e2011659118. doi:10.1073/pnas.2011659118

Ishiwata, S. i., Miyazaki, M., Sato, K., Nakagome, K., Shintani, S. A., Kobirumaki-Shimozawa, F., et al. (2017). Dynamic Properties of Bio-Motile Systems with a Liquid-Crystalline Structure. *Mol. Crystals Liquid Crystals* 647, 127–150. doi:10.1080/15421406.2017.1289445

Linke, W. A., Bartoo, M. L., and Pollack, G. H. (1993). Spontaneous Sarcomeric Oscillations at Intermediate Activation Levels in Single Isolated Cardiac Myofibrils. *Circ. Res.* 73, 724–734. doi:10.1161/01.res.73.4.724

Okamura, N., and Ishiwata, S. i. (1988). Spontaneous Oscillatory Contraction of Sarcomeres in Skeletal Myofibrils. *J. Muscle Res. Cel Motil* 9, 111–119. doi:10.1007/BF01773733

Pearson, J. T., Shirai, M., Tsuchimochi, H., Schwenke, D. O., Ishida, T., Kangawa, K., et al. (2007). Effects of Sustained Length-dependent Activation on *In Situ* Cross-Bridge Dynamics in Rat Hearts. *Biophysical J.* 93, 4319–4329. doi:10.1529/biophysj.107.111740

Sasaki, D., Fukuda, N., and Ishiwata, S. i. (2006). Myocardial Sarcomeres Spontaneously Oscillate with the Period of Heartbeat under Physiological Conditions. *Biochem. Biophysical Res. Commun.* 343, 1146–1152. doi:10.1016/j.bbrc.2006.03.070

Shintani, S. A. (2021). Effects of High-Pressure Treatment on the Structure and Function of Myofibrils. *Biophysics* 18, 85–95. doi:10.2142/biophysico.bppb-v18.010

Shintani, S. A., Oyama, K., Fukuda, N., and Ishiwata, S. i. (2015). High-frequency Sarcomeric Auto-Oscillations Induced by Heating in Living Neonatal Cardiomyocytes of the Rat. *Biochem. Biophysical Res. Commun.* 457, 165–170. doi:10.1016/j.bbrc.2014.12.077

Shintani, S. A., Oyama, K., Kobirumaki-Shimozawa, F., Ohki, T., Ishiwata, S. i., and Fukuda, N. (2014). Sarcomere Length Nanometry in Rat Neonatal Cardiomyocytes Expressed with α-actinin-AcGFP in Z Discs. *J. Gen. Physiol.* 143, 513–524. doi:10.1085/jgp.201311118

Shintani, S. A., Washio, T., and Higuchi, H. (2020). Mechanism of Contraction Rhythm Homeostasis for Hyperthermal Sarcomeric Oscillations of Neonatal Cardiomyocytes. *Sci. Rep.* 10, 20468. doi:10.1038/s41598-020-77443-x

Washio, T., Hisada, T., Shintani, S. A., and Higuchi, H. (2017). Analysis of Spontaneous Oscillations for a Three-State Power-Stroke Model. *Phys. Rev. E* 95, 02411. doi:10.1103/PhysRevE.95.022411

Washio, T., Shintani, S. A., Higuchi, H., Sugiura, S., and Hisada, T. (2019). Effect of Myofibril Passive Elastic Properties on the Mechanical Communication between Motor Proteins on Adjacent Sarcomeres. *Sci. Rep.* 9, 9355. doi:10.1038/s41598-019-45772-1

Yoda, T., Crawshaw, L. I., Yoshida, K., Su, L., Hosono, T., Shido, O., et al. (2000). Effects of Food Deprivation on Daily Changes in Body Temperature and Behavioral Thermoregulation in Rats. *Am. J. Physiology-Regulatory, Integr. Comp. Physiol.* 278, R134–R139. doi:10.1152/ajpregu.2000.278.1.R134

Yoneda, K., Okada, J.-i., Watanabe, M., Sugiura, S., Hisada, T., and Washio, T. (2021). A Multiple Step Active Stiffness Integration Scheme to Couple a Stochastic Cross-Bridge Model and Continuum Mechanics for Uses in Both Basic Research and Clinical Applications of Heart Simulation. *Front. Physiol.* 12, 712816. doi:10.3389/fphys.2021.712816

Conflict of Interest: The authors declare that the research was conducted in the absence of any commercial or financial relationships that could be construed as a potential conflict of interest.

Publisher's Note: All claims expressed in this article are solely those of the authors and do not necessarily represent those of their affiliated organizations, or those of the publisher, the editors and the reviewers. Any product that may be evaluated in this article, or claim that may be made by its manufacturer, is not guaranteed or endorsed by the publisher.

frontiers | Frontiers in Physiology

REVIEW
published: 26 May 2022
doi: 10.3389/fphys.2022.902079

Hypertrophic Cardiomyopathy Mutations of Troponin Reveal Details of Striated Muscle Regulation

J. M. Chalovich, L. Zhu and D. Johnson†*

Department of Biochemistry and Molecular Biology, Brody School of Medicine, East Carolina University, Greenville, NC, United States

Striated muscle contraction is inhibited by the actin associated proteins tropomyosin, troponin T, troponin I and troponin C. Binding of Ca^{2+} to troponin C relieves this inhibition by changing contacts among the regulatory components and ultimately repositioning tropomyosin on the actin filament creating a state that is permissive for contraction. Several lines of evidence suggest that there are three possible positions of tropomyosin on actin commonly called Blocked, Closed/Calcium and Open or Myosin states. These states are thought to correlate with different functional states of the contractile system: inactive-Ca^{2+}-free, inactive-Ca^{2+}-bound and active. The inactive-Ca^{2+}-free state is highly occupied at low free Ca^{2+} levels. However, saturating Ca^{2+} produces a mixture of inactive and active states making study of the individual states difficult. Disease causing mutations of troponin, as well as phosphomimetic mutations change the stabilities of the states of the regulatory complex thus providing tools for studying individual states. Mutants of troponin are available to stabilize each of three structural states. Particular attention is given to the hypertrophic cardiomyopathy causing mutation, Δ14 of TnT, that is missing the last 14 C-terminal residues of cardiac troponin T. Removal of the basic residues in this region eliminates the inactive-Ca^{2+}-free state. The major state occupied with Δ14 TnT at inactivating Ca^{2+} levels resembles the inactive-Ca^{2+}-bound state in function and in displacement of TnI from actin-tropomyosin. Addition of Ca^{2+}, with Δ14TnT, shifts the equilibrium between the inactive-Ca^{2+}-bound and the active state to favor that latter state. These mutants suggest a unique role for the C-terminal region of Troponin T as a brake to limit Ca^{2+} activation.

Keywords: cardiomyopathy, troponin, striated muscle, states of actin, troponin T, troponin I, acrylodan tropomyosin, muscle contraction regulation

OPEN ACCESS

Edited by:
Shin'Ichi Ishiwata, Waseda University, Japan

Reviewed by:
Thomas Charles Irving, Illinois Institute of Technology, United States
Sachio Morimoto, International University of Health and Welfare (IUHW), Japan

****Correspondence:***
J. M. Chalovich
chalovichj@ecu.edu

†Present address:
D. Johnson, University of North Florida, Jacksonville, FL, United States

Specialty section:
This article was submitted to Striated Muscle Physiology, a section of the journal Frontiers in Physiology

Received: *22 March 2022*
Accepted: *05 May 2022*
Published: *26 May 2022*

Citation:
Chalovich JM, Zhu L and Johnson D (2022) Hypertrophic Cardiomyopathy Mutations of Troponin Reveal Details of Striated Muscle Regulation. Front. Physiol. 13:902079. doi: 10.3389/fphys.2022.902079

THE SCOPE OF TROPONIN MUTANTS

Naturally occurring mutants of troponin have been identified that stabilize each of the states of regulated actin. Those states of actin have different abilities to stimulate myosin ATPase activity. In addition to giving insight into muscle disorders, these mutants have provided tools to study normal muscle function and regulation. The use of troponin mutants as tools will be apparent in the first part of this document as we review concepts of regulation, the states of regulated actin and quantitation of those states. These concepts are essential as the mutants of troponin that we studied function by changing the distribution of those actin states.

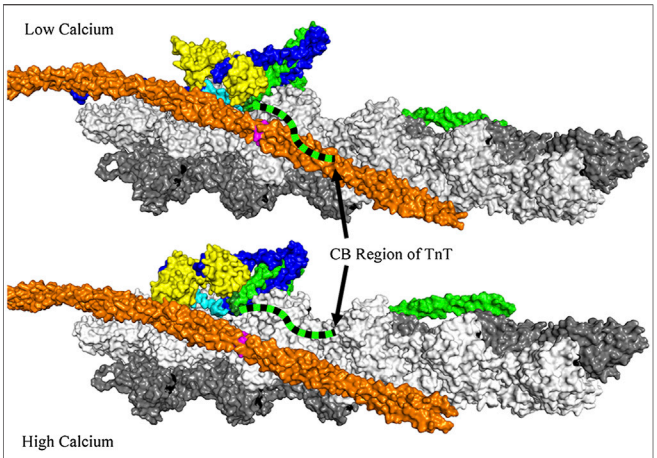

FIGURE 1 | View of actin (grey and white), tropomyosin (orange), TnT (green), TnC (yellow) and TnI (blue) with the inhibitory region of TnI (light blue). Also shown are Cys 190 of tropomyosin (pink) and Cys 374 of actin (black). The coordinates for this figure were taken from PDB deposition 6kn7 (low calcium) and 6kn8 (high calcium) (Yamada et al., 2020). Superimposed on this figure is a possible location of the C-terminal basic region of TnT (green dashed ribbon). This ribbon extends from the end of the IT helix. Both the inhibitory region of TnI and the C-terminal basic region of TnT move away from actin-tropomyosin in the Ca^{2+}-bound state. Actin filaments containing HAHA TnT at low free Ca^{2+} would resemble the wild type at high Ca^{2+} in some respects (see text). Note that the tropomyosin and troponin on the opposite face of the actin filament are not shown for clarity.

REGULATION OF CONTRACTION

Muscle movement occurs as two filamentous protein complexes (myosin and actin) slide past each other in a process that is driven by the concentration gradient of ATP and the free energy of ATP hydrolysis. Actin binding to myosin greatly increases the rate of ATP hydrolysis by myosin; the conformational changes that occur during the cycle of ATP hydrolysis are coupled to force production. Cardiac and skeletal muscles are regulated primarily through modulation of the cofactor activity of actin through tropomyosin and troponin. This modulation may be fine-tuned by post translational modification such as phosphorylation of sites in TnI and TnT (Noland et al., 1989; Kobayashi and Solaro, 2005) and tropomyosin (Rao et al., 2009). Additional regulation may occur *via* C protein (Harris et al., 2004) or nebulin (Root and Wang, 2001). Phosphorylation of myosin light chains plays a modulatory role even in striated muscle (Sweeney and Stull, 1990). Here we limit our comments to regulation that occurs through the actin binding proteins tropomyosin and troponin.

Actin Based Regulation

Actin filaments from striated mammalian muscle have tropomyosin bound along the length of both sides of the double actin helix (**Figure 1**). Each tropomyosin molecule covers seven actin protomers. A troponin complex is bound to each tropomyosin. The troponin complex contains 3 subunits: TnT (tropomyosin binding), TnI (inhibitory) and TnC (calcium binding). The inhibitory region of TnI and the C-terminal region of TnI remain bound to actin, in the relaxed state, resulting in positioning tropomyosin on the outer edge of the actin helical groove (intersection of the white and grey actin strands). Ca^{2+} binding to TnC opens a hydrophobic patch to which the switch region of TnI can bind (Herzberg and James, 1985) thus moving TnI away from actin (see the light blue region in **Figure 1**) and permitting tropomyosin to exist in an equilibrium between an inactive state and an active state that can support high ATPase activity and movement.

The Role of Calcium and Force Producing Crossbridge Attachment

Calcium alone increases the k_{cat} for ATPase activity by about 18-fold and decreases the K_M for actin by about 2-fold, giving about a 36-fold activation at low actin concentrations (Chalovich and Eisenberg, 1982; El-Saleh and Potter, 1985). Full activation occurs when force producing myosin crossbridges accumulate and bind to actin and fix tropomyosin in the active state. The ATPase rate can be increased a further 4-fold or more by allowing binding of "activating" or force producing-like myosin subfragments to actin such as occurs when myosin subfragment-1 has bound ADP. We will describe this in more detail in the following section.

Initial observations of the activating effects of force producing crossbridges were at low ATP levels where myosin-ADP levels could rise and stabilize the active state of regulated actin filaments. Limiting experimentation to very low ATP concentrations precluded some questions of physiological significance as physiological levels of ATP are high relative to ADP. For example, determining the effects of the regulatory proteins on the binding of myosin to actin or on the kinetic constants that define actin activated ATP hydrolysis during contraction must be measured at saturating concentrations of ATP.

Activation With N-Ethylmaleimide Labeled S1 (NEM-S1)

One way to study the role of both Ca^{2+} and "force producing" crossbridges, under saturating ATP conditions, is to dope the system with myosin or myosin subfragments that were treated with the sulfhydryl alkylating reagent N-ethylmaleimide (NEM). S1 that is extensively modified with NEM binds with high affinity to regulated actin even at saturating ATP levels and is able to activate regulated actin under those conditions (Pemrick and Weber, 1976; Meeusen and Cande, 1979; Heeley et al., 2006).

The activating effect of NEM-S1 does not stem directly from its high affinity but results from a change in the way that some chemical forms of S1, like NEM-S1, bind to actin as the free Ca^{2+} level increases. NEM-S1 binds more tightly to regulated actin at high free Ca^{2+} levels whereas S1-ATP binds with about the same affinity irrespective of the free Ca^{2+} level (Chalovich and Eisenberg, 1982; Kraft et al., 1995). Furthermore, increasing saturation of regulated actin with the stable S1-ATP analogue, pPDM-S1-ATP, at low ionic strength is not cooperative (Chalovich et al., 1983). However, S1-AMP-PNP binding to regulated actin is cooperative over the same level of saturation of actin sites even with the affinity of binding adjusted to the same

level by using a higher salt concentration (Chalovich et al., 1983). Cooperativity occurs because of a transition from a low affinity state to a high affinity state of the regulated actin. S1-ATP and pPDM-S1-ATP bind with a similar affinity to both actin states so no stabilization of the high affinity state of actin occurs. Thus, we often distinguish chemical and nucleotide states of myosin as either being "activating" or "non-activating." S1-AMP-PNP, S1-ADP, NEM-S1 and rigor S1 are activating while S1-ATP, S1-ADP-Pi and pPDM-S1-ATP are non-activating states. More will be said about this cooperative transition in the discussion of mutations that increase activation at all Ca^{2+} levels.

The additional activation that NEM-S1 provides over activation by Ca^{2+} occurs largely because of a decrease in the K_M for actin (Williams et al., 1988). Note that the K_M is the actin concentration required to reach ½ of the V_{max} and should not be confused with binding affinity. The affinity of unmodified S1-ATP for regulated actin was not appreciably increased by the presence of activating levels of NEM-S1.

It is interesting that the combination of two cardiomyopathy associated mutants, Δ14-TnT and A8V-TnC, together yield full activation by Ca^{2+} without the need of high affinity attachment of myosin to actin (Baxley et al., 2017). This is a clue that activation by force producing crossbridge binding and by mutations of troponin may share a common mechanism. The C-terminal region of TnT is essential for the ability of activating crossbridges to increase contractile activity.

DISORDERS OF SKELETAL AND CARDIAC MUSCLE REGULATIORY PROTEINS

Many naturally occurring mutants of tropomyosin and troponin produce defects in regulation that lead to contractile dysfunction. Some mutations affect protein folding or binding affinity leaving some actin units unregulated. Other mutations create regulatory complexes that have: 1) decreased activation at all Ca^{2+} levels 2) decreased activation at saturating Ca^{2+} but increased activation at low free Ca^{2+} or 3) increased activation at all Ca^{2+} levels. Several examples of these three classes have altered equilibrium constants among the inactive and active states of regulated actin (Chalovich, 2012; Lehrer and Geeves, 2014). Altering the distribution among the states of regulated actin is reasonable as it is troponin that stabilizes tropomyosin into the various positions on actin that define the states.

Our survey of mutations of TnT and TnI showed that five TnT mutants, associated with dilated cardiomyopathy, have decreased Ca^{2+} sensitivity. It is likely that these mutations stabilize the inactive states of regulated actin. Fifteen mutants of TnT and six mutants of TnI, associated with hypertrophic cardiomyopathy, have increased Ca^{2+} sensitivity; those mutants likely stabilize the active state. The association between the effect of mutations on Ca^{2+}-sensitivity and the type of disorder has been previously noted (Robinson et al., 2002), (Robinson et al., 2007). Several mutations of TnI had a mixed effect on Ca^{2+} sensitivity that could be explained by stabilization of an inactive intermediate state. Before exploring these cases in detail, it is necessary to discuss the states of regulated actin and how they are measured.

States of Regulated Actin

Many studies support the idea that troponin controls the ability of actin to accelerate myosin ATPase activity by changing the position of tropomyosin on actin (Huxley, 1972; Haselgrove, 1972); Parry and Squire, 1973; Wakabayashi et al., 1975; Pirani et al., 2005). Although the regulation of ATPase activity can be described by two states (inactive and active) (Hill et al., 1981), there appear to be three structurally distinct positions of tropomyosin on actin separated by relatively low energy barriers (Poole et al., 2006; Risi et al., 2017). Two of these three structural states are degenerate in terms of their inability to support rapid ATP hydrolysis by myosin (Johnson et al., 2016). The merits of two state (Heeley et al., 2019) vs. 3 state (Geeves et al., 2019) models have recently been discussed.

A 1981 model described two classes of states: 1 (inactive) and 2 (active). State 1 had two substates: one without Ca^{2+} and the other with bound Ca^{2+}. A later model (McKillop and Geeves, 1993) described three states: blocked (B), closed or calcium (C) and either O (open) or M (myosin stabilized). Although the models differ in some fundamental respects, the states appear to be equivalent. Others make a further distinction between the active state stabilized by Ca^{2+} or by rigor myosin binding (Lehrer and Geeves, 2014). The ATPase activity of myosin is proportional to the fraction of actin in the active state. When myosin-linked regulation is present, the rate is also proportional to the fraction of myosin in the active state. We will not deal with myosin-linked regulation here.

Determining the Fraction of Each Actin State

Quantitation of the active state is most confidently done by measuring a relative activity such as ATPase activity. The fraction of actin in the active state, F_A, is then given by $(v_{obs}—v_{min})/(v_{max}—v_{min})$ where v_{obs} is the measured ATPase rate, v_{min} is 0.67* the rate with zero calcium added and in the presence of EGTA, v_{max} is the rate measured at saturating Ca^{2+} and NEM-S1 and at the same actin concentration used in the other measurements. The term 0.67 comes from the rate of ATPase activity with a phosphomimetic mutant of TnI having Glu replacing the 3 phosphorylatable residues (Mathur et al., 2008). This lower rate may better reflect the inactive state. The value of v_{max} can be estimated by stabilizing the active state with both Ca^{2+} and activating or force-producing type crossbridges. The use of NEM-S1 to stabilize the active state (mentioned earlier) may involve rather large corrections (Baxley et al., 2017). By using Δ14-TnT, F_A is increased from 0.25 to 0.7 with Ca^{2+} alone. Thus, small amounts of NEM-S1 are sufficient to reach full activation and the corrections are minimized. The combination of Δ14-TnT and A8V-TnC gives $F_A = 1$ without the need of NEM-S1 at all (Baxley et al., 2017).

Actin filaments in the two inactive states can be distinguished based on differences in the rate of non-ATP containing myosin S1 binding to regulated actin in the presence and absence of Ca^{2+} (Trybus and Taylor, 1980; McKillop and Geeves, 1993), by the use of environmentally sensitive probes on tropomyosin (Ishii and Lehrer, 1993; Gafurov and Chalovich, 2007; Borrego-Diaz and

Chalovich, 2010) and by FRET between different proteins of the thin filament (Shitaka et al., 2004; Shitaka et al., 2005; Johnson et al., 2019). However, there is uncertainty in quantitating the relative populations of the two inactive states because we do not know the values of these parameters when actin is 100% in each of the two inactive states. That is, at low Ca^{2+} there is a mixture of the two inactive states while at saturating Ca^{2+} there is a mixture of the two Ca^{2+}-bound states, one inactive and one active.

One approach to determining the fraction of each of the inactive states is to use a model of regulation to calculate the values based on a series of assumptions. This approach was taken for estimating the state distribution based on the kinetics of ATP-free S1 binding to regulated actin (McKillop and Geeves, 1993). In that study, the values of the parameters K_b, K_2 and n were fixed at what were seen to be reasonable values, the rate of binding to the inactive-Ca^{2+}-free state (B state) was set to zero and the rate of binding to actin in the presence of saturating Ca^{2+} (a mixture of the C and O states) was assumed to be at its maximum value. Although useful, such estimates are model dependent. Relaxing the restrictions led to different estimates of the actin distributions (Gafurov et al., 2004a). Furthermore, the assumption that Ca^{2+} is sufficient to produce the maximum rate of binding does not appear to be true with cardiac regulatory proteins (Gafurov et al., 2004a).

While current measurements of actin state distributions are imperfect, these methods accurately report changes in the distribution of states. These methods are also invaluable for measuring the kinetics of state transitions (Shitaka et al., 2005; McKillop and Geeves, 1993; Borrego-Diaz and Chalovich, 2010; Johnson et al., 2019).

TROPONIN MUTANTS SERVE AS BENCHMARKS OF ACTIN STATES AND DEMONSTRATE ADDITIONAL COMPLEXITIES OF REGULATION

Because some troponin mutants stabilize a particular state of actin, they can be used to calibrate measurements of actin state distributions. The S45E mutation of TnI gives a better estimate of the inactive amplitude as it gives a signal for acrylodan tropomyosin fluorescence 1.3x the wild type amplitude (Franklin et al., 2012). It is yet unclear if this represents 100% occupancy of the inactive-Ca^{2+}-free state. Stabilization of a state that is functionally similar to the inactive-Ca^{2+}-bound state can be achieved using Δ14-TnT mutant at low Ca^{2+} levels. The fully active state can be stabilized with the combination of A8V TnC and Δ14 TnT. A description of these and other mutants is given below.

Mutations That Decrease Activation at all Ca^{2+} Levels

The example that we give here is not that of a disease-causing mutation but of the simulation of a normal regulatory event. PKC pseudo-phosphorylation of TnI at Ser-43, Ser-45 and Thr-144 (mouse sequence) reduces Ca^{2+} sensitivity and ATPase activity (Burkart et al., 2003). Actin filaments containing TnI with Glu inserted at positions 45, 43 and 45 or 43, 45 and 144 all had reduced ATPase activities which were especially pronounced at saturating Ca^{2+} (Mathur et al., 2008). The rates at saturating Ca^{2+} approached the same maximum limit as wild type upon activation with NEM-S1. Thus, the decreased rate was likely due to stabilization of the inactive state of regulated actin. The S45E mutant had a rate 0.89 times wild type while the 43/45/144 mutant was even lower at 0.67 times the wild type rate. Our working assumption is that the minimum value of ATPase activity, at low free Ca^{2+} is 0.67x the wild type rate. As already stated, the amplitude of acrylodan-tropomyosin fluorescence of S45E-TnI was 1.3x that of wild type actin filaments. Together with the lower ATPase activity observed with S45E-TnI, it is clear that wild type troponin does not fully stabilize the inactive-Ca^{2+}-free state.

The idea that these phosphomimetic mutants stabilize the inactive-Ca^{2+}-free state was reinforced by comparing the equilibrium binding of S1-ADP to actin filaments containing wild type and mutant TnI. Binding to actin filaments containing mutant TnI had a more sigmoidal cooperative binding curve than did wild type actin filaments. Increasing the fraction of actin filaments in the low affinity state has the effect of exaggerating the cooperative transition. The affinity of regulated actin containing the 45 and 43/45/144 mutants for Ca^{2+} was also decreased as expected for stabilization of the inactive state. Thus, it appeared that these phosphomimetic mutants of TnI shifted the equilibrium constants among the states to favor the inactive state.

Mutations That Decrease Activation at Saturating Ca^{2+} but Increase Activation at Low Free Ca^{2+}: Stabilization of an Inactive Intermediate State

Several missense mutations of TnI are associated with hypertrophic cardiomyopathy (Kimura et al., 1997). The R146G mutations were shown to reduce regulation with an elevated fiber force at low free Ca^{2+} levels and a depressed force at saturating Ca^{2+} (Lang et al., 2002). These TnI mutants increased Ca^{2+} sensitivity. The D191H, R146G and R146W mutations of mouse TnI stabilized the active state at low free Ca^{2+} and the inactive state at saturating Ca^{2+} (Mathur et al., 2009). The effects of R146G-TnI could not be attributed to a change in affinity for actin-tropomyosin. We proposed that these mutations of TnI stabilized a form of regulated actin that was between the inactive and active states (Mathur et al., 2009).

The intermediate state of regulated actin that was stabilized by R146G-TnI was inactive toward stimulating myosin catalyzed ATPase activity (Mathur et al., 2009). This state had been assumed to be inactive in models of regulation of ATPase activity (Hill et al., 1981) and of myosin S1 binding to regulated actin (McKillop and Geeves, 1993).

R146G and R146W occur within the inhibitory region of TnI that is essential for forming the inactive-Ca^{2+}-free state. The inhibitory region (Tao et al., 1990) and the COOH terminal mobile region of TnI (Tripet et al., 1997) are bound to actin in the

inactive-Ca^{2+}-free state and are released at saturating Ca^{2+} levels. Other residues within the inhibitory region of TnI are likely to have an equal or greater effect on activity than the R146 mutations (Van Eyk and Hodges, 1988). Elimination of the inhibitory region of TnI is sufficient to eliminate the inactive-Ca^{2+}-free state. However, the inhibitory and COOH regions of TnI are insufficient to form the inactive- Ca^{2+}-free state of regulated actin. Rather, the C-terminal basic region of TnT is also required as shown later in this document.

TABLE 1 | Mammalian C-terminal troponin T sequences compared with the C-terminal TnI sequence.

Troponin type	C-terminal
Cardiac TnT	QKVSKTRGKAKVTGRWK
Fast Skeletal TnT	QKHSKKAGTPAKGKVGGRWK
Slow Skeletal TnT	QKFRKGAGKGRVGGRWK
Cardiac TnI	RGKFKRPTLRRVRISAD 152

Mutations That Increase Activation at all Ca^{2+} Levels

Hypertrophic cardiomyopathy is most often associated with those mutations of troponin that cause an increase in Ca^{2+} activation (Robinson et al., 2007). These mutants are characterized by increased sensitivity to Ca^{2+} in muscle fiber preparations and an increase in actin-activated ATPase activity in solution studies. We have focused our attention on one TnT mutation that gives the largest increase in activity that we are aware of, that is Δ14-TnT.

Two splice variants of TnT were identified in a family that resulted in a deletion of the last 14 amino acids of TnT (Δ14-TnT) in one case and that replaced the last 28 amino acids with a novel stretch of 7 amino acids in the other case (Thierfelder et al., 1994). Muscle fibers having Δ14-TnT had an increased activity (Nakaura et al., 1999) and had an increased response to both Ca^{2+} and to high affinity, ATP-free myosin binding (Stelzer et al., 2004). The actin activated ATPase activity produced with actin filaments containing Δ14-TnT was higher than that with wild type filaments at both low and high Ca^{2+} concentrations (Gafurov et al., 2004b; Baxley et al., 2017) provided that the actin concentration was sub-saturating. The rates of wild type filaments and those containing Δ14-TnT were also the same when maximum activation was achieved by the addition of NEM-S1 (Gafurov et al., 2004b; Baxley et al., 2017).

Some hypertrophic cardiomyopathy mutations of TnC also moderately enhance Ca^{2+} activation of ATPase activity and sensitize fibers to Ca^{2+} (Landstrom et al., 2008). Whereas Δ14-TnT increased the actin activated ATPase activity by 2.2-fold, A8V-TnC increased the rate by 1.8-fold (Baxley et al., 2017). The combined effects of A8V-TnC and Δ14-TnT increased the ATPase activity 3.2-fold giving a rate identical to that of wild type filaments that were fully activated with Ca^{2+} and NEM-S1 (Baxley et al., 2017). These results suggest that troponin has the inherent ability to stabilize the active state of actin (Baxley et al., 2017) as well as the more well-known ability to stabilize the inactive state at low Ca^{2+} levels. The basic C-terminal region of TnT attenuates the stabilization of the active state that would otherwise occur at saturating Ca^{2+}. Higher animals having the CB region have gained a dual activation system requiring Ca^{2+} and force producing crossbridges (Johnson et al., 2020).

The ATPase rates used to estimate the activation by Ca^{2+} were measured at low actin concentrations so that the values obtained were proportional to k_{cat}/K_M. When ATPase rates were measured with increasing concentrations of regulated actin, the values with Δ14-TnT-A8V-TnC and with actin in the absence of tropomyosin or troponin approached the same maximum rate. Troponin-tropomyosin increases the effectiveness of actin as a cofactor in accelerating ATPase activity by decreasing the K_M, that is the concentration of regulated actin required to reach half of the maximum rate. This agrees with an earlier study that used NEM-S1 to fully activate the system (Williams et al., 1988). That study showed that the decrease in K_M occurred without a change in the affinity of S1-ATP for regulated actin.

This brings up a point that is incompletely understood. Ca^{2+} increases the ATPase activity of regulated actin primarily by increasing the k_{cat}, with little change in K_M or in affinity of S1-ATP for actin (Chalovich and Eisenberg, 1982). Reaching full activation by using NEM-S1 or Δ14-TnT and A8V-TnC increases the rate another 3-4-fold and that increase occurs primarily with a decrease in K_M with a smaller change in k_{cat} and no appreciable change in S1-ATP affinity for actin (Williams et al., 1988). If these increases in rate are due only to the increase in the population of actin in the active state, then one would have expected full activation to also be driven primarily by an increase in k_{cat}.

Further evidence that the Δ14 mutant of TnT stabilizes the active state of regulated actin came from studies of equilibrium binding of myosin S1 to regulated actin. The affinity and shape of the binding curves are dependent on the free Ca^{2+} level, ionic strength and nucleotide bound to S1 (Greene and Eisenberg, 1980), (Chalovich et al., 1983). At low free Ca^{2+} levels, binding of species such as S1-AMPPNP, S1-ADP and rigor S1 increases in a sigmoidal fashion as the free concentration of S1 increases. This occurs, as was stated earlier, because the regulated actin exists in an equilibrium between a lower affinity form and a higher affinity form for binding of non-ATP containing species of S1 with the lower affinity form being favored at low free Ca^{2+} (Hill et al., 1980). The binding of activating species of S1 stabilizes the higher affinity form of regulated actin in a cooperative manner. Binding is characterized by the equilibrium constant between the two binding configurations of regulated actin, the cooperativity of the transition and the affinities of the low and high affinity states for actin (Hill et al., 1980).

Replacing Δ14-TnT for wild type TnT made the binding in the virtual absence of Ca^{2+} become more similar to that observed at saturating Ca^{2+} (Gafurov et al., 2004b). Removing the C-terminal 14 amino acid residues from human cardiac TnT stabilized the high affinity configuration of actin over a range of ionic strengths (L' increased in the Hill model). That is, the C-terminal region of TnT stabilized the low affinity binding state of regulated actin.

HAHA-TnT and Other Constructs of Troponin T for the Study of Regulation

Just as NEM-S1 was created as a tool for studying activation by "activating" myosin species, HAHA-TnT was designed to permit study of the involvement of TnT in that activation. HAHA stands for High Ala, High Activity. HAHA-TnT was created by replacing the Lys and Arg residues in the CB region of cardiac or skeletal TnT (in bold in **Table 1**) with Ala. This produces a TnT that has effects on regulation much like those of Δ14-TnT without eliminating the entire C-terminal region (Johnson et al., 2019). We also produced 289C-HAHA-TnT that has an added C-terminal Cys residue that can incorporate reporter groups. The wild type control for the 289C-HAHA-TnT is 289C-TnT. Reporter groups have also been placed on 275C of both HAHA and wild type TnT.

Actin Filaments Containing Δ14-TnT or HAHA-TnT do Not Occupy the Inactive-Ca^{2+}-free State in the Virtual Absence of Ca^{2+}

Wild type regulated actin filaments containing acrylodan-labeled tropomyosin show an increase in fluorescence when they progress to the inactive-Ca^{2+}-free state. There was no such fluorescence change with regulated actin containing either Δ14-TnT (Franklin et al., 2012), or 289C-HAHA-TnT (Johnson et al., 2019) indicating that the inactive-Ca^{2+}-free state (or B state) was not formed.

The S45E mutant of TnI that stabilizes the inactive-Ca^{2+}-free state and gives a 30% enhancement of the acrylodan-tropomyosin signal did not rescue the total absence of signal with Δ14-TnT (Franklin et al., 2012). The lack of additivity suggests that the C-terminal region of TnT is essential for forming the inactive-Ca^{2+}-free state. We predict from these observations that the CB region of TnT stabilizes the binding of the switch and C-terminal regions of TnI to the actin filament. That hypothesis is supported by FRET measurements between these regions of TnI and both actin-374 and tropomyosin-190 (Zhu et al., 2022).

DETERMINATION OF FUNCTIONAL REGIONS WITHIN THE C-TERMINUS OF TNT

Both the N- and C-terminal regions of TnT have regulatory roles. The N-terminal region of TnT is isoform specific and alters the properties, such as Ca^{2+} sensitivity, to specific muscle types (Jin, 2016). The constancy of the C-terminal region suggests that it functions on a more basic level to maintain normal regulation. The CB region of TnT does vary among animal species and that may give clues to its function.

The C-terminal region of TnT from mammals shows a preponderance of basic residues and a terminal sequence of GRWK (**Table 1**). The inhibitory region of TnI is also highly basic and there is a suggestion of an evolutionary link between these regions (Brunet et al., 2014). Such patches of basic residues may indicate that electrostatic interactions involving the C-terminal region of TnT may be important in its observed functions.

Figure 2 shows that the CB region of TnT is highly conserved in cardiac muscle of mammals. Reptiles, birds, amphibians, and fish have different C-terminal sequences but maintain a large number of basic residues. Based on the results of stepwise truncation of residues from the C-terminal of cardiac TnT, the limitation of Ca^{2+} activation is proportional to the fraction of basic residues conserved (Johnson et al., 2018). Some fish TnT have a C-terminus that is highly basic while lacking the terminal GRWK.

The basic C-terminal region is absent in Protostomia. Some members of Protostomia have a long stretch of Glu residues at their C-terminal. There is evidence that this acidic region is a Ca^{2+} buffer that assists the high frequency oscillations of insect flight muscle (Cao et al., 2020). It is interesting, in this regard, that the flight muscle of some birds also has a long stretch of Glu residues but at the N-terminal region (Jin et al., 2008). It will be interesting to see how the regulatory properties of avian and mammalian TnT compare.

Mutants of TnT Demonstrate the Importance of Overall Positive Charge of the CB Region

To identify key residues within the CB region of TnT, we made a series of C-terminal truncation mutants. **Figure 3** shows the approximate fraction of regulated actin in the active state and in the inactive-Ca^{2+}-free state as a function of the number of deleted positive charges. At saturating Ca^{2+}, the fraction of regulated actin in the active state increased in roughly a linear fashion as the CB region was shortened. Likewise, the fraction of regulated actin in the inactive-Ca^{2+}-free state decreased in a linear manner as the number of positive charges was reduced. These data show that the basic residues are responsible for stabilizing the inactive state at low Ca^{2+} and for destabilizing the active state at saturating Ca^{2+}. That the loss of positive charges from the C-terminal region of TnT can produce an activating effect has also been shown with the R278C mutation (Morimoto et al., 1999), (Szczesna et al., 2000), the K273E mutation (Venkatraman et al., 2003), (Messer et al., 2016) and the K280N mutation (Messer et al., 2016).

The rate of rigor S1 binding to regulated actin containing wild type cardiac troponin was about 4-fold faster at high Ca^{2+} than at low free Ca^{2+} indicating that the C and M states (inactive-Ca^{2+}-bound and active states) permit faster binding (Trybus and Taylor, 1980), (McKillop and Geeves, 1993). The rate of binding of rigor S1 to actin filaments containing 289C-HAHA at low Ca^{2+} was similar to that observed with wild type regulated actin at saturating Ca^{2+}. That is, removal of the C-terminal basic residues of TnT increased the occupancy of these faster binding states. It was also interesting that the rate of binding of rigor S1 to 289C-HAHA containing actin filaments at saturating Ca^{2+} was 1.8x that of wild type at saturating Ca^{2+}. That is, with cardiac troponin, the rate of binding to actin in the active state (M state) is faster than to

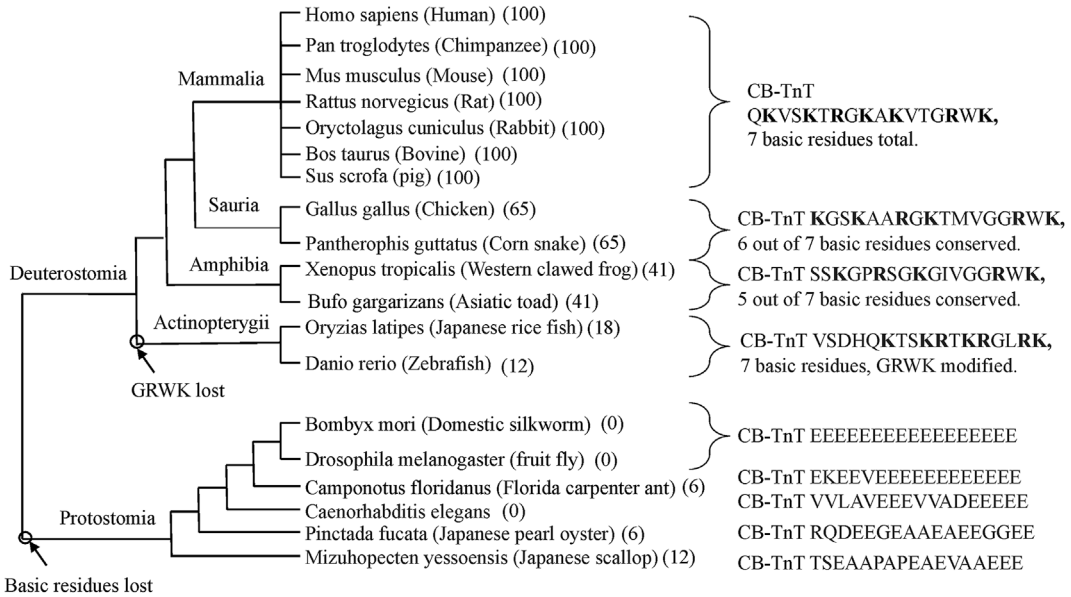

FIGURE 2 | Cladogram of the last 17 residues of cardiac TnT. The mammalian sequences are all identical. They contain seven basic residues within this 17 residue stretch and have a terminal GRWK. Sauria have 65% sequence conservation with 6 basic residues and a terminal GRWK. Amphibia are 41% conserved with five basic residues and a terminal GRWK. Actinopterygii have 18% sequence conservation but have seven basic residues with the terminal sequence GLRK. Protostomia lack the C-terminal basic region altogether. Note that the Protostomia have the same type of TnT in all striated muscles.

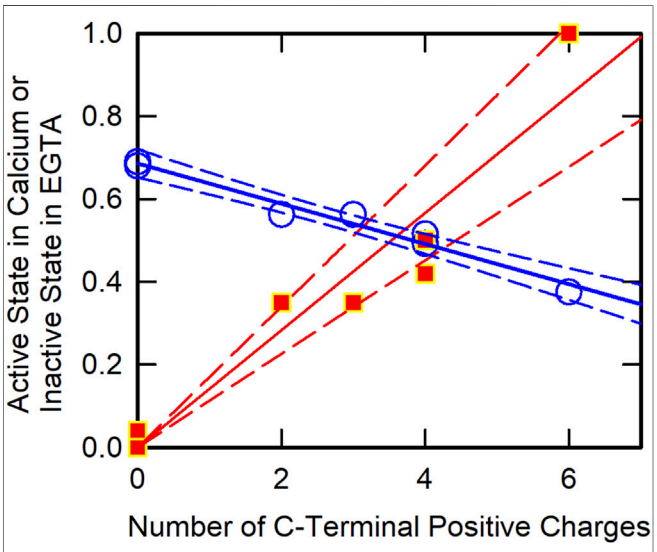

FIGURE 3 | C-Terminal TnT Charge Effects on Actin Filament States. The fraction of actin in the active state at saturating Ca^{2+} was determined by ATPase assays (green circles). The fraction of actin in the inactive state in the virtual absence of Ca^{2+} was determined by acrylodan tropomyosin fluorescence (red squares). Data were obtained from earlier publications (Johnson et al., 2018), (Johnson et al., 2019) with linear least square fits (solid lines) and 95% confidence limits (broken lines).

actin in the inactive-Ca^{2+}-bound state (C state) (Johnson et al., 2019). That difference was not observed in the case of skeletal troponin (Lopez Davila et al., 2020).

The HAHA mutant of TnT had other similarities to Δ14 TnT. For example, the acrylodan-tropomyosin fluorescence assay failed to detect evidence of the B state in the virtual absence of Ca^{2+} (Johnson et al., 2019). However, the ATPase activity remained very low indicating that the active state was not populated. We concluded that actin filaments containing HAHA TnT exist in a state that is functionally like the C (inactive-Ca^{2+}-bound) state even at low free Ca^{2+}.

HAHA TnT increased the ATPase activity at saturating Ca^{2+} over values obtained with wild type actin filaments. Placing 289C-HAHA TnT into a cardiac fiber preparation increased the Ca^{2+} sensitivity by 0.24 pCa units. Overall, HAHA TnT behaved similarly to Δ14 TnT.

The Cys residues engineered into the CB region of TnT made it possible to follow changes in this region. The transition from the inactive-Ca^{2+}-bound state of wild type actin filaments to the inactive-Ca^{2+}-free state was accompanied by movement of TnT-289 toward tropomyosin-190 (Johnson et al., 2019). Furthermore, the apparent rate constant of this transition was similar to the rate constant for acrylodan tropomyosin fluorescence over a range of temperatures. When the same study was done with 289C-HAHA-TnT there was no change in FRET as removal of the basic residues made it virtually impossible to occupy the inactive-Ca^{2+}-free state.

Muscle Fiber Studies Confirm the Role of Positively Charged Residues Within the CB Region of TnT

The previous solution studies raise an interesting question of how muscle contraction would change if there were no B state and if

Ca^{2+} gave ≥ 3-fold greater activation of ATPase activity than normally observed. This question was examined with the *in vitro* motility assay and with a cardiac fiber preparation (Johnson et al., 2020).

Actin filaments containing Δ14-TnT had an enhanced rate of movement at both low and high Ca^{2+} levels (Johnson et al., 2020). The maximum speed of movement was about 1.8x faster than wild type at saturating Ca^{2+}. There was no movement of wild type filaments at low Ca^{2+} but Δ14-TnT-containing filaments moved at 13% of the maximum observed rate. No change in Ca^{2+} sensitivity was observed.

Cardiac muscle fiber preparations containing Δ14-TnT produced the same maximum force as fibers with wild type troponin and had an increased Ca^{2+} sensitivity by 0.2 pCa units (Gafurov et al., 2004b). Fibers containing both Δ14-TnT and A8V-TnC produced about 18% more force than fibers with wild type troponin (Johnson et al., 2020). Both Δ14-TnT and the combination of Δ14-TnT & A8V-TnC increased the basal activity by about 3-fold and increased the Ca^{2+} sensitivity by 0.3–0.34 pCa units.

Taken together, these results show that eliminating the inactive-Ca^{2+}-free state results in increased basal activity. The force produced by fiber preparations increased at all Ca^{2+} levels. The results of the solution assays and the *in vitro* motility assay were very similar; in both cases the loads were small as were the number of attached myosin molecules. Muscle fiber preparations had greater activation at low Ca^{2+} levels but did not have large increases, over wild type, in maximally activated force.

Many of these results were recapitulated in skeletal troponin-tropomyosin using a skeletal version 251C-HAHA-TnT or Δ16 skeletal TnT (Lopez Davila et al., 2020). Effects of the loss of charges at the C-terminal region of skeletal TnT included increased ATPase activity at low and high Ca^{2+}, loss of the acrylodan tropomyosin fluorescence increase in transitioning to the B state, and an increase in Ca^{2+} sensitivity by 0.8–1.2 pCa units. Skeletal fibers containing the mutant TnT varieties produced force even at pCa 7.5 where fibers are normally relaxed. The C-terminal basic region of skeletal TnT, like that of cardiac TnT, is required for forming the inactive-Ca^{2+}-free state and for limiting the activation by Ca^{2+}.

TROPONIN STRUCTURE ALTERATION BY MUTATIONS

Regulation of mammalian striated muscle contraction involves alterations in protein-protein contacts among TnC, TnI, TnT, tropomyosin and actin. Because the CB region of TnT causes large changes in the response to Ca^{2+}, it seems likely that substantial changes in these protein-protein associations also occur. We investigated Ca^{2+}-dependent changes in the CB region of TnT and the effect that the CB region has on the well documented changes in TnI contacts that occur during activation. The CB region is natively unstructured and is invisible in high resolution structures of troponin. We utilized Förster Resonance Energy Transfer (FRET) to monitor changes in the CB region of TnT and to map the changes that the CB region of TnT produces in other key regions of troponin.

Readers may wish to consult more detailed descriptions of troponin structure than are present in this manuscript. A detailed description of the structure of a large part of the troponin complex is available (Takeda et al., 2003). Most recently, the structure of much of regulated actin complex has been published (Yamada et al., 2020) along with a helpful commentary on that structure (Tobacman, 2021). Several reviews, while predating the most recent findings, are useful for understanding the key regions of the components (Marston and Zamora, 2020; Cheng and Regnier, 2016). The latter paper includes a useful diagram of the troponin components showing the position of many mutations along the primary structure.

The CB Region of TnT is Localized Near Actin-Tropomyosin in the Inactive State

FRET measurements showed that in forming the inactive-Ca^{2+}-free state from the inactive-Ca^{2+}-bound state, CB residues 275 and 289 approach tropomyosin-190 (Johnson et al., 2019; Zhu et al., 2022). Residue 275 was closer to tropomyosin-190 than residue 289 of TnT.

These FRET results as well as the effects of truncating residues from the C-terminal region of TnT suggest that the C-terminal 14 amino acids of human cardiac TnT are important for positioning tropomyosin in the inactive state. The C-terminal region of TnT likely binds to actin or tropomyosin in order to hold tropomyosin in the inactive state (or bind to a position that blocks tropomyosin movement into the active states). Other data suggests that a site in the C-terminal region of TnT binds to tropomyosin near Cys 190 under conditions of very low free Ca^{2+} (Morris and Lehrer, 1984). That second tropomyosin binding site of TnT was reported to be between residues 197 and 239 of human cardiac TnT (Jin and Chong, 2010), or within the terminal 31 residues (Pearlstone and Smillie, 1981), or within the terminal 17 residues (Tanokura et al., 1983).

Further FRET studies showed that Ca^{2+} binding to TnC caused the CB region of TnT to move away from actin as well as from tropomyosin (Zhu et al., 2022). That is, there appears to be a coordinated movement of regions of TnT and TnI away from actin-tropomyosin upon Ca^{2+} binding. The extent of movement of the CB region away from actin-tropomyosin increased when Ala replaced the basic residues within the CB region of TnT. This further movement reflects the shift from about 30% occupancy of the active state to 70% occupancy under these conditions.

The Location of the CB Region of TnT in the Active State

Ca^{2+} binding to the regulatory site(s) of TnC opens a hydrophobic pocket to which the switch region of TnI can bind (Herzberg and James, 1985) but it was unclear whether this was sufficient to release the inhibitory region of TnI from actin. There is an indication that the N-lobe of TnC is able to nudge the inhibitory region of TnI off of actin (Tobacman, 2021)

allowing the switch region of TnI to bind to the hydrophobic pocket of TnC.

The CB region of TnT might also bind near the N-lobe of TnC in the active state (Johnston et al., 2019). However, FRET measurements show that the CB region of TnT remains far from TNC at both low and high free Ca^{2+} levels (Zhu et al., 2022). Because of the potential importance of the CB region in regulation, this discrepancy must be resolved.

The CB Region of TnT is Critical for Normal Changes in TnI Interactions

Removal of the basic residues of the CB region of TnT caused the switch and inhibitory regions of TnI to move away from actin-tropomyosin in the same manner observed with Ca^{2+} binding to wild type regulated actin filaments. Formation of the inactive-Ca^{2+}-bound state requires both the inhibitory region on TnI (Van Eyk and Hodges, 1988) and the long C-terminal region of TnI (residues 164–210), known as the mobile region (Ramos, 1999), (Wong et al., 2019). Now it appears that the CB region of TnT is also required to position tropomyosin into the inhibitory position. The ribbon diagram of the CB region of TnT in **Figure 1** illustrates the possible change in position of the CB region of TnT in going from the relaxed to the active, high Ca^{2+}-state.

The basic amino acid residues in the C-terminal region of TnI also appear to be critical for forming the inactive-Ca^{2+}-free state. Charge replacements near the end of the IT helix (TnI-R145G and TnT-R278C) increased the resting force and increased the Ca^{2+} sensitivity of fibers (Brunet et al., 2014). Furthermore, these effects of the I and T mutations on the inactive state were additive.

We mentioned earlier that an inactive-Ca^{2+}-bound state forms even in the virtual absence of Ca^{2+} when wild type TnT is replaced with Δ14 TnT or HAHA TnT. Although that seems to be a contradiction of terms that idea is clarified by FRET studies. Actin filaments containing HAHA TnT at low free Ca^{2+}, would have the inhibitory region of TnI (light blue in **Figure 1**) and the CB region of TnT (blue and black dashed curve) positioned away from actin tropomyosin as they are for wild type filaments at saturating Ca^{2+}. The switch region of TnI is also detached from actin but is not bound to the hydrophobic pocket of TnC as opening of the hydrophobic pocket of TnC is a rare event in the absence of bound Ca^{2+}.

FURURE PROSPECTS

Investigations of mutations of troponin have shown that having a population of regulated actin filaments with too little Ca^{2+} activation, too much Ca^{2+} activation or with too little difference between the inactive and active states (stabilization of the intermediate state) all result in cardiomyopathies. This observation complicates treatment of cardiomyopathies as it is critical to establish the natural balance. For example, the Ca^{2+}-sensitizer Bepridil does increase activity at low free Ca^{2+} levels but it inhibits activity at high Ca^{2+} levels and seems to stabilize the inactive intermediate state of the actin filament (Varughese et al., 2011).

The many naturally occurring mutants of troponin as well as post-translationally modified forms of troponin provide opportunities to uncover additional details of actin-based regulation of contraction. The C-terminal region of TnT is an added region of TnT that limits Ca^{2+} activation providing additional activation possibilities upon binding of activating or force producing states of myosin. This region may be a future target for therapies. The function of the CB region of TnT is not entirely understood. Although this region is closer to actin-tropomyosin in the relaxed state than in the active state, we do not know if it is bound to either actin or tropomyosin. Even more uncertainty exists over the location of the CB region of TnT in the Ca^{2+} active state and in the fully active state.

The CB region of TnT reduces basal activity of regulated actin and limits Ca^{2+} activation in solution and decreases Ca^{2+} sensitivity in muscle fibers. Binding of force producing myosin crossbridges to actin restores full activation. This CB region is common in higher animal forms and its preservation suggests that this dual regulation by Ca^{2+} and binding of "activating" forms of myosin to actin is an advantage to the striated muscles of these organisms. It is unclear, at present, what that advantage is. A full understanding of this question requires knowledge of how all of the other modulators of contraction (phosphorylation, C protein etc.) operate together. Fortunately, troponin mutants may contribute to answering these and other questions.

AUTHOR CONTRIBUTIONS

JC conceived and wrote the article. LZ prepared the cladogram and assisted in writing. DJ prepared the structural figure and assisted in writing.

FUNDING

JC wishes to thank Victor and Leepo C. Yu for supporting this work with a personal grant. The late Dr. Leepo Yu was well known to many in the muscle community for her use of X-ray diffraction techniques to study muscle contraction. She was a valued colleague, and a kind soul who was liked by all who knew her.

REFERENCES

Baxley, T., Johnson, D., Pinto, J. R., and Chalovich, J. M. (2017). Troponin C Mutations Partially Stabilize the Active State of Regulated Actin and Fully Stabilize the Active State when Paired with Δ14 TnT. *Biochemistry* 56, 2928–2937. doi:10.1021/acs.biochem.6b01092

Borrego-Diaz, E., and Chalovich, J. M. (2010). Kinetics of Regulated Actin Transitions Measured by Probes on Tropomyosin. *Biophysical J.* 98, 2601–2609. doi:10.1016/j.bpj.2010.02.030

Brunet, N. M., Chase, P. B., Mihajlović, G., and Schoffstall, B. (2014). Ca^{2+}-regulatory Function of the Inhibitory Peptide Region of Cardiac Troponin I Is Aided by the C-Terminus of Cardiac Troponin T: Effects of Familial Hypertrophic Cardiomyopathy Mutations cTnI R145G and cTnT R278C, Alone and in Combination, on Filament Sliding. *Archives Biochem. Biophysics* 552-553, 11–20. doi:10.1016/j.abb.2013.12.021

Burkart, E. M., Sumandea, M. P., Kobayashi, T., Nili, M., Martin, A. F., Homsher, E., et al. (2003). Phosphorylation or Glutamic Acid Substitution at Protein Kinase C Sites on Cardiac Troponin I Differentially Depress Myofilament Tension and Shortening Velocity. *J. Biol. Chem.* 278, 11265–11272. doi:10.1074/jbc.m210712200

Cao, T., Sujkowski, A., Cobb, T., Wessells, R. J., and Jin, J.-P. (2020). The Glutamic Acid-Rich-Long C-Terminal Extension of Troponin T Has a Critical Role in Insect Muscle Functions. *J. Biol. Chem.* 295, 3794–3807. doi:10.1074/jbc.ra119.012014

Chalovich, J. M. (2012). Disease Causing Mutations of Troponin Alter Regulated Actin State Distributions. *J. Muscle Res. Cell Motil.* 33, 493–499. doi:10.1007/s10974-012-9305-x

Chalovich, J. M., and Eisenberg, E. (1982). Inhibition of Actomyosin ATPase Activity by Troponin-Tropomyosin without Blocking the Binding of Myosin to Actin. *J. Biol. Chem.* 257, 2432–2437. doi:10.1016/s0021-9258(18)34942-1

Chalovich, J. M., Greene, L. E., and Eisenberg, E. (1983). Crosslinked Myosin Subfragment 1: a Stable Analogue of the subfragment-1.ATP Complex. *Proc. Natl. Acad. Sci. U.S.A.* 80, 4909–4913. doi:10.1073/pnas.80.16.4909

Cheng, Y., and Regnier, M. (2016). Cardiac Troponin Structure-Function and the Influence of Hypertrophic Cardiomyopathy Associated Mutations on Modulation of Contractility. *Archives Biochem. Biophysics* 601, 11–21. doi:10.1016/j.abb.2016.02.004

El-Saleh, S. C., and Potter, J. D. (1985). Calcium-insensitive Binding of Heavy Meromyosin to Regulated Actin at Physiological Ionic Strength. *J. Biol. Chem.* 260, 14775–14779. doi:10.1016/s0021-9258(17)38640-4

Franklin, A. J., Baxley, T., Kobayashi, T., and Chalovich, J. M. (2012). The C-Terminus of Troponin T Is Essential for Maintaining the Inactive State of Regulated Actin. *Biophysical J.* 102, 2536–2544. doi:10.1016/j.bpj.2012.04.037

Gafurov, B., and Chalovich, J. M. (2007). Equilibrium Distribution of Skeletal Actin-Tropomyosin-Troponin States, Determined by Pyrene-Tropomyosin Fluorescence. *FEBS J.* 274, 2287–2299. doi:10.1111/j.1742-4658.2007.05765.x

Gafurov, B., Chen, Y.-D., and Chalovich, J. M. (2004a). Ca^{2+} and Ionic Strength Dependencies of S1-ADP Binding to Actin-Tropomyosin-Troponin: Regulatory Implications. *Biophysical J.* 87, 1825–1835. doi:10.1529/biophysj.104.043364

Gafurov, B., Fredricksen, S., Cai, A., Brenner, B., Chase, P. B., and Chalovich, J. M. (2004b). The Δ14 Mutation of Human Cardiac Troponin T Enhances ATPase Activity and Alters the Cooperative Binding of S1-ADP to Regulated Actin. *Biochemistry* 43, 15276–15285. doi:10.1021/bi048646h

Geeves, M. A., Lehrer, S. S., and Lehman, W. (2019). The Mechanism of Thin Filament Regulation: Models in Conflict? *J. Gen. Physiol.* 151, 1265–1271. doi:10.1085/jgp.201912446

Greene, L. E., and Eisenberg, E. (1980). Cooperative Binding of Myosin Subfragment-1 to the Actin-Troponin-Tropomyosin Complex. *Proc. Natl. Acad. Sci. U.S.A.* 77, 2616–2620. doi:10.1073/pnas.77.5.2616

Harris, S. P., Rostkova, E., Gautel, M., and Moss, R. L. (2004). Binding of Myosin Binding Protein-C to Myosin Subfragment S2 Affects Contractility Independent of a Tether Mechanism. *Circulation Res.* 95, 930–936. doi:10.1161/01.res.0000147312.02673.56

Haselgrove, J. C. (1972). X-ray Evidence for a Conformational Change in the Actin Containing Filaments of Vertebrate Striated Muscle. *Cold Spring Harb. Symp. Quant. Biol.* 37, 341–352.

Heeley, D. H., Belknap, B., and White, H. D. (2006). Maximal Activation of Skeletal Muscle Thin Filaments Requires Both Rigor Myosin S1 and Calcium. *J. Biol. Chem.* 281, 668–676. doi:10.1074/jbc.m505549200

Heeley, D. H., White, H. D., and Taylor, E. W. (2019). Investigation into the Mechanism of Thin Filament Regulation by Transient Kinetics and Equilibrium Binding: Is There a Conflict? *J. Gen. Physiol.* 151, 628–634. doi:10.1085/jgp.201812198

Herzberg, O., and James, M. N. G. (1985). Structure of the Calcium Regulatory Muscle Protein Troponin-C at 2.8 Å Resolution. *Nature* 313, 653–659. doi:10.1038/313653a0

Hill, T. L., Eisenberg, E., and Chalovich, J. M. (1981). Theoretical Models for Cooperative Steady-State ATPase Activity of Myosin Subfragment-1 on Regulated Actin. *Biophysical J.* 35, 99–112. doi:10.1016/s0006-3495(81)84777-7

Hill, T. L., Eisenberg, E., and Greene, L. (1980). Theoretical Model for the Cooperative Equilibrium Binding of Myosin Subfragment 1 to the Actin-Troponin-Tropomyosin Complex. *Proc. Natl. Acad. Sci. U.S.A.* 77, 3186–3190. doi:10.1073/pnas.77.6.3186

Huxley, H. E. (1972). Structural Changes in the Actin and Myosin Containing Filaments during Contraction. *Cold Spring Harb. Symp. Quant. Biol.* 37, 361–376.

Ishii, Y., and Lehrer, S. S. (1993). Kinetics of the "On-Off" Change in Regulatory State of the Muscle Thin Filament. *Archives Biochem. Biophysics* 305, 193–196. doi:10.1006/abbi.1993.1410

Jin, J.-P., and Chong, S. M. (2010). Localization of the Two Tropomyosin-Binding Sites of Troponin T. *Archives Biochem. Biophysics* 500, 144–150. doi:10.1016/j.abb.2010.06.001

Jin, J.-P. (2016). Evolution, Regulation, and Function of N-Terminal Variable Region of Troponin T: Modulation of Muscle Contractility and beyond. *Int. Rev. Cell Mol. Biol.* 321, 1–28. doi:10.1016/bs.ircmb.2015.09.002

Jin, J.-P., Zhang, Z., and Bautista, J. A. (2008). Isoform Diversity, Regulation, and Functional Adaptation of Troponin and Calponin. *Crit. Rev. Eukar Gene Expr.* 18, 93–124. doi:10.1615/critreveukargeneexpr.v18.i2.10

Johnson, D., Angus, C. W., and Chalovich, J. M. (2018). Stepwise C-Terminal Truncation of Cardiac Troponin T Alters Function at Low and Saturating Ca^{2+}. *Biophysical J.* 115, 702–712. doi:10.1016/j.bpj.2018.06.028

Johnson, D., Landim-Vieira, M., Solı´s, C., Zhu, L., Robinson, J. M., Pinto, J. R., et al. (2020). Eliminating the First Inactive State and Stabilizing the Active State of the Cardiac Regulatory System Alters Behavior in Solution and in Ordered Systems. *Biochemistry* 59, 3487–3497. doi:10.1021/acs.biochem.0c00430

Johnson, D., Mathur, M. C., Kobayashi, T., and Chalovich, J. M. (2016). The Cardiomyopathy Mutation, R146G Troponin I, Stabilizes the Intermediate "C" State of Regulated Actin under High- and Low-free Ca^{2+} Conditions. *Biochemistry* 55, 4533–4540. doi:10.1021/acs.biochem.5b01359

Johnson, D., Zhu, L., Landim-Vieira, M., Pinto, J. R., and Chalovich, J. M. (2019). Basic Residues within the Cardiac Troponin T C Terminus Are Required for Full Inhibition of Muscle Contraction and Limit Activation by Calcium. *J. Biol. Chem.* 294, 19535–19545. doi:10.1074/jbc.ra119.010966

Johnston, J. R., Landim-Vieira, M., Marques, M. A., de Oliveira, G. A. P., Gonzalez-Martinez, D., Moraes, A. H., et al. (2019). The Intrinsically Disordered C Terminus of Troponin T Binds to Troponin C to Modulate Myocardial Force Generation. *J. Biol. Chem.* 294, 20054–20069. doi:10.1074/jbc.ra119.011177

Kimura, A., Harada, H., Park, J.-E., Nishi, H., Satoh, M., Takahashi, M., et al. (1997). Mutations in the Cardiac Troponin I Gene Associated with Hypertrophic Cardiomyopathy. *Nat. Genet.* 16, 379–382. doi:10.1038/ng0897-379

Kobayashi, T., and Solaro, R. J. (2005). Calcium, Thin Filaments, and the Integrative Biology of Cardiac Contractility. *Annu. Rev. Physiol.* 67, 39–67. doi:10.1146/annurev.physiol.67.040403.114025

Kraft, T., Chalovich, J. M., Yu, L. C., and Brenner, B. (1995). Parallel Inhibition of Active Force and Relaxed Fiber Stiffness by Caldesmon Fragments at Physiological Ionic Strength and Temperature Conditions: Additional Evidence that Weak Cross-Bridge Binding to Actin Is an Essential Intermediate for Force Generation. *Biophysical J.* 68, 2404–2418. doi:10.1016/s0006-3495(95)80423-6

Landstrom, A. P., Parvatiyar, M. S., Pinto, J. R., Marquardt, M. L., Bos, J. M., Tester, D. J., et al. (2008). Molecular and Functional Characterization of Novel Hypertrophic Cardiomyopathy Susceptibility Mutations in TNNC1-Encoded Troponin C. *J. Mol. Cell. Cardiol.* 45, 281–288. doi:10.1016/j.yjmcc.2008.05.003

Lang, R., Gomes, A. V., Zhao, J., Miller, T., Potter, J. D., and Housmans, P. R. (2002). Functional Analysis of a Troponin I (R145G) Mutation Associated with Familial Hypertrophic Cardiomyopathy. *J. Biol. Chem.* 277, 11670–11678. doi:10.1074/jbc.m108912200

Lehrer, S. S., and Geeves, M. A. (2014). The Myosin-Activated Thin Filament Regulatory State, M^{-}Oopen: a Link to Hypertrophic Cardiomyopathy (HCM). *J. Muscle Res. Cell Motil.* 35, 153–160. doi:10.1007/s10974-014-9383-z

Lopez Davila, A. J., Zhu, L., Fritz, L., Kraft, T., and Chalovich, J. M. (2020). The Positively Charged C-Terminal Region of Human Skeletal Troponin T Retards

Activation and Decreases Calcium Sensitivity. *Biochemistry* 59, 4189–4201. doi:10.1021/acs.biochem.0c00499

Marston, S., and Zamora, J. E. (2020). Troponin Structure and Function: a View of Recent Progress. *J. Muscle Res. Cell Motil.* 41, 71–89. doi:10.1007/s10974-019-09513-1

Mathur, M. C., Kobayashi, T., and Chalovich, J. M. (2008). Negative Charges at Protein Kinase C Sites of Troponin I Stabilize the Inactive State of Actin. *Biophysical J.* 94, 542–549. doi:10.1529/biophysj.107.113944

Mathur, M. C., Kobayashi, T., and Chalovich, J. M. (2009). Some Cardiomyopathy-Causing Troponin I Mutations Stabilize a Functional Intermediate Actin State. *Biophysical J.* 96, 2237–2244. doi:10.1016/j.bpj.2008.12.3909

McKillop, D. F., and Geeves, M. A. (1993). Regulation of the Interaction between Actin and Myosin Subfragment 1: Evidence for Three States of the Thin Filament. *Biophysical J.* 65, 693–701. doi:10.1016/s0006-3495(93)81110-x

Meeusen, R. L., and Cande, W. Z. (1979). N-ethylmaleimide-modified Heavy Meromyosin. A Probe for Actomyosin Interactions. *J. Cell Biol.* 82, 57–65. doi:10.1083/jcb.82.1.57

Messer, A. E., Bayliss, C. R., El-Mezgueldi, M., Redwood, C. S., Ward, D. G., Leung, M.-C., et al. (2016). Mutations in Troponin T Associated with Hypertrophic Cardiomyopathy Increase Ca^{2+}-Sensitivity and Suppress the Modulation of Ca^{2+}-Sensitivity by Troponin I Phosphorylation. *Archives Biochem. Biophysics* 601, 113–120. doi:10.1016/j.abb.2016.03.027

Morimoto, S., Nakaura, H., Yanaga, F., and Ohtsuki, I. (1999). Functional Consequences of a Carboxyl Terminal Missense Mutation Arg278Cys in Human Cardiac Troponin T. *Biochem. Biophysical Res. Commun.* 261, 79–82. doi:10.1006/bbrc.1999.1000

Morris, E. P., and Lehrer, S. S. (1984). Troponin-tropomyosin Interactions. Fluorescence Studies of the Binding of Troponin, Troponin T and Chymotryptic Troponin T Fragments to Specifically Labeled Tropomyosin. *Biochemistry* 23, 2214–2220. doi:10.1021/bi00305a018

Nakaura, H., Morimoto, S., Yanaga, F., Nakata, M., Nishi, H., Imaizumi, T., et al. (1999). Functional Changes in Troponin T by a Splice Donor Site Mutation that Causes Hypertrophic Cardiomyopathy. *Am. J. Physiology-Cell Physiology* 277, C225–C232. doi:10.1152/ajpcell.1999.277.2.c225

Noland, T. A., JR., Raynor, R. L., and Kuo, J. F. (1989). Identification of Sites Phosphorylated in Bovine Cardiac Troponin I and Troponin T by Protein Kinase C and Comparative Substrate Activity of Synthetic Peptides Containing the Phosphorylation Sites. *J. Biol. Chem.* 264, 20778–20785. doi:10.1016/s0021-9258(19)47130-5

Parry, D. A. D., and Squire, J. M. (1973). Structural Role of Tropomyosin in Muscle Regulation: Analysis of the X-Ray Diffraction Patterns from Relaxed and Contracting Muscles. *J. Mol. Biol.* 75, 33–55. doi:10.1016/0022-2836(73)90527-5

Pearlstone, J. R., and Smillie, L. B. (1981). Identification of a Second Binding Region on Rabbit Skeletal Troponin-T for α-tropomyosin. *FEBS Lett.* 128, 119–122. doi:10.1016/0014-5793(81)81095-2

Pemrick, S., and Weber, A. (1976). Mechanism of Inhibition of Relaxation by N-Ethylmaleimide Treatment of Myosin. *Biochemistry* 15, 5193–5198. doi:10.1021/bi00668a038

Pirani, A., Xu, C., Hatch, V., Craig, R., Tobacman, L. S., and Lehman, W. (2005). Single Particle Analysis of Relaxed and Activated Muscle Thin Filaments. *J. Mol. Biol.* 346, 761–772. doi:10.1016/j.jmb.2004.12.013

Poole, K. J. V., Lorenz, M., Evans, G., Rosenbaum, G., Pirani, A., Craig, R., et al. (2006). A Comparison of Muscle Thin Filament Models Obtained from Electron Microscopy Reconstructions and Low-Angle X-Ray Fibre Diagrams from Non-overlap Muscle. *J. Struct. Biol.* 155, 273–284. doi:10.1016/j.jsb.2006.02.020

Ramos, C. H. I. (1999). Mapping Subdomains in the C-Terminal Region of Troponin I Involved in its Binding to Troponin C and to Thin Filament. *J. Biol. Chem.* 274, 18189–18195. doi:10.1074/jbc.274.26.18189

Rao, V. S., Marongelli, E. N., and Guilford, W. H. (2009). Phosphorylation of Tropomyosin Extends Cooperative Binding of Myosin beyond a Single Regulatory Unit. *Cell Motil. Cytoskelet.* 66, 10–23. doi:10.1002/cm.20321

Risi, C., Eisner, J., Belknap, B., Heeley, D. H., White, H. D., Schröder, G. F., et al. (2017). Ca^{2+}-induced Movement of Tropomyosin on Native Cardiac Thin Filaments Revealed by Cryoelectron Microscopy. *Proc. Natl. Acad. Sci. U.S.A.* 114, 6782–6787. doi:10.1073/pnas.1700868114

Robinson, P., Griffiths, P. J., Watkins, H., and Redwood, C. S. (2007). Dilated and Hypertrophic Cardiomyopathy Mutations in Troponin and α-Tropomyosin Have Opposing Effects on the Calcium Affinity of Cardiac Thin Filaments. *Circulation Res.* 101, 1266–1273. doi:10.1161/circresaha.107.156380

Robinson, P., Mirza, M., Knott, A., Abdulrazzak, H., Willott, R., Marston, S., et al. (2002). Alterations in Thin Filament Regulation Induced by a Human Cardiac Troponin T Mutant that Causes Dilated Cardiomyopathy Are Distinct from Those Induced by Troponin T Mutants that Cause Hypertrophic Cardiomyopathy. *J. Biol. Chem.* 277, 40710–40716. doi:10.1074/jbc.m203446200

Root, D. D., and Wang, K. (2001). High-affinity Actin-Binding Nebulin Fragments Influence the actoS1 Complex. *Biochemistry* 40, 1171–1186. doi:10.1021/bi0015010

Shitaka, Y., Kimura, C., Iio, T., and Miki, M. (2004). Kinetics of the Structural Transition of Muscle Thin Filaments Observed by Fluorescence Resonance Energy Transfer. *Biochemistry* 43, 10739–10747. doi:10.1021/bi0492713

Shitaka, Y., Kimura, C., and Miki, M. (2005). The Rates of Switching Movement of Troponin T between Three States of Skeletal Muscle Thin Filaments Determined by Fluorescence Resonance Energy Transfer. *J. Biol. Chem.* 280, 2613–2619. doi:10.1074/jbc.m408553200

Stelzer, J. E., Patel, J. R., Olsson, M. C., Fitzsimons, D. P., Leinwand, L. A., and Moss, R. L. (2004). Expression of Cardiac Troponin T with COOH-Terminal Truncation Accelerates Cross-Bridge Interaction Kinetics in Mouse Myocardium. *Am. J. Physiology-Heart Circulatory Physiology* 287, H1756–H1761. doi:10.1152/ajpheart.00172.2004

Sweeney, H. L., and Stull, J. T. (1990). Alteration of Cross-Bridge Kinetics by Myosin Light Chain Phosphorylation in Rabbit Skeletal Muscle: Implications for Regulation of Actin-Myosin Interaction. *Proc. Natl. Acad. Sci. U.S.A.* 87, 414–418. doi:10.1073/pnas.87.1.414

Szczesna, D., Zhang, R., Zhao, J., Jones, M., Guzman, G., and Potter, J. D. (2000). Altered Regulation of Cardiac Muscle Contraction by Troponin T Mutations that Cause Familial Hypertrophic Cardiomyopathy. *J. Biol. Chem.* 275, 624–630. doi:10.1074/jbc.275.1.624

Takeda, S., Yamashita, A., Maeda, K., and Maéda, Y. (2003). Structure of the Core Domain of Human Cardiac Troponin in the Ca^{2+}-Saturated Form. *Nature* 424, 35–41. doi:10.1038/nature01780

Tanokura, M., Tawada, Y., Ono, A., and Ohtsuki, I. (1983). Chymotryptic Subfragments of Troponin T from Rabbit Skeletal Muscle. Interaction with Tropomyosin, Troponin I and Troponin C1. *J. Biochem.* 93, 331–337. doi:10.1093/oxfordjournals.jbchem.a134185

Tao, T., Gong, B.-J., and Leavis, P. C. (1990). Calcium-induced Movement of Troponin-I Relative to Actin in Skeletal Muscle Thin Filaments. *Science* 247, 1339–1341. doi:10.1126/science.2138356

Thierfelder, L., Watkins, H., Macrae, C., Lamas, R., Mckenna, W., Vosberg, H.-P., et al. (1994). α-Tropomyosin and Cardiac Troponin T Mutations Cause Familial Hypertrophic Cardiomyopathy: A Disease of the Sarcomere. *Cell* 77, 701–712. doi:10.1016/0092-8674(94)90054-x

Tobacman, L. S. (2021). Troponin Revealed: Uncovering the Structure of the Thin Filament On-Off Switch in Striated Muscle. *Biophysical J.* 120, 1–9. doi:10.1016/j.bpj.2020.11.014

Tripet, B., van Eyk, J. E., and Hodges, R. S. (1997). Mapping of a Second Actin-Tropomyosin and a Second Troponin C Binding Site within the C Terminus of Troponin I, and Their Importance in the Ca^{2+}-dependent Regulation of Muscle Contraction. *J. Mol. Biol.* 271, 728–750. doi:10.1006/jmbi.1997.1200

Trybus, K. M., and Taylor, E. W. (1980). Kinetic Studies of the Cooperative Binding of Subfragment 1 to Regulated Actin. *Proc. Natl. Acad. Sci. U.S.A.* 77, 7209–7213. doi:10.1073/pnas.77.12.7209

Van Eyk, J. E., and Hodges, R. S. (1988). The Biological Importance of Each Amino Acid Residue of the Troponin I Inhibitory Sequence 104-115 in the Interaction with Troponin C and Tropomyosin-Actin. *J. Biol. Chem.* 263, 1726–1732. doi:10.1016/s0021-9258(19)77936-8

Varughese, J. F., Baxley, T., Chalovich, J. M., and Li, Y. (2011). A Computational and Experimental Approach to Investigate Bepridil Binding with Cardiac Troponin. *J. Phys. Chem. B* 115, 2392–2400. doi:10.1021/jp1094504

Venkatraman, G., Harada, K., Gomes, A. V., Kerrick, W. G. L., and Potter, J. D. (2003). Different Functional Properties of Troponin T Mutants that Cause Dilated Cardiomyopathy. *J. Biol. Chem.* 278, 41670–41676. doi:10.1074/jbc.m302148200

Wakabayashi, T., Huxley, H. E., Amos, L. A., and Klug, A. (1975). Three-dimensional Image Reconstruction of Actin-Tropomyosin Complex and Actin-Tropomyosin-Troponin T-Troponin I Complex. *J. Mol. Biol.* 93, 477–497. doi:10.1016/0022-2836(75)90241-7

Williams, D. L., Greene, L. E., and Eisenberg, E. (1988). Cooperative Turning on of Myosin Subfragment 1 Adenosine Triphosphatase Activity by the Troponin-Tropomyosin-Actin Complex. *Biochemistry* 27, 6987–6993. doi:10.1021/bi00418a048

Wong, S., Feng, H.-Z., and Jin, J.-P. (2019). The Evolutionarily Conserved C-Terminal Peptide of Troponin I Is an Independently Configured Regulatory Structure to Function as a Myofilament Ca^{2+}-Desensitizer. *J. Mol. Cell. Cardiol.* 136, 42–52. doi:10.1016/j.yjmcc.2019.09.002

Yamada, Y., Namba, K., and Fujii, T. (2020). Cardiac Muscle Thin Filament Structures Reveal Calcium Regulatory Mechanism. *Nat. Commun.* 11, 153. doi:10.1038/s41467-019-14008-1

Zhu, L., Johnson, D., and Chalovich, J. M. (2022). The C-Terminal Basic Region of Troponin T Alters the Ca^{2+}-dependent Changes in Troponin I Interactions. *Biochemistry* [Epub ahead of print]. doi:10.1021/acs.biochem.2c00090

Conflict of Interest: The authors declare that the research was conducted in the absence of any commercial or financial relationships that could be construed as a potential conflict of interest.

Publisher's Note: All claims expressed in this article are solely those of the authors and do not necessarily represent those of their affiliated organizations, or those of the publisher, the editors and the reviewers. Any product that may be evaluated in this article, or claim that may be made by its manufacturer, is not guaranteed or endorsed by the publisher.

frontiers | Frontiers in Physiology

ORIGINAL RESEARCH
published: 08 June 2022
doi: 10.3389/fphys.2022.892979

Small Molecule RPI-194 Stabilizes Activated Troponin to Increase the Calcium Sensitivity of Striated Muscle Contraction

Zabed Mahmud[1], Svetlana Tikunova[2], Natalya Belevych[3], Cory S. Wagg[4], Pavel Zhabyeyev[5], Philip B. Liu[5], David V. Rasicci[6], Christopher M. Yengo[6], Gavin Y. Oudit[5], Gary D. Lopaschuk[4], Peter J. Reiser[3], Jonathan P. Davis[2]* and Peter M. Hwang[1,5]**

[1]Department of Biochemistry, University of Alberta, Edmonton, AB, Canada, [2]Department of Physiology and Cell Biology, The Ohio State University, Columbus, OH, United States, [3]Division of Biosciences, College of Dentistry, The Ohio State University, Columbus, OH, United States, [4]Department of Pediatrics, University of Alberta, Edmonton, AB, Canada, [5]Department of Medicine, University of Alberta, Edmonton, AB, Canada, [6]Department of Cellular and Molecular Physiology, College of Medicine, Pennsylvania State University, University Park, PA, United States

OPEN ACCESS

Edited by:
Shin'Ichi Ishiwata,
Waseda University, Japan

Reviewed by:
Thomas Charles Irving,
Illinois Institute of Technology, United States
P. Bryant Chase,
Florida State University, United States

***Correspondence:**
Peter M. Hwang
phwang1@ualberta.ca
Peter J. Reiser
reiser.17@osu.edu
Jonathan P. Davis
davis.812@osu.edu

Specialty section:
This article was submitted to Striated Muscle Physiology, a section of the journal Frontiers in Physiology

Received: 09 March 2022
Accepted: 10 May 2022
Published: 08 June 2022

Citation:
Mahmud Z, Tikunova S, Belevych N, Wagg CS, Zhabyeyev P, Liu PB, Rasicci DV, Yengo CM, Oudit GY, Lopaschuk GD, Reiser PJ, Davis JP and Hwang PM (2022) Small Molecule RPI-194 Stabilizes Activated Troponin to Increase the Calcium Sensitivity of Striated Muscle Contraction. Front. Physiol. 13:892979. doi: 10.3389/fphys.2022.892979

Small molecule cardiac troponin activators could potentially enhance cardiac muscle contraction in the treatment of systolic heart failure. We designed a small molecule, RPI-194, to bind cardiac/slow skeletal muscle troponin (Cardiac muscle and slow skeletal muscle share a common isoform of the troponin C subunit.) Using solution NMR and stopped flow fluorescence spectroscopy, we determined that RPI-194 binds to cardiac troponin with a dissociation constant K_D of 6–24 μM, stabilizing the activated complex between troponin C and the switch region of troponin I. The interaction between RPI-194 and troponin C is weak (K_D 311 μM) in the absence of the switch region. RPI-194 acts as a calcium sensitizer, shifting the pCa_{50} of isometric contraction from 6.28 to 6.99 in mouse slow skeletal muscle fibers and from 5.68 to 5.96 in skinned cardiac trabeculae at 100 μM concentration. There is also some cross-reactivity with fast skeletal muscle fibers (pCa_{50} increases from 6.27 to 6.52). In the slack test performed on the same skinned skeletal muscle fibers, RPI-194 slowed the velocity of unloaded shortening at saturating calcium concentrations, suggesting that it slows the rate of actin-myosin cross-bridge cycling under these conditions. However, RPI-194 had no effect on the ATPase activity of purified actin-myosin. In isolated unloaded mouse cardiomyocytes, RPI-194 markedly decreased the velocity and amplitude of contractions. In contrast, cardiac function was preserved in mouse isolated perfused working hearts. In summary, the novel troponin activator RPI-194 acts as a calcium sensitizer in all striated muscle types. Surprisingly, it also slows the velocity of unloaded contraction, but the cause and significance of this is uncertain at this time. RPI-194 represents a new class of non-specific troponin activator that could potentially be used either to enhance cardiac muscle contractility in the setting of systolic heart failure or to enhance skeletal muscle contraction in neuromuscular disorders.

Keywords: cardiac troponin activator, calcium sensitizer, inotrope, systolic heart failure, striated muscle, thin filament

INTRODUCTION

Heart failure is a common disease condition in which the heart is unable to pump enough blood to satisfy the metabolic demands of the body. Systolic heart failure, also known as heart failure with reduced ejection fraction (HFrEF), occurs when inadequate contraction results in an ejection fraction of less than 40% (Murphy et al., 2020). Over time, the heart becomes increasingly thinned and dilated, which further exacerbates muscle wall tension to impair contraction. Atherosclerotic ischemic heart disease is the most common etiology causing HFrEF (Curtis et al., 2003). In decompensated heart failure, blood pressure is often low, the perfusion of vital organs is barely adequate, and fluid accumulates throughout the body due to maladaptive sodium retention by the kidneys. The most well-established drug therapies in heart failure are diuretics to reverse volume overload and blood pressure medications that attenuate long term pathologic remodeling of the heart. What is missing from the therapeutic arsenal is an effective positive inotrope, a drug that increases the contractility of the heart, because to date no existing positive inotrope has been shown to improve survival.

The oldest therapy for heart failure, digoxin, inhibits cellular Na, K-ATPase function and increases cardiac muscle contraction through an increase in cytoplasmic calcium concentration. Digoxin therapy improves symptoms and reduces hospitalization rates for heart failure (Bourge et al., 2013), but a narrow therapeutic index has limited its use so that it is no longer a recommended therapy. The most commonly used positive inotropes in the intensive care unit, β_1-agonists like dobutamine and downstream type 3/4-phosphodiesterase (PDE3/PDE4) inhibitors like milrinone increase cardiac output, but they also confer a risk of tachyarrhythmias and promote peripheral vasodilation and hypotension. Due to adverse side effects, these agents do not provide a survival benefit in chronic or acute decompensated heart failure (Tacon et al., 2012).

In theory, directly targeting the sarcomeric proteins that generate cardiac muscle contraction could enhance cardiac output with fewer side effects (Kitada et al., 1989; Wolska et al., 1996; Brixius et al., 2000; Li et al., 2000; Tikunova et al., 2010; Hwang and Sykes, 2015; Shettigar et al., 2016). Omecamtiv mecarbil is a compound that binds to cardiac myosin to stabilize its pre-powerstroke conformation (Planelles-Herrero et al., 2017). This increases the number of strong actin-myosin cross-bridges, enhancing cooperative activation of the cardiac thin filament. Though omecamtiv enhances actin-myosin interactions, it was also found to suppress the myosin working stroke (Woody et al., 2018) and to decrease actin sliding velocity in *in vitro* motility assay (Swenson et al., 2017), giving it a mixed activation/inhibition mechanism of action. Omecamtiv mecarbil prolongs the systolic phase of the cardiac cycle and increases the ejection fraction of the left ventricle, though it does not enhance the speed or force of contraction (Malik et al., 2011). Phase III clinical trials of omecamtiv mecarbil have not shown a statistically significant survival benefit in chronic (Teerlink et al., 2021) or acute decompensated heart failure (Teerlink et al., 2016).

It may be more advantageous to enhance activation of the thin filament without modulating the force-generating ATPase cycle of myosin (Shettigar et al., 2016). Thin filaments in cardiac sarcomeres are activated by cardiac troponin (cTn) (Li et al., 2004; Metzger and Westfall, 2004; Shettigar et al., 2016), which consists of three protein subunits: calcium-binding cTnC, actin binding inhibitory cTnI, and tropomyosin binding cTnT (Ebashi and Ebashi, 1964; Ebashi et al., 1967; Greaser and Gergely, 1973). X-ray crystallography (Takeda et al., 2003) and NMR (Sia et al., 1997) studies revealed that the cTnC subunit is a dumbbell-shaped protein with two globular domains, the N-terminal regulatory domain (cNTnC) and the C-terminal structural domain (cCTnC). The cNTnC domain has two EF-hand motifs, EF-I and EF-II, but only EF-II is active and binds calcium with micromolar affinity, attuned to sense the increase in free cytoplasmic calcium concentration during systole (the contractile phase of the cardiac cycle). Calcium ions come on and off cNTnC very rapidly (rate of exchange, $k_{ex} > 5{,}000\ s^{-1}$) (Li et al., 2002), with the calcium-bound state experiencing a rapid equilibrium between closed and partially open conformations (Sia et al., 1997; Spyracopoulos et al., 1997). Binding of the switch region of cTnI ($cTnI_{148\text{-}158}$) to cNTnC stabilizes its calcium-bound open state, substantially slowing calcium dissociation (Li et al., 2002; Siddiqui et al., 2016). Cryo-EM structures of cTn (Oda et al., 2020; Yamada et al., 2020) showed that residues 135–209 of cTnI bind to actin to maintain the thin filament in a blocked state, but binding of cNTnC to $cTnI_{148\text{-}158}$ relieves the inhibition of the thin filament, shifting tropomyosin from its blocked position and facilitating strong actin-myosin interaction.

Troponin exists in three different isoforms found in fast skeletal, slow skeletal, and cardiac muscle. For troponin I and troponin T, there are three different isoforms which are specific for each muscle type, but cardiac muscle and slow skeletal muscle share the same isoform of for troponin C (*i.e.*, cTnC = ssTnC) (Li and Hwang, 2015). The fast skeletal isoform of TnC (fsTnC) has been specifically targeted by the drugs tirasemtiv and reldesemtiv, which completed clinical trials for the treatment of amyotrophic lateral sclerosis, though benefit was limited (Shefner et al., 2019; Shefner et al., 2021). Reldesemtiv is currently undergoing clinical trials for the treatment of spinal muscular atrophy (Rudnicki et al., 2021). These fsTnC-targeting drugs bind to a hydrophobic cavity in fsTnC that lies beneath the binding site for the fsTnI switch region (Li et al., 2021). In theory, it should be possible to develop a compound that targets the homologous binding cavity in cTnC/ssTnC, though it would likely be active for both cardiac and slow skeletal muscle. Cytokinetics has developed a cardio-selective troponin activator, CK-136, formerly known as AMG 594, which appears to be selective for cardiac muscle, though a structure of its binding site on cardiac troponin is not yet available (He et al., 2021).

Previous attempts to design positive inotropes appeared to target cardiac troponin but in fact resulted in compounds that also bind to other targets in cardiomyocytes. Such compounds include levosimendan, pimobendan, MCI-154, and EMD 57033. Of these, levosimendan (Orstavik et al., 2015), pimobendan (Bohm et al., 1991), and MCI-154 (Bethke et al., 1993; Li et al., 2018) were found to have potent PDE3-inhibitory

activity, whereas EMD 57033 was found to interact with cardiac myosin (Brixius et al., 2000). These compounds have lower affinity for cTnC than for these other proteins.

We, therefore, designed and screened compounds for binding to the cTn complex using a unique cNTnC-cTnI chimeric construct, which we named "gChimera" (Cai et al., 2018). We synthesized a novel small molecule cardiac troponin modulator, RPI-194, and measured its binding to both gChimera and to the isolated cNTnC domain, as well as its activity in skinned cardiac muscle trabeculae, individual cardiomyocytes, and isolated perfused working mouse hearts. Since cardiac muscle shares the same TnC isoform as slow skeletal muscle, we have also examined its activity in skinned skeletal muscle fibers. Slow skeletal muscle has a distinct isoform of troponin I [ssTnI], but the switch region of ssTnI that binds cNTnC is very similar to the corresponding region in cTnI. Our goal was to develop a compound that can be used as a positive inotropic agent in the treatment of systolic heart failure, but it turns out that our compound interacts with troponin from all striated muscle types.

MATERIALS AND METHODS

Preparation of Proteins for NMR Studies

Three human protein constructs were used in the NMR study: 1) recombinant human aCys-cNTnC (C35S, C84S double mutant), 2) chimeric construct (gChimera) of the cNTnC-cTnI switch peptide complex, aCys-cNTnC$_{1\text{-}85}$—SSGGSSGGSSGG linker - cTnI$_{145\text{-}167}$ and 3) slow skeletal troponin I switch peptide (ssTnI). The protocol used to express and purify both cNTnC and gChimera in *Escherichia coli* was previously described (Cai et al., 2016). The ssTnI peptide was synthesized and purified by GL Biochem Ltd. (Shanghai).

NMR Titration of RPI-194 Against gChimera and cNTnC

RPI-194 was synthesized by Rane Pharmaceuticals, Inc. in Edmonton, Alberta, Canada. Chemical structure was confirmed by NMR. For each NMR titration experiment, recombinant ^{15}N-labeled gChimera or cNTnC was dissolved in 500 µL NMR buffer (90% H_2O/10% D_2O) consisting of 100 mM KCl, 10 mM imidazole, and 0.5 mM 4, 4-dimethyl-4-silapentane-1-sulfonic acid as a chemical shift reference. Purified lyophilized forms of gChimera or cNTnC were dissolved in NMR buffer. Protein quantitation by acid hydrolysis followed by amino acid quantitation showed the lyophilized form was 54% pure protein by weight. The pH of each NMR sample was maintained at a slightly acidic pH ~ 6.7 by adjusting with microliter quantities of either 1 M NaOH or 1 M HCl. An acidic pH is typically employed in NMR to slow down base-catalyzed solvent-amide exchange, improving the signal intensity for rapidly exchanging amide groups in the protein. Since the proteins of interest are not known to have native side chains that become ionized near pH 6.7 (typically histidine), the use of a slightly acidic pH should not impact the electrostatic surface of the protein at all.

RPI-194 compound was dissolved into d_6-DMSO to make a 68 mM stock solution, which was then diluted ten-fold in d_6-DMSO to perform titrations. For both cNTnC and gChimera, the starting concentration was 115 µM. RPI-194 was titrated to 0.1, 0.2, 0.3, 0.4, 0.6, 0.8, 1, 1.5, 2, 2.5, 3, 3.5, 4, 5, 6 and 8 equivalents of cNTnC. For gChimera-RPI-194 titration, RPI-194 was titrated to 0.2, 0.4, 0.6, 0.8, 1, 1.2 and 1.4 equivalents of gChimera. Each titration point was monitored by recording a two dimensional ^{1}H, ^{15}N heteronuclear single quantum coherence (HSQC) spectrum. Dilution factors were applied at each titration point to calculate the final concentration of cNTnC and RPI-194 in the calculation of binding affinities.

NMR Titration of ssTnI Against cNTnC and cNTnC·RPI-194 Complex

Titration of ssTnI was performed against free cNTnC and against cNTnC complexed with RPI-194. A 10 mM stock concentration of ssTnI was made by dissolving it into d_6-DMSO. ssTnI was titrated to 0.5, 1, 1.5, 2, 2.5, 3, 3.5, 4, 5, 6, 8, 10, 13, 16, 20, 25 and 30 equivalents of cNTnC. For titrating ssTnI into cNTnC·RPI-194 complex, RPI-194 was first titrated into free cTnC (115 µM) until both protein and drug were 1:1 equivalent. Then ssTnI was titrated with 0.1, 0.2, 0.4, 0.6, 0.8, 1, 1.5, 2, 2.5, and 3 equivalents of cNTnC·RPI-194 complex (115 µM).

NMR Spectroscopy

All titrations were performed on a Varian Inova 500 MHz NMR spectrometer equipped with triple resonance ^{1}H, ^{13}C, ^{15}N probe. 2D ^{1}H, ^{15}N HSQC spectra were collected for each titration point at 30°C. All titration data were processed using NMRPipe (Delaglio et al., 1995). A MATLAB runtime-based two dimensional lineshape analysis program called TITAN was used to calculate the dissociation constant (K_D) from titration experiments (Waudby et al., 2016). First, the protein and ligand concentration of each titration point were specified in the program. Individual NMR spectra for each titration point were uploaded into TITAN, and a specific region of interest (ROI) was selected for peaks we selected for large chemical shift perturbations. TITAN only considers chemical shift changes within the selected ROI for fitting and calculating dissociation constants. Simplified two-state binding models were used to calculate binding dissociation constants and on/off rate constants.

Determination of Binding Affinities by Steady State Fluorescence

All steady-state fluorescence measurements were obtained on a SpectraMax i3x multi-mode microplate reader at 15°C. RPI-194 has intrinsic fluorescence with peak excitation and emission wavelengths at 335 and 470 nm, respectively. The same cNTnC and gChimera proteins (0–297 µM) used for NMR were titrated into a solution containing 5 µM RPI-194, 50 mM HEPES, 150 mM KCl, 5 mM $MgCl_2$, 1 mM DTT and 10 mM $CaCl_2$, and the intrinsic fluorescence spectrum of RPI-194 was monitored for changes. Binding affinities were calculated using

GraphPad Prism version 9.0.2 (San Diego, California, United States).

Determination of Ca^{2+} Dissociation Rates by Stopped-Flow Fluorescence

Recombinant human cTnC (T53C, C35S, and C84S), cTnI and cTnT were used to reconstitute the cardiac troponin complex for stopped flow fluorescence studies. Expression, purification, production, and labeling of cTnC T53C with 2-(4′-(iodoacetamido) anilino) naphthalene-6-sulfonic acid (IAANS) were previously published (Davis et al., 2007). Expression and purification of recombinant cTnI, cTnT and reconstitution of the cardiac troponin complex (cTnC cTnI·cTnT) were as previously described (Davis et al., 2007).

Calcium release rates of IAANS-labeled, reconstituted cardiac troponin complex as a function of RPI-194 concentration were measured in a stopped-flow spectrometer (Applied Photophysics model SX.18 MV). IAANS excitation and emission were monitored at 330 nm and 420–470 nm, respectively. The calcium release rate was monitored by mixing calcium saturated (500 μM Ca^{2+}) cardiac troponin complex with a stopped flow buffer containing calcium chelating solution (EGTA 10 mM, 10 mM MOPS and 150 mM KCl, pH 7.0) with a dead mixing time ~ 1.24 ms. EGTA (10 mM) was used to sequester calcium from reconstituted cardiac troponin complex (0.3 μM) in the absence or presence of RPI-194. Increasing concentrations of RPI-194 were used in this reaction. P.J. King data analysis software, developed by Applied Photophysics (Leatherhead, Surrey, UK), was used to analyze stopped flow data. It uses a nonlinear Levenberg–Marquardt algorithm for data fitting.

Analysis of Force *Versus* pCa Relationship in Skinned Ventricular Trabeculae and Skeletal Muscle Fibers

Heart, soleus, and tibialis anterior muscles were isolated from each of 8 male Sprague-Dawley rats, ranging in age from 6–9 months. The rats were euthanized (anesthesia induced by isoflurane, followed by rapid cardiectomy) in accordance with a protocol approved by Institutional Animal Care and Use Committee of Ohio State University. The soleus and anterior tibialis muscles were immediately placed in cold relaxing solution, and fiber bundles were prepared and stored in relaxing solution containing 50% glycerol (v/v) at −20°C (Reiser et al., 2013). A single large cut was made through the free wall of both ventricles of the heart, which was then placed in ice-cold relaxing solution with 1% Triton X-100 for 30 min (Tikunova et al., 2019). The heart was removed from this solution, gently compressed, and blotted and transferred to cold glycerinating solution (Reiser et al., 2013).

Single trabeculae were isolated and studied as previously described (Tikunova et al., 2019). Briefly, a trabecula was mounted in the experimental chamber that was controlled at 15°C (Tikunova et al., 2019). In the chamber, one end of the trabecula was attached to a motor and another end was attached to a transducer. The trabecula was set to the resting striation spacing, the equivalent of sarcomere length. Striation spacing was determined using a camera mounted on the microscope and the SPOT image analysis software (https://www.spotimaging.com) (Tikunova et al., 2019). The distance spanned by ~ 20 striations was measured to calculate resting sarcomere length. Fiber width and depth were measured, and fiber cross-sectional area (CSA) was calculated, assuming an ellipsoidal cross section. The average resting sarcomere length of the twenty-four trabeculae that were studied was set to 2.07 ± 0.02 μm. Each trabecula was then subjected to two series, A and B, of activations. Series A was always without RPI-194. Series B was with 0, 20, 50 or 100 μM RPI-194.

The force versus pCa relationship was measured in six trabeculae for each concentration of RPI-194, first without (series A), then with (series B) RPI-194 (100 mM stock dissolved in DMSO) (Tikunova et al., 2019). RPI-194 was added to all of the solutions to which the trabeculae were exposed during the measurements of the force/pCa relationship: pCa 9.0 solution, HDTA pre-activating solution and each of the maximal (pCa 4.0) and submaximal activating solutions. The trabeculae were soaked in pCa 9.0 solution with RPI-194 at 15°C for 30 min before initiating the second series of force measurements. We reported previously that DMSO had no effect on the force/pCa relationship (Reiser et al., 2013). We initially determined, in three skeletal muscle fibers, that the control (no added compound) force/pCa relationship is essentially identical when measured twice in a given preparation. The trabecula was treated with series of pCa solutions as previously described (Reiser et al., 2013). The force versus pCa data were fit as previously described (Black et al., 2000; Tikunova et al., 2002; Tikunova et al., 2019).

The sarcomere length in slow and fast fibers was measured using the Fast Fourier Transform in ImageJ (https://imagej.nih.gov/ij/). The fiber type (slow or fast) of each studied skeletal muscle fiber was determined from an analysis of the myosin heavy chain isoform composition using SDS-PAGE, as described (Tikunova et al., 2018). The maximal velocity of shortening (V_o) was measured, using the slack test (Edman, 1979), in slow and fast fibers when activated in pCa 4.0 solution (every third activation in the force/pCa measurements series). Thus, two V_o determinations were made in each slow and fast fiber, first without, then with, RPI-194 (series A and B).

A total of 24 slow fibers, 24 fast fibers and 24 trabeculae were studied. The group size for each concentration of RPI-194 was six and each preparation was studied at one concentration. An analysis of variance (ANOVA) Tukey's post-hoc test was used when comparing the effects of all four concentrations (0, 20, 50 and 100 μM) of RPI-194 in each preparation (slow fibers, fast fibers or trabeculae) or when comparing effects of a given concentration of RPI-194 in all three preparations (slow fibers, fast fibers and trabeculae). Student's t-test was used to assess the significance of differences in maximal shortening velocity in fast and slow fibers at a given concentration of RPI-194. Pearson's correlation was used to test for a relationship between the shift in pCa_{50} and the change in V_o induced by RPI-194.

Isolation of Mouse Ventricular Myocytes, Contractility Assays and cAMP Measurements

Adult ventricular cardiomyocytes were isolated and perfused as previously described (Sah et al., 2002). Contractility assays from isolated cardiomyocytes were conducted as previously described (Crackower et al., 2002). Briefly, a Grass S44 stimulator with a pulse duration of 3 milliseconds at 1 Hz was used to stimulate cardiomyocytes. Myocyte contraction was tracked at 240 Hz using a video edge detector. In addition, myocyte steady state contractions at 1 Hz and a subsequent equilibrium period for 4 min at 240 Hz were recorded. We determined fractional shortening, shortening rate (+dL/dT) and relaxation rate (dl/dT) in the isolated cardiomyocytes.

Isolated Mouse Working Heart Perfusion and Measurement of Metabolic Rates

All animals used in isolated working heart perfusion experiments were treated in accordance with the guidelines of the Canadian Council of Animal Care and approved by the University of Alberta Health Sciences Animal Welfare Committee. All animal experiments were conducted on male C57BL/6 mice (7–10 weeks) obtained from Charles River Laboratories (Wilmington, MA, United States) and regularly fed with chow diet (Harlan Teklad, Madison, WI, United States). Animals were anesthetized with 60 mg kg^{-1} isoflurane administered through the peritoneum. Isolated working heart perfusions were performed as previously described (Kuang et al., 2004). Rapidly excised hearts were immediately placed on an ice-cold Krebs-Henseleit solution. A recirculating perfusate solution was used for the isolation of working hearts. It consisted of a modified Krebs-Henseleit solution (100 ml) which was a mixture of 1.2 mM KH_2PO_4, 1.2 mM MgSO4, 2.5 mM $CaCl_2$, 4.7 mM KCl, 25 mM $NaHCO_3$ and 118 mM NaCl. The perfusate was supplemented with 1.2 mM palmitate prebound to 3% bovine serum albumin and 5 mM glucose as energy substrates. Glycolysis and glucose oxidation rates were calculated from the perfused heart by adding a small amount of radiolabeled [5-^{3}H] glucose and [U-^{14}C] glucose in the Krebs-Henseleit solution (Kovacic et al., 2003; Kuang et al., 2004). The perfusate was continuously supplied with a gas mixture of 95% O_2, 5% CO_2. Cardiac output, cardiac work, heart rate and peak systolic pressure were also assessed from the perfused hearts.

Impact of RPI-194 on Cardiac Myosin ATPase Activity

The ATPase activity of human beta-cardiac myosin subfragment 1 (amino acids 1–843) containing a C-terminal green fluorescent protein tag (M2β-S1 GFP) was examined using the NADH coupled assay (Swenson et al., 2017; Tang et al., 2019). M2β-S1 GFP was produced using the C2C12 cell expression system and purified as previously described (Swenson et al., 2017; Tang et al., 2019). The ATPase activity was examined in the presence of 40 μM actin and varying RPI-194 concentrations with 1% DMSO present.

RESULTS

RPI-194 Binds Ca^{2+} Saturated cNTnC-cTnI Chimera

During systole, cardiac muscle contraction is triggered by the calcium dependent binding of the cTnI switch region to the regulatory cNTnC. A cardiac troponin activator drug promotes and stabilizes formation of this activated complex. We previously produced multiple variations of the cNTnC-cTnI chimera with different linkers (Pineda-Sanabria et al., 2014; Cai et al., 2016). In the current study we used a further refined version that we call "gChimera", which utilizes a linker containing multiple Ser and Gly residues for maximum flexibility and solubility while maintaining charge neutrality (amino acid sequence shown in **Figure 1A**).

Based on our previous work, 3-chlorodiphenylamine was a promising starting compound to develop a cardiac troponin activator (Cai et al., 2016). Addition of hydrophobic substituents to the aryl rings of 3-chlorodiphenylamine tends to improve binding affinity but greatly reduces solubility, whereas more polar substituents are not well tolerated. We aimed to add at least one hydrophilic group to enhance solubility and specificity of binding. We designed a total of 54 3-chlorodiphenylamine-based compounds that were synthesized by Rane Pharmaceutical Inc., Edmonton, AB, Canada. The compounds were assessed for binding to gChimera by NMR, and we identified a compound, RPI-194,

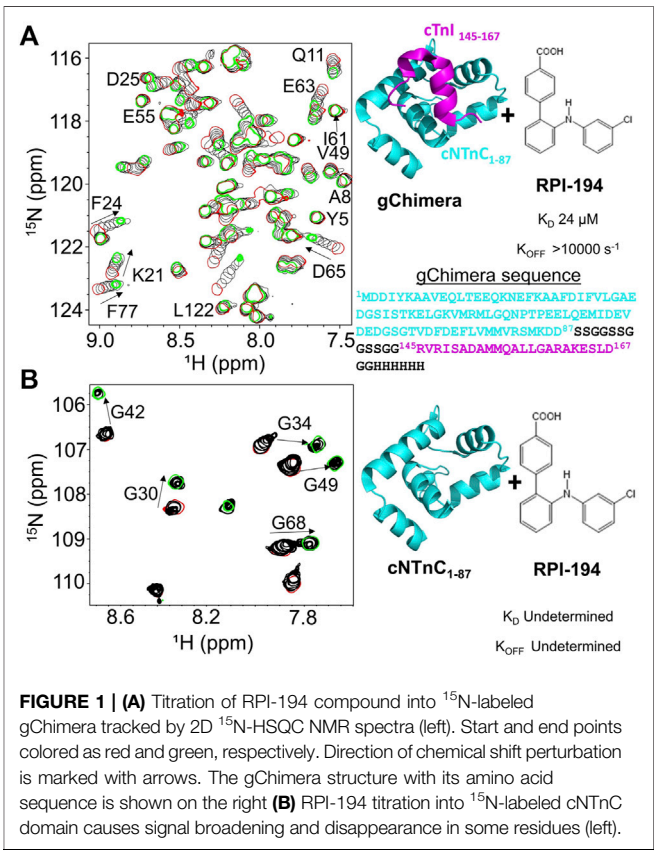

FIGURE 1 | (A) Titration of RPI-194 compound into ^{15}N-labeled gChimera tracked by 2D ^{15}N-HSQC NMR spectra (left). Start and end points colored as red and green, respectively. Direction of chemical shift perturbation is marked with arrows. The gChimera structure with its amino acid sequence is shown on the right **(B)** RPI-194 titration into ^{15}N-labeled cNTnC domain causes signal broadening and disappearance in some residues (left).

which has an additional *p*-benzoic acid in the ortho position of the aniline group, with a measured dissociation constant, K_D, of 24 μM (see **Figure 1A**). Linear migration of the NMR signals suggests 1:1 binding kinetics in the fast exchange regime. ("Fast" exchange means fast relative to the frequency differences between NMR signals in the two different states.) We also calculated the binding affinity by titrating gChimera into RPI-194, monitoring the steady state intrinsic fluorescence of the RPI-194 compound to yield a measured dissociation constant, K_D, of 14 μM (see **Supplementary Figure S1**).

RPI-194 Binds Weakly to Ca^{2+}-Saturated cNTnC in the Absence of cTnI Switch Peptide

RPI-194 binds to the isolated cNTnC domain with a lower affinity than gChimera (K_D = 300 μM), as measured by steady state fluorescence (see **Supplementary Figure S1**). Compared with gChimera, the isolated cNTnC domain lacks the cTnI switch region, which shifts it to an open conformation and binds to small molecules like RPI-194 via the side chains of residues Ile148 and Met153.

NMR titration experiments show a complex equilibrium when RPI-194 is titrated into the cNTnC domain, precluding binding affinity determination by NMR, as was done for gChimera. Prior to addition of RPI-194, the NMR spectrum of isolated cNTnC domain demonstrates signal broadening due to fast timescale conformational exchange between closed and open states (Sia et al., 1997; Spyracopoulos et al., 1997), undergoing a closed-to-open transition with a k_{ex} of about 30,000 s^{-1} (Eichmuller and Skrynnikov, 2005), with the more open conformation representing a minor population of about 5% (Mckay et al., 2000; Paakkonen et al., 2000). Peaks shift and then rapidly disappear upon addition of RPI-194, indicating intermediate timescale binding, consistent with selective binding of RPI-194 to the less populated open state (see **Figure 1B**). As more RPI-194 is added, new NMR signals corresponding to RPI-194-cNTnC complex abruptly re-appear, but in some cases (for example, for residues G30 and G42) they appear in a different position than one would expect based on the start of the titration. This suggests a new conformational process occurring different from the initial 1:1 binding of cNTnC to RPI-194. Other peaks in the spectrum that do not shift become visibly reduced in intensity, suggesting a large increase in molecular weight consistent with dimerization.

Similar changes occur when the drug trifluoperazine is titrated into calmodulin, a protein homologous to troponin C (Feldkamp et al., 2010; Waudby et al., 2016). Each homologous domain of calmodulin binds two molecules of trifluoperazine, and this promotes association of the N-terminal domain with the C-terminal domain through hydrophobic interactions. We propose that at high concentrations of RPI-194, one or two molecules of RPI-194 bind and stabilize the open conformation of the cNTnC domain, which then has a tendency to dimerize. Physiologically, the cNTnC domain does not dimerize because cTnC is tethered to fixed positions along the thin filament. Moreover, the cNTnC domain is predominantly in the closed state unless the cTnI switch region is bound. Thus, while the behaviour of free cNTnC domain in the presence of RPI-194 (and many other compounds) is interesting in terms of its tendency to dimerize, it is not physiologically relevant, except to note that RPI-194 does bind to calcium-saturated cNTnC domain in the absence of cTnI switch region, though binding is substantially more effective once the cTnI switch region is bound. This suggests that RPI-194 is more effective at stabilizing the activated troponin complex once it is formed, rather than promoting the formation of the activated complex.

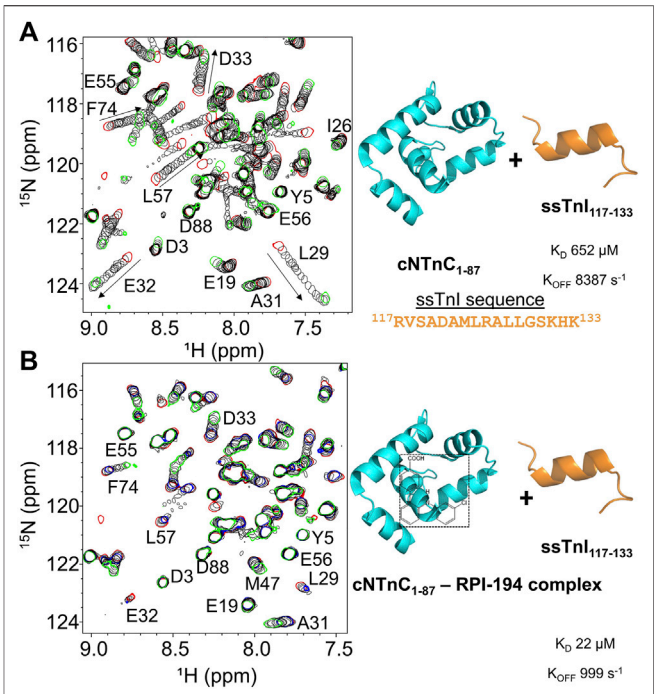

FIGURE 2 | (A) 2D ^{15}N-HSQC spectra of ssTnI titration into ^{15}N-labeled cNTnC (left). Titration start and end points are colored as red and green, respectively. The direction of chemical shift perturbation is indicated with arrows **(B)** The 2D ^{15}N-HSQC spectra of ssTnI titration into ^{15}N-labeled cNTnC and unlabeled RPI-194 complex (left). cNTnC·RPI-194 titration start and end points are colored as red and blue, respectively. End of cNTnC·RPI-194·ssTnI titration is colored green.

RPI-194 Enhances Binding of ssTnI Switch Peptide to cNTnC

To examine the impact of RPI-194 on binding of TnI switch peptide to cNTnC, we titrated TnI switch peptide into isolated cNTnC domain. Cardiac muscle troponin C (cTnC) is the same isoform as slow skeletal muscle troponin C (ssTnC), though slow skeletal muscle possesses different isoforms of troponin I (ssTnI) and troponin T (ssTnT). We used the ssTnI switch peptide instead of the cardiac isoform because of its superior solubility. The cTnI switch peptide readily precipitates out of solution when titrated into solutions containing cTnC and RPI-194, making determination of binding constants unreliable.

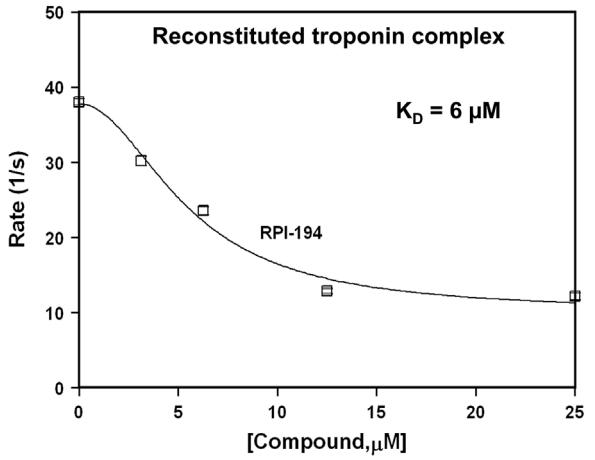

FIGURE 3 | Stopped flow fluorescence experiments. Rate of calcium release from IAANS-labeled reconstituted troponin complex as a function of RPI-194 concentration. *N* = 10 for all measurements.

When ssTnI switch peptide (as opposed to small molecule RPI-194) is titrated into cNTnC, signals that were broad at the start of the titration progressively become narrower as the switch peptide shifts the cNTnC conformational equilibrium to a fully open state (see **Figure 2A**), indicating fast kinetics of binding. This is in marked contrast to when RPI-194 is titrated into cNTnC, in which peaks that were broad at the beginning of the titration become broadened beyond detection as RPI-194 is added. Thus, the ssTnI switch peptide appears able to bind cNTnC via a rapid induced fit mechanism, whereby it stimulates the transition of cNTnC from a closed to an open state, whereas RPI-194 binds via conformational selection, requiring a stochastic transition to the open state prior to binding. Using a two-dimensional lineshape analysis tool, TITAN, we calculated the ssTnI switch peptide binding affinity for cNTnC (K_D 652 μM) that is weaker than that previously determined for the corresponding cTnI switch peptide (K_D 154 μM) (Li et al., 2002).

We then titrated ssTnI switch peptide into cNTnC domain in the presence of RPI-194 (**Figure 2B**). The presence of one equivalent of RPI-194 significantly enhances the binding of ssTnI switch peptide to cNTnC. The binding affinity of ssTnI switch peptide for the cNTnC: RPI-194 complex is K_D 22 μM as calculated by TITAN, which is significantly tighter than the value of 652 μM determined for cNTnC-ssTnI binding in the absence RPI-194, over an order of magnitude change. Improved binding of the TnI switch peptide is consistent with previous NMR studies of the cardiac troponin activator dfbp-o (Robertson et al., 2010; Lindert et al., 2015).

RPI-194 Slows Calcium Release From the Trimeric Cardiac Troponin Complex

We used stopped-flow fluorescence of IAANS-labeled troponin C to measure the impact of RPI-194 on calcium release rates in troponin. RPI-194 binding to reconstituted heterotrimeric cardiac troponin complex slowed the rate of calcium release from 38 s^{-1} to 13 s^{-1} (**Figure 3**), with an apparent dissociation constant, K_D, of 6 μM, in agreement with NMR and steady state fluorescence measurements. This is consistent with our NMR studies demonstrating that RPI-194 stabilizes the calcium-saturated activated troponin complex.

RPI-194 Activates Cardiac, Slow Skeletal, and Fast Skeletal Muscle in Isometric Contraction, but Slows the Velocity of Unloaded Contraction in Skeletal Muscle

At baseline and in the absence of drug, the intrinsic calcium sensitivity of skeletal muscle fibers is about the same for limb slow (pCa_{50} 6.28 ± 0.03) and fast (6.27 ± 0.03) muscle fibers (see **Figure 4** and **Table 1**). The calcium sensitivity of cardiac trabeculae is significantly lower (5.68 ± 0.02). Slow skeletal muscle has a higher calcium affinity than cardiac muscle, even though both muscle types utilize the same cTnC/ssTnC isoform.

RPI-194 has a greater effect on slow skeletal muscle than cardiac muscle. The effects of RPI-194 were tested at 20, 50 and 100 μM concentrations. Six cardiac trabeculae, six slow fibers and six fast fibers were studied at each concentration, and each trabecula/fiber was used to study one concentration of the compound. The shift in the pCa_{50} (i.e., ΔpCa_{50}) is significant between each tested concentration of RPI-194 within each muscle group. At 50 μM RPI-194, the pCa_{50} of slow fibers shifted +0.35 units, while the fast fibers and cardiac trabeculae shifted +0.14 and +0.16, respectively (**Figure 4** and **Table 1**). Therefore, there is a larger calcium sensitizing effect of RPI-194 on limb slow fibers, compared to cardiac trabeculae and limb fast fibers. Although RPI-194 was designed and tested to bind to the cardiac/slow skeletal troponin complex, there is some cross-reactivity with fast skeletal muscle, but the effect is not nearly as large as that observed with tirasemtiv (+0.89) (Russell et al., 2012), which was designed specifically for fast skeletal muscle.

RPI-194 did not increase the maximum isometric force (P_o) generated under saturating calcium concentrations in any of the muscle types (**Supplementary Table S1**). In fact, upon addition of 20, 50, or 100 μM RPI-194, there was an initial 15% decrease in P_o for the slow muscle fibers and a 10% decrease for fast muscle fibers and cardiac trabeculae, with no apparent concentration dependence at the concentrations tested. There was a trend towards recovery in P_o with time seen at higher concentrations of RPI-194 in cardiac trabeculae. The reasons behind these phenomena are not known. The skinned muscle fiber experiments are described in more detail in the **Supplementary Material**.

There was a marked effect of RPI-194 on maximal shortening velocity in unloaded slow and fast skeletal muscle fibers, with velocity generally decreasing with higher concentrations of RPI-194. The overall slowing effect of RPI-194 was similar in slow and fast fibers, with the velocity V_o being reduced to about half in the presence of 100 μM RPI-194 (**Table 1**).

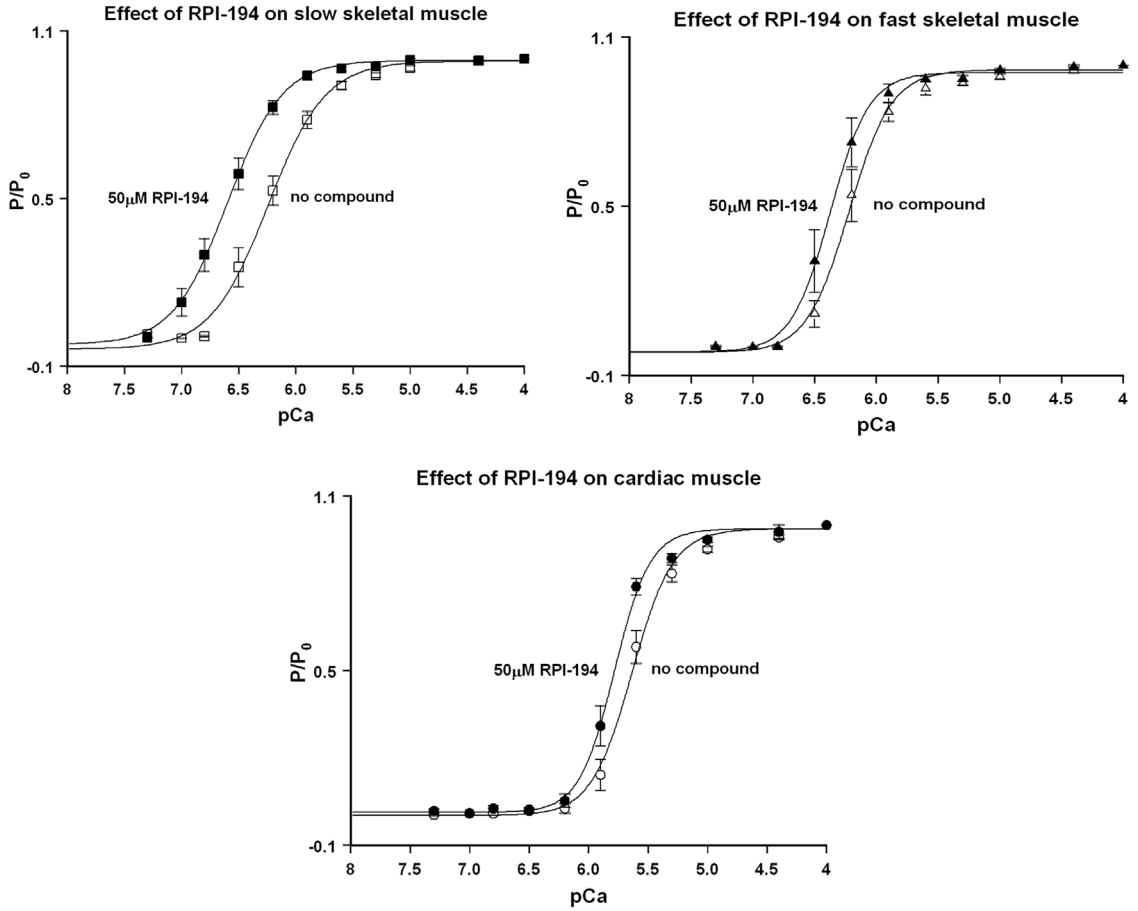

FIGURE 4 | Normalized force (P/P_o) versus pCa curves for rat skinned cardiac trabeculae, fast skeletal, and slow skeletal muscle fibers in the presence of 50 μM RPI-194. Representative number of experiments, *N* = 6 fibers or trabeculae for all measurements.

TABLE 1 | Fundamental properties of slow and fast fibers and of cardiac trabeculae, in the absence or presence of 20, 50 and 100 μM RPI-194.

	Slow Fibers	Fast Fibers	Cardiac Trabeculae
pCa_{50}, series A, *N* = 24 of each	6.28 ± 0.03 (6.10–6.58)	6.27 ± 0.02 (6.03–6.46)	5.68 ± 0.01 (5.49–5.80)
ΔpCa_{50} with 0 μM RPI-194 (series B), *N* = 6 of each	–0.01 ± 0.02 (–0.04–0.01)	0.04 ± 0.02 (–0.01–0.06)	0.00 ± 0.01 (–0.01–0.01)
ΔpCa_{50} with 20 μM RPI-194 (series B), *N* = 6 of each	0.14 ± 0.02 (0.10–0.24)	0.04 ± 0.02 (–0.01–0.12)	0.03 ± 0.02 (–0.01–0.10)
ΔpCa_{50} with 50 μM RPI-194 (series B), *N* = 6 of each	0.35 ± 0.02 (0.30–0.42)	0.14 ± 0.02 (0.07–0.19)	0.16 ± 0.02 (0.09–0.20)
ΔpCa_{50} with 100 μM RPI-194 (series B), *N* = 6 of each	0.71 ± 0.05 (0.58–0.84)	0.25 ± 0.02 (0.14–0.27)	0.28 ± 0.02 (0.21–0.32)
V_o (FL/s), in the absence of RPI-194 (series A), *N* = 24 of each[a]	1.35 ± 0.04 (1.04–1.68)	4.53 ± 0.17 (3.19–6.31)	—
V_o ratio with 0 μM RPI-194 (series B/series A), *N* = 6 of each	0.94 ± 0.07 (0.83–1.02)	0.89 ± 0.04 (0.68–1.00)	—
V_o ratio with 20 μM RPI-194 (series B/series A), *N* = 6 of each	0.75 ± 0.03 (0.69–0.86)	0.67 ± 0.06 (0.51–0.82)	—
V_o ratio with 50 μM RPI-194 (series B/series A), *N* = 6 of each[a]	0.58 ± 0.04 (0.51–0.68)	0.61 ± 0.06 (0.49–0.85)	—
V_o ratio with 100 μM RPI-194 (series B/series A), *N* = 6 of each	0.50 ± 0.01 (0.48–0.52)	0.52 ± 0.04 (0.42–0.64)	—

[a]*Values are mean ± SEM (range in parentheses). Here, V_o = maximal shortening velocity.*

Shortening velocity is determined by the load-dependent rate of actin-myosin cycling. It is possible that RPI-194 slows the velocity of unloaded contraction, V_0, via a direct interaction with actin-myosin. We therefore proceeded to examine the effect of RPI-194 on human beta-cardiac myosin S1 ATPase activity in the presence of 40 μM actin. We found no effect whatsoever (see **Supplementary Figure S2**), suggesting that the reduction in V_0 by RPI-194 seen in slow and fast skeletal muscle is not due to direct binding to actin-myosin S1, but rather, an effect on another myosin domain or light chain, troponin, or some other unknown off-target effect.

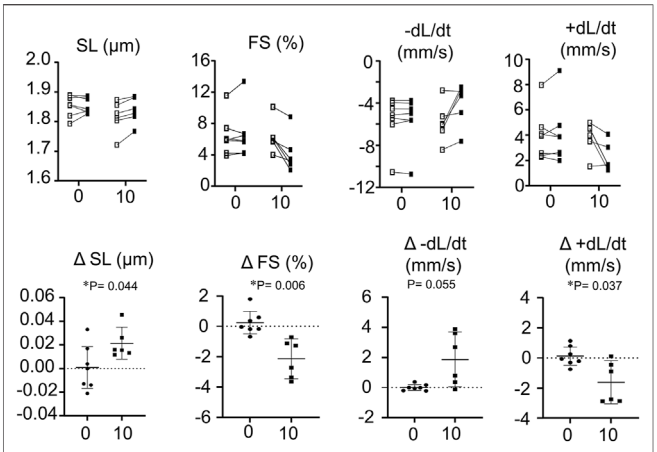

FIGURE 5 | Top panel shows measurement of resting sarcomere length (SL), fractional shortening (FS), rate of contraction (-dL/dt) and rate of relaxation (+dL/dt) of isolated single cardiomyocytes. Open boxes represent baseline and filled boxes represent addition of either 0 or 10 μM RPI-194 (10). Bottom panel shows absolute changes of measurements from wild type values. $N = 6$ for all measurements. *$p < 0.05$ compared between placebo (0) or 10 μM RPI-194 (10) with Tukey post-hoc test.

RPI-194 Decreases Velocity and Amplitude of Contraction in Unloaded Individual Mouse Cardiomyocytes

The addition of RPI-194 to individual unloaded cardiomyocytes caused a decrease in observed contractility. 10 μM RPI-194 significantly increased resting sarcomere length, decreased fractional shortening, and decreased the velocity of contraction and relaxation (**Figure 5**). At a concentration of 100 μM, cardiomyocyte contractions ceased completely, with sarcomere lengths suggestive of a relaxed state (rather than a contracted state). The inhibition of contractility observed in cardiomyocytes contrasts with the increased calcium sensitivity of isometric contraction seen in skinned cardiac trabeculae. This raises the possibility that RPI-194 interferes with excitation-contraction coupling in living cells, for example, the inhibition of ion channels. When we attempted to measure calcium transients in cardiomyocytes using calcium-sensitive fluorophores, the strong intrinsic fluorescence of RPI-194 created too much background signal. It is therefore necessary to assess cardiac contractility in another system that includes intact cells.

Cardiac Work is Maintained in Mouse Isolated Perfused Working Hearts

We studied the impact of RPI-194 in a mouse isolated perfused working heart model, which was maintained at constant pressure. There was no consistent trend in heart rate or heart rate times peak systolic pressure product as RPI-194 was added to the system up to a maximum of 100 μM (**Figure 6**). Cardiac output and cardiac work increased with increasing RPI-194 levels, but the trend was not statistically significant, and similar changes could also be observed in controls over the course of 60 min (see **Supplementary Figure S3**). As RPI-194 was added, the observed increase in cardiac work was accompanied by higher rates of glucose utilization and oxygen consumption. Thus, it appears that metabolic pathways are generally intact in the presence of RPI-194. The severe inhibitory effect of RPI-194 observed in individual unloaded cardiomyocytes was not observed in isolated perfused working hearts, making it less likely that the inhibitory effect observed in cardiomyocytes is due to modulation of ion channels.

DISCUSSION

Perhaps the most unexpected result in the current study is the effect of RPI-194 in slowing the velocity of unloaded shortening, both in skinned skeletal muscle fibers and in isolated cardiomyocytes. This could be due to an unknown off-target effect, although it is reassuring that cardiac function was preserved in mouse isolated perfused working hearts. It is possible that the decreased velocity of unloaded shortening seen with RPI-194 is a consequence of troponin activation itself. The ideal duty ratio (proportion of myosin heads strongly bound to actin) is dependent on load, with more myosin-actin interactions needed for higher loads, while for smaller loads excessive interactions might only contribute to drag. In isometric muscle contraction, actin-myosin interaction is maximal, with a duty ratio of about 0.25 (Land and Niederer, 2015). This value decreases to <0.05 in unloaded shortening, and it could be that excessive formation of actin-myosin cross-bridges beyond this lower duty ratio slows unloaded contraction (O'connell et al., 2007; Brizendine et al., 2015).

The effect of RPI-194 on unloaded cardiomyocytes is similar to that observed with mutations in cTnI or cTnT associated with hypertrophic cardiomyopathy (HCM) (Willott et al., 2010). Such mutations increase calcium sensitivity and shift the thin filament towards the activated state (Ren et al., 2018), much like the effect of RPI-194. Feline cardiomyocytes showed decreased amplitude and velocity of shortening after being transfected with R92Q-cTnT versus wildtype cTnT (Marian et al., 1997). A similar effect was observed in R92Q-cTnT transgenic mouse cardiomyocytes (Tardiff et al., 1999). Slowed contractility was also observed in isolated guinea pig cardiomyocytes transfected with R145G-cTnI. Thus, decreased and slowed contractions in unloaded cardiomyocytes appears to be a feature of HCM mutations, so it is possible that cardiac troponin activation by RPI-194 has a similar effect. Nevertheless, an off-target effect remains a possibility.

RPI-194 was designed to bind and stabilize the calcium-bound activated complex between cardiac TnC and TnI. The structure of RPI-194 can be further engineered to improve its specificity by adding aromatic ring substituents or restricting its degrees of freedom. This would help to resolve whether the observed slowing of unloaded shortening seen with RPI-194 is due to its impact on troponin or an off-target effect.

It is unlikely that any modifications of RPI-194 would enhance its specificity for cardiac troponin with respect to slow skeletal muscle troponin. Both use the same troponin C isoform, and the residues in the switch region binding the RPI-194 molecule are highly homologous in the troponin I isoforms

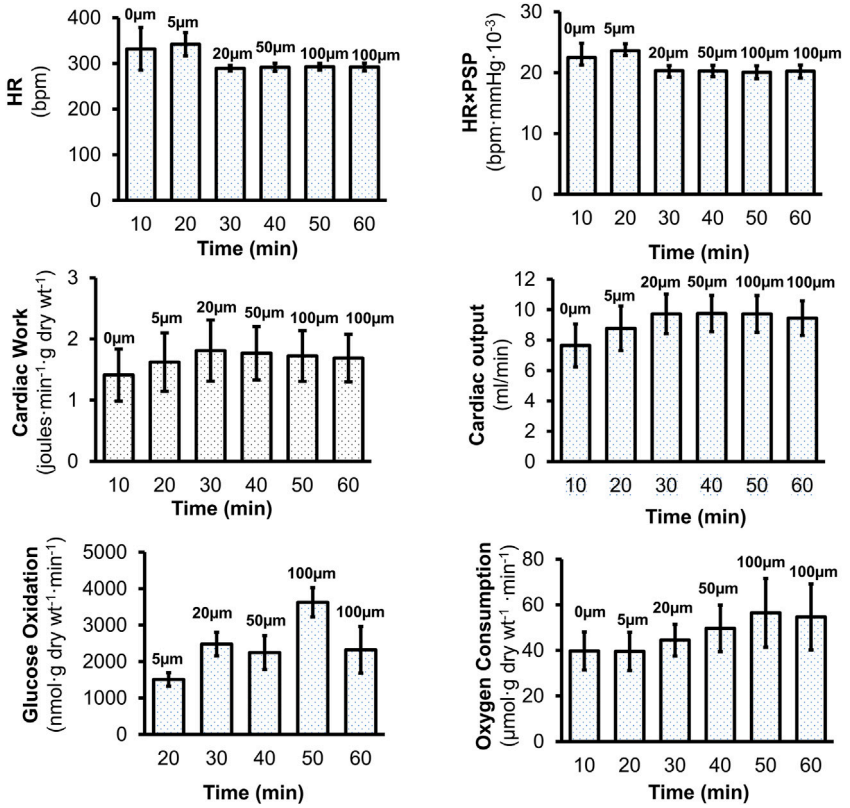

FIGURE 6 | Effects of RPI-194 on heart rate (HR), heart rate×peak systolic pressure (HR×PSP), cardiac work, cardiac output, glucose oxidation, and oxygen consumption in isolated, perfused working mouse hearts. *N* = 4 for all measurements.

(compare Ile148 and Met153, cTnI, in **Figure 1A** *versus* Val118 and Met123, ssTnI, in **Figure 2A**). It is possible that RPI-194 could be modified to decrease cross-reactivity with fast skeletal troponin, for which there are selective activators, tirasemtiv and reldesemtiv (Russell et al., 2012; Hwee et al., 2014; Hwee et al., 2015; Calder et al., 2016). Whether or not cross-reactivity with skeletal muscle, particularly slow skeletal muscle, would limit potential use of a cardiac troponin activator, remains to be seen. On the other hand, it is also unknown whether the cardiac effects of a general troponin activator would limit its use as slow skeletal muscle activator. Whole animal models examining the impact of compounds like RPI-194 are needed.

Finally, we note that our cardiac troponin activator RPI-194 likely has a different mechanism of activity from the recently published cardiac troponin activator TA1, a closely related analog of the drug AMG-594/CK-136, which has undergone Phase 1 clinical trials (https://cytokinetics.com/ck-136/). TA1/AMG-594/CK-136 is highly selective for cardiac muscle over slow skeletal muscle, which would not be possible if it were targeting the same binding site as RPI-194. Moreover, TA1 is more potent, not only causing a greater leftward shift for pCa_{50} in cardiac trabeculae, but also markedly increasing the maximum force generated at saturating calcium concentrations, unlike RPI-194 (He et al., 2021). Increased force was also observed at resting calcium concentrations, along with increased myosin ATP consumption in cardiac myofibrils. The behaviour of RPI-194 is more in keeping with what was observed for fast skeletal troponin activator tirasemtiv, with a leftward pCa_{50} but no significant change in force generated at low or saturating calcium concentrations (Russell et al., 2012), which is not surprising given that they both target the same homologous binding pocket (Li et al., 2021). It is possible that TA1 is able to activate the thin filament through cTnI/cTnT, independent of the calcium binding activity of cTnC, unlike RPI-194 and tirasemtiv. Further comparative studies are needed to delineate the differences between RPI-194 and TA1/AMG-594/CK-136 in terms of mechanism of action and physiologic impact.

DATA AVAILABILITY STATEMENT

The original contributions presented in the study are included in the article/**Supplementary Material**, further inquiries can be directed to the corresponding authors.

ETHICS STATEMENT

The animal study was reviewed and approved by Institutional Animal Care and Use Committee of The Ohio State University.

AUTHOR CONTRIBUTIONS

ZM performed protein expression and purification, NMR and steady state fluorescence spectroscopy data acquisition for screening drug compounds, and wrote the original manuscript. ST and JD performed stopped-flow fluorescence data acquisition, analysis and reviewed the manuscript. NB and PR tested compounds in slow/fast skeletal muscle fibers and trabeculae. CW tested compounds in the isolated perfused working mouse hearts. PZ tested compounds in isolated single cardiomyocytes. PL expressed and purified proteins. DR expressed and purified human cardiac myosin and tested compounds using the myosin ATPase assay. CY, GO, GL, ST, JD, and PR provided their lab facilities, analyzed data, and reviewed the manuscript. PH was involved in conceptualization, funding acquisition, supervision, writing, and reviewing the manuscript.

FUNDING

This work was funded by the Hwang Professional Corporation, which allows PMH to use his salary as a professor to pay for laboratory personnel and operating costs. PMH was previously supported by a Heart and Stroke Foundation of Canada / Mazankowski Alberta Heart Institute early career investigator award and a Canadian Institutes of Health Research Phase 2 Clinician Scientist Salary Award. NIH grant HL127699 to CMY. NIH grants R01HL132213 and R01HL138579 to JPD, and and CIHR Foundation grant to GDL.

SUPPLEMENTARY MATERIAL

The Supplementary Material for this article can be found online at: https://www.frontiersin.org/articles/10.3389/fphys.2022.892979/full#supplementary-material

Supplementary Figure S1 | Fluorescence signal of 5 μM RPI-194 with titration of gChimera protein (left), or titration of cNTnC protein (right). *N* = 3 for all measurements.

Supplementary Figure S2 | Lack of impact of RPI-194 on myosin ATPase activity. The ATPase activity of human beta-cardiac myosin subfragment 1 (0.1 μM) was measured in the presence of 40 μM actin and varying concentrations of drug (RPI-194P). The ATPase activity is reported as moles of Pi per mole of myosin per second. Number of experiments with separate protein preparations, *N* = 3.

Supplementary Figure S3 | Effects of DMSO in heart rate (HR), heart rate×peak systolic pressure (HR×PSP), cardiac work, and cardiac output in isolated, perfused working mouse hearts. N = 7 for all measurements.

REFERENCES

Bethke, T., Meyer, W., Schmitz, W., Scholz, H., Wenzlaff, H., Armah, B. I., et al. (1993). High Selectivity for Inhibition of Phosphodiesterase III and Positive Inotropic Effects of MCI-154 in guinea Pig Myocardium. *J. Cardiovasc. Pharmacol.* 21, 847–855. doi:10.1097/00005344-199306000-00001

Black, D. J., Tikunova, S. B., Johnson, J. D., and Davis, J. P. (2000). Acid Pairs Increase the N-Terminal Ca2+ Affinity of CaM by Increasing the Rate of Ca2+ Association,. *Biochemistry* 39, 13831–13837. doi:10.1021/bi001106+

Böhm, M., Morano, I., Pieske, B., Rüegg, J. C., Wankerl, M., Zimmermann, R., et al. (1991). Contribution of cAMP-Phosphodiesterase Inhibition and Sensitization of the Contractile Proteins for Calcium to the Inotropic Effect of Pimobendan in the Failing Human Myocardium. *Circ. Res.* 68, 689–701. doi:10.1161/01.res.68.3.689

Bourge, R. C., Fleg, J. L., Fonarow, G. C., Cleland, J. G. F., Mcmurray, J. J. V., Van Veldhuisen, D. J., et al. (2013). Digoxin Reduces 30-day All-Cause Hospital Admission in Older Patients with Chronic Systolic Heart Failure. *Am. J. Med.* 126, 701–708. doi:10.1016/j.amjmed.2013.02.001

Brixius, K., Mehlhorn, U., Bloch, W., and Schwinger, R. H. (2000). Different Effect of the Ca(2+) Sensitizers EMD 57033 and CGP 48506 on Cross-Bridge Cycling in Human Myocardium. *J. Pharmacol. Exp. Ther.* 295, 1284–1290.

Brizendine, R. K., Alcala, D. B., Carter, M. S., Haldeman, B. D., Facemyer, K. C., Baker, J. E., et al. (2015). Velocities of Unloaded Muscle Filaments Are Not Limited by Drag Forces Imposed by Myosin Cross-Bridges. *Proc. Natl. Acad. Sci. U.S.A.* 112, 11235–11240. doi:10.1073/pnas.1510241112

Cai, F., Hwang, P. M., and Sykes, B. D. (2018). Structural Changes Induced by the Binding of the Calcium Desensitizer W7 to Cardiac Troponin. *Biochemistry* 57, 6461–6469. doi:10.1021/acs.biochem.8b00882

Cai, F., Li, M. X., Pineda-Sanabria, S. E., Gelozia, S., Lindert, S., West, F., et al. (2016). Structures Reveal Details of Small Molecule Binding to Cardiac Troponin. *J. Mol. Cell. Cardiol.* 101, 134–144. doi:10.1016/j.yjmcc.2016.10.016

Calder, A. N., Androphy, E. J., and Hodgetts, K. J. (2016). Small Molecules in Development for the Treatment of Spinal Muscular Atrophy. *J. Med. Chem.* 59, 10067–10083. doi:10.1021/acs.jmedchem.6b00670

Crackower, M. A., Oudit, G. Y., Kozieradzki, I., Sarao, R., Sun, H., Sasaki, T., et al. (2002). Regulation of Myocardial Contractility and Cell Size by Distinct PI3K-PTEN Signaling Pathways. *Cell* 110, 737–749. doi:10.1016/s0092-8674(02)00969-8

Curtis, J. P., Sokol, S. I., Wang, Y., Rathore, S. S., Ko, D. T., Jadbabaie, F., et al. (2003). The Association of Left Ventricular Ejection Fraction, Mortality, and Cause of Death in Stable Outpatients with Heart Failure. *J. Am. Coll. Cardiol.* 42, 736–742. doi:10.1016/s0735-1097(03)00789-7

Davis, J. P., Norman, C., Kobayashi, T., Solaro, R. J., Swartz, D. R., and Tikunova, S. B. (2007). Effects of Thin and Thick Filament Proteins on Calcium Binding and Exchange with Cardiac Troponin C. *Biophysical J.* 92, 3195–3206. doi:10.1529/biophysj.106.095406

Delaglio, F., Grzesiek, S., Vuister, G., Zhu, G., Pfeifer, J., and Bax, A. (1995). NMRPipe: a Multidimensional Spectral Processing System Based on UNIX Pipes. *J. Biomol. NMR* 6, 277–293. doi:10.1007/BF00197809

Ebashi, S., Ebashi, F., and Kodama, A. (1967). Troponin as the Ca++-Receptive Protein in the Contractile System. *J. Biochem.* 62, 137–138. doi:10.1093/oxfordjournals.jbchem.a128628

Ebashi, S., Ebashi, F., and Maruyama, K. (1964). A New Protein Factor Promoting Contraction of Actomyosin. *Nature* 203, 645–646. doi:10.1038/203645a0

Edman, K. A. (1979). The Velocity of Unloaded Shortening and its Relation to Sarcomere Length and Isometric Force in Vertebrate Muscle Fibres. *J. Physiol.* 291, 143–159. doi:10.1113/jphysiol.1979.sp012804

Eichmüller, C., and Skrynnikov, N. R. (2005). A New Amide Proton R1ρ Experiment Permits Accurate Characterization of Microsecond Time-Scale Conformational Exchange. *J. Biomol. NMR* 32, 281–293. doi:10.1007/s10858-005-0658-y

Feldkamp, M. D., O'donnell, S. E., Yu, L., and Shea, M. A. (2010). Allosteric Effects of the Antipsychotic Drug Trifluoperazine on the Energetics of Calcium Binding by Calmodulin. *Proteins* 78, 2265–2282. doi:10.1002/prot.22739

Greaser, M. L., and Gergely, J. (1973). Purification and Properties of the Components from Troponin. *J. Biol. Chem.* 248, 2125–2133. doi:10.1016/s0021-9258(19)44195-1

He, H., Baka, T., Balschi, J., Motani, A. S., Nguyen, K. K., Liu, Q., et al. (2022). Novel Small-Molecule Troponin Activator Increases Cardiac Contractile Function without Negative Impact on Energetics. *Circ. Heart Fail.* 15, e009195. doi:10.1161/CIRCHEARTFAILURE.121.009195

Hwang, P. M., and Sykes, B. D. (2015). Targeting the Sarcomere to Correct Muscle Function. *Nat. Rev. Drug Discov.* 14, 313–328. doi:10.1038/nrd4554

Hwee, D. T., Kennedy, A. R., Hartman, J. J., Ryans, J., Durham, N., Malik, F. I., et al. (2015). The Small-Molecule Fast Skeletal Troponin Activator, CK-2127107,

Improves Exercise Tolerance in a Rat Model of Heart Failure. *J. Pharmacol. Exp. Ther.* 353, 159–168. doi:10.1124/jpet.114.222224

Hwee, D. T., Kennedy, A., Ryans, J., Russell, A. J., Jia, Z., Hinken, A. C., et al. (2014). Fast Skeletal Muscle Troponin Activator Tirasemtiv Increases Muscle Function and Performance in the B6SJL-Sod1g93a ALS Mouse Model. *PLoS One* 9, e96921. doi:10.1371/journal.pone.0096921

Kitada, Y., Kobayashi, M., Narimatsu, A., and Ohizumi, Y. (1989). Potent Stimulation of Myofilament Force and Adenosine Triphosphatase Activity of Canine Cardiac Muscle through a Direct Enhancement of Troponin C Ca++ Binding by MCI-154, a Novel Cardiotonic Agent. *J. Pharmacol. Exp. Ther.* 250, 272–277.

Kovacic, S., Soltys, C.-L. M., Barr, A. J., Shiojima, I., Walsh, K., and Dyck, J. R. B. (2003). Akt Activity Negatively Regulates Phosphorylation of AMP-Activated Protein Kinase in the Heart. *J. Biol. Chem.* 278, 39422–39427. doi:10.1074/jbc.M305371200

Kuang, M., Febbraio, M., Wagg, C., Lopaschuk, G. D., and Dyck, J. R. B. (2004). Fatty Acid translocase/CD36 Deficiency Does Not Energetically or Functionally Compromise Hearts before or after Ischemia. *Circulation* 109, 1550–1557. doi:10.1161/01.CIR.0000121730.41801.12

Land, S., and Niederer, S. A. (2015). A Spatially Detailed Model of Isometric Contraction Based on Competitive Binding of Troponin I Explains Cooperative Interactions between Tropomyosin and Crossbridges. *PLoS Comput. Biol.* 11, e1004376. doi:10.1371/journal.pcbi.1004376

Li, M., Saude, E., Wang, X., Pearlstone, J., Smillie, L., and Sykes, B. (2002). Kinetic Studies of Calcium and Cardiac Troponin I Peptide Binding to Human Cardiac Troponin C Using NMR Spectroscopy. *Eur. Biophysics J.* 31, 245–256. doi:10.1007/s00249-002-0227-1

Li, M. X., Gelozia, S., Danmaliki, G. I., Wen, Y., Liu, P. B., Lemieux, M. J., et al. (2018). The Calcium Sensitizer Drug MCI-154 Binds the Structural C-Terminal Domain of Cardiac Troponin C. *Biochem. Biophysics Rep.* 16, 145–151. doi:10.1016/j.bbrep.2018.10.012

Li, M. X., and Hwang, P. M. (2015). Structure and Function of Cardiac Troponin C (TNNC1): Implications for Heart Failure, Cardiomyopathies, and Troponin Modulating Drugs. *Gene* 571, 153–166. doi:10.1016/j.gene.2015.07.074

Li, M. X., Mercier, P., Hartman, J. J., and Sykes, B. D. (2021). Structural Basis of Tirasemtiv Activation of Fast Skeletal Muscle. *J. Med. Chem.* 64, 3026–3034. doi:10.1021/acs.jmedchem.0c01412

Li, M. X., Wang, X., and Sykes, B. D. (2004). Structural Based Insights into the Role of Troponin in Cardiac Muscle Pathophysiology. *J. Muscle Res. Cell Motil.* 25, 559–579. doi:10.1007/s10974-004-5879-2

Li, Y., Love, M. L., Putkey, J. A., and Cohen, C. (2000). Bepridil Opens the Regulatory N-Terminal Lobe of Cardiac Troponin C. *Proc. Natl. Acad. Sci. U.S.A.* 97, 5140–5145. doi:10.1073/pnas.090098997

Lindert, S., Li, M. X., Sykes, B. D., and Mccammon, J. A. (2015). Computer-aided Drug Discovery Approach Finds Calcium Sensitizer of Cardiac Troponin. *Chem. Biol. Drug Des.* 85, 99–106. doi:10.1111/cbdd.12381

Malik, F. I., Hartman, J. J., Elias, K. A., Morgan, B. P., Rodriguez, H., Brejc, K., et al. (2011). Cardiac Myosin Activation: a Potential Therapeutic Approach for Systolic Heart Failure. *Science* 331, 1439–1443. doi:10.1126/science.1200113

Marian, A. J., Zhao, G., Seta, Y., Roberts, R., and Yu, Q.-t. (1997). Expression of a Mutant (Arg92Gln) Human Cardiac Troponin T, Known to Cause Hypertrophic Cardiomyopathy, Impairs Adult Cardiac Myocyte Contractility. *Circulation Res.* 81, 76–85. doi:10.1161/01.res.81.1.76

Mckay, R. T., Saltibus, L. F., Li, M. X., and Sykes, B. D. (2000). Energetics of the Induced Structural Change in a Ca2+ Regulatory Protein: Ca2+ and Troponin I Peptide Binding to the E41A Mutant of the N-Domain of Skeletal Troponin C. *Biochemistry* 39, 12731–12738. doi:10.1021/bi001240u

Metzger, J. M., and Westfall, M. V. (2004). Covalent and Noncovalent Modification of Thin Filament Action: The Essential Role Of Troponin In Cardiac Muscle Regulation. *Circulation Res.* 94, 146–158. doi:10.1161/01.RES.0000110083.17024.60

Murphy, S. P., Ibrahim, N. E., and Januzzi, J. L., Jr. (2020). Heart Failure with Reduced Ejection Fraction: A Review. *JAMA* 324, 488–504. doi:10.1001/jama.2020.10262

O'connell, C. B., Tyska, M. J., and Mooseker, M. S. (2007). Myosin at Work: Motor Adaptations for a Variety of Cellular Functions. *Biochimica Biophysica Acta (BBA) - Mol. Cell Res.* 1773, 615–630. doi:10.1016/j.bbamcr.2006.06.012

Oda, T., Yanagisawa, H., and Wakabayashi, T. (2020). Cryo-EM Structures of Cardiac Thin Filaments Reveal the 3D Architecture of Troponin. *J. Struct. Biol.* 209, 107450. doi:10.1016/j.jsb.2020.107450

Ørstavik, Ø., Manfra, O., Andressen, K. W., Andersen, G. Ø., Skomedal, T., Osnes, J.-B., et al. (2015). The Inotropic Effect of the Active Metabolite of Levosimendan, OR-1896, Is Mediated through Inhibition of PDE3 in Rat Ventricular Myocardium. *PLoS One* 10, e0115547. doi:10.1371/journal.pone.0115547

Pääkkönen, K., Sorsa, T., Drakenberg, T., Pollesello, P., Tilgmann, C., Permi, P., et al. (2000). Conformations of the Regulatory Domain of Cardiac Troponin C Examined by Residual Dipolar Couplings. *Eur. J. Biochem.* 267, 6665–6672. doi:10.1046/j.1432-1327.2000.01763.x

Pineda-Sanabria, S. E., Julien, O., and Sykes, B. D. (2014). Versatile Cardiac Troponin Chimera for Muscle Protein Structural Biology and Drug Discovery. *ACS Chem. Biol.* 9, 2121–2130. doi:10.1021/cb500249j

Planelles-Herrero, V. J., Hartman, J. J., Robert-Paganin, J., Malik, F. I., and Houdusse, A. (2017). Mechanistic and Structural Basis for Activation of Cardiac Myosin Force Production by Omecamtiv Mecarbil. *Nat. Commun.* 8, 190. doi:10.1038/s41467-017-00176-5

Reiser, P. J., Welch, K. C., Jr., Suarez, R. K., and Altshuler, D. L. (2013). Very Low Force-Generating Ability and Unusually High Temperature-Dependency in Hummingbird Flight Muscle Fibers. *J. Exp. Biol.* 216, 2247–2256. doi:10.1242/jeb.068825

Ren, X., Hensley, N., Brady, M. B., and Gao, W. D. (2018). The Genetic and Molecular Bases for Hypertrophic Cardiomyopathy: The Role for Calcium Sensitization. *J. Cardiothorac. Vasc. Anesth.* 32, 478–487. doi:10.1053/j.jvca.2017.05.035

Robertson, I. M., Sun, Y.-B., Li, M. X., and Sykes, B. D. (2010). A Structural and Functional Perspective into the Mechanism of Ca2+-Sensitizers that Target the Cardiac Troponin Complex. *J. Mol. Cell. Cardiol.* 49, 1031–1041. doi:10.1016/j.yjmcc.2010.08.019

Rudnicki, S. A., Andrews, J. A., Duong, T., Cockroft, B. M., Malik, F. I., Meng, L., et al. (2021). Reldesemtiv in Patients with Spinal Muscular Atrophy: a Phase 2 Hypothesis-Generating Study. *Neurotherapeutics* 18, 1127–1136. doi:10.1007/s13311-020-01004-3

Russell, A. J., Hartman, J. J., Hinken, A. C., Muci, A. R., Kawas, R., Driscoll, L., et al. (2012). Activation of Fast Skeletal Muscle Troponin as a Potential Therapeutic Approach for Treating Neuromuscular Diseases. *Nat. Med.* 18, 452–455. doi:10.1038/nm.2618

Sah, R., Oudit, G. Y., Nguyen, T.-T. T., Lim, H. W., Wickenden, A. D., Wilson, G. J., et al. (2002). Inhibition of Calcineurin and Sarcolemmal Ca2+ Influx Protects Cardiac Morphology and Ventricular Function in K(v)4.2N Transgenic Mice. *Circulation* 105, 1850–1856. doi:10.1161/01.cir.0000014211.47830.4d

Shefner, J. M., Andrews, J. A., Genge, A., Jackson, C., Lechtzin, N., Miller, T. M., et al. (2021). A Phase 2, Double-Blind, Randomized, Dose-Ranging Trial of Reldesemtiv in Patients with ALS. *Amyotroph. Lateral Scler. Frontotemporal Degener.* 22, 287–299. doi:10.1080/21678421.2020.1822410

Shefner, J. M., Cudkowicz, M. E., Hardiman, O., Cockroft, B. M., Lee, J. H., Malik, F. I., et al. (2019). A Phase III Trial of Tirasemtiv as a Potential Treatment for Amyotrophic Lateral Sclerosis. *Amyotroph. Lateral Scler. Frontotemporal Degener.* 20, 584–594. doi:10.1080/21678421.2019.1612922

Shettigar, V., Zhang, B., Little, S. C., Salhi, H. E., Hansen, B. J., Li, N., et al. (2016). Rationally Engineered Troponin C Modulates *In Vivo* Cardiac Function and Performance in Health and Disease. *Nat. Commun.* 7, 10794. doi:10.1038/ncomms10794

Sia, S. K., Li, M. X., Spyracopoulos, L., Gagné, S. M., Liu, W., Putkey, J. A., et al. (1997). Structure of Cardiac Muscle Troponin C Unexpectedly Reveals a Closed Regulatory Domain. *J. Biol. Chem.* 272, 18216–18221. doi:10.1074/jbc.272.29.18216

Siddiqui, J. K., Tikunova, S. B., Walton, S. D., Liu, B., Meyer, M., De Tombe, P. P., et al. (2016). Myofilament Calcium Sensitivity: Consequences of the Effective Concentration of Troponin I. *Front. Physiol.* 7, 632. doi:10.3389/fphys.2016.00632

Spyracopoulos, L., Li, M. X., Sia, S. K., Gagné, S. M., Chandra, M., Solaro, R. J., et al. (1997). Calcium-Induced Structural Transition in the Regulatory Domain of Human Cardiac Troponin C,. *Biochemistry* 36, 12138–12146. doi:10.1021/bi971223d

Swenson, A. M., Tang, W., Blair, C. A., Fetrow, C. M., Unrath, W. C., Previs, M. J., et al. (2017). Omecamtiv Mecarbil Enhances the Duty Ratio of Human β-Cardiac Myosin Resulting in Increased Calcium Sensitivity and Slowed Force Development in Cardiac Muscle. *J. Biol. Chem.* 292, 3768–3778. doi:10.1074/jbc.M116.748780

Tacon, C. L., Mccaffrey, J., and Delaney, A. (2012). Dobutamine for Patients with Severe Heart Failure: a Systematic Review and Meta-Analysis of Randomised Controlled Trials. *Intensive Care Med.* 38, 359–367. doi:10.1007/s00134-011-2435-6

Takeda, S., Yamashita, A., Maeda, K., and Maéda, Y. (2003). Structure of the Core Domain of Human Cardiac Troponin in the Ca(2+)-Saturated Form. *Nature* 424, 35–41. doi:10.1038/nature01780

Tang, W., Unrath, W. C., Desetty, R., and Yengo, C. M. (2019). Dilated Cardiomyopathy Mutation in the Converter Domain of Human Cardiac Myosin Alters Motor Activity and Response to Omecamtiv Mecarbil. *J. Biol. Chem.* 294, 17314–17325. doi:10.1074/jbc.RA119.010217

Tardiff, J. C., Hewett, T. E., Palmer, B. M., Olsson, C., Factor, S. M., Moore, R. L., et al. (1999). Cardiac Troponin T Mutations Result in Allele-specific Phenotypes in a Mouse Model for Hypertrophic Cardiomyopathy. *J. Clin. Invest.* 104, 469–481. doi:10.1172/JCI6067

Teerlink, J. R., Diaz, R., Felker, G. M., Mcmurray, J. J. V., Metra, M., Solomon, S. D., et al. (2021). Cardiac Myosin Activation with Omecamtiv Mecarbil in Systolic Heart Failure. *N. Engl. J. Med.* 384, 105–116. doi:10.1056/NEJMoa2025797

Teerlink, J. R., Felker, G. M., Mcmurray, J. J. V., Ponikowski, P., Metra, M., Filippatos, G. S., et al. (2016). Acute Treatment with Omecamtiv Mecarbil to Increase Contractility in Acute Heart Failure: The ATOMIC-AHF Study. *J. Am. Coll. Cardiol.* 67, 1444–1455. doi:10.1016/j.jacc.2016.01.031

Tikunova, S. B., Cuesta, A., Price, M., Li, M. X., Belevych, N., Biesiadecki, B. J., et al. (2019). 3-Chlorodiphenylamine Activates Cardiac Troponin by a Mechanism Distinct from Bepridil or TFP. *J. Gen. Physiol.* 151, 9–17. doi:10.1085/jgp.201812131

Tikunova, S., Belevych, N., Doan, K., and Reiser, P. J. (2018). Desensitizing Mouse Cardiac Troponin C to Calcium Converts Slow Muscle towards a Fast Muscle Phenotype. *J. Physiol.* 596, 4651–4663. doi:10.1113/JP276296

Tikunova, S. B., Liu, B., Swindle, N., Little, S. C., Gomes, A. V., Swartz, D. R., et al. (2010). Effect of Calcium-Sensitizing Mutations on Calcium Binding and Exchange with Troponin C in Increasingly Complex Biochemical Systems. *Biochemistry* 49, 1975–1984. doi:10.1021/bi901867s

Tikunova, S. B., Rall, J. A., and Davis, J. P. (2002). Effect of Hydrophobic Residue Substitutions with Glutamine on Ca(2+) Binding and Exchange with the N-Domain of Troponin C. *Biochemistry* 41, 6697–6705. doi:10.1021/bi011763h

Waudby, C. A., Ramos, A., Cabrita, L. D., and Christodoulou, J. (2016). Two-Dimensional NMR Lineshape Analysis. *Sci. Rep.* 6, 24826. doi:10.1038/srep24826

Willott, R. H., Gomes, A. V., Chang, A. N., Parvatiyar, M. S., Pinto, J. R., and Potter, J. D. (2010). Mutations in Troponin that Cause HCM, DCM and RCM: what Can We Learn about Thin Filament Function? *J. Mol. Cell. Cardiol.* 48, 882–892. doi:10.1016/j.yjmcc.2009.10.031

Wolska, B. M., Kitada, Y., Palmiter, K. A., Westfall, M. V., Johnson, M. D., and Solaro, R. J. (1996). CGP-48506 Increases Contractility of Ventricular Myocytes and Myofilaments by Effects on Actin-Myosin Reaction. *Am. J. Physiology-Heart Circulatory Physiology* 270, H24–H32. doi:10.1152/ajpheart.1996.270.1.H24

Woody, M. S., Greenberg, M. J., Barua, B., Winkelmann, D. A., Goldman, Y. E., and Ostap, E. M. (2018). Positive Cardiac Inotrope Omecamtiv Mecarbil Activates Muscle Despite Suppressing the Myosin Working Stroke. *Nat. Commun.* 9, 3838. doi:10.1038/s41467-018-06193-2

Yamada, Y., Namba, K., and Fujii, T. (2020). Cardiac Muscle Thin Filament Structures Reveal Calcium Regulatory Mechanism. *Nat. Commun.* 11, 153. doi:10.1038/s41467-019-14008-1

Conflict of Interest: The authors declare that the research was conducted in the absence of any commercial or financial relationships that could be construed as a potential conflict of interest.

Publisher's Note: All claims expressed in this article are solely those of the authors and do not necessarily represent those of their affiliated organizations, or those of the publisher, the editors and the reviewers. Any product that may be evaluated in this article, or claim that may be made by its manufacturer, is not guaranteed or endorsed by the publisher.

frontiers | Frontiers in Physiology

MINI REVIEW
published: 22 June 2022
doi: 10.3389/fphys.2022.932333

Modeling Human Cardiac Thin Filament Structures

Michael J. Rynkiewicz, Elumalai Pavadai and William Lehman*

Department of Physiology and Biophysics, Boston University School of Medicine, Boston, MA, United States

Striated muscle contraction is regulated in a calcium-dependent manner through dynamic motions of the tropomyosin/troponin polymer, a multicomponent complex wrapped around actin-containing thin filaments. Tropomyosin/troponin sterically blocks myosin-binding at low-calcium concentrations but moves to expose myosin-binding sites at high-calcium concentrations leading to force development. Understanding the key intermolecular interactions that define these dynamic motions will promote our understanding of mutation-induced contractile dysfunction that eventually leads to hypertrophic cardiomyopathy, dilated cardiomyopathy, and skeletal myopathies. Advancements in cryoelectron microscopy (cryoEM) have resulted in a partial elucidation of structures of the thin filament, revealing many atomic-level interactions between the component proteins and critical calcium-dependent conformational alterations. However, building models at the resolutions achieved can be challenging since landmarks in the maps are often missing or ambiguous. Therefore, current computational analyses including *de novo* structure prediction, protein-protein docking, molecular dynamics flexible fitting, and molecular dynamics simulations are needed to ensure good quality models. We review here our efforts to model the troponin T domain spanning the head-to-tail overlap domain of tropomyosin, improving previous models. Next, we refined the published cryoEM modeled structures, which had mistakenly compressed alpha helices, with a model that has expected helical parameters while matching densities in the cryoEM volume. Lastly, we used this model to reinterpret the interactions between tropomyosin and troponin I showing key features that hold the tropomyosin cable in its low-calcium, sterically blocking position. These revised thin filament models show improved intermolecular interactions in the key low- and high-calcium regulatory states, providing novel insights into function.

Keywords: tropomyosin, actin, troponin, cryoEM, protein-protein docking

OPEN ACCESS

Edited by:
Shin'Ichi Ishiwata,
Waseda University, Japan

Reviewed by:
Murali Chandra,
Washington State University, United States
Neil Kad,
University of Kent, United Kingdom

****Correspondence:***
Michael J. Rynkiewicz
rynkiemj@bu.edu

Specialty section:
This article was submitted to Striated Muscle Physiology, a section of the journal Frontiers in Physiology

Received: *03 May 2022*
Accepted: *31 May 2022*
Published: *22 June 2022*

Citation:
Rynkiewicz MJ, Pavadai E and Lehman W (2022) Modeling Human Cardiac Thin Filament Structures. Front. Physiol. 13:932333. doi: 10.3389/fphys.2022.932333

INTRODUCTION

The improvements in methodology of cryoelectron microscopy (cryoEM) have pushed the limit of resolution achievable by this technique to unprecedented levels, allowing visualization of previously unseen structural details in the thin filament of the sarcomere in striated muscle (Doran et al., 2020; Yamada et al., 2020; Risi et al., 2021a; Risi et al., 2021b; Wang et al., 2021; Wang et al., 2022). These thin filaments consist of actin, tropomyosin, and the troponin complex whose structural transitions regulate contraction in a calcium-dependent manner (reviewed in Lehman, 2016). Tropomyosin is an alpha-helical, coiled-coil protein that forms a head-to-tail polymeric cable wrapped helically around the central actin core of the filament (Hitchcock-DeGregori, 2008; Holmes and Lehman,

2008). The head-to-tail region stabilizing the polymer is formed by an overlap between adjacent tropomyosin dimers of about 11 amino acids where the coiled coil becomes a 4-helix bundle (Greenfield et al., 2006; Frye et al., 2010). The troponin complex consists of three proteins—troponin C (TnC), troponin I (TnI), and troponin T (TnT) (Gordon et al., 2000). TnC along with the N-terminal domains of TnI and the C-terminal domains of TnT form a central core (Takeda et al., 2003; Yamada et al., 2020; also reviewed in Tobacman, 2021). The N-terminal domains of TnT extend from the core to anchor the troponin complex to tropomyosin. Under low calcium conditions, the C-terminus of TnI extends outward from the core where it binds actin and tropomyosin, thus locking the cable in a blocked state position that sterically inhibits myosin access to the thin filament leading to relaxation of the muscle. Higher calcium concentrations lead to conformational changes in calcium-bound TnC that recruit TnI back to the core, releasing the steric block and forming a closed state. Myosin binding to the closed state then results in a further shift of the cable to an open state leading to contraction of the muscle. Thus, the thin filament accesses three structural states—B-state (blocked), C-state (closed), and M-state (open) in its regulatory transitions, as originally proposed by McKillop and Geeves (1993) and by Vibert et al. (1997). All three of these states have now been elucidated by cryoEM (Doran et al., 2020; Yamada et al., 2020) using cardiac muscle filaments (**Figure 1**).

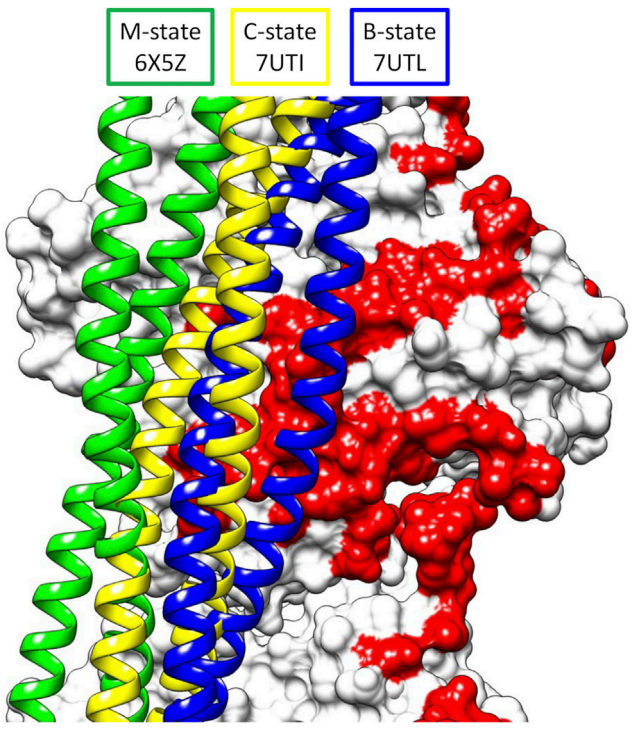

FIGURE 1 | Superposition of the three structural states of tropomyosin during thin filament activation of the M-state (green), C-state (yellow), and B-state (blue) showing the movement of tropomyosin over actin (white surface, pointed end up). Note the steric blocking of the myosin binding site (red) is relieved as tropomyosin moves from B- to M-state.

The development of inherited cardiomyopathies starts with an insult to the contractile machinery that alters the force characteristics of the heart and eventually leads to pathological remodeling (Deranek et al., 2019). Therefore, these cryo-EM structures offer vast potential to increase our understanding of the genesis of cardiomyopathies or to develop novel therapeutics. However, it is critical that accurate atomic-level details are incorporated into the models of the thin filament being used. Otherwise, errors in the structure will propagate into the predictions, leading to misleading or incorrect data, and impeding efforts to develop therapeutics. As will be shown, some regions of the thin filament structure require extra consideration to achieve this needed accuracy.

MODELING CARDIAC THIN FILAMENT STRUCTURES FROM CRYOELECTRON MICROSCOPY ELECTRON DENSITY MAPS

Challenges of Interpreting Electron Density Maps

A quality structure should not only fit the cryoEM density map well but have good chemical parameters, including optimized interactions between proteins or domains, and ideally representing the global energy minimum structure. Unfortunately, the resolutions achieved in the current cryoEM structures may be insufficient to unambiguously build a model in some sections of the electron density map. While programs such as MolProbity (Chen et al., 2010) can be used to check the bonds, angles, and backbone/side chain dihedrals of a structure, they do not check the reasonableness of the tertiary or quaternary structures. The register of the protein side chains to the map may be difficult to determine due to lack of visible landmarks such as large side chains. Additionally, starting models based on x-ray crystal structures of isolated domains or fragments may have errors, such as packing artefacts, that may not be resolved to the global energy minimum during refinement, instead getting trapped in a local energy minimum. Thus, a search method that quickly tests a large number of possible structures is needed. In our group, we have been using protein-protein docking to search billions of possible binding poses for a low-energy structure that fits the density map using ClusPro2.0 (Kozakov et al., 2017). These initial poses are ranked by an energy function containing terms such as attractive and repulsive van der Waals' energy, electrostatic energy, and the desolvation energy. The representative structures from the largest clusters using the top 1,000 poses are then side-chain minimized to optimize the final energies in the output rankings. The top scoring poses, which can be calculated with a number of different weighting schemes, are then analyzed by the experimentalist to incorporate any available outside data (fit to an electron density map, mutational analysis, and known close residue-residue contacts) and the highest scoring pose(s) that satisfy the data are selected. As a check of the quality of the docked models, molecular dynamics simulations are performed to check the stability of model as well as fine tune structural interfaces by exploring conformations not tested during the rigid-body docking calculations.

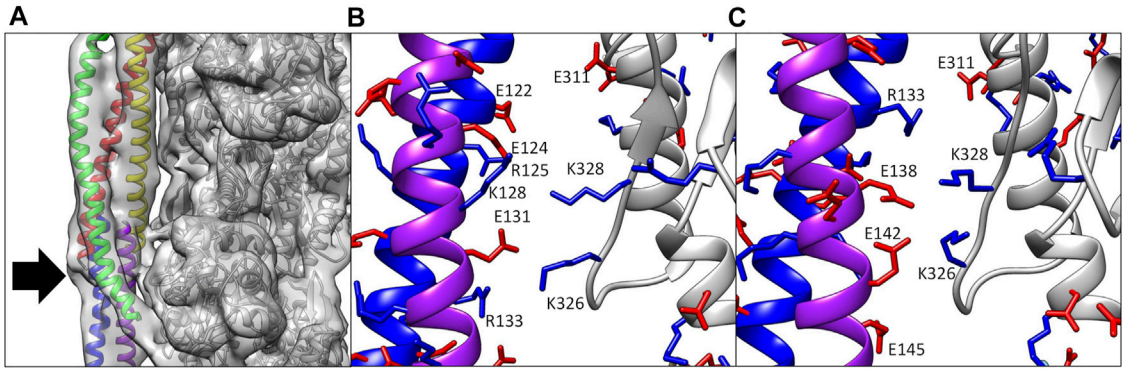

FIGURE 2 | (A) Electron density map of the cardiac thin filament solved in calcium-free conditions. Note the tubular density for both tropomyosin (red, yellow, blue, and purple ribbon) and TnT1 (green ribbon), which could be fit by a number of potential structures. The only landmark here for the modeler is the N- and C-termini of tropomyosin (arrow). **(B)** Ca^{2+}-bound model (Yamada et al., 2020) showing poor alignment of positive (blue sticks) and negative residues (red sticks) between actin (gray ribbon) and tropomyosin (blue and purple ribbons). **(C)** Ca^{2+}-bound model (Pavadai et al., 2020) in a similar orientation as **(B)**. Note the improved alignment of charged residues after rebuilding.

Of particular interest here, the coiled-coil structure of tropomyosin appears in the maps as two intertwined tubes and the TnT domain (TnT1) that extends over the polymeric overlap domain of tropomyosin is also a simple tube (**Figure 2A**). By translating and/or rotating the helices in the tropomyosin or TnT1 models, a large number of models that satisfy the electron density map can be generated, and selection of the final model requires careful consideration. Using ideal models, secondary structure prediction, and protein-protein docking, we were able to refine the models of the TnT1/tropomyosin overlap domain (Pavadai et al., 2019) and the coiled coil of tropomyosin in thin filaments solved in calcium-free and calcium-bound conditions (Pavadai et al., 2020; Lehman et al., 2021).

Tropomyosin Contacts With Actin in Cryoelectron Microscopy Structures

The solution of the cryoEM structure of the cardiac thin filament in calcium-free and calcium-bound states by Yamada et al. revealed many key relationships between tropomyosin, actin, and troponin. Analysis of the structure by our group, however, revealed unfavorable interactions between tropomyosin and actin in the Yamada modeling. The authors had started with a homology model of tropomyosin based on a low resolution (7 Å) crystal structure (Whitby and Phillips, 2000) whose coiled-coil pitch was longer than that present in the electron density maps [147 Å vs. 138 Å, as measured by the program Twister (Strelkov and Burkhard, 2002)]. In the final structure, both the end-to-end length of tropomyosin and the alpha helical rise were smaller than the expected values (see Table 4 in Pavadai et al., 2020). This may have been a result of compression of the helices during refinement as the coiled-coil pitch was reduced to match the maps. The result is that the tropomyosin present in these structures makes poor interactions with actin and cannot be extended into a polymeric cable.

We took two approaches to fitting tropomyosin into the electron density maps. First, we generated ideal, computer generated coiled-coil structures (Lorenz et al., 1995) with different rotations around their super-helical axis. Side chains in these models were derived from high resolution crystal structures of tropomyosin fragments (Li et al., 2010; Li et al., 2011; Rynkiewicz et al., 2015). After rigid body fitting of these models into the electron density maps in Chimera (Pettersen et al., 2004), the model that most closely matched the observed position of the C-terminus in the maps was selected for further fitting with molecular dynamics flexible fitting (MDFF) (Trabuco et al., 2008). The fitted coiled coil then had the previously published overlap domain/TnT1 model (Pavadai et al., 2019) grafted on to create the model used for molecular dynamics.

The above method does not account for any localized twisting, which can optimize tropomyosin/actin interactions (Lehman et al., 2018). Therefore, we used protein-protein docking to sample tropomyosin-actin interactions over a broader range of conformational space. We used a "divide and conquer" strategy whereby tropomyosin was divided into four pieces of about 60 amino acids in the middle of the molecule and an overlap domain of about 100 amino acids, each having about 20 amino acids overlapping with their neighboring segments. The list of poses docked to a model comprising two actin subunits was analyzed for fit to the electron density map, proper polarity, and overlap with neighboring poses. Through fusion of the overlapping regions in the various docked poses, the entire tropomyosin cable was built out and further fit into the cryo-EM density using MDFF, yielding a structure that has locally optimized interactions with actin. The models from the two methods are very similar, with both showing improved electrostatic interactions with actin (compare **Figures 2B,C**; see also Table 1 in Pavadai et al., 2020).

We also used this approach to model tropomyosin in the calcium-free (B-state) structure (Pavadai et al., 2020; Lehman et al., 2021), which shows similar compression in the tropomyosin helices as observed in the calcium-bound (C-state) structure. Again, we built models from ideal coiled coils and docking of smaller fragments of tropomyosin. Here, the

docking models were key to guiding the building process, since the twist of tropomyosin is not equal across the entire molecule in the calcium-free maps, thus an ideal coiled coil structure does not fit in the map well without real space refinements. Analysis of the resulting models showed improvements to the interactions with actin, showing key salt bridges between actin residues Lys326, Lys328, and Asp311 and oppositely charged amino acids along the entire tropomyosin chain.

Lastly, the docking method was used to model tropomyosin in the M-state by fitting to the nucleotide-free rigor actomyosin-tropomyosin complex cryoEM map (Doran et al., 2020). This map also shows tropomyosin as two, intertwined tubes with no landmarks to guide positioning. Thus, assignment of the tropomyosin residues required the above approaches. The resulting model shows that tropomyosin movement from C-state to M-state is mostly a rotation around the actin helical axis, with little longitudinal movement or rotation around its own axis. The model also showed interactions between tropomyosin and loop four of myosin, notably between Arg369 and oppositely charged residues on tropomyosin.

Tropomyosin Contacts With Troponin T and Troponin I in Cryoelectron Microscopy Structures

In addition to actin, tropomyosin also makes key interactions with TnT and TnI. TnT contains a TnT1 domain (residues 89–151 in cardiac TnT isoform 6) that is bound to the tropomyosin overlap domain in the cryoEM structure (Yamada et al., 2020), where it anchors the troponin complex to the thin filament, stabilizes the tropomyosin overlap domain, and maintains the 1:1 stoichiometry of troponin with tropomyosin in the thin filament (Flicker et al., 1982). Previously, a complex of peptides of TnT1 and the tropomyosin overlap domain had been solved in an x-ray crystal structure (Murakami et al., 2008). However, this crystal structure has poor density for the TnT and N-terminal tropomyosin peptides as well as a stoichiometry inconsistent with the thin filament. This crystal structure was used to guide the placement of the TnT1 domain by several groups (Manning et al., 2011; Gangadharan et al., 2017; Williams et al., 2018; Yamada et al., 2020) resulting in models that show poor contacts between TnT1 and tropomyosin. Thus, a method such as protein-protein docking, with a much larger exploration of conformational space and therefore a lower potential bias, seemed ideal for this system.

We started by docking alpha helical segments of TnT1 [residues 70–170 of cardiac TnT are ~90% alpha helix as measured by circular dichroism (Palm et al., 2001)] to a model of the tropomyosin overlap domain based on the NMR solution structure and extended to a full filament (Greenfield et al., 2006; Orzechowski et al., 2014). The docking poses were analyzed to select poses that span the overlap in the expected antiparallel orientation to tropomyosin (Flicker et al., 1982; Cabral-Lilly et al., 1997; Jin and Chong, 2010). We used small, helical fragments with overlapping residues to extend TnT1 across the curved overlap domain of tropomyosin using multiple docking runs. The docking studies were terminated when high-scoring poses that could be reasonably added to the growing chain were predicted to make major clashes with actin.

In this way, cardiac TnT1 residues 89–151 and skeletal muscle TnT1 residues 79–141 were docked onto the tropomyosin overlap domain. The structures were similar with the exception of a pocket in the protein-protein interface of the cardiac TnT1/tropomyosin model not found in the skeletal muscle model. The models were stable in molecular dynamics simulations, with small fluctuations of the TnT1 termini. Consistent with the approximately 20 nM dissociation constant for TnT1/tropomyosin (Tobacman et al., 2002; Jin and Chong, 2010; Gangadharan et al., 2017), the cardiac TnT1 model showed a large, buried solvent-accessible surface area between the two proteins (an average of 2,295 $Å^2$ during molecular dynamics) and many strong electrostatic interactions—representing an improvement over the previous models (Pavadai et al., 2020). After publication of the cryoEM maps from Yamada et al. (2020), we found that our TnT1/tropomyosin model had an excellent fit to the electron density map, thus cross-validating the two models.

The final part of the tropomyosin model to analyze was its interaction with the C-terminus of TnI. The C-terminus of TnI consists of several domains—the inhibitory peptide (residues 137–148 in cardiac TnI) which binds to actin, then the switch peptide (residues 149–163) which binds either actin or TnC in a calcium-dependent manner, and finally a H_4-helix (residues 164–184) and C-terminal tail domain (residues 185–210) that bind actin in the calcium-free structure locking it in the sterically blocking position, but are unresolved and presumably disordered in the calcium-bound maps (Yamada et al., 2020). The latter three domains make potential calcium-dependent interactions with tropomyosin in the Yamada et al. structure; however, as discussed above, they were refined against a compressed tropomyosin. For example, analysis of the deposited coordinates show several charged tropomyosin residues (Arg133, Lys136, Glu138, Lys140 and Glu145) interacting with hydrophobic patch on TnI formed by residues 155–173, thus suggesting a modeling error.

After docking and refitting of the tropomyosin model, the TnI C-terminus was also docked to the model to check the proper placement of this domain. The refined structure shows hydrophobic residues on tropomyosin (Ala155, Ile154, Ala151, Leu148, Ile146, and Ile143) now in contact with TnI residues 155–173 (see Figure 3 in Lehman et al., 2021). Energy analysis of the tropomyosin/TnI contacts showed that most of the binding energy comes from association of the helix H_4 and C-terminal domains with tropomyosin. On the other hand, most of the actin/TnI binding energy is contained in the inhibitory peptide.

DISCUSSION

As stated in the Introduction, accurate models of the thin filament are essential for understanding regulation of muscle contraction and early events in the development of inherited cardiomyopathies. Here, our group has used protein-protein

docking methods along with molecular dynamics to refine cryoEM-derived models (Yamada et al., 2020). The regulatory function of the thin filament requires dynamic motions of tropomyosin/troponin and it is essential that the models accurately represent the key interactions of these proteins in their various structural states. The cooperative nature of the regulatory transitions suggests that long-range effects could be common for cardiomyopathy-causing mutations, therefore a globally accurate model of the thin filament is crucial for formation of mechanistic hypotheses. For example, in the hypertrophic cardiomyopathy tropomyosin mutant E192K (Sewanan et al., 2021), residue 192 was found to pass over a charged patch on actin that would be unfavorable for the mutant, potentially impairing tropomyosin's ability to return to a sterically-blocking state. In the case of the dilated cardiomyopathy tropomyosin mutant M8R (Racca et al., 2020), the mutational effects in molecular dynamics simulations are local on the structure of the overlap domain, but there are also long-range shifts in the middle residues of tropomyosin to azimuthal positions predicted to enhance steric-blocking in low calcium conditions leading to hypocontractility. In this case, since the mutation is in the head-to-tail overlap domain, having proper helical structure in the tropomyosin model and coiled-coil helical symmetry matching that of actin was critical to accurately propagate mutational effects in the simulation both within and across tropomyosin dimers in the thin filament cable. Most recently, we have used the docking techniques discussed here to model the cardiac-specific N-terminus on TnI (Pavadai et al., 2022) which is the target of protein kinase A phosphorylation at serine residues 23 and 24. The model proposes that positively charged residues on tropomyosin, notably Arg 160, can interact with the phosphoserines, potentially biasing tropomyosin to a sterically blocking state and contributing to the observed increased relaxation rate found during adrenergic stimulation in the heart. Interestingly, E40K, E54K, and D230N mutations in cardiac tropomyosin have been shown to abolish cardiac TnI phosphorylation-dependent effects on calcium sensitivity *in vitro* assays of tissue-purified proteins (Memo et al., 2013), and the new model will help to understand the molecular basis of these observations. In the above examples, the derived mechanistic hypotheses critically rely on accurate representations of the thin filament proteins and their interactions along the entire length of the filament.

There are still some unresolved portions of the thin filament which may contribute to thin filament energetics, and these need to be accurately modeled to fully unlock the predictive power of the thin filament models. These include the linker region of TnT, which connects the TnT1 domain to the troponin core and the hypervariable N-terminus of TnT, an intriguing part of the thin filament, which may act as a calcium reservoir in insect muscle (Cao et al., 2020). These regions show weak or no density in the maps so they are presumably disordered, making modeling challenging. They could be represented by a small ensemble of structures generated using the computational techniques discussed here using biochemical data to guide the selection of the docking poses included in the final structure. The structures presented here could also be used as templates to make homology models of skeletal muscle thin filaments to propose mechanistic hypotheses explaining mutations that lead to skeletal myopathies. However, one must always inspect the intra- and intermolecular interactions formed by the proteins in the filament to ensure that these interactions are chemically reasonable and the resulting models are of the highest quality achievable.

AUTHOR CONTRIBUTIONS

MJR wrote the manuscript and made the figures. WL and EP edited the manuscript. All authors contributed to the formulation of the models of the thin filament discussed in the article.

FUNDING

This work was funded by National Institutes of Health grants R01HL036153 (to WL).

REFERENCES

Cabral-Lilly, D., Tobacman, L. S., Mehegan, J. P., and Cohen, C. (1997). Molecular Polarity in Tropomyosin-Troponin T Co-crystals. *Biophysical J.* 73, 1763–1770. doi:10.1016/s0006-3495(97)78206-7

Cao, T., Sujkowski, A., Cobb, T., Wessells, R. J., and Jin, J.-P. (2020). The Glutamic Acid-Rich-Long C-Terminal Extension of Troponin T Has a Critical Role in Insect Muscle Functions. *J. Biol. Chem.* 295, 3794–3807. doi:10.1074/jbc.ra119.012014

Chen, V. B., Arendall, W. B., 3rd, Headd, J. J., Keedy, D. A., Immormino, R. M., Kapral, G. J., et al. (2010). MolProbity: All-Atom Structure Validation for Macromolecular Crystallography. *Acta Crystallogr. D. Biol. Cryst.* 66, 12–21. doi:10.1107/s0907444909042073

Deranek, A. E., Klass, M. M., and Tardiff, J. C. (2019). Moving beyond Simple Answers to Complex Disorders in Sarcomeric Cardiomyopathies: the Role of Integrated Systems. *Pflugers Arch. - Eur. J. Physiol.* 471, 661–671. doi:10.1007/s00424-019-02269-0

Doran, M. H., Pavadai, E., Rynkiewicz, M. J., Walklate, J., Bullitt, E., Moore, J. R., et al. (2020). Cryo-EM and Molecular Docking Shows Myosin Loop 4 Contacts Actin and Tropomyosin on Thin Filaments. *Biophysical J.* 119, 821–830. doi:10.1016/j.bpj.2020.07.006

Flicker, P. F., Phillips, G. N., Jr, and Cohen, C. (1982). Troponin and its Interactions with Tropomyosin. *J. Mol. Biol.* 162, 495–501. doi:10.1016/0022-2836(82)90540-x

Frye, J., Klenchin, V. A., and Rayment, I. (2010). Structure of the Tropomyosin Overlap Complex from Chicken Smooth Muscle: Insight into the Diversity of N-Terminal Recognition, *Biochemistry* 49, 4908–4920. doi:10.1021/bi100349a

Gangadharan, B., Sunitha, M. S., Mukherjee, S., Chowdhury, R. R., Haque, F., Sekar, N., et al. (2017). Molecular Mechanisms and Structural Features of Cardiomyopathy-Causing Troponin T Mutants in the Tropomyosin Overlap Region. *Proc. Natl. Acad. Sci. U.S.A.* 114, 11115–11120. doi:10.1073/pnas.1710354114

Gordon, A. M., Homsher, E., and Regnier, M. (2000). Regulation of Contraction in Striated Muscle. *Physiol. Rev.* 80, 853–924. doi:10.1152/physrev.2000.80.2.853

Greenfield, N. J., Huang, Y. J., Swapna, G. V. T., Bhattacharya, A., Rapp, B., Singh, A., et al. (2006). Solution NMR Structure of the Junction between Tropomyosin Molecules: Implications for Actin Binding and Regulation. *J. Mol. Biol.* 364, 80–96. doi:10.1016/j.jmb.2006.08.033

Hitchcock-DeGregori, S. E. (2008). Tropomyosin: Function Follows Structure. *Adv. Exp. Med. Biol.* 644, 60–72. doi:10.1007/978-0-387-85766-4_5

Holmes, K. C., and Lehman, W. (2008). Gestalt-binding of Tropomyosin to Actin Filaments. *J. Muscle Res. Cell Motil.* 29, 213–219. doi:10.1007/s10974-008-9157-6

Jin, J.-P., and Chong, S. M. (2010). Localization of the Two Tropomyosin-Binding Sites of Troponin T. *Archives Biochem. Biophysics* 500, 144–150. doi:10.1016/j.abb.2010.06.001

Kozakov, D., Hall, D. R., Xia, B., Porter, K. A., Padhorny, D., Yueh, C., et al. (2017). The ClusPro Web Server for Protein-Protein Docking. *Nat. Protoc.* 12, 255–278. doi:10.1038/nprot.2016.169

Lehman, W., Li, X., Kiani, F. A., Moore, J. R., Campbell, S. G., Fischer, S., et al. (2018). Precise Binding of Tropomyosin on Actin Involves Sequence-dependent Variance in Coiled-Coil Twisting. *Biophysical J.* 115, 1082–1092. doi:10.1016/j.bpj.2018.08.017

Lehman, W., Pavadai, E., and Rynkiewicz, M. J. (2021). C-terminal Troponin-I Residues Trap Tropomyosin in the Muscle Thin Filament Blocked-State. *Biochem. Biophysical Res. Commun.* 551, 27–32. doi:10.1016/j.bbrc.2021.03.010

Lehman, W. (2016). Thin Filament Structure and the Steric Blocking Model. *Compr. Physiol.* 6, 1043–1069. doi:10.1002/cphy.c150030

Li, X., Holmes, K. C., Lehman, W., Jung, H., and Fischer, S. (2010). The Shape and Flexibility of Tropomyosin Coiled Coils: Implications for Actin Filament Assembly and Regulation. *J. Mol. Biol.* 395, 327–339. doi:10.1016/j.jmb.2009.10.060

Li, X., Tobacman, L. S., Mun, J. Y., Craig, R., Fischer, S., and Lehman, W. (2011). Tropomyosin Position on F-Actin Revealed by EM Reconstruction and Computational Chemistry. *Biophysical J.* 100, 1005–1013. doi:10.1016/j.bpj.2010.12.3697

Lorenz, M., Poole, K. J. V., Popp, D., Rosenbaum, G., and Holmes, K. C. (1995). An Atomic Model of the Unregulated Thin Filament Obtained by X-Ray Fiber Diffraction on Oriented Actin-Tropomyosin Gels. *J. Mol. Biol.* 246, 108–119. doi:10.1006/jmbi.1994.0070

Manning, E. P., Tardiff, J. C., and Schwartz, S. D. (2011). A Model of Calcium Activation of the Cardiac Thin Filament. *Biochemistry* 50, 7405–7413. doi:10.1021/bi200506k

McKillop, D. F., and Geeves, M. A. (1993). Regulation of the Interaction between Actin and Myosin Subfragment 1: Evidence for Three States of the Thin Filament. *Biophysical J.* 65, 693–701. doi:10.1016/s0006-3495(93)81110-x

Memo, M., Leung, M.-C., Ward, D. G., dos Remedios, C., Morimoto, S., Zhang, L., et al. (2013). Familial Dilated Cardiomyopathy Mutations Uncouple Troponin I Phosphorylation from Changes in Myofibrillar Ca2+ Sensitivity. *Cardiovasc Res.* 99, 65–73. doi:10.1093/cvr/cvt071

Murakami, K., Stewart, M., Nozawa, K., Tomii, K., Kudou, N., Igarashi, N., et al. (2008). Structural Basis for Tropomyosin Overlap in Thin (Actin) Filaments and the Generation of a Molecular Swivel by Troponin-T. *Proc. Natl. Acad. Sci. U.S.A.* 105, 7200–7205. doi:10.1073/pnas.0801950105

Orzechowski, M., Li, X., Fischer, S., and Lehman, W. (2014). An Atomic Model of the Tropomyosin Cable on F-Actin. *Biophysical J.* 107, 694–699. doi:10.1016/j.bpj.2014.06.034

Palm, T., Graboski, S., Hitchcock-DeGregori, S. E., and Greenfield, N. J. (2001). Disease-causing Mutations in Cardiac Troponin T: Identification of a Critical Tropomyosin-Binding Region. *Biophysical J.* 81, 2827–2837. doi:10.1016/s0006-3495(01)75924-3

Pavadai, E., Rynkiewicz, M. J., Ghosh, A., and Lehman, W. (2019). Docking Troponin T onto the Tropomyosin Overlapping Domain of Thin Filaments. *Biophys. J.* 118, 325–336. doi:10.1016/j.bpj.2019.11.3393

Pavadai, E., Lehman, W., and Rynkiewicz, M. J. (2020). Protein-Protein Docking Reveals Dynamic Interactions of Tropomyosin on Actin Filaments. *Biophysical J.* 119, 75–86. doi:10.1016/j.bpj.2020.05.017

Pavadai, E., Rynkiewicz, M. J., Yang, Z., Gould, I. R., Marston, S. B., and Lehman, W. (2022). Modulation of Cardiac Thin Filament Structure by Phosphorylated Troponin-I Analyzed by Protein-Protein Docking and Molecular Dynamics Simulation. *Archives Biochem. Biophysics* 725, 109282. In press. doi:10.1016/j.abb.2022.109282

Pettersen, E. F., Goddard, T. D., Huang, C. C., Couch, G. S., Greenblatt, D. M., Meng, E. C., et al. (2004). UCSF Chimera?A Visualization System for Exploratory Research and Analysis. *J. Comput. Chem.* 25, 1605–1612. doi:10.1002/jcc.20084

Racca, A. W., Rynkiewicz, M. J., LaFave, N., Ghosh, A., Lehman, W., and Moore, J. R. (2020). M8R Tropomyosin Mutation Disrupts Actin Binding and Filament Regulation: The Beginning Affects the Middle and End. *J. Biol. Chem.* 295, 17128–17137. doi:10.1074/jbc.ra120.014713

Risi, C. M., Pepper, I., Belknap, B., Landim-Vieira, M., White, H. D., Dryden, K., et al. (2021a). The Structure of the Native Cardiac Thin Filament at Systolic Ca2+ Levels. *Proc. Natl. Acad. Sci. U. S. A.* 118, e2024288118. doi:10.1073/pnas.2024288118

Risi, C., Schäfer, L. U., Belknap, B., Pepper, I., White, H. D., Schröder, G. F., et al. (2021b). High-Resolution Cryo-EM Structure of the Cardiac Actomyosin Complex. *Structure* 29, 50–60. doi:10.1016/j.str.2020.09.013

Rynkiewicz, M. J., Schott, V., Orzechowski, M., Lehman, W., and Fischer, S. (2015). Electrostatic Interaction Map Reveals a New Binding Position for Tropomyosin on F-Actin. *J. Muscle Res. Cell Motil.* 36, 525–533. doi:10.1007/s10974-015-9419-z

Sewanan, L. R., Park, J., Rynkiewicz, M. J., Racca, A. W., Papoutsidakis, N., Schwan, J., et al. (2021). Loss of Crossbridge Inhibition Drives Pathological Cardiac Hypertrophy in Patients Harboring the TPM1 E192K Mutation. *J. Gen. Physiol.* 153, e202012640. doi:10.1085/jgp.202012640

Strelkov, S. V., and Burkhard, P. (2002). Analysis of α-Helical Coiled Coils with the Program TWISTER Reveals a Structural Mechanism for Stutter Compensation. *J. Struct. Biol.* 137, 54–64. doi:10.1006/jsbi.2002.4454

Takeda, S., Yamashita, A., Maeda, K., and Maéda, Y. (2003). Structure of the Core Domain of Human Cardiac Troponin in the Ca2+-Saturated Form. *Nature* 424, 35–41. doi:10.1038/nature01780

Tobacman, L. S., Nihli, M., Butters, C., Heller, M., Hatch, V., Craig, R., et al. (2002). The Troponin Tail Domain Promotes a Conformational State of the Thin Filament that Suppresses Myosin Activity. *J. Biol. Chem.* 277, 27636–27642. doi:10.1074/jbc.m201768200

Tobacman, L. S. (2021). Troponin Revealed: Uncovering the Structure of the Thin Filament On-Off Switch in Striated Muscle. *Biophysical J.* 120, 1–9. doi:10.1016/j.bpj.2020.11.014

Trabuco, L. G., Villa, E., Mitra, K., Frank, J., and Schulten, K. (2008). Flexible Fitting of Atomic Structures into Electron Microscopy Maps Using Molecular Dynamics. *Structure* 16, 673–683. doi:10.1016/j.str.2008.03.005

Vibert, P., Craig, R., and Lehman, W. (1997). Steric-model for Activation of Muscle Thin Filaments. *J. Mol. Biol.* 266, 8–14. doi:10.1006/jmbi.1996.0800

Wang, Z., Grange, M., Pospich, S., Wagner, T., Kho, A. L., Gautel, M., et al. (2022). Structures from Intact Myofibrils Reveal Mechanism of Thin Filament Regulation through Nebulin. *Science* 375, eabn1934. doi:10.1126/science.abn1934

Wang, Z., Grange, M., Wagner, T., Kho, A. L., Gautel, M., and Raunser, S. (2021). The Molecular Basis for Sarcomere Organization in Vertebrate Skeletal Muscle. *Cell* 184, 2135–2150. e13. doi:10.1016/j.cell.2021.02.047

Whitby, F. G., and Phillips, G. N., Jr. (2000). Crystal Structure of Tropomyosin at 7 Ångstroms Resolution. *Proteins* 38, 49–59. doi:10.1002/(sici)1097-0134(20000101)38:1<49:aid-prot6>3.0.co;2-b

Williams, M. R., Tardiff, J. C., and Schwartz, S. D. (2018). Mechanism of Cardiac Tropomyosin Transitions on Filamentous Actin as Revealed by All-Atom Steered Molecular Dynamics Simulations. *J. Phys. Chem. Lett.* 9, 3301–3306. doi:10.1021/acs.jpclett.8b00958

Yamada, Y., Namba, K., and Fujii, T. (2020). Cardiac Muscle Thin Filament Structures Reveal Calcium Regulatory Mechanism. *Nat. Commun.* 11, 153. doi:10.1038/s41467-019-14008-1

Conflict of Interest: The authors declare that the research was conducted in the absence of any commercial or financial relationships that could be construed as a potential conflict of interest.

Publisher's Note: All claims expressed in this article are solely those of the authors and do not necessarily represent those of their affiliated organizations, or those of the publisher, the editors and the reviewers. Any product that may be evaluated in this article, or claim that may be made by its manufacturer, is not guaranteed or endorsed by the publisher.

frontiers | Frontiers in Physiology

REVIEW
published: 30 June 2022
doi: 10.3389/fphys.2022.914296

Protein Quality Control at the Sarcomere: Titin Protection and Turnover and Implications for Disease Development

Sebastian Kötter and Martina Krüger*

Department of Cardiovascular Physiology, Medical Faculty and University Hospital Düsseldorf, Heinrich-Heine-University Düsseldorf, Düsseldorf, Germany

Sarcomeres are mainly composed of filament and signaling proteins and are the smallest molecular units of muscle contraction and relaxation. The sarcomere protein titin serves as a molecular spring whose stiffness mediates myofilament extensibility in skeletal and cardiac muscle. Due to the enormous size of titin and its tight integration into the sarcomere, the incorporation and degradation of the titin filament is a highly complex task. The details of the molecular processes involved in titin turnover are not fully understood, but the involvement of different intracellular degradation mechanisms has recently been described. This review summarizes the current state of research with particular emphasis on the relationship between titin and protein quality control. We highlight the involvement of the proteasome, autophagy, heat shock proteins, and proteases in the protection and degradation of titin in heart and skeletal muscle. Because the fine-tuned balance of degradation and protein expression can be disrupted under pathological conditions, the review also provides an overview of previously known perturbations in protein quality control and discusses how these affect sarcomeric proteins, and titin in particular, in various disease states.

Keywords: connectin, degradation, proteasome, autophagy, proteases, heat-shock-proteins

OPEN ACCESS

Edited by:
Norio Fukuda,
Jikei University School of Medicine, Japan

Reviewed by:
Charles S. Chung,
Wayne State University, United States
Mathias Gautel,
King's College London, United Kingdom

****Correspondence:***
Sebastian Kötter
sebastian.koetter@uni-duesseldorf.de

Specialty section:
This article was submitted to Striated Muscle Physiology, a section of the journal Frontiers in Physiology

Received: *06 April 2022*
Accepted: *10 June 2022*
Published: *30 June 2022*

Citation:
Kötter S and Krüger M (2022) Protein Quality Control at the Sarcomere: Titin Protection and Turnover and Implications for Disease Development. Front. Physiol. 13:914296. doi: 10.3389/fphys.2022.914296

1 INTRODUCTION

The sarcomere scaffold of striated muscle cells is formed by three filaments: The thick filament consisting of myosin, the thin filament formed by actin, and the titin filament. While myosin and actin are mainly responsible for the Ca^{2+}-dependent force development of the sarcomere, several different functions are attributed to the titin filament. Due to its very specific structure and position in the sarcomere, titin plays a particularly important role in shaping the viscoelastic properties of myofilaments. In this role, titin acts as a molecular spring and, along with collagen, is the main determinant of passive elastic force in muscle cells (Granzier and Irving, 1995; Linke, 2008; Tskhovrebova and Trinick, 2010; Gautel, 2011b). In addition, titin participates in the complex mechanisms determining length-dependent activation, is responsible for keeping thick filaments in the center of the sarcomere, assists in sarcomere assembly, and is a hotspot for various processes of mechano-chemical signal transduction (Krüger and Linke, 2011). The elastic properties of cardiac titin change dynamically during cardiac development and may also be pathologically altered during the course of cardiac disease (Linke and Hamdani, 2014). These changes in the titin molecule have a strong impact on diastolic function of the myocardium (Koser et al., 2019). The central position of titin in the

sarcomere, coupled with its role as a signaling node allows it to function as an important mechanosensor (Krüger and Linke, 2011). Because the protein is subjected to high mechanical stress in the working sarcomere, the titin filament must be subject to tightly regulated quality control. However, in a sarcomere that is constantly contracting and relaxing, quality control of a giant protein like titin is a huge challenge. In this review, we provide a brief overview on the mechanisms of protein quality control (PQC) in the sarcomere with a particular focus on the mechanisms of titin degradation known to date. In addition, we compile some well-characterized pathologies in which PQC mechanisms are impaired, leading to a significant loss of myocyte function.

2 TITIN—A BRIEF OVERVIEW ON STRUCTURE AND FUNCTION

The giant protein titin is encoded by a single gene with 364 exons resulting in a theoretical (maximum) size of 4.2 MDa (Bang et al., 2001). A single titin molecule spans the distance of 1 μm from the Z-disk to the M-line. Titin consists mainly of serially linked immunoglobulin-like domains (Ig domains), fibronectin type III domains (FN3 domains), and some unique sequences (us) (Bang et al., 2001). The NH_2 terminus of titin is anchored to the sarcomeric Z-disk by interaction with nebulin or the cardiac isoform nebulette (Witt et al., 2006), α-actinin 2 (Sorimachi et al., 1997; Labeit et al., 2006), and telethonin (Mues et al., 1998; Granzier and Labeit, 2004; Miller et al., 2004; Lange et al., 2006). Telethonin connects the NH_2-terminal parts of two titin molecules from one sarcomere in a palindromic manner (Zou et al., 2006). In a complex with the Z-disk component actinin and the muscle LIM protein (MLP), titin and telethonin form a mechanical stretch-sensing complex (Knöll et al., 2002). The I-band part of titin is not firmly attached to the adjacent filaments and can thus act like an elastic molecular spring that contributes to the passive stiffness of cardiac and skeletal muscles. It is composed of the proximal Ig domains, a heart-specific N2B domain (including the unique N2-B sequence, N2-bus), the middle Ig domains, the N2A domain (N2BA isoform), the PEVK domain [named for the high abundance of proline (P), glutamic acid (E), valine (V), and lysine (K) residues], and finally the distal Ig domains. With a size of ~ 2 MDa, the A-band part of titin is the largest part of the molecule (Bang et al., 2001) and mainly consists of fibronectin type III and Ig-domains, organized in 7-domain and 11-domain super repeats, respectively (Labeit et al., 1992). Titin is tightly connected to myosin and myosin-binding protein C (Tskhovrebova and Trinick, 2004; Lange et al., 2006). The M-band portion of titin contains several inserted sequences and the titin-kinase-domain in the M-band periphery (Bang et al., 2001; Gautel, 2011a).

In cardiac muscle cells, titin occurs in two isoforms: the longer and more compliant N2BA isoform (~3.2–3.3 MDa) and the shorter and more rigid N2B isoform (~3.0 MDa). Skeletal muscle cells contain a third isoform type, the N2A isoform with the slightly longer muscle-specific splice variants (3.3–3.7 MDa) (Freiburg et al., 2000; Neagoe et al., 2003; Prado et al., 2005). In cardiac muscle cells the ratio of N2BA and N2B largely determines titin based passive stiffness (Krüger and Linke, 2011).

The composition of titin isoforms can be dynamically adjusted. For example, the composition of titin isoforms changes from a predominant fetal N2BA isoform to adult N2BA and N2B isoforms during cardiac development, which is enhanced by stimulation with thyroid hormone 3 or insulin through triggering the PI3-K/AKT/mTOR pathway (Krüger et al., 2008; Krüger et al., 2010). The ratio of N2BA:N2B in human cardiomyocytes is about 30%:70% (Neagoe, 2002). All titin isoforms are transcribed and translated from a single gene by alternative splicing, which is strongly regulated by the splicing factor RNA-binding motif 20 (RBM20) Silencing of RBM20 leads to the formation of a giant titin isoform (N2BA-G, 3.9 MDa) (Guo et al., 2012; Zhu et al., 2017). Splicing events occur mainly within the I-band portion of titin but can also involve the Z-disk and M-band (Krüger and Linke, 2011). In heart failure, severe deviations in the composition of titin isoforms may occur due to altered splicing behaviour. In this context, a shift towards an either elevated or decreased N2BA:N2B ratio has been observed in several systolic or diastolic heart failure models (Linke and Hamdani, 2014).

While changing isoform composition is a long-term mechanism, posttranslational modification of elastic I-band domains can affect titin-based stiffness more dynamically. The most intensively studied posttranslational modification is phosphorylation of elastic spring elements in the I-band part of titin (Linke and Hamdani, 2014). Phosphorylation of the cardiac N2-B-domain by Protein Kinase A (PKA) (Yamasaki, 2002), Protein Kinase G (PKG) (Krüger et al., 2009), Cam-Kinase IIδ and Extracellular regulated Kinase 1/2 (ERK1/2) lowers titin-based passive stiffness whereas phosphorylation of the PEVK domain by PKCα increases titin-based passive stiffness (Hidalgo et al., 2009). Alterations of the phosphorylation levels have been demonstrated for different human pathologies with elevation of PEVK and reduced N2B phosphorylation in DCM, HCM and diabetes type 2 (van Heerebeek et al., 2012; Hamdani et al., 2013; Kötter et al., 2013; Hopf et al., 2018) resulting in higher stiffness compared to healthy controls. Higher PEVK and lower N2B phosphorylation has also been observed in the remote myocardium of mice after 3 days of permanent LAD ligature (Kötter et al., 2016). Acute and chronic elevation of titin-based passive stiffness could be tantamount with higher mechanical strain, increased working load and subsequent abrasion potentially lowering titin filament lifetime. This could lead to the necessity of faster replacement and degradation of titin filaments.

Oxidative stress due to higher levels of reactive oxygen species (ROS) can result in oxidative modification of myofilament components, thereby affecting myocyte contractility. Oxidative modification of sarcomere proteins and especially titin has been reported for several conditions like ischemia/reperfusion, in heart failure or muscular dystrophies (Beckendorf and Linke, 2015). S-glutathionylation lowers titin-based passive stiffness, disulphide bonding increases it (Grützner et al., 2009; Alegre-Cebollada et al., 2014). Unfolded domain oxidation within Ig-domains of the I-band also affects titin elasticity (Loescher et al., 2020). Although most cysteines are buried within folded Ig-

domains and can only be oxidatively modified in an unfolded state, Ig-domain unfolding occurs already at physiological sarcomere lengths (Rivas-Pardo et al., 2016). Another effect of oxidative stress is a reduced activity of NOS, resulting in lower amounts of NO (De Pascali et al., 2014). Since PKG activity depends on NO availability, oxidative stress can cause hypo-phosphorylation of the N2-B*us* (Beckendorf and Linke, 2015) (**Section 5.1**).

Within the PEVK domain a ubiquitination site (K11877) is directly neighbouring the well-established PKCα phosphorylation site S11878, according to the full-length human titin sequence (UniProtKB accession number, Q8WZ42) (Wagner et al., 2012). Crosstalk between ubiquitination and phosphorylation events have become a regularly discussed topic especially in cell signaling regulation (Hunter, 2007; Nguyen et al., 2013). The PEVK domain has been described as an unstructured, random-coiled region (Watanabe et al., 2002) and, therefore, potential conformational changes caused by incorporation of polyubiquitin chains can hardly be predicted. Nevertheless, it seems likely that posttranslational modifications adjacent to ubiquitination motifs influence not only local signaling events but also ubiquitin-mediated degradation, and vice versa (**Section 4.1.1**).

3 MECHANISMS OF PROTEIN QUALITY CONTROL

Intracellular PQC is essential for maintaining the balance between protein degradation and synthesis. In long-lived striated muscle cells, maintaining proteome balance is demanding. A large number of components must be correctly synthesized, folded and incorporated into the sarcomere (Hnia et al., 2019). Imbalance of protein homeostasis leads to accumulation of misfolded proteins and cytosolic aggregation with severe proteotoxicity (Wang and Hill, 2015). Dysregulated PQC has been implicated in various diseases such as cardiovascular diseases (Wang and Hill, 2015; Sciarretta et al., 2018), skeletal muscle myopathies (Kley et al., 2016) and diabetes (Sciarretta et al., 2015). In post-mitotic cardiomyocytes with low regenerative capacity and permanent mechanical stress, it becomes even more complicated as components have to be incorporated into the working sarcomere. Therefore, integration into the Z-disk, the A-band and the M-line or excision of the giant protein titin from the sarcomere to allow further degradation seems to be the *ultimate challenge*. To date, the exact mechanisms of PQC for titin are not fully understood.

The following sections provide an overview of the central processes of PQC and summarize the current state of knowledge on the degradation and remodeling of the protein giant titin. Major components of PQC are the ubiquitin-proteasome-system (UPS), the autophagosomal-lysosomal system (autophagy), proteases such as calpains and matrix metalloproteinase 2 and heat shock proteins (**Figures 1, 2**).

Degradation usually begins with the labeling of target proteins by polyubiquitin chains (**Section 3.1**), which specifically direct the proteins to the respective degradation machinery of the proteasome (**Section 3.2**) or autophagosome (**Section 3.3**). Depending on the substrate, additional pre-digestion by proteases is required to make the substrates accessible for further degradation (**Section 3.4**). In the sarcomere, calpains have been shown to be involved in the disassembly of myofilament complexes so that they can be degraded by the proteasome (Kramerova et al., 2005; Galvez et al., 2007). Heat shock proteins (HSPs) take on the role of protective chaperones, primarily to prevent misfolding and premature degradation (**Section 3.5**). In the following section, the individual stations will be discussed in more detail.

3.1 E3-Ligases

Ubiquitination of proteins is a three-step reaction performed by E1 (ubiquitin-activating), E2 (ubiquitin-conjugating) or E3 ligases (ubiquitin-ligating) (**Figure 1A**). Substrate specificity is based on the diversity and large number of E3 ligases performing the final step (Wang et al., 2011). To date, 2 E1-ligases and 38 E2 ligases have been identified within human tissues (Gundogdu and Walden, 2019). In contrast, hundreds of E3-ligases are known that can be classified into different types. The Really Interesting New Gene (RING) family is the largest type of E3 ubiquitin ligases with more than 600 members in humans alone (Morreale and Walden, 2016). Other families are the Homologous to E6AP C-terminus (HECT) E3 ubiquitin ligases (Lorenz, 2018), the Cullin-RING ubiquitin ligases (CRLs) and the U-box containing E3 ligases, also named E4 ligases (Morreale and Walden, 2016) and Ring Between Ring (RBR) E3-ubiquitin ligases (Dove and Klevit, 2017). Several muscle specific E3-ligases have already been identified in the past including the members of the muscle specific ring finger (MuRF) family members MuRF-1, -2, -3, also called tripartite motif containing (TRIM), and F-box protein 32 (Fbx32) also called atrogin-1 or MAFbx (Willis et al., 2008). In cardiomyocytes MuRF-1 negatively regulates cardiac hypertrophy through proteasomal degradation of calcineurin. Mutations in the gene encoding MuRF-1 have been found in patients with cardiac hypertrophy (Chen et al., 2012). Fbx32 is another muscle specific E3-ligase that, like MuRF-1, promotes protein degradation and is thought to inhibit cardiac hypertrophy. In contrast, inhibition of Fbx32 supresses hypertrophy through subsequent activation of nuclear factor kappa B signaling (Usui et al., 2011). MuRF-2 plays an important role in myofibril assembly in neonatal cardiomyocytes (Perera et al., 2011). MuRF-1 and Fbx32 are known to be key regulators of skeletal muscle atrophy and are involved in proteasomal degradation of myosin and myosin binding protein C (Gomes et al., 2001; Clarke et al., 2007; Cohen et al., 2009).

Carboxy terminus of HSP70 interacting protein CHIP (also named STUB1) is expressed in several tissues, but shows highest expression levels in cardiac and skeletal muscle. CHIP is capable of forming both K48 as well as K63 polyubiquitin chains (Zhang et al., 2005; Shaid et al., 2012) suggesting a role in proteasomal and autophagosomal degradation of substrate proteins or organelles. CHIP is critical for quality control processes and ubiquitinates misfolded proteins when correct folding cannot be achieved (Demand et al., 2001). It plays a cardioprotective role during ischemia and reperfusion by increasing PQC in a PKG-

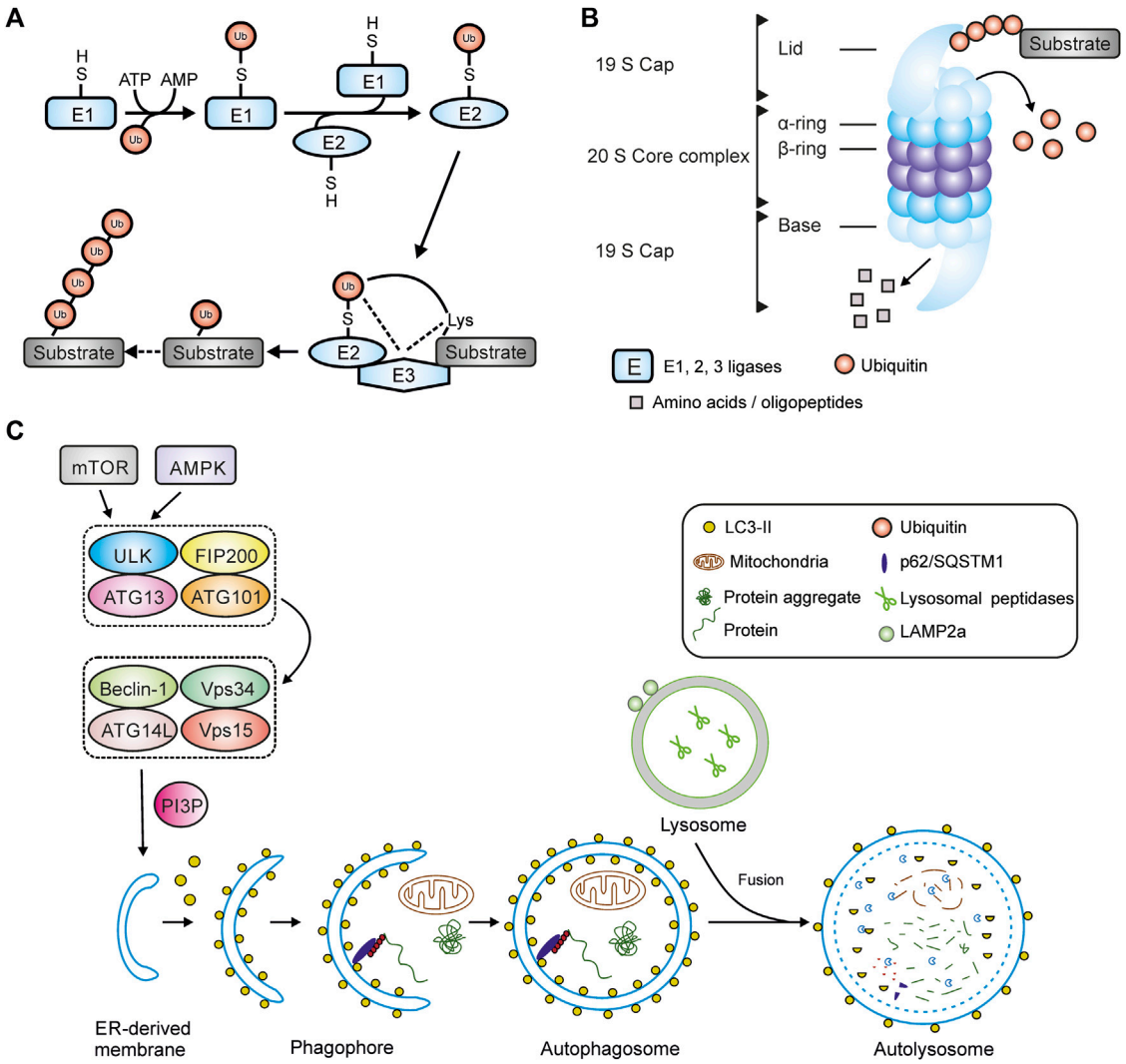

FIGURE 1 | Main components of protein quality control. **(A)** Ubiquitination of a substrate protein by E1-, E2- and E3-ligases. **(B)** Structure of the 26S-proteasome. **(C)** Schematic overview of macroautophagy including autophagy initiation complexes, autophagosome maturation and fusion with a lysosome. Abbreviations: AMPK, AMP activated protein kinase; Atg, autophagy-related (gene); FIP200, focal adhesion kinase family-interacting protein of 200 kD; LAMP2a, lysosomal-associated membrane protein 2a; LC3, microtubule-associated protein 1 light chain 3; mTOR, mammalian target of rapamycin; PI3P, phosphatidylinositol 3-phosphate; ULK1, unc-51–like autophagy-activating kinase 1; Vps34, class III phosphoinositide 3-kinase; Vps15, serine-threonine kinase Vps15/ird1.

dependent manner (Ranek et al., 2020). In a complex with Bcl2-associated anthanogene 3 (BAG3), HSPB8, HSC70 and p62, CHIP is involved in the degradation of Z-disk components including filamin c (**Figure 3**) (Arndt et al., 2010). It has been reported that BAG3/CHIP dependent sarcomere protein turnover is essential for maintenance of myofilament function (Martin et al., 2021).

In skeletal muscle, MuRF-1 and 2 are reported to ubiquitinate titin fragments from the M-line-A-band transition zone (Witt et al., 2005; Higashikuse et al., 2019). Inhibition of MuRF-1 by small molecules improves diastolic function in heart failure with preserved ejection fraction (HFpEF) and attenuates skeletal muscle wasting in cardiac cachexia (Bowen et al., 2017; Adams et al., 2022). Recently, the involvement of MuRF-1, -2, -3, Fbx32 and CHIP in proteasome- and autophagosome dependent titin filament ubiquitination has been demonstrated (**Section 4.1** and **Figure 2**) (Müller et al., 2021).

3.2 Ubiquitin-Proteasome System

The ubiquitin-proteasome system (UPS) is a large, multi-subunit protease complex that functions in an ATP-dependent manner and is responsible for the regulated non-lysosomal degradation of most misfolded or defective cytoplasmic proteins (Livneh et al., 2016). Proteins degraded by the proteasome must be tagged with a poly-ubiquitin chain (Lander et al., 2012), however, mono-ubiquitination of some substrates has also been reported to lead to proteasomal degradation (Braten et al., 2016). Ubiquitin is a small, highly conserved protein composed of 76 amino acids. *Via* the

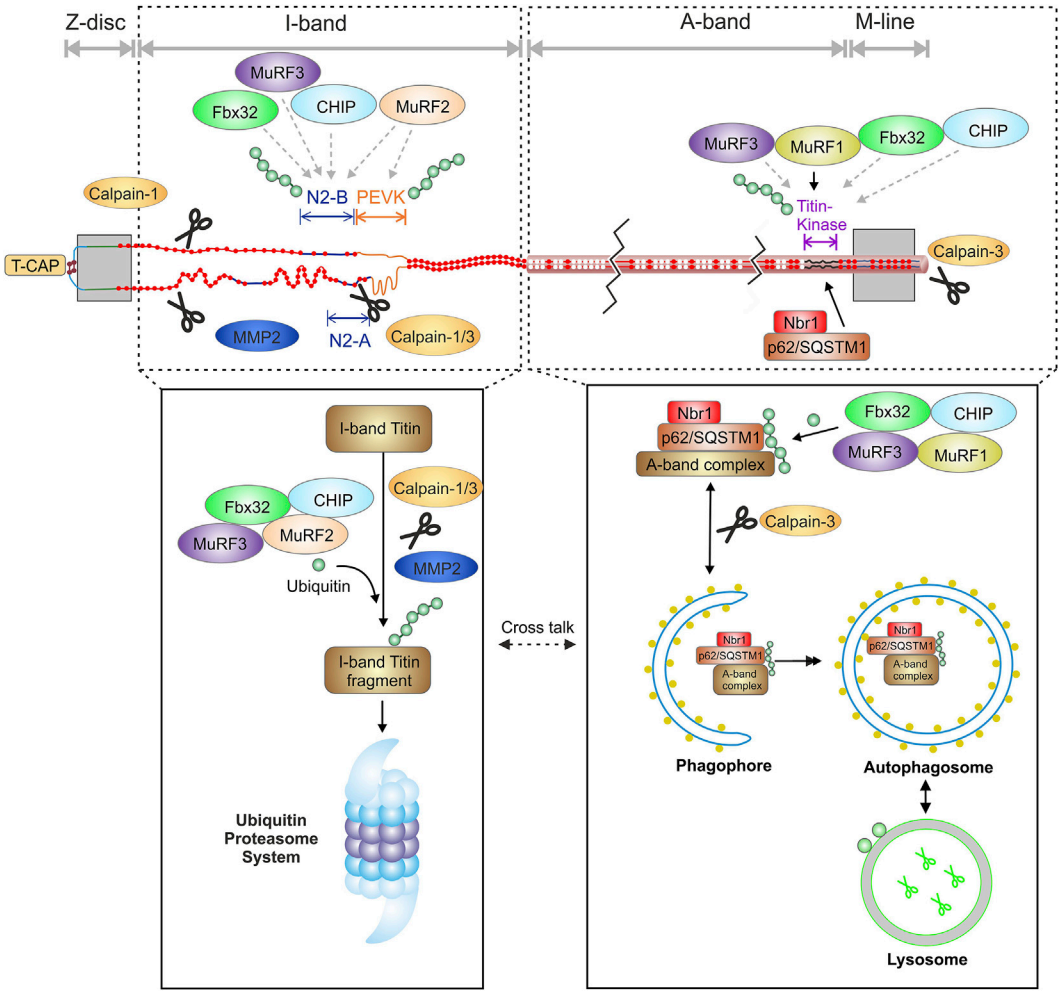

FIGURE 2 | Schematic overview of the interaction of the titin filament with components of the protein quality control and suggested domain specific degradation of titin by the proteasome and autophagy. MMP2, matrix metalloproteinase-2; T-CAP, titin cap/telethonin; N2-B, cardiac specific domain; PEVK, Prolin, glutamate, valine and lysine rich domain.

N-terminal methionine, ubiquitin molecules are bound to lysine residues of substrate proteins. Polyubiquitin chains consist of at least four ubiquitin molecules that are linked to each other *via* different lysine residues within the ubiquitin molecule (K6, K11, K27, K29, K33, K48, K63) (Swatek and Komander, 2016). In proteasomal degradation, the linkage occurs *via* K48 (Thrower et al., 2000).

A catalytic 20S core and one or two regulatory 19S subunits form the 26S proteasome (Bard et al., 2018) (**Figure 1B**). The 20S core is arranged in a stack of four rings, each with 7 subunits, two α-rings (α1-α7) and two β-rings (β1-β7) (Lander et al., 2012). Degradation of substrate proteins occurs through three key protease activities: caspase-like activity (β1-subunit), trypsin-like (β2-subunit) and chymotrypsin-like activity (β5-subunit). These subunits can be replaced by the inducible β1i, β2i and β5i subunits under different physiological and pathophysiological conditions (Scruggs et al., 2011). The 19S regulatory subunit consists of 19 subunits that can be divided into the lid and the base. The base consists of six regulatory particle AAA ATPase subunits (Rpt1-Rpt6) building a ring structure and four non-ATPase subunits (Rpn1, Rpn2, Rpn10 and Rpn13) (Díaz-Villanueva et al., 2015). The lid contains nine different subunits (Rpn3, Rpn5-9, Rpn11, Rpn12 and Rpn15). Ubiquitinated proteins are recognized by the ubiquitin binding proteins Rpn1, 10 and 13 within the 19S lid and ubiquitin chains are partially removed and rescued from degradation primarily by the Rpn11 subunit (Verma et al., 2002; Yao and Cohen, 2002). The substrates are unfolded and transported through a narrow central pore into the catalytic core where they are degraded (Lander et al., 2012). This central pore is formed by the N-termini of a subgroup of α-subunits that blocks the unregulated entry of substrates into the catalytic core (Groll et al., 2000).

3.3 Autophagy

The autophagosomal-lysosomal system processes individual proteins, larger protein complexes, aggregates and complete

organelles (Shaid et al., 2012). It is regulated by specific autophagy-related genes (Atg) that control the initiation, maturation and fusion of autophagosomes with lysosomes to form autolysosomes (Sciarretta et al., 2018). To date, more than 35 Atg genes have been identified, most of which are conserved between yeast and mammals (Ravikumar et al., 2010). Autophagy is activated by various stresses such as nutrient/glucose deprivation or oxidative stress (Sciarretta et al., 2018). In recent years, autophagy has gained attention as an important regulator of cardiac protein homeostasis and function. By eliminating misfolded proteins and damaged organelles, autophagy is central to maintaining cardiac structure and function (Nakai et al., 2007; Ikeda et al., 2015). There are three different types of autophagy: macroautophagy, chaperone-mediated autophagy (CMA or CASA for chaperone assisted selective autophagy) and microautophagy. In CMA, soluble substrates containing a KFERQ sequence are bound to the chaperone heat shock cognate protein 70 (HSC70/HSPA8), and the proteins are delivered directly to the lysosome by binding to lysosome-associated membrane protein 2a (LAMP2a) (Arndt et al., 2010). In the process of microautophagy, a small portion of the cytosol is directly engulfed by the lysosomal membrane. Macroautophagy describes the degradation process of proteins, protein aggregates, macromolecules or cellular organelles, which involves encapsulation in a double-membraned vesicle, the autophagosome (Shaid et al., 2012). In a first step, small endoplasmatic/sarcoplasmatic reticulum-derived vesicular sacs form around the target proteins, the autophagophore. Substrates are anchored to the membrane by autophagy-related proteins such as microtubule-associated light chain 3 (LC3/Atg8) and the ubiquitin binding protein p62/SQSTM1 (Shaid et al., 2012). Once the membrane closes around the target substrates, it is called autophagosome. Eventually, the autophagosome is fused to a lysosome and the substrates are degraded by lysosomal proteases (Levine and Kroemer, 2008; Gatica et al., 2015). In the following macroautophagy is referred to as autophagy. For autolysosomal degradation, unfolded protein substrates and protein aggregates are also labelled by polyubiquitin chains. In this case the ubiquitin molecules are typically linked *via* lysine residue 63 (K63) (Ji and Kwon, 2017).

A key element of autophagy initiation is the autophagy-initiating kinase Ulk1 (mammalian homologue of yeast ATG1) as part of the ULK1-ATG13-FIP200 protein complex (Mizushima, 2010). ULK1 contains multiple phosphorylation sites that regulate their activity when targeted e.g., by AMP activated protein kinase (AMPK) or mammalian target of rapamycin (mTOR) (Kim et al., 2011). Under glucose starvation, AMPK-mediated phosphorylation of ULK1 (e.g., at S317, S777 and S555) activates autophagy (Egan et al., 2011; Kim et al., 2011). In contrast, mTOR, a cell growth regulator, associates with the ULK1-ATG13-FIP200 complex, leading to phosphorylation of ULK1 at S757, thereby disrupting the AMPK-ULK1 interaction and inhibiting autophagy (Egan et al., 2011). Activated ULK1 phosphorylates and recruits a class III phosphoinositide-3-kinase (PI3-K) complex to the site of formation of the isolation membrane to start phagophore assembly (Feng et al., 2014) (**Figure 1C**).

3.4 Calpains and MMP2

The calpain family in humans consists of 15 members and all are Ca^{2+}-dependent, non-lysosomal cysteine proteases (Chen et al., 2021). Unlike other proteases that catalyse the degradation of their substrates, calpains recognize and proteolyze their substrates, but do not degrade them (Ono and Sorimachi, 2012). Three members have been identified in muscle tissues, calpain-1 (μ-calpain) and -2 (m-calpain) are ubiquitously expressed whereas calpain-3 is predominantly found in skeletal muscle (Portbury et al., 2011; Letavernier et al., 2012). The inhibitory protein calpastatin serves as the primary negative allosteric modifier of calpain activity by interaction between calpain and inhibitory domains of calpastatin (Hyatt and Powers, 2020). All three calpains have been associated with the degradation of sarcomere proteins including titin (Lim et al., 2004; Portbury et al., 2011).

Matrix metalloproteinase 2 (MMP2) is a zinc-dependent protease that degrades components of the extracellular matrix. Although normally localized in the extracellular matrix, MMP2 does not exclusively degrade matrix components and intracellular and particularly sarcomeric localization of MMPs has been demonstrated (Ali et al., 2010). Under increased oxidative stress, MMP-2 has been shown to degrade various sarcomere proteins such as troponin, myosin-light chain and α -actinin (Wang et al., 2002; Gao et al., 2003; Sawicki et al., 2005; Sung et al., 2007). In cardiomyocytes intracellular MMP2 can be found in the Z-disc region where it has been suggested to degrade the titin filament, particularly after experimental ischemia/reperfusion. (Ali et al., 2010).

3.5 Heat Shock Proteins

Another important element of PQC are the heat shock proteins that help other proteins fold or maintain their secondary structure under extreme conditions. They are produced in increased amounts after cells have been exposed to heat or other types of stressful environmental influences such as ultraviolet radiation, heavy metals or ethanol. In these situations of cellular stress, heat shock proteins stabilise cellular proteins to protect them from denaturation or accelerate the degradation of non-functional proteins *via* the proteasome. There are several different types of heat shock proteins, including the ATP-dependent HSP90 and HSP70, chaperonin containing TCP1 [CCT; also called TCP1-ring complex (TRiC)] and the non-ATP-dependent small heat shock proteins (sHSP) (Willis and Patterson, 2010). sHSPs, a family of molecular chaperones with 10 members in humans (HSPB1-10) (Kappé et al., 2010) and a molecular weight of 12–43 kDa, play a central role the PQC machinery. Despite their low molecular weight, sHSPs can form huge oligomers of up to several hundred kilo Dalton (Vos et al., 2008). As non ATP-dependent chaperones, sHSPs are not able to refold, but bind damaged or partially unfolded client proteins to keep them in a folding-prone state and protect them from aggregation (Mymrikov et al., 2011). Under several stress conditions like oxidative stress or energy depletion expression levels of sHSPs are increased in order to protect the cell (Mymrikov et al., 2011). Overexpression of HSP20 (HSPB6) protects against ischemia/reperfusion injury by activating autophagy (Fan et al., 2005; Qian et al., 2009). HSP22 (HSPB8)

and HSP27 (HSPB1) have also been shown to have a protective effect after ischemia/reperfusion (Vander Heide, 2002; Depre et al., 2006). HSP27 and αB-crystallin (HSPB5) are ubiquitously expressed in mammalian tissues (Klemenz et al., 1993). The chaperone activity of HSP27 and αB-crystallin is regulated by their oligomeric structure and the phosphorylation status (Ahmad et al., 2008; Jovcevski et al., 2015). αB-crystallin interacts with the 20S core of the proteasome and phosphorylation-independent with Fbx4, a subunit of the ubiquitin ligase complex SCF, suggesting the degradation of bound substrates by the proteasome (Boelens et al., 2001; den Engelsman et al., 2003). HSP27 has been shown to interact with the 19S unit of the proteasome and with ubiquitin, suggesting a role in substrate degradation by the proteasome also for this heat shock protein (Garrido et al., 2006). Both, HSP27 and αB-crystallin can translocate from the cytosol to the sarcomere under different stimuli and pathological conditions (Kötter et al., 2014; Unger et al., 2017).

The ATP-dependent chaperone HSP90 is ubiquitously expressed and has been reported to be a chaperone for myosin in the sarcomere (Smith et al., 2014). HSP90 does not directly interact with titin, but it can associate to the N2A domain of titin in a complex with the titin binding partner SET and MYND domain containing protein 2 (SMYD2) thereby exerting a protective effect on the Z-disc/I-band structure. For this interaction, HSP90 has to be methylated by SMYD2 at lysine K616 (Donlin et al., 2012). Following glutathionylation or oxidation of SMYD2, the complex dissociates and titin/N2A can be degraded by calpain-1 and/or MMP2 pointing to a positive role of SMYD2 and HSP90 in regulation of titin stability (Donlin et al., 2012; Munkanatta Godage et al., 2018).

4 PROTEIN QUALITY CONTROL OF SARCOMERE PROTEINS

4.1 Protection and Degradation of Titin

As mentioned earlier, controlling the protein quality of the titin filament is particularly challenging because the filament consists of a single protein and replacing a defective titin molecule in a functioning sarcomere is a difficult task. The reported half-life of a titin molecule under baseline conditions is about 3–5 days (Isaacs et al., 1989), but exchange of titin filaments in the sarcomere can occur within hours (da Silva Lopes et al., 2011). During neonatal development titin isoforms switching from foetal isoforms to the adult isoforms occurs within in days in small mammals (Opitz et al., 2004; Krüger et al., 2008) and weeks to months in larger animals (Lahmers et al., 2004). In adult heart, interventions such as pharmacologically induced hypothyroidism (Wu et al., 2007) and transverse aortic constriction (Han et al., 2020) have been reported to alter titin isoform composition within weeks. This process includes incorporation of newly synthesised titin filaments into growing sarcomeres as well as turnover of the foetal isoforms.

It was shown that translation of titin mRNA occurs predominantly at the Z-disk and the I-band of the sarcomere, i.e., in close proximity to the subsequent site of incorporation (Rudolph et al., 2019). The study by Rudolph et al. also partially refutes the long-discussed hypothesis of gradual integration of the titin filament into the Z-disc and subsequently into the M-lineage, by showing the placement of fluorescently labelled full-length titin filaments in the sarcomere. According to the study, integrated titin filaments originate primarily from a soluble cytosolic pool that represents approximately 10–15% of total titin (Rudolph et al., 2019). The exact mechanisms of titin filament integration into the sarcomere are not resolved yet, however, it is likely impeded by ongoing contraction of the sarcomeres.

Similarly, only little information is available on the mechanisms involved in titin PQC and turnover. Its gigantic size makes titin highly susceptible to fragmentation and degradation, suggesting that a continuous, well-functioning mechanism for protein turnover is required.

The sHSPs αB-crystallin and HSP27 as well as HSP90 have been identified as direct or indirect binding partners of titin I-band domains and likely play an important role in the PQC of the giant molecule (Bullard et al., 2004; Kötter et al., 2014). Under ischemic conditions and mechanical stretch of cardiac myocytes, conditions that occur during high mechanical stress, titin domain unfolding and subsequent interfilament aggregation can occur, leading to increased passive stiffness of muscle cells. It could be shown *in vitro*, that the presence of the small heat shock proteins HSP27 or αB-crystallin titin aggregation is blocked and an increase in passive stiffness is prevented (Kötter et al., 2014). HSP27 and αB-crystallin also showed translocation from the Z-disk to I-band domains e.g., in failing hearts and skeletal muscle dystrophies indicating a protective effect on these domains under pathological conditions. HSP27 and αB-crystallin have been shown to interact with the proximal Ig-region, the N2B and the N2A domain but not the PEVK, indicating a translocation to and a protection for these domains (Bullard et al., 2004; Kötter et al., 2014). *In vitro* experiments in human cardiomyocytes from failing hearts showed that treatment with αB-crystallin can decrease pathologically increased titin-based passive stiffness (Franssen et al., 2017). Thus, one might speculate that αB-crystallin not only prevents the formation of titin aggregates, but can also dissolve them. which would be a finding with significant potential for novel therapeutic strategies. However, caution is required here, because there is no reported evidence at the molecular level that sHSPs alone are capable of refolding proteins or even dissolving aggregates.

Due to the size of a titin filament, its degradation is an extremely complex and probably energy-consuming task for the cell. A first sign of elevated titin degradation is a higher abundance of the T2 fragment with a size of approximately 2–2.5 MDa, a specific degradation intermediate mainly existing of the A-band part of titin (Linke and Hamdani, 2014). The recently identified titin cronos isoform (~2 MDa) (Zou et al., 2015; Zaunbrecher et al., 2019) appears in the same molecular weight range than the T2 band and cannot be easily distinguished by electrophoresis alone. Gelelectrophoretic separation of full-length titin and the T2 revealed 2, 3 or more separate T2 bands (Neagoe, 2002; Lahmers et al., 2004; Kruger and Linke, 2006; Krüger et al., 2008). Since the A-band portion of titin is identical in most isoforms, the different molecular weights of the T2 product indicate a different composition of the I-band domain

of the degradation intermediate, similar to variable I-band length in the N2BA isoforms. This could also imply that multiple excision sites exist within the titin I-band resulting in different degradation products.

Current evidence suggests that both the proteasome (Kötter et al., 2016; Higashikuse et al., 2019) and autophagy (Lange et al., 2005; Bogomolovas et al., 2021; Müller et al., 2021), are involved in the degradation of titin and that the degradation of the different titin domains might occur specifically *via* one or the other system. This hypothesis was lately supported by experimental *in vitro* inhibition of the proteasome, which lead to increased proteasome-dependent K48 polyubiquitination, and inhibition of autophagy, causing increased autophagy-dependent K63 polyubiquitination of titin (Kötter et al., 2016; Müller et al., 2021).

The observed titin ubiquitination is at least in part performed by the muscle specific E3-ligases MuRF-1, -2, -3, CHIP and Fbx32/atrogin-1. Importantly, polyubiquitination occurs at full-length titin indicating is fully accessible for ubiquitination while still incorporated into the sarcomere (Müller et al., 2021). This is in accordance with other studies showing ubiquitination of other sarcomere proteins within the sarcomere (Martin et al., 2021). It can therefore be concluded that also for a giant protein like titin, a predigest is not necessarily needed for the ubiquitination reaction itself (Müller et al., 2021). Nevertheless, predigest of titin is important for further processing by autophagy or the proteasome and could be performed by the proteases calpain 1 and/or 3 as well as MMP2 (Barta et al., 2005; Hayashi et al., 2008; Azevedo et al., 2014). Calpain-1 has been identified as a binding partner of the N2A domain and the proximal Ig-domains of titin (Raynaud et al., 2005; Coulis et al., 2008). *In vitro* experiments have demonstrated that calpain-1 proteolyzes recombinant titin N2A constructs, suggesting that N2A is one of the titin subdomains susceptible to proteolysis by calpain-1 (Hayashi et al., 2008). The sequences within N2A that are degraded by calpain-1 were analyzed and mapped to two sites at the N- and C-terminal borders of N2A's unique insertion (uN2A). Calpain-3 also interacts with the N2A domain of titin (Hayashi et al., 2008). The release of calpain-3 from the N2A domain seems to be necessary for the activation and proteolysis of titin (Adewale and Ahn, 2021). Calpain-3 additionally binds to the C-terminal part of titin in the M-line region and leads to its proteolysis (Sorimachi and Ono, 2012; Charton et al., 2015).

MMP2 has been shown to associate to titin in Z-disk proximity at regions that share >60% sequence identity with MMP2 cleavage sites (Ali et al., 2010). The Z-disk proximity of MMP2 binding makes it highly likely that MMP2 is preferentially involved in the degradation of the readily accessible I-band region of titin. Calpains and MMP2 digest I-band titin into smaller fragments that can be readily recognized and degraded by the proteasome. This supports the idea that the accessible I-band part of titin could be preferentially degraded *via* the proteasome. Of note, the specific titin degradation band T2 was increased after inhibition of autophagy or the proteasome suggesting that under these conditions the titin degradation is stalled after proteolytic pre-digest, resulting in accumulation of the pre-digest product T2 containing titins A-band (Müller et al., 2021). The A-band portion of titin, which is tightly linked to myosin and myosin-binding protein C (Linke and Hamdani, 2014) is thought to be embedded in an autophagosome and degraded after fusion with a lysosome. The hypothesis of domain dependent degradation is supported by recent studies demonstrating localization of proteasome subunits of the 20S core at the Z-disk/I-band region of the sarcomere in adult cardiomyocytes (Rudolph et al., 2019) and localization of the autophagy-related Nbr1/p62/MuRF-1 complex at the titin kinase region upon MuRF-1 mediated ubiquitination of titin (Lange et al., 2005; Bogomolovas et al., 2021). **Figure 2** summarizes recent findings supporting the hypothesis of a domain specific degradation of titin by the proteasome and autophagy.

4.1.1 Potential Degradation-independent Effects of Titin Ubiquitination

Given the important role of titin as a mechanosensitive protein and its function as a molecular spring excessive modification of the protein may also have significant effects on its biomechanical properties. A polyubiquitin chain of 5 molecules has a molecular weight of about 40 kDa, so the size in itself could lead to steric hindrance of other posttranslational modifications. Whether titin ubiquitination directly or indirectly affects titin mechanical properties remains to be investigated. In mice, a previous study reported ubiquitination of titin within the PEVK domain at lysine residue K11877 (Wagner et al., 2012). This site is adjacent to a well-described PKCα phosphorylation site (S11878) that regulates titin-based passive tension. It can be speculated that mono- and/or poly-ubiquitination of K11877 alters the accessibility of the phosphorylation site, thereby preventing phosphorylation or de-phosphorylation of the S11878 residue. Such changes in the phosphorylation status of titin may in turn affect its elastic properties and cardiomyocyte function. Monoubiquitination of titin, e.g., within the N2-B domain, may also have implications for titin-based signal transduction by altering hypertrophic signaling *via* the N2B/four and a half LIM domain protein 1 and 2 (FHL1, FHL2)/MAPK complex.

4.2 Degradation of Other Sarcomere Proteins

Several studies have shown that the E3 ligase MuRF-1 plays a key role in the degradation of sarcomere proteins. MuRF-1 ubiquitinates myofibrillar proteins such as troponin I (Kedar et al., 2004), myosin heavy chains (Clarke et al., 2007; Fielitz et al., 2007), actin (Polge et al., 2011), myosin binding protein C and myosin light chain 1 and 2 (Cohen et al., 2009). Subsequently, all of these substrates are degraded by the proteasome (**Figure 3**).

The giant protein obscurin, binding partner of titin and myomesin (Fukuzawa et al., 2008), is localized in the M-band of the sarcomere. Small ankyrin-1 isoform 5 (sAnk1.5) is localized at the membrane of the sarcoplasmatic reticulum (SR) from where it interacts with the C-terminus of obscurin in cardiac and skeletal muscle (Lange et al., 2009) (**Figure 3**). This structural interaction of sarcomeric obscurin and sAnk1.5 in the membrane of the SR is necessary to anchor the SR in close proximity to the myofibrils. In the absence of sAnk1.5 longitudinal SR architecture is disrupted (Giacomello et al., 2015). In addition, interaction

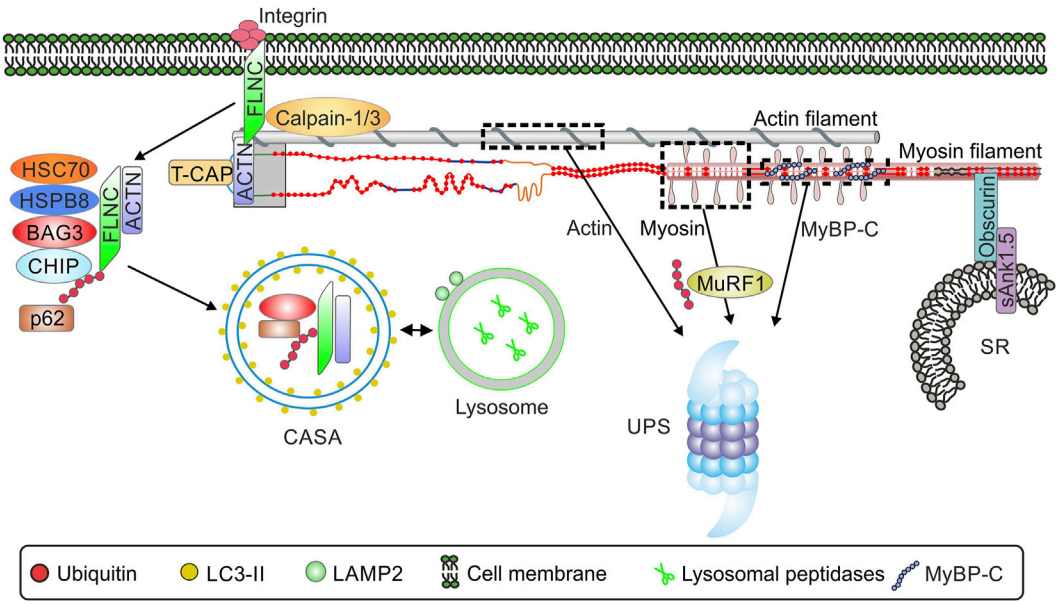

FIGURE 3 | Schematic overview of the interaction of sarcomere and selected sarcomere-associated proteins and protein quality control. Abbreviations: ACTN, α-actinin; BAG3, Bcl2-associated anthanogene 3; CASA, chaperone assisted selective autophagy; CHIP, Carboxy terminus of HSP70 interacting protein; HSP70, heat shock protein 70; HSPB8, heat shock protein family B member 8; LAMP2, Lysosome-associated membrane protein 2; LC3, microtubule-associated protein 1 light chain 3; MuRF-1, muscle specific ring finger 1; p62, sequestosome-1/p62; sAnk1.5, Small ankyrin-1 isoform 5; FLNC, filamin-C ; UPS, ubiquitin-proteasome system; SR, sarcoplasmatic reticulum. TCAP, telethonin/titin-cap.

with obscurin prevents the degradation of sAnk1.5. Disruption of thi obscurin-sAnk1.5 interaction leads to dislocation of sAnk1.5 to the sarcomeric Z-disc and cullin-3-mediated degradation (Lange et al., 2012).

The chaperone UNC-45 promotes folding and formation of myosin molecules (Gaiser et al., 2011; Melkani et al., 2011). Together with HSP70 and HSP90, UNC-45 builds a multisite docking platform for the assembly of myosin filaments (Gazda et al., 2013). Mutations in conserved regions of UNC-45 leading to reduced protein levels and/or chaperone activity results in paralysis and dysregulated thick filaments in *Caenorhabditis elegans* (Moncrief et al., 2021).

Another important mediator of sarcomere protein degradation is the co-chaperone BAG3 (Ulbricht et al., 2013; Behl, 2016). In skeletal muscle, BAG3 induces the formation of a protein complex that includes HSC70, the small heat shock protein HSP22 (HSPB8) and the carboxy-terminus of HSP70 interacting protein CHIP (Arndt et al., 2010). CHIP ubiquitinates the chaperone-bound substrate proteins and BAG3, facilitating interaction of the complex with p62 and potentially resulting in co-degradation of the ubiquitinated substrate and BAG3. The complex induces the degradation of Z-disk components, such as filamin-C by chaperone assisted selective autophagy (CASA, **Figure 3**) (Arndt et al., 2010). The exact function of filamin-C has not yet been elucidated. Filamin-C is found in subsarcolemmal regions as well as at Z-disks, so it is likely that the function of filamin-C is to act as a communication pathway between the membrane and the sarcomere. Alterations in the subcellular localization of filamin-C have been noted in limb-girdle muscular dystrophy and Duchenne muscular dystrophy (Mao and Nakamura, 2020). Filamin C is necessary for muscle formation and in the absence of FLNC mice develop a severe muscle phenotype including defects in embryonic myogenesis with decreased number of primary fibers, massive fiber size variation, and a disturbed sarcomere architecture (Dalkilic et al., 2006). The importance of the BAG3-dependent CASA mechanism has also been demonstrated in cardiac muscle, for which 8 proteins have been identified to date whose degradation is dependent on BAG3, including the sarcomere proteins α-actinin and the myosin-binding protein C. Insufficient turnover of sarcomere proteins as a result of impaired BAG3/CHIP-mediated degradation has been suggested to lead to impaired contractility of the myocardium (Martin et al., 2021).

5 PATHOLOGICAL CHANGES OF PROTEIN QUALITY CONTROL IN HEART AND SKELETAL MUSCLE

Striated muscle is a tissue with very high metabolic activity and is subject to strong mechanical stress. For this reason, highly effective and precisely regulated protein homeostasis is critical for cardiac and skeletal muscle function. As described in the previous sections, the UPS and autophagy play a central role in protein homeostasis. While the proteasome is already constantly active under normal conditions, autophagic activity is usually low in the heart (Levine and Kroemer, 2008). Dysregulation of proteasome and autophagosomal activity occurs in response to stress situations and diseases like ischemia/reperfusion, cardiac hypertrophy, heart failure and skeletal muscle atrophy (Gustafsson and Gottlieb, 2008; Portbury et al., 2011; Schlossarek and Carrier, 2011; Schiaffino

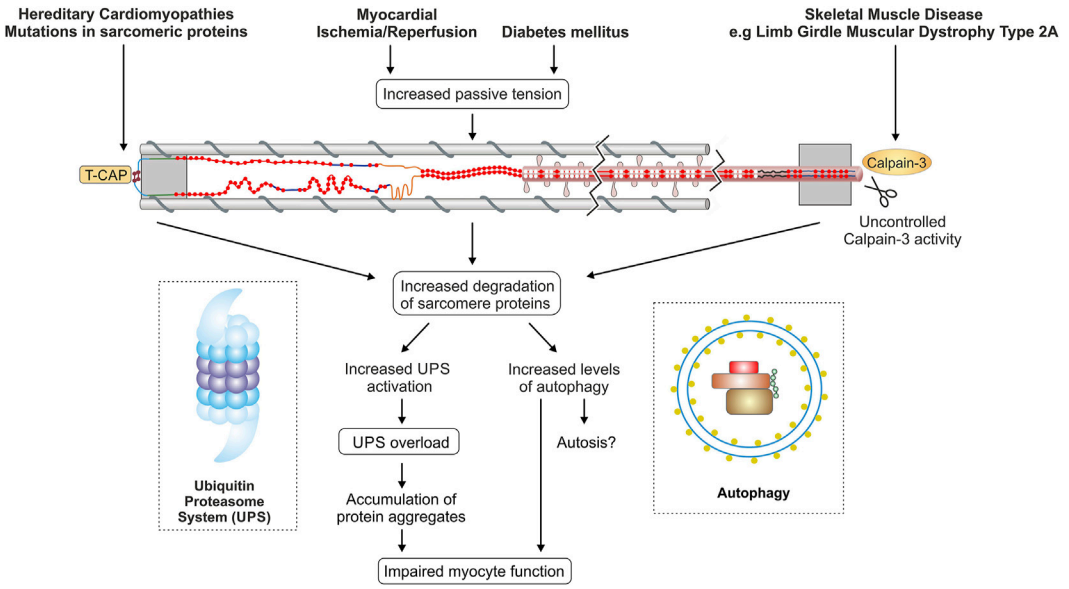

FIGURE 4 | Titin and protein quality control in different disease settings. The figure summarizes currently discussed mechanisms of disturbed PQC affecting titin in cardiac and skeletal muscle diseases. TCAP, telethonin/titin-cap.

et al., 2013) In addition, metabolic diseases such as diabetes are associated to alterations in proteasomal and autophagosomal activity (Queisser et al., 2010; Xu et al., 2013). The accumulation of ubiquitinated proteins may indicate impaired or overloaded UPS and/or autophagy, and is commonly observed in various muscle diseases. Accumulation of misfolded protein is an age-related symptom in mammals caused, at least partially, by downregulation of the activity of the UPS (Tomaru et al., 2012) and the autophagosomal system (Shirakabe et al., 2016). Aging affects several cellular targets. Titin isoform composition or titin based passive stiffness do not seem to be altered during aging but proteasomal activity and calpain-1 activity declines during aging leading to an accumulation of aggregated proteins (Salcan et al., 2020). According to various studies, autophagic activity also appears to generally decrease during aging (Aman et al., 2021) Only for aged primary human fibroblast cells an increased autophagic activity for the turnover of ubiquitinated proteins has been reported (Gamerdinger et al., 2009). For this reason, it has to be considered that in some pathological situations, especially in heart diseases, PQC could also be affected by aging alone. The following sections will briefly review a selection of pathological changes observed in the context of striated muscle diseases, again with a specific focus on their impact on protein homeostasis and function of the sarcomere protein titin.

5.1 Altered Protein Quality Control in Response to Cardiac Ischemic Injury

Myocardial ischemia is characterized by a brief interruption of blood supply to the working myocardium, resulting in a greater or lesser degree of myocardial tissue death depending on the duration of ischemia. Additional tissue damage occurs during the reperfusion phase and is a result of complex processes such as increased production of reactive oxygen species (ROS), impaired Ca^{2+} handling, and altered cellular metabolism (Kalogeris et al., 2012). During ischemia/reperfusion the UPS becomes dysfunctional by oxidative modification of 20S core subunits and loses the ability to process ubiquitinated substrate proteins (Bulteau et al., 2001; Powell et al., 2005). In contrast, autophagosomal activity is increased during ischemia/reperfusion by activation of the AMPK pathway and inhibition of the Rheb/mTOR pathway (Matsui et al., 2007; Sciarretta et al., 2012), apparently to compensate for the greater amount of damaged and ubiquitinated proteins due to an impaired or overloaded UPS. In turn, experimental activation of autophagy during ischemia has been shown to be cardioprotective and to reduce infarct size (Mizushima and Komatsu, 2011; Choi et al., 2013; Kroemer, 2015; Mo et al., 2016). However, during reperfusion, the massive activation of autophagy through beclin-1-dependent but AMPK-independent pathways could be maladaptive (Shi et al., 2019). One explanation for the deleterious effect of hyperactivated autophagy could be the induction of autosis leading to death of cardiomyocytes and further contractile impairment of the affected ventricle (Liu et al., 2013).

Oxidative stress plays an important role in cardiac damage of infarcted hearts and is known to induce modifications of sarcomeric and Ca^{2+}-handling proteins, thereby altering their function, expression and activity. This oxidative stress can be mediated by increased production of ROS, such as superoxide radical ($O2^{\bullet-}$) hydroxyl radical ($OH^{\bullet-}$) and the non-radical reactive species hydrogen peroxide (H_2O_2).

It is suggested that oxidative stress may be increased beyond physiological levels not only in the infarcted but also in the non-ischemic regions of the heart (remote myocardium) after myocardial infarction (Cave et al., 2006; Sun, 2009). Oxidative stress strongly affects myofibrillar proteins, e.g., by increasing

proteolysis of myofilament proteins by ROS-activated proteases (Steinberg, 2013). Oxidative changes in actin and myosin have also been observed during reperfusion of ischemic rat hearts (Eaton et al., 2002; Prochniewicz et al., 2008). Myosin Ca^{2+}-ATPase activity was decreased after experimental induction of myocardial infarction (MI) (Avner et al., 2012). Moreover, glutathionylation levels in the myofibrillar protein fraction of the remote myocardium were greatly increased after infarction.

In vitro analyses have shown that S-glutathionylation and disulfide bonding of titin fragments could alter the elastic properties of titin in response to oxidative stress (Grützner et al., 2009; Alegre-Cebollada et al., 2014). The authors demonstrated that under conditions of high mechanical strain titin Ig-domains are unfolded and become S-glutathionylated in the presence of oxidized glutathione (GSSG), which then prevents the re-folding of the domain and lowers titin-based stiffness. However, after myocardial infarction S-glutathionylation of unfolded I-band Ig-domains of titin was increased only in the infarcted area, but not in the remote region. (Loescher et al., 2020).

During ischemia-induced sarcomere breakdown titin is among the first proteins to be degraded (Hein et al., 1994). In response to ischemic injury, MMP2 translocates to the Z-disk/I-band region and contributes to titin degradation (Ali et al., 2010). Cardiac Ischemia is associated with both hypoxia and acidosis due to increased glycolysis and lactic acid production of the ischemic myocytes (Webster et al., 2000). The resulting acidic conditions in combination with the increased mechanical load of the sarcomeres are likely to induce Ig-domain unfolding and aggregation of titin filaments as recently demonstrated *in vitro* (Kötter et al., 2014). Such aggregation leads to increased titin-based passive tension. This is in partial conflict with the reported elevated S-glutathionylation of unfolded Ig-domains having the opposite effect (Loescher et al., 2020). Nevertheless, the presence of αB-crystallin or HSP27 could prevent aggregation of unfolded titin domains and the increase in passive stiffness in this setting.

Titin phosphorylation and titin-based stiffness was also increased within the viable remote myocardium of mice 3 days after permanent ligature of the LAD. This is thought to be a protective mechanism to stabilize and promote the function of the vital myocardium after massive loss of cardiomyocytes in the infarcted region. As long as the scar within the infarct region is not formed, rapidly increased titin stiffness in the non-ischemic region may prevent load-induced overstretching and disruption of non-ischemic cardiac myocytes and thereby reduce sarcomeric and cellular damage in the first hours and days after myocardial injury (Kötter et al., 2016). It cannot be excluded that aggregation contributes to the observed increase in passive stiffness and the stability of the remote myocardium. While titin aggregation could possibly help stabilizing the sarcomere under conditions of high mechanical stress, aggregation cannot be easily reversed to retrieve functional filaments, and aggregated titin filaments eventually lose their elastic properties. In addition, titin aggregation has been reported to occur in the area of the N2A domain, a region of calpain-1 interaction in heart muscle (Barta et al., 2005). This interaction is potentially affected by aggregation leading to higher calpain activity and proteolysis of titin and other substrates. The increased mechanical stress on the remaining vital myocardium results in greatly increased proteasomal activity. However, despite the higher proteasomal activity in remote myocardium, erosion and ubiquitination of titin appeared to be too high to be compensated by increased proteasomal turnover, and thus led to the accumulation of K48-dependent poly-ubiquitinated titin (Kötter et al., 2016). In the end partially damaged and ubiquitinated titin filaments may remain within the sarcomere and could negatively affect cardiomyocyte function.

Taken together, the exact interplay of the described mechanisms and their role in the functional adaptation of sarcomere function after myocardial infarction or ischemia/reperfusion injury requires further investigation.

5.2 Muscle Atrophy and Skeletal Muscle Myopathies

Muscular atrophy occurs when the rate of muscle protein breakdown/turnover exceeds muscle protein synthesis. It is a predominant symptom of several pathologies including muscle myopathies or cardiac and cancer cachexia (Bonaldo and Sandri, 2013). A hallmark of muscle atrophy is a massive loss of skeletal muscle triggered by activation of the UPS and autophagy (Schiaffino et al., 2013). High muscle loss apparently includes increased sarcomere protein turnover.

Lang et al. reported changes in titin ubiquitination, particularly within the C-terminal region, after sciatic nerve section in mouse gastrocnemius muscle, indicating elevated titin turnover during atrophy (Lang et al., 2017). The E3-ligases MuRF-1, that targets several sarcomeric proteins like myosin or MyBP-C for degradation by the UPS (**Section 4.2**), and Fbx32/atrogin-1 are strongly upregulated during muscle atrophy (Bodine et al., 2001; Gomes et al., 2001). Since titin has been shown to be a polyubiquitination target of both these E3-ligases, significant degradation of titin during atrophy/cachexia development is likely (Müller et al., 2021).

Hereditary myopathies are a heterogeneous group of disorders with a highly variable age at onset. These myopathies are due to mutations in several genes, including dystrophin (Duchenne muscular dystrophy, DMD), calpain-3 (Limb girdle muscular dystrophies, LGMD2A), or titin [muscular dystrophy with myositis (MDM); tibial muscular dystrophy (TMD) and limb-girdle muscular dystrophy 2J (LGMD2J)] (Hackman et al., 2002; Huebsch et al., 2005; Udd et al., 2005). DMD is an X-linked inherited muscular dystrophy based on mutations in the dystrophin gene and is the most common form of dystrophy in childhood (Koenig et al., 1987). Typically, the muscles of the thighs and pelvis affected first. In later stages of the disease, the heart is also concerned, leading to the development of cardiomyopathy (Ryder et al., 2017). Autophagic activity is decreased in DMD patients and in mdx mice by constitutive activation of mTOR, which leads to downregulation of Atg proteins and inhibition of autophagy function (De Palma et al., 2012). In the urine of DMD patients and in mdx mice N-terminal titin fragments have been identified, which may have the potential to serve as non-invasive biomarkers of DMD (Robertson et al., 2017).

LGMD2A is an autosomal recessive human muscular dystrophy characterized by muscle wasting, cell death and

decreased calpain-3 activity and expression (Nishino and Ozawa, 2002). MDM is caused by a deletion mutation of 83 amino acids that includes part of the titin N2A domain responsible for the interaction with calpain-3 (Huebsch et al., 2005; Nishikawa et al., 2020). Deletion of this fragment in skeletal muscle of mdm mice results in reduced association of calpain-3 to titin N2A (Huebsch et al., 2005). The lack of interaction between calpain-3 and N2A leads to increased activity of calpain-3 and increased substrate digestion (Huebsch et al., 2005; Nishikawa et al., 2020). Patients with missense or truncating mutation in either of the two last exons of TTN, Mex5 and Mex6, encoding the is7 region and the M10 domain in the M-band proximity, respectively, develop TMD and LGMD2J (Hackman et al., 2008; Evilä et al., 2014).

Myofibrillar myopathies (MFMs) are characterized by histological alterations such as focal disintegration of myofibrils predominantly at the Z-disk and protein aggregation in myofibers (Kley et al., 2016). Overexpression of HSPs significantly reduces aberrant protein aggregation in various models of MFMs (Chávez Zobel et al., 2003; Sanbe et al., 2007; Sanbe et al., 2009). A common feature in hereditary myopathies is the translocation of the small heat shock proteins HSP27 and αB-crystallin and the ATP-dependent chaperone HSP90 from the z-disk region or the cytosol to the elastic titin I-band increasing the passive tension of skeletal muscle fibers (Unger et al., 2017). This suggests a protective mechanism that prevents aggregation of unfolded titin domains as well as other affected sarcomeric proteins.

Hereditary myopathy with early respiratory failure (HMERF, MFM-Titinopathy) is a slowly progressive myopathy with onset in adulthood. In addition to the limb girdle and leg muscles, it typically affects the diaphragm muscle, resulting in a severe reduction in forced vital capacity. However, cardiac involvement in the disease has not yet been observed to date (Tasca and Udd, 2018). All HMERF-associated pathogenic titin variants are located in the 119th FN3 domain of titin resulting in misfolding of the FN3 domain *in vitro* (Hedberg et al., 2014; Pfeffer et al., 2014; Tasca and Udd, 2018). In contrast to disease-causing proteins in many other myopathies, the mutant titin protein could not be found in cytoplasmic bodies but in other myofibrillar proteins (Palmio et al., 2014). One possible explanation is the loss of dynamic interaction of the FN3 119-domain with neighbouring proteins, which alters autophagy processes and subsequently leads to aggregation of other proteins (Edström et al., 1990; Tasca and Udd, 2018).

5.3 Protein Quality Control in Diabetes Mellitus

Another condition associated with altered PQC is diabetes mellitus (DM). DM describes metabolic diseases that lead to elevated blood glucose levels due to a lack of insulin or a reduced effectiveness of insulin. The pathology of diabetes mellitus is associated with increased morbidity and mortality due to coronary artery disease, peripheral artery disease, stroke, cardiomyopathy and congestive heart failure (King et al., 1998; Plutzky, 2011). Diabetes patients have a 2 fold higher case fatality rate during acute phase of myocardial infarction and long term follow up (Milazzo et al., 2021). Patients with type 2 diabetes mellitus (T2DM) often show a very early manifestation of left ventricular dysfunction due to increased diastolic passive stiffness of the left ventricle. This increased passive ventricular stiffness is associated with cellular and systemic abnormalities often leading to the progression of heart failure (Boyer et al., 2004).

Hyperglycemia has been shown to inhibit autophagy-mediated degradation of cellular components and alter proteasomal activity (Queisser et al., 2010; Kobayashi et al., 2012). It is suggested that perturbations of PQC may be important factors in the development of diabetic cardiac failure. Indeed, therapeutic activation of autophagy in experimental diabetes type 1 and 2 models lead to improved cardiac function and reduced the incidence of cardiac abnormalities (Sciarretta et al., 2015). Both type 1 and type 2 diabetes mellitus have been shown to affect cellular mechanisms of PQC. Type 1 diabetes has been reported to decrease proteasomal activity but also increase the expression of proteasomal subunits (Powell et al., 2008; Li et al., 2017). In type 2 diabetes skeletal muscle showed increased expression of selected proteasomal subunits (Hwang et al., 2010). Whether autolysosomal activity is generally increased or impaired in type-1 and type-2 diabetes is still under debate (Mellor et al., 2011; Kobayashi et al., 2012; Xu et al., 2013). It was recently (Kanamori et al., 2015) reported that autophagy is increased in diabetic cardiomyopathy in type 1 diabetes, whereas it is reduced in hearts of patients with type 2 diabetes. Their conclusion of increased autophagy was partially based on findings of increased LC3-II and p62/sequestosome-1 level in a type 1 diabetes model. This observation was challenged by recent findings, showing elevated LC3-II and p62 protein levels also after pharmacological inhibition of autophagy in cultured cardiomyocytes (Müller et al., 2021). Apart from disunity concerning elevated or reduced autophagy, modification of PQC seems to be a general phenomenon in the setting of diabetes. However, the specific effects on sarcomere protein turnover particularly of titin and cardiomyocyte function have not been studied, to date. Diverging alterations in PQC in type -1 and type- 2 diabetes are likely to differentially affect the sarcomere and the titin filament and should be elucidated in future studies.

5.4 Mutations in Sarcomeric/Myofibrillar Proteins

Emerging evidence suggests that not only sarcomeric proteins but also non-filament proteins play an essential role in the development of various muscle diseases. A substantial overview of disease causing mutations in myofibrillar myopathy associated proteins has recently been given in a series of reviews [e.g., (Kley et al., 2016; Dorsch et al., 2019; Kellermayer et al., 2019; Rees et al., 2021)]. Therefore, we briefly highlight selected disease causing mutation in the titin sequence and other filamentous proteins.

5.4.1 Titin Truncating and Missense Variants

Whole genome sequencing studies have revealed titin as an important human disease gene (Bang et al., 2001; Begay et al., 2015; Kellermayer et al., 2019). Due to the enormous size of the titin gene, diverse missense mutations have been observed at extremely high frequency (Karczewski et al., 2020). Because many

of the missense mutations have also been found in control subjects and not only in cardiomyopathy patients, it was assumed that most of the mutations do not cause the disease (Thomson et al., 2019). Nonetheless, about 130 pathogenic *TTN* coding mutations were reported in relation to skeletal and/or cardiac myopathies (Chauveau et al., 2014; Savarese et al., 2016). Recessive truncation mutations adjacent to the C-terminal M-band were related to Salih myopathy that affects skeletal and cardiac muscle (Carmignac et al., 2007), while recessive mutations in centronuclear myopathy with potential cardiac involvement (Ceyhan-Birsoy et al., 2013) and other neuromuscular phenotypes were identified within the N-terminal region, and comprise compound heterozygosity of either two truncating mutations or a truncation and a missense mutation (Chauveau et al., 2013; Palmio et al., 2014).

The titin missense variant A178D was identified as the most likely cause of cardiac disease in a family affected by the uncommon autosomal dominant left ventricular non-compaction (LVNC) and dilated cardiomyopathy (DCM) (Hastings et al., 2016). In a mouse model carrying this mutation, the variant was sufficient to cause a mild phenotype of DCM (Jiang et al., 2021). The missense variant A178D causes disruption of the interaction between titin and telethonin (T-cap), leading to dissociation of telethonin from the Z-disc and cytosolic telethonin accumulation (Jiang et al., 2021). Subsequent depletion of cytosolic telethonin by the UPS leads to proteasome overload and functional impairment (Hastings et al., 2016).

The most common form of cardiomyopathy is dilated Cardiomyopathy (DCM) with a prevalence of ~1:250 (Hershberger et al., 2013; Schafer et al., 2017). Up to 25% of familial DCM cases are associated with heterozygous titin mutations, and many are titin truncating variants (*TTNtv*) (Herman et al., 2012; Roberts et al., 2015). Truncations in the constitutively expressed A-band region of titin, which stabilizes myosin filaments in the A-band, show the most obvious pathogenicity of *TTNtv* (Herman et al., 2012; Roberts et al., 2015; Schafer et al., 2017). Correction of truncated titin proteins using CRISPR/CAS technique results in functional recovery and appears to be a promising therapeutic target for the treatment of titin mutation-based cardiomyopathy (Fomin et al., 2021). **Figure 4** summarizes alterations of PQC and titin in different disease settings.

5.4.2 Mutations in Other Sarcomeric Proteins

Mutations in the *MYBPC3* gene coding for MyBP-C are the most common cause of familial hypertrophic cardiomyopathy (HCM) (Ho et al., 2018). Most *MYBPC3* variants are frameshift, nonsense or splice variants resulting in premature stop codons. Truncated transcripts are targeted for degradation by nonsense mediated RNA decay and result in reduced levels of MyBP-C protein (Helms et al., 2020). In heart tissues of HCM patients MyBP-C protein level was reduced by approximately 40% and lower synthesis rates are compensated by diminished MyBP-C degradation (Marston et al., 2009; O'Leary et al., 2019; Helms et al., 2020). Non-truncating variants account for up to 15% and a subset of domain specific variants causes loss of function due to failure of myofilament incorporation (Helms et al., 2020). Heat shock cognate 70 kDa (HSC70) was identified as a central player in the turnover of the wild type as well as the mutated MyBP-C (Glazier et al., 2018).

Mutations in *FLNC*, the gene coding for filamin C, causes myofibrillar myopathy (filaminopathy) characterized by disintegration of myofibrils predominantly at the Z-disc and massive protein aggregates in cytosolic deposits within the muscle fibers (Kley et al., 2013). Components of the CASA complex HSPA8, HSPB8 and SQSTM1/p62, were accumulated in the aggregates while BAG3 and STUB1 localizes around the deposits. These results indicate that abnormal muscle fibers compensate the massive protein aggregation with a strongly increased expression of proteins involved in proteasomal and autophagic degradation (Kley et al., 2013).

The scientific community is just beginning to recognize the absolute number of involved proteins and disease causing mutations, triggered by new RNA and DNA sequencing technologies. More research is required to uncover the pathomechanisms by which mutations in myofibrillar and non-myofibrillar proteins induce myopathies. Future studies will uncover new exciting insights with potentials for therapeutic interventions.

6 CONCLUSION

In summary, the turnover of titin filaments and other sarcomere proteins depends on a whole range of PQC mechanisms. Loss of the physiological balance of synthesis and degradation under pathological conditions could lead to either insufficient or even excessive turnover of sarcomere proteins and titin. Decreased titin turnover due to impaired autophagy or reduced proteasomal activity results in partially damaged titin filaments within the sarcomere, which then compromise the contractile and elastic properties of the sarcomere (**Figure 4**). In contrast, abnormally increased degradation possibly leads to turnover of the still functional and not only the heavily stressed and worn titin filaments. More detailed knowledge of the finely tuned ubiquitination and turnover process of sarcomere proteins is necessary to understand how pathological changes in these processes affect sarcomere function and cardiac and skeletal muscle properties. In the future, the targeted use/modification of PQC components may represent a promising option for therapeutic intervention.

AUTHOR CONTRIBUTIONS

SK made the conception of the review, wrote the manuscript draft and prepared Figures 1, 2, and 3. MK and SK prepared Figure 4, discussed and structured the content and made the proof reading.

FUNDING

Some of the work reviewed here was supported by a grant from the German research foundation (SFB1116-1/2 TPA02 to MK), the research commission of the Heinrich-Heine-University Düsseldorf (Grant to SK; 11/2014) and the Else-Kröner-Fresenius Stiftung (Grant to SK; 2017_A01).

REFERENCES

Adams, V., Schauer, A., Augstein, A., Kirchhoff, V., Draskowski, R., Jannasch, A., et al. (2022). Targeting MuRF1 by Small Molecules in a HFpEF Rat Model Improves Myocardial Diastolic Function and Skeletal Muscle Contractility. *J. Cachexia Sarcopenia Muscle* 13, 1565–1581. doi:10.1002/jcsm.12968

Adewale, A. O., and Ahn, Y.-H. (2021). Titin N2A Domain and its Interactions at the Sarcomere. *Ijms* 22 (14), 7563. doi:10.3390/ijms22147563

Ahmad, M. F., Raman, B., Ramakrishna, T., and Rao, C. M. (2008). Effect of Phosphorylation on αB-crystallin: Differences in Stability, Subunit Exchange and Chaperone Activity of Homo and Mixed Oligomers of αB-Crystallin and its Phosphorylation-Mimicking Mutant. *J. Mol. Biol.* 375 (4), 1040–1051. doi:10.1016/j.jmb.2007.11.019

Alegre-Cebollada, J., Kosuri, P., Giganti, D., Eckels, E., Rivas-Pardo, J. A., Hamdani, N., et al. (2014). S-glutathionylation of Cryptic Cysteines Enhances Titin Elasticity by Blocking Protein Folding. *Cell* 156 (6), 1235–1246. doi:10.1016/j.cell.2014.01.056

Ali, M. A. M., Cho, W. J., Hudson, B., Kassiri, Z., Granzier, H., and Schulz, R. (2010). Titin Is a Target of Matrix Metalloproteinase-2: Implications in Myocardial Ischemia/reperfusion Injury. *Circulation* 122 (20), 2039–2047. doi:10.1161/CIRCULATIONAHA.109.930222

Aman, Y., Schmauck-Medina, T., Hansen, M., Morimoto, R. I., Simon, A. K., Bjedov, I., et al. (2021). Autophagy in Healthy Aging and Disease. *Nat. Aging* 1 (8), 634–650. doi:10.1038/s43587-021-00098-4

Arndt, V., Dick, N., Tawo, R., Dreiseidler, M., Wenzel, D., Hesse, M., et al. (2010). Chaperone-assisted Selective Autophagy Is Essential for Muscle Maintenance. *Curr. Biol.* 20 (2), 143–148. doi:10.1016/j.cub.2009.11.022

Avner, B. S., Shioura, K. M., Scruggs, S. B., Grachoff, M., Geenen, D. L., Helseth, D. L. Jr., et al. (2012). Myocardial Infarction in Mice Alters Sarcomeric Function via Post-Translational Protein Modification.. *Mol. Cell Biochem.* 363 (1–2), 203–215. doi:10.1007/s11010-011-1172-z

Azevedo, A., Prado, A. F., Antonio, R. C., Issa, J. P., and Gerlach, R. F. (2014). Matrix Metalloproteinases Are Involved in Cardiovascular Diseases. *Basic Clin. Pharmacol. Toxicol.* 115 (4), 301–314. doi:10.1111/bcpt.12282

Bang, M.-L., Centner, T., Fornoff, F., Geach, A. J., Gotthardt, M., McNabb, M., et al. (2001). The Complete Gene Sequence of Titin, Expression of an Unusual 700-kDa Titin Isoform, and its Interaction with Obscurin Identify a Novel Z-Line to I-Band Linking System. *Circulation Res.* 89 (11), 1065–1072. doi:10.1161/hh2301.100981

Bard, J. A. M., Goodall, E. A., Greene, E. R., Jonsson, E., Dong, K. C., and Martin, A. (2018). Structure and Function of the 26S Proteasome. *Annu. Rev. Biochem.* 87, 697–724. doi:10.1146/annurev-biochem-062917-011931

Barta, J., Tóth, A., Édes, I., Vaszily, M., Papp, J. G., Varró, A., et al. (2005). Calpain-1-sensitive Myofibrillar Proteins of the Human Myocardium. *Mol. Cell Biochem.* 278 (1), 1–8. doi:10.1007/s11010-005-1370-7

Beckendorf, L., and Linke, W. A. (2015). Emerging Importance of Oxidative Stress in Regulating Striated Muscle Elasticity. *J. Muscle Res. Cell Motil.* 36 (1), 25–36. doi:10.1007/s10974-014-9392-y

Begay, R. L., Graw, S., Sinagra, G., Merlo, M., Slavov, D., Gowan, K., et al. (2015). Role of Titin Missense Variants in Dilated Cardiomyopathy. *Jaha* 4 (11). doi:10.1161/jaha.115.002645

Behl, C. (2016). Breaking BAG: The Co-chaperone BAG3 in Health and Disease. *Trends Pharmacol. Sci.* 37 (8), 672–688. doi:10.1016/j.tips.2016.04.007

Bodine, S. C., Latres, E., Baumhueter, S., Lai, V. K.-M., Nunez, L., Clarke, B. A., et al. (2001). Identification of Ubiquitin Ligases Required for Skeletal Muscle Atrophy. *Science* 294 (5547), 1704–1708. doi:10.1126/science.1065874

Boelens, W. C., Croes, Y., and de Jong, W. W. (2001). Interaction between alphaB-Crystallin and the Human 20S Proteasomal Subunit C8/alpha7. *Biochim. Biophys. Acta* 1544 (1-2), 311–319. doi:10.1016/s0167-4838(00)00243-0

Bogomolovas, J., Fleming, J. R., Franke, B., Manso, B., Simon, B., Gasch, A., et al. (2021). Titin Kinase Ubiquitination Aligns Autophagy Receptors with Mechanical Signals in the Sarcomere. *EMBO Rep.* 22, e48018. doi:10.15252/embr.201948018

Bonaldo, P., and Sandri, M. (2013). Cellular and Molecular Mechanisms of Muscle Atrophy. *Dis. Model Mech.* 6 (1), 25–39. doi:10.1242/dmm.010389

Bowen, T. S., Adams, V., Werner, S., Fischer, T., Vinke, P., Brogger, M. N., et al. (2017). Small-molecule Inhibition of MuRF1 Attenuates Skeletal Muscle Atrophy and Dysfunction in Cardiac Cachexia. *J. Cachexia, Sarcopenia Muscle* 8 (6), 939–953. doi:10.1002/jcsm.12233

Boyer, J. K., Thanigaraj, S., Schechtman, K. B., and Pérez, J. E. (2004). Prevalence of Ventricular Diastolic Dysfunction in Asymptomatic, Normotensive Patients with Diabetes Mellitus. *Am. J. Cardiol.* 93 (7), 870–875. doi:10.1016/j.amjcard.2003.12.026

Braten, O., Livneh, I., Ziv, T., Admon, A., Kehat, I., Caspi, L. H., et al. (2016). Numerous Proteins with Unique Characteristics Are Degraded by the 26S Proteasome Following Monoubiquitination. *Proc. Natl. Acad. Sci. U.S.A.* 113 (32), E4639–E4647. doi:10.1073/pnas.1608644113

Bullard, B., Ferguson, C., Minajeva, A., Leake, M. C., Gautel, M., Labeit, D., et al. (2004). Association of the Chaperone αB-crystallin with Titin in Heart Muscle. *J. Biol. Chem.* 279 (9), 7917–7924. doi:10.1074/jbc.M307473200

Bulteau, A.-L., Lundberg, K. C., Humphries, K. M., Sadek, H. A., Szweda, P. A., Friguet, B., et al. (2001). Oxidative Modification and Inactivation of the Proteasome during Coronary Occlusion/reperfusion. *J. Biol. Chem.* 276 (32), 30057–30063. doi:10.1074/jbc.M100142200

Carmignac, V., Salih, M. A. M., Quijano-Roy, S., Marchand, S., Al Rayess, M. M., Mukhtar, M. M., et al. (2007). C-terminal Titin Deletions Cause a Novel Early-Onset Myopathy with Fatal Cardiomyopathy. *Ann. Neurol.* 61 (4), 340–351. doi:10.1002/ana.21089

Cave, A. C., Brewer, A. C., Narayanapanicker, A., Ray, R., Grieve, D. J., Walker, S., et al. (2006). NADPH Oxidases in Cardiovascular Health and Disease. *Antioxidants Redox Signal.* 8 (5-6), 691–728. doi:10.1089/ars.2006.8.691

Ceyhan-Birsoy, O., Agrawal, P. B., Hidalgo, C., Schmitz-Abe, K., DeChene, E. T., Swanson, L. C., et al. (2013). Recessive Truncating Titin Gene, TTN, Mutations Presenting as Centronuclear Myopathy. *Neurology* 81 (14), 1205–1214. doi:10.1212/WNL.0b013e3182a6ca62

Charton, K., Sarparanta, J., Vihola, A., Milic, A., Jonson, P. H., Suel, L., et al. (2015). CAPN3-mediated Processing of C-Terminal Titin Replaced by Pathological Cleavage in Titinopathy. *Hum. Mol. Genet.* 24 (13), 3718–3731. doi:10.1093/hmg/ddv116

Chauveau, C., Bonnemann, C. G., Julien, C., Kho, A. L., Marks, H., Talim, B., et al. (2013). Recessive TTN Truncating Mutations Define Novel Forms of Core Myopathy with Heart Disease. *Hum. Mol. Genet.* 23 (4), 980–991. doi:10.1093/hmg/ddt494

Chauveau, C., Rowell, J., and Ferreiro, A. (2014). A Rising Titan:TTNReview and Mutation Update. *Hum. Mutat.* 35 (9), 1046–1059. doi:10.1002/humu.22611

Chávez Zobel, A. T., Loranger, A., Marceau, N., Thériault, J. R., Lambert, H., and Landry, J. (2003). Distinct Chaperone Mechanisms Can Delay the Formation of Aggresomes by the Myopathy-Causing R120G alphaB-Crystallin Mutant. *Hum. Mol. Genet.* 12 (13), 1609–1620. doi:10.1093/hmg/ddg173

Chen, L., Tang, F., Gao, H., Zhang, X., Li, X., and Xiao, D. (2021). CAPN3: A Muscle-specific C-alpain with an I-mportant R-ole in the P-athogenesis of D-iseases (Review). *Int. J. Mol. Med.* 48 (5). doi:10.3892/ijmm.2021.5036

Chen, S. N., Czernuszewicz, G., Tan, Y., Lombardi, R., Jin, J., Willerson, J. T., et al. (2012). Human Molecular Genetic and Functional Studies Identify TRIM63 , Encoding Muscle RING Finger Protein 1, as a Novel Gene for Human Hypertrophic Cardiomyopathy. *Circ. Res.* 111 (7), 907–919. doi:10.1161/CIRCRESAHA.112.270207

Choi, A. M. K., Ryter, S. W., and Levine, B. (2013). Autophagy in Human Health and Disease. *N. Engl. J. Med.* 368 (7), 651–662. doi:10.1056/NEJMra1205406

Clarke, B. A., Drujan, D., Willis, M. S., Murphy, L. O., Corpina, R. A., Burova, E., et al. (2007). The E3 Ligase MuRF1 Degrades Myosin Heavy Chain Protein in Dexamethasone-Treated Skeletal Muscle. *Cell Metab.* 6 (5), 376–385. doi:10.1016/j.cmet.2007.09.009

Cohen, S., Brault, J. J., Gygi, S. P., Glass, D. J., Valenzuela, D. M., Gartner, C., et al. (2009). During Muscle Atrophy, Thick, but Not Thin, Filament Components Are Degraded by MuRF1-dependent Ubiquitylation. *J. Cell Biol.* 185 (6), 1083–1095. doi:10.1083/jcb.200901052

Coulis, G., Becila, S., Herrera-Mendez, C. H., Sentandreu, M. A., Raynaud, F., Richard, I., et al. (2008). Calpain 1 Binding Capacities of the N1-Line Region of Titin Are Significantly Enhanced by Physiological Concentrations of Calcium†. *Biochemistry* 47 (35), 9174–9183. doi:10.1021/bi800315v

da Silva Lopes, K., Pietas, A., Radke, M. H., and Gotthardt, M. (2011). Titin Visualization in Real Time Reveals an Unexpected Level of Mobility within and between Sarcomeres. *J. Cell Biol.* 193 (4), 785–798. doi:10.1083/jcb.201010099

Dalkilic, I., Schienda, J., Thompson, T. G., and Kunkel, L. M. (2006). Loss of FilaminC (FLNc) Results in Severe Defects in Myogenesis and Myotube Structure. *Mol. Cell Biol.* 26 (17), 6522–6534. doi:10.1128/mcb.00243-06

De Palma, C., Morisi, F., Cheli, S., Pambianco, S., Cappello, V., Vezzoli, M., et al. (2012). Autophagy as a New Therapeutic Target in Duchenne Muscular Dystrophy. *Cell Death Dis.* 3 (11), e418. doi:10.1038/cddis.2012.159

De Pascali, F., Hemann, C., Samons, K., Chen, C.-A., and Zweier, J. L. (2014). Hypoxia and Reoxygenation Induce Endothelial Nitric Oxide Synthase Uncoupling in Endothelial Cells through Tetrahydrobiopterin Depletion and S-Glutathionylation. *Biochemistry* 53 (22), 3679–3688. doi:10.1021/bi500076r

Demand, J., Alberti, S., Patterson, C., and Höhfeld, J. (2001). Cooperation of a Ubiquitin Domain Protein and an E3 Ubiquitin Ligase during Chaperone/proteasome Coupling. *Curr. Biol.* 11 (20), 1569–1577. doi:10.1016/s0960-9822(01)00487-0

den Engelsman, J., Keijsers, V., de Jong, W. W., and Boelens, W. C. (2003). The Small Heat-Shock Protein αB-Crystallin Promotes FBX4-dependent Ubiquitination. *J. Biol. Chem.* 278 (7), 4699–4704. doi:10.1074/jbc.M211403200

Depre, C., Wang, L., Sui, X., Qiu, H., Hong, C., Hedhli, N., et al. (2006). H11 Kinase Prevents Myocardial Infarction by Preemptive Preconditioning of the Heart. *Circulation Res.* 98 (2), 280–288. doi:10.1161/01.RES.0000201284.45482.e8

Díaz-Villanueva, J., Díaz-Molina, R., and García-González, V. (2015). Protein Folding and Mechanisms of Proteostasis. *Ijms* 16 (8), 17193–17230. doi:10.3390/ijms160817193

Donlin, L. T., Andresen, C., Just, S., Rudensky, E., Pappas, C. T., Kruger, M., et al. (2012). Smyd2 Controls Cytoplasmic Lysine Methylation of Hsp90 and Myofilament Organization. *Genes Dev.* 26 (2), 114–119. doi:10.1101/gad.177758.111

Dorsch, L. M., Schuldt, M., Knežević, D., Wiersma, M., Kuster, D. W. D., van der Velden, J., et al. (2019). Untying the Knot: Protein Quality Control in Inherited Cardiomyopathies. *Pflugers Arch. - Eur. J. Physiol.* 471 (5), 795–806. doi:10.1007/s00424-018-2194-0

Dove, K. K., and Klevit, R. E. (2017). RING-Between-RING E3 Ligases: Emerging Themes amid the Variations. *J. Mol. Biol.* 429 (22), 3363–3375. doi:10.1016/j.jmb.2017.08.008

Eaton, P., Byers, H. L., Leeds, N., Ward, M. A., and Shattock, M. J. (2002). Detection, Quantitation, Purification, and Identification of Cardiac Proteins S-Thiolated during Ischemia and Reperfusion. *J. Biol. Chem.* 277 (12), 9806–9811. doi:10.1074/jbc.M111454200

Edström, L., Thornell, L. E., Albo, J., Landin, S., and Samuelsson, M. (1990). Myopathy with Respiratory Failure and Typical Myofibrillar Lesions. *J. Neurol. Sci.* 96 (2), 211–228. doi:10.1016/0022-510X(90)90134-9

Egan, D., Kim, J., Shaw, R. J., and Guan, K.-L. (2011). The Autophagy Initiating Kinase ULK1 Is Regulated via Opposing Phosphorylation by AMPK and mTOR. *Autophagy* 7 (6), 643–644. doi:10.4161/auto.7.6.15123

Evilä, A., Vihola, A., Sarparanta, J., Raheem, O., Palmio, J., Sandell, S., et al. (2014). Atypical Phenotypes in Titinopathies Explained by Second Titin Mutations. *Ann. Neurol.* 75 (2), 230–240. doi:10.1002/ana.24102

Fan, G.-C., Ren, X., Qian, J., Yuan, Q., Nicolaou, P., Wang, Y., et al. (2005). Novel Cardioprotective Role of a Small Heat-Shock Protein, Hsp20, against Ischemia/reperfusion Injury. *Circulation* 111 (14), 1792–1799. doi:10.1161/01.cir.0000160851.41872.c6

Feng, Y., He, D., Yao, Z., and Klionsky, D. J. (2014). The Machinery of Macroautophagy. *Cell Res.* 24 (1), 24–41. doi:10.1038/cr.2013.168

Fielitz, J., Kim, M.-S., Shelton, J. M., Latif, S., Spencer, J. A., Glass, D. J., et al. (2007). Myosin Accumulation and Striated Muscle Myopathy Result from the Loss of Muscle RING Finger 1 and 3. *J. Clin. Invest.* 117 (9), 2486–2495. doi:10.1172/jci32827

Fomin, A., Gärtner, A., Cyganek, L., Tiburcy, M., Tuleta, I., Wellers, L., et al. (2021). Truncated Titin Proteins and Titin Haploinsufficiency Are Targets for Functional Recovery in Human Cardiomyopathy Due to TTN Mutations. *Sci. Transl. Med.* 13 (618), eabd3079. doi:10.1126/scitranslmed.abd3079

Franssen, C., Kole, J., Musters, R., Hamdani, N., and Paulus, W. J. (2017). α-B Crystallin Reverses High Diastolic Stiffness of Failing Human Cardiomyocytes. *Circ. Heart Fail.* 10 (3), e003626. doi:10.1161/CIRCHEARTFAILURE.116.003626

Freiburg, A., Trombitas, K., Hell, W., Cazorla, O., Fougerousse, F., Centner, T., et al. (2000). Series of Exon-Skipping Events in the Elastic Spring Region of Titin as the Structural Basis for Myofibrillar Elastic Diversity. *Circulation Res.* 86 (11), 1114–1121. doi:10.1161/01.res.86.11.1114

Fukuzawa, A., Lange, S., Holt, M., Vihola, A., Carmignac, V., Ferreiro, A., et al. (2008). Interactions with Titin and Myomesin Target Obscurin and Obscurin-like 1 to the M-Band - Implications for Hereditary Myopathies. *J. Cell Sci.* 121 (11), 1841–1851. doi:10.1242/jcs.028019

Gaiser, A. M., Kaiser, C. J. O., Haslbeck, V., and Richter, K. (2011). Downregulation of the Hsp90 System Causes Defects in Muscle Cells of *Caenorhabditis elegans*. *PLoS One* 6 (9), e25485. doi:10.1371/journal.pone.0025485

Galvez, A. S., Diwan, A., Odley, A. M., Hahn, H. S., Osinska, H., Melendez, J. G., et al. (2007). Cardiomyocyte Degeneration with Calpain Deficiency Reveals a Critical Role in Protein Homeostasis. *Circulation Res.* 100 (7), 1071–1078. doi:10.1161/01.RES.0000261938.28365.11

Gamerdinger, M., Hajieva, P., Kaya, A. M., Wolfrum, U., Hartl, F. U., and Behl, C. (2009). Protein Quality Control during Aging Involves Recruitment of the Macroautophagy Pathway by BAG3. *Embo J.* 28 (7), 889–901. doi:10.1038/emboj.2009.29

Garrido, C., Brunet, M., Didelot, C., Zermati, Y., Schmitt, E., and Kroemer, G. (2006). Heat Shock Proteins 27 and 70: Anti-apoptotic Proteins with Tumorigenic Properties. *Cell Cycle* 5 (22), 2592–2601. doi:10.4161/cc.5.22.3448

Gatica, D., Chiong, M., Lavandero, S., and Klionsky, D. J. (2015). Molecular Mechanisms of Autophagy in the Cardiovascular System. *Circ. Res.* 116 (3), 456–467. doi:10.1161/CIRCRESAHA.114.303788

Gautel, M. (2011a). Cytoskeletal Protein Kinases: Titin and its Relations in Mechanosensing. *Pflugers Arch. - Eur. J. Physiol.* 462 (1), 119–134. doi:10.1007/s00424-011-0946-1

Gautel, M. (2011b). The Sarcomeric Cytoskeleton: Who Picks up the Strain? *Curr. Opin. Cell Biol.* 23 (1), 39–46. doi:10.1016/j.ceb.2010.12.001

Gazda, L., Pokrzywa, W., Hellerschmied, D., Löwe, T., Forné, I., Mueller-Planitz, F., et al. (2013). The Myosin Chaperone UNC-45 Is Organized in Tandem Modules to Support Myofilament Formation in *C. elegans*. *Cell* 152 (1-2), 183–195. doi:10.1016/j.cell.2012.12.025

Giacomello, E., Quarta, M., Paolini, C., Squecco, R., Fusco, P., Toniolo, L., et al. (2015). Deletion of Small Ankyrin 1 (sAnk1) Isoforms Results in Structural and Functional Alterations in Aging Skeletal Muscle Fibers. *Am. J. Physiology-Cell Physiology* 308 (2), C123–C138. doi:10.1152/ajpcell.00090.2014

Glazier, A. A., Hafeez, N., Mellacheruvu, D., Basrur, V., Nesvizhskii, A. I., Lee, L. M., et al. (2018). HSC70 Is a Chaperone for Wild-type and Mutant Cardiac Myosin Binding Protein C. *JCI Insight* 3 (11). doi:10.1172/jci.insight.99319

Gomes, M. D., Lecker, S. H., Jagoe, R. T., Navon, A., and Goldberg, A. L. (2001). Atrogin-1, a Muscle-specific F-Box Protein Highly Expressed during Muscle Atrophy. *Proc. Natl. Acad. Sci. U.S.A.* 98 (25), 14440–14445. doi:10.1073/pnas.251541198

Granzier, H. L., and Irving, T. C. (1995). Passive Tension in Cardiac Muscle: Contribution of Collagen, Titin, Microtubules, and Intermediate Filaments. *Biophysical J.* 68 (3), 1027–1044. doi:10.1016/s0006-3495(95)80278-x

Granzier, H. L., and Labeit, S. (2004). The Giant Protein Titin: a Major Player in Myocardial Mechanics, Signaling, and Disease. *Circulation Res.* 94 (3), 284–295. doi:10.1161/01.RES.0000117769.88862.F8

Groll, M., Glickman, M. H., Finley, D., Bajorek, M., Köhler, A., Moroder, L., et al. (2000). A Gated Channel into the Proteasome Core Particle. *Nat. Struct. Biol.* 7 (11), 1062–1067. doi:10.1038/80992

Grützner, A., Garcia-Manyes, S., Kötter, S., Badilla, C. L., Fernandez, J. M., and Linke, W. A. (2009). Modulation of Titin-Based Stiffness by Disulfide Bonding in the Cardiac Titin N2-B Unique Sequence. *Biophysical J.* 97 (3), 825–834. doi:10.1016/j.bpj.2009.05.037

Gundogdu, M., and Walden, H. (2019). Structural Basis of Generic versus Specific E2-RING E3 Interactions in Protein Ubiquitination. *Protein Sci.* 28 (10), 1758–1770. doi:10.1002/pro.3690

Guo, W., Schafer, S., Greaser, M. L., Radke, M. H., Liss, M., Govindarajan, T., et al. (2012). RBM20, a Gene for Hereditary Cardiomyopathy, Regulates Titin Splicing. *Nat. Med.* 18 (5), 766–773. doi:10.1038/nm.2693

Gustafsson, Å. B., and Gottlieb, R. A. (2008). Recycle or die: the role of autophagy in cardioprotection. *J. Mol. Cell. Cardiol.* 44 (4), 654–661. doi:10.1016/j.yjmcc.2008.01.010

Hackman, P., Marchand, S., Sarparanta, J., Vihola, A., Pénisson-Besnier, I., Eymard, B., et al. (2008). Truncating Mutations in C-Terminal Titin May

Cause More Severe Tibial Muscular Dystrophy (TMD). *Neuromuscul. Disord.* 18 (12), 922–928. doi:10.1016/j.nmd.2008.07.010

Hackman, P., Vihola, A., Haravuori, H., Marchand, S., Sarparanta, J., De Seze, J., et al. (2002). Tibial Muscular Dystrophy Is a Titinopathy Caused by Mutations in TTN, the Gene Encoding the Giant Skeletal-Muscle Protein Titin. *Am. J. Hum. Genet.* 71 (3), 492–500. doi:10.1086/342380

Hamdani, N., Franssen, C., Lourenço, A., Falcão-Pires, I., Fontoura, D., Leite, S., et al. (2013). Myocardial Titin Hypophosphorylation Importantly Contributes to Heart Failure with Preserved Ejection Fraction in a Rat Metabolic Risk Model. *Circ. Heart Fail.* 6 (6), 1239–1249. doi:10.1161/CIRCHEARTFAILURE.113.000539

Han, X., Wang, Y., Fu, M., Song, Y., Wang, J., Cui, X., et al. (2020). Effects of Adiponectin on Diastolic Function in Mice Underwent Transverse Aorta Constriction. *J. Cardiovasc. Trans. Res.* 13 (2), 225–237. doi:10.1007/s12265-019-09913-1

Hastings, R., de Villiers, C. P., Hooper, C., Ormondroyd, L., Pagnamenta, A., Lise, S., et al. (2016). Combination of Whole Genome Sequencing, Linkage, and Functional Studies Implicates a Missense Mutation in Titin as a Cause of Autosomal Dominant Cardiomyopathy with Features of Left Ventricular Noncompaction. *Circ. Cardiovasc Genet.* 9 (5), 426–435. doi:10.1161/circgenetics.116.001431

Hayashi, C., Ono, Y., Doi, N., Kitamura, F., Tagami, M., Mineki, R., et al. (2008). Multiple Molecular Interactions Implicate the Connectin/titin N2A Region as a Modulating Scaffold for P94/calpain 3 Activity in Skeletal Muscle. *J. Biol. Chem.* 283 (21), 14801–14814. doi:10.1074/jbc.M708262200

Hedberg, C., Toledo, A. G., Gustafsson, C. M., Larson, G., Oldfors, A., and Macao, B. (2014). Hereditary Myopathy with Early Respiratory Failure Is Associated with Misfolding of the Titin Fibronectin III 119 Subdomain. *Neuromuscul. Disord.* 24 (5), 373–379. doi:10.1016/j.nmd.2014.02.003

Hein, S., Scholz, D., Fujitani, N., Rennollet, H., Brand, T., Friedl, A., et al. (1994). Altered Expression of Titin and Contractile Proteins in Failing Human Myocardium. *J. Mol. Cell. Cardiol.* 26 (10), 1291–1306. doi:10.1006/jmcc.1994.1148

Helms, A. S., Thompson, A. D., Glazier, A. A., Hafeez, N., Kabani, S., Rodriguez, J., et al. (2020). Spatial and Functional Distribution of MYBPC3 Pathogenic Variants and Clinical Outcomes in Patients with Hypertrophic Cardiomyopathy. *Circ Genomic Precis. Med.* 13 (5), 396–405. doi:10.1161/circgen.120.002929

Herman, D. S., Lam, L., Taylor, M. R. G., Wang, L., Teekakirikul, P., Christodoulou, D., et al. (2012). Truncations of Titin Causing Dilated Cardiomyopathy. *N. Engl. J. Med.* 366 (7), 619–628. doi:10.1056/NEJMoa1110186

Hershberger, R. E., Hedges, D. J., and Morales, A. (2013). Dilated Cardiomyopathy: the Complexity of a Diverse Genetic Architecture. *Nat. Rev. Cardiol.* 10 (9), 531–547. doi:10.1038/nrcardio.2013.105

Hidalgo, C., Hudson, B., Bogomolovas, J., Zhu, Y., Anderson, B., Greaser, M., et al. (2009). PKC Phosphorylation of Titin's PEVK Element: a Novel and Conserved Pathway for Modulating Myocardial Stiffness. *Circulation Res.* 105 (7), 631–638. doi:10.1161/CIRCRESAHA.109.198465

Higashikuse, Y., Mittal, N., Arimura, T., Yoon, S. H., Oda, M., Enomoto, H., et al. (2019). Perturbation of the titin/MURF1 Signaling Complex Is Associated with Hypertrophic Cardiomyopathy in a Fish Model and in Human Patients. *Dis. Model Mech.* 12 (11). doi:10.1242/dmm.041103

Hnia, K., Clausen, T., and Moog-Lutz, C. (2019). Shaping Striated Muscles with Ubiquitin Proteasome System in Health and Disease. *Trends Mol. Med.* 25 (9), 760–774. doi:10.1016/j.molmed.2019.05.008

Ho, C. Y., Day, S. M., Ashley, E. A., Michels, M., Pereira, A. C., Jacoby, D., et al. (2018). Genotype and Lifetime Burden of Disease in Hypertrophic Cardiomyopathy. *Circulation* 138(14), 1387–1398. doi:10.1161/CIRCULATIONAHA.117.033200

Hopf, A.-E., Andresen, C., Kötter, S., Isić, M., Ulrich, K., Sahin, S., et al. (2018). Diabetes-Induced Cardiomyocyte Passive Stiffening Is Caused by Impaired Insulin-dependent Titin Modification and Can Be Modulated by Neuregulin-1. *Circ. Res.* 123 (3), 342–355. doi:10.1161/CIRCRESAHA.117.312166

Huebsch, K. A., Kudryashova, E., Wooley, C. M., Sher, R. B., Seburn, K. L., Spencer, M. J., et al. (2005). Mdm Muscular Dystrophy: Interactions with Calpain 3 and a Novel Functional Role for Titin's N2A Domain. *Hum. Mol. Genet.* 14 (19), 2801–2811. doi:10.1093/hmg/ddi313

Hunter, T. (2007). The Age of Crosstalk: Phosphorylation, Ubiquitination, and beyond. *Mol. Cell* 28 (5), 730–738. doi:10.1016/j.molcel.2007.11.019

Hwang, H., Bowen, B. P., Lefort, N., Flynn, C. R., De Filippis, E. A., Roberts, C., et al. (2010). Proteomics Analysis of Human Skeletal Muscle Reveals Novel Abnormalities in Obesity and Type 2 Diabetes. *Diabetes* 59 (1), 33–42. doi:10.2337/db09-0214

Hyatt, H. W., and Powers, S. K. (2020). The Role of Calpains in Skeletal Muscle Remodeling with Exercise and Inactivity-Induced Atrophy. *Int. J. Sports Med.* 41 (14), 994–1008. doi:10.1055/a-1199-7662

Ikeda, Y., Shirakabe, A., Maejima, Y., Zhai, P., Sciarretta, S., Toli, J., et al. (2015). Endogenous Drp1 Mediates Mitochondrial Autophagy and Protects the Heart against Energy Stress. *Circ. Res.* 116 (2), 264–278. doi:10.1161/circresaha.116.303356

Isaacs, W. B., Kim, I. S., Struve, A., and Fulton, A. B. (1989). Biosynthesis of Titin in Cultured Skeletal Muscle Cells. *J. Cell Biol.* 109 (5), 2189–2195. doi:10.1083/jcb.109.5.2189

Ji, C. H., and Kwon, Y. T. (2017). Crosstalk and Interplay between the Ubiquitin-Proteasome System and Autophagy. *Mol. Cells* 40 (7), 441–449. doi:10.14348/molcells.2017.0115

Jiang, H., Hooper, C., Kelly, M., Steeples, V., Simon, J. N., Beglov, J., et al. (2021). Functional Analysis of a Gene-Edited Mouse Model to Gain Insights into the Disease Mechanisms of a Titin Missense Variant. *Basic Res. Cardiol.* 116 (1), 14. doi:10.1007/s00395-021-00853-z

Jovcevski, B., Kelly, M. A., Rote, A. P., Berg, T., Gastall, H. Y., Benesch, J. L. P., et al. (2015). Phosphomimics Destabilize Hsp27 Oligomeric Assemblies and Enhance Chaperone Activity. *Chem. Biol.* 22 (2), 186–195. doi:10.1016/j.chembiol.2015.01.001

Kalogeris, T., Baines, C. P., Krenz, M., and Korthuis, R. J. (2012). Cell Biology of Ischemia/reperfusion Injury. *Int. Rev. Cell Mol. Biol.* 298, 229–317. doi:10.1016/b978-0-12-394309-5.00006-7

Kanamori, H., Takemura, G., Goto, K., Tsujimoto, A., Mikami, A., Ogino, A., et al. (2015). Autophagic Adaptations in Diabetic Cardiomyopathy Differ between Type 1 and Type 2 Diabetes. *Autophagy* 11 (7), 1146–1160. doi:10.1080/15548627.2015.1051295

Kappé, G., Boelens, W. C., and de Jong, W. W. (2010). Why Proteins without an α-crystallin Domain Should Not Be Included in the Human Small Heat Shock Protein Family HSPB. *Cell Stress Chaperones* 15 (4), 457–461. doi:10.1007/s12192-009-0155-4

Karczewski, K. J., Francioli, L. C., Tiao, G., Cummings, B. B., Alföldi, J., Wang, Q., et al. (2020). The Mutational Constraint Spectrum Quantified from Variation in 141,456 Humans. *Nature* 581 (7809), 434–443. doi:10.1038/s41586-020-2308-7

Kedar, V., McDonough, H., Arya, R., Li, H.-H., Rockman, H. A., and Patterson, C. (2004). Muscle-specific RING Finger 1 Is a Bona Fide Ubiquitin Ligase that Degrades Cardiac Troponin I. *Proc. Natl. Acad. Sci. U.S.A.* 101 (52), 18135–18140. doi:10.1073/pnas.0404341102

Kellermayer, D., Smith, J. E., 3rd, and Granzier, H. (2019). Titin Mutations and Muscle Disease. *Pflugers Arch. - Eur. J. Physiol.* 471 (5), 673–682. doi:10.1007/s00424-019-02272-5

Kim, J., Kundu, M., Viollet, B., and Guan, K.-L. (2011). AMPK and mTOR Regulate Autophagy through Direct Phosphorylation of Ulk1. *Nat. Cell Biol.* 13 (2), 132–141. doi:10.1038/ncb2152

King, H., Aubert, R. E., and Herman, W. H. (1998). Global Burden of Diabetes, 1995-2025: Prevalence, Numerical Estimates, and Projections. *Diabetes Care* 21 (9), 1414–1431. doi:10.2337/diacare.21.9.1414

Klemenz, R., Andres, A. C., Fröhli, E., Schäfer, R., and Aoyama, A. (1993). Expression of the Murine Small Heat Shock Proteins Hsp 25 and Alpha B Crystallin in the Absence of Stress. *J. Cell Biol.* 120 (3), 639–645. doi:10.1083/jcb.120.3.639

Kley, R. A., Olivé, M., and Schröder, R. (2016). New Aspects of Myofibrillar Myopathies. *Curr. Opin. Neurol.* 29 (5), 628–634. doi:10.1097/wco.0000000000000357

Kley, R. A., van der Ven, P. F. M., Olivé, M., Höhfeld, J., Goldfarb, L. G., Fürst, D. O., et al. (2013). Impairment of Protein Degradation in Myofibrillar Myopathy Caused by FLNC/filamin C Mutations. *Autophagy* 9 (3), 422–423. doi:10.4161/auto.22921

Knöll, R., Hoshijima, M., Hoffman, H. M., Person, V., Lorenzen-Schmidt, I., Bang, M.-L., et al. (2002). The Cardiac Mechanical Stretch Sensor Machinery Involves a Z Disc Complex that Is Defective in a Subset of Human Dilated Cardiomyopathy. *Cell* 111 (7), 943–955. doi:10.1016/s0092-8674(02)01226-6

Kobayashi, S., Xu, X., Chen, K., and Liang, Q. (2012). Suppression of Autophagy Is Protective in High Glucose-Induced Cardiomyocyte Injury. *Autophagy* 8 (4), 577–592. doi:10.4161/auto.18980

Koenig, M., Hoffman, E. P., Bertelson, C. J., Monaco, A. P., Feener, C., and Kunkel, L. M. (1987). Complete Cloning of the Duchenne Muscular Dystrophy (DMD) cDNA and Preliminary Genomic Organization of the DMD Gene in Normal and Affected Individuals. *Cell* 50 (3), 509–517. doi:10.1016/0092-8674(87)90504-6

Koser, F., Loescher, C., and Linke, W. A. (2019). Posttranslational Modifications of Titin from Cardiac Muscle: How, where, and what for? *Febs J.* 286 (12), 2240–2260. doi:10.1111/febs.14854

Kötter, S., Gout, L., Von Frieling-Salewsky, M., Müller, A. E., Helling, S., Marcus, K., et al. (2013). Differential Changes in Titin Domain Phosphorylation Increase Myofilament Stiffness in Failing Human Hearts. *Cardiovasc Res.* 99 (4), 648–656. doi:10.1093/cvr/cvt144

Kötter, S., Kazmierowska, M., Andresen, C., Bottermann, K., Grandoch, M., Gorressen, S., et al. (2016). Titin-Based Cardiac Myocyte Stiffening Contributes to Early Adaptive Ventricular Remodeling after Myocardial Infarction. *Circ. Res.* 119 (9), 1017–1029. doi:10.1161/CIRCRESAHA.116.309685

Kötter, S., Unger, A., Hamdani, N., Lang, P., Vorgerd, M., Nagel-Steger, L., et al. (2014). Human Myocytes Are Protected from Titin Aggregation-Induced Stiffening by Small Heat Shock Proteins. *J. Cell Biol.* 204 (2), 187–202. doi:10.1083/jcb.201306077

Kramerova, I., Kudryashova, E., Venkatraman, G., and Spencer, M. J. (2005). Calpain 3 Participates in Sarcomere Remodeling by Acting Upstream of the Ubiquitin-Proteasome Pathway. *Hum. Mol. Genet.* 14 (15), 2125–2134. doi:10.1093/hmg/ddi217

Kroemer, G. (2015). Autophagy: a Druggable Process that Is Deregulated in Aging and Human Disease. *J. Clin. Invest.* 125 (1), 1–4. doi:10.1172/jci78652

Krüger, M., Babicz, K., von Frieling-Salewsky, M., and Linke, W. A. (2010). Insulin Signaling Regulates Cardiac Titin Properties in Heart Development and Diabetic Cardiomyopathy. *J. Mol. Cell. Cardiol.* 48 (5), 910–916. doi:10.1016/j.yjmcc.2010.02.012

Krüger, M., and Linke, W. A. (2006). Protein Kinase-A Phosphorylates Titin in Human Heart Muscle and Reduces Myofibrillar Passive Tension. *J. Muscle Res. Cell Motil.* 27 (5-7), 435–444. doi:10.1007/s10974-006-9090-5

Krüger, M., and Linke, W. A. (2011). The Giant Protein Titin: a Regulatory Node that Integrates Myocyte Signaling Pathways. *J. Biol. Chem.* 286 (12), 9905–9912. doi:10.1074/jbc.R110.173260

Krüger, M., Kötter, S., Grützner, A., Lang, P., Andresen, C., Redfield, M. M., et al. (2009). Protein Kinase G Modulates Human Myocardial Passive Stiffness by Phosphorylation of the Titin Springs. *Circulation Res.* 104 (1), 87–94. doi:10.1161/CIRCRESAHA.108.184408

Krüger, M., Sachse, C., Zimmermann, W. H., Eschenhagen, T., Klede, S., and Linke, W. A. (2008). Thyroid Hormone Regulates Developmental Titin Isoform Transitions via the Phosphatidylinositol-3-Kinase/AKT Pathway. *Circulation Res.* 102 (4), 439–447. doi:10.1161/CIRCRESAHA.107.162719

Labeit, S., Gautel, M., Lakey, A., and Trinick, J. (1992). Towards a Molecular Understanding of Titin. *EMBO J.* 11 (5), 1711–1716. doi:10.1002/j.1460-2075.1992.tb05222.x

Labeit, S., Lahmers, S., Burkart, C., Fong, C., McNabb, M., Witt, S., et al. (2006). Expression of Distinct Classes of Titin Isoforms in Striated and Smooth Muscles by Alternative Splicing, and Their Conserved Interaction with Filamins. *J. Mol. Biol.* 362 (4), 664–681. doi:10.1016/j.jmb.2006.07.077

Lahmers, S., Wu, Y., Call, D. R., Labeit, S., and Granzier, H. (2004). Developmental Control of Titin Isoform Expression and Passive Stiffness in Fetal and Neonatal Myocardium. *Circulation Res.* 94 (4), 505–513. doi:10.1161/01.Res.0000115522.52554.86

Lander, G. C., Estrin, E., Matyskiela, M. E., Bashore, C., Nogales, E., and Martin, A. (2012). Complete Subunit Architecture of the Proteasome Regulatory Particle. *Nature* 482 (7384), 186–191. doi:10.1038/nature10774

Lang, F., Aravamudhan, S., Nolte, H., Tuerk, C., Hölper, S., Müller, S., et al. (2017). Dynamic Changes in the Skeletal Muscle Proteome during Denervation-Induced Atrophy. *Dis. Model Mech.* 10 (7), 881–896. doi:10.1242/dmm.028910

Lange, S., Ehler, E., and Gautel, M. (2006). From A to Z and Back? Multicompartment Proteins in the Sarcomere. *Trends Cell Biol.* 16 (1), 11–18. doi:10.1016/j.tcb.2005.11.007

Lange, S., Ouyang, K., Meyer, G., Cui, L., Cheng, H., Lieber, R. L., et al. (2009). Obscurin Determines the Architecture of the Longitudinal Sarcoplasmic Reticulum. *J. Cell Sci.* 122 (Pt 15), 2640–2650. doi:10.1242/jcs.046193

Lange, S., Perera, S., Teh, P., and Chen, J. (2012). Obscurin and KCTD6 Regulate Cullin-dependent Small Ankyrin-1 (sAnk1.5) Protein Turnover. *MBoC* 23 (13), 2490–2504. doi:10.1091/mbc.E12-01-0052

Lange, S., Xiang, F., Yakovenko, A., Vihola, A., Hackman, P., Rostkova, E., et al. (2005). The Kinase Domain of Titin Controls Muscle Gene Expression and Protein Turnover. *Science* 308 (5728), 1599–1603. doi:10.1126/science.1110463

Letavernier, E., Zafrani, L., Perez, J., Letavernier, B., Haymann, J.-P., and Baud, L. (2012). The Role of Calpains in Myocardial Remodelling and Heart Failure. *Cardiovasc. Res.* 96 (1), 38–45. doi:10.1093/cvr/cvs099

Levine, B., and Kroemer, G. (2008). Autophagy in the Pathogenesis of Disease. *Cell* 132 (1), 27–42. doi:10.1016/j.cell.2007.12.018

Li, J., Ma, W., Yue, G., Tang, Y., Kim, I.-m., Weintraub, N. L., et al. (2017). Cardiac Proteasome Functional Insufficiency Plays a Pathogenic Role in Diabetic Cardiomyopathy. *J. Mol. Cell. Cardiol.* 102, 53–60. doi:10.1016/j.yjmcc.2016.11.013

Lim, C. C., Zuppinger, C., Guo, X., Kuster, G. M., Helmes, M., Eppenberger, H. M., et al. (2004). Anthracyclines Induce Calpain-dependent Titin Proteolysis and Necrosis in Cardiomyocytes. *J. Biol. Chem.* 279 (9), 8290–8299. doi:10.1074/jbc.M308033200

Linke, W. A., and Hamdani, N. (2014). Gigantic Business: Titin Properties and Function through Thick and Thin. *Circ. Res.* 114 (6), 1052–1068. doi:10.1161/CIRCRESAHA.114.301286

Linke, W. (2008). Sense and Stretchability: the Role of Titin and Titin-Associated Proteins in Myocardial Stress-Sensing and Mechanical Dysfunction. *Cardiovasc. Res.* 77 (4), 637–648. doi:10.1016/j.cardiores.2007.03.029

Liu, Y., Shoji-Kawata, S., Sumpter, R. M., Jr., Wei, Y., Ginet, V., Zhang, L., et al. (2013). Autosis Is a Na+,K+-ATPase-regulated Form of Cell Death Triggered by Autophagy-Inducing Peptides, Starvation, and Hypoxia-Ischemia. *Proc. Natl. Acad. Sci. U.S.A.* 110 (51), 20364–20371. doi:10.1073/pnas.1319661110

Livneh, I., Cohen-Kaplan, V., Cohen-Rosenzweig, C., Avni, N., and Ciechanover, A. (2016). The Life Cycle of the 26S Proteasome: from Birth, through Regulation and Function, and onto its Death. *Cell Res.* 26 (8), 869–885. doi:10.1038/cr.2016.86

Loescher, C. M., Breitkreuz, M., Li, Y., Nickel, A., Unger, A., Dietl, A., et al. (2020). Regulation of Titin-Based Cardiac Stiffness by Unfolded Domain Oxidation (UnDOx). *Proc. Natl. Acad. Sci. U.S.A.* 117 (39), 24545–24556. doi:10.1073/pnas.2004900117

Lorenz, S. (2018). Structural Mechanisms of HECT-type Ubiquitin Ligases. *Biol. Chem.* 399 (2), 127–145. doi:10.1515/hsz-2017-0184

Mao, Z., and Nakamura, F. (2020). Structure and Function of Filamin C in the Muscle Z-Disc. *Ijms* 21 (8), 2696. doi:10.3390/ijms21082696

Marston, S., Copeland, O. N., Jacques, A., Livesey, K., Tsang, V., McKenna, W. J., et al. (2009). Evidence from Human Myectomy Samples that MYBPC3 Mutations Cause Hypertrophic Cardiomyopathy through Haploinsufficiency. *Circulation Res.* 105 (3), 219–222. doi:10.1161/circresaha.109.202440

Martin, T. G., Myers, V. D., Dubey, P., Dubey, S., Perez, E., Moravec, C. S., et al. (2021). Cardiomyocyte Contractile Impairment in Heart Failure Results from Reduced BAG3-Mediated Sarcomeric Protein Turnover. *Nat. Commun.* 12 (1), 2942. doi:10.1038/s41467-021-23272-z

Matsui, Y., Takagi, H., Qu, X., Abdellatif, M., Sakoda, H., Asano, T., et al. (2007). Distinct Roles of Autophagy in the Heart during Ischemia and Reperfusion: Roles of AMP-Activated Protein Kinase and Beclin 1 in Mediating Autophagy. *Circulation Res.* 100 (6), 914–922. doi:10.1161/01.RES.0000261924.76669.36

Melkani, G. C., Bodmer, R., Ocorr, K., and Bernstein, S. I. (2011). The UNC-45 Chaperone Is Critical for Establishing Myosin-Based Myofibrillar Organization and Cardiac Contractility in the Drosophila Heart Model. *PLoS One* 6 (7), e22579. doi:10.1371/journal.pone.0022579

Mellor, K. M., Bell, J. R., Young, M. J., Ritchie, R. H., and Delbridge, L. M. D. (2011). Myocardial Autophagy Activation and Suppressed Survival Signaling Is Associated with Insulin Resistance in Fructose-Fed Mice. *J. Mol. Cell. Cardiol.* 50 (6), 1035–1043. doi:10.1016/j.yjmcc.2011.03.002

Milazzo, V., Cosentino, N., Genovese, S., Campodonico, J., Mazza, M., De Metrio, M., et al. (2021). Diabetes Mellitus and Acute Myocardial Infarction: Impact on Short and Long-Term Mortality. *Adv. Exp. Med. Biol.* 1307, 153–169. doi:10.1007/5584_2020_481

Miller, M., Granzier, H., Ehler, E., and Gregorio, C. C. (2004). The Sensitive Giant: the Role of Titin-Based Stretch Sensing Complexes in the Heart. *Trends Cell Biol.* 14 (3), 119–126. doi:10.1016/j.tcb.2004.01.003

Mizushima, N., and Komatsu, M. (2011). Autophagy: Renovation of Cells and Tissues. *Cell* 147 (4), 728–741. doi:10.1016/j.cell.2011.10.026

Mizushima, N. (2010). The Role of the Atg1/ULK1 Complex in Autophagy Regulation. *Curr. Opin. Cell Biol.* 22 (2), 132–139. doi:10.1016/j.ceb.2009.12.004

Mo, Y., Tang, L., Ma, Y., and Wu, S. (2016). Pramipexole Pretreatment Attenuates Myocardial Ischemia/reperfusion Injury through Upregulation of Autophagy. *Biochem. Biophysical Res. Commun.* 473 (4), 1119–1124. doi:10.1016/j.bbrc.2016.04.026

Moncrief, T., Matheny, C. J., Gaziova, I., Miller, J. M., Qadota, H., Benian, G. M., et al. (2021). Mutations in Conserved Residues of the Myosin Chaperone UNC -45 Result in Both Reduced Stability and Chaperoning Activity. *Protein Sci.* 30 (11), 2221–2232. doi:10.1002/pro.4180

Morreale, F. E., and Walden, H. (2016). Types of Ubiquitin Ligases. *Cell* 165 (1), 248. e241. doi:10.1016/j.cell.2016.03.003

Mues, A., van der Ven, P. F., Young, P., Fürst, D. O., and Gautel, M. (1998). Two Immunoglobulin-like Domains of the Z-Disc Portion of Titin Interact in a Conformation-dependent Way with Telethonin. *FEBS Lett.* 428 (1-2), 111–114. doi:10.1016/s0014-5793(98)00501-8

Müller, E., Salcan, S., Bongardt, S., Barbosa, D. M., Krüger, M., and Kötter, S. (2021). E3-ligase Knock Down Revealed Differential Titin Degradation by Autophagy and the Ubiquitin Proteasome System. *Sci. Rep.* 11 (1), 21134. doi:10.1038/s41598-021-00618-7

Munkanatta Godage, D. N. P., VanHecke, G. C., Samarasinghe, K. T. G., Feng, H.-Z., Hiske, M., Holcomb, J., et al. (2018). SMYD2 Glutathionylation Contributes to Degradation of Sarcomeric Proteins. *Nat. Commun.* 9 (1), 4341. doi:10.1038/s41467-018-06786-x

Mymrikov, E. V., Seit-Nebi, A. S., and Gusev, N. B. (2011). Large Potentials of Small Heat Shock Proteins. *Physiol. Rev.* 91 (4), 1123–1159. doi:10.1152/physrev.00023.2010

Nakai, A., Yamaguchi, O., Takeda, T., Higuchi, Y., Hikoso, S., Taniike, M., et al. (2007). The Role of Autophagy in Cardiomyocytes in the Basal State and in Response to Hemodynamic Stress. *Nat. Med.* 13 (5), 619–624. doi:10.1038/nm1574

Neagoe, C., Kulke, M., del Monte, F., Gwathmey, J. K., de Tombe, P. P., Hajjar, R. J., et al. (2002). Titin Isoform Switch in Ischemic Human Heart Disease. *Circulation* 106 (11), 1333–1341. doi:10.1161/01.cir.0000029803.93022.93

Neagoe, C., Opitz, C. A., Makarenko, I., and Linke, W. A. (2003). Gigantic Variety: Expression Patterns of Titin Isoforms in Striated Muscles and Consequences for Myofibrillar Passive Stiffness. *J. Muscle Res. Cell Motil.* 24 (2-3), 175–189. doi:10.1023/a:1026053530766

Nguyen, L. K., Kolch, W., and Kholodenko, B. N. (2013). When Ubiquitination Meets Phosphorylation: a Systems Biology Perspective of EGFR/MAPK Signalling. *Cell Commun. Signal.* 11 (1), 52. doi:10.1186/1478-811X-11-52

Nishikawa, K., Lindstedt, S. L., Hessel, A., and Mishra, D. (2020). N2A Titin: Signaling Hub and Mechanical Switch in Skeletal Muscle. *Ijms* 21 (11), 3974. doi:10.3390/ijms21113974

Nishino, I., and Ozawa, E. (2002). Muscular Dystrophies. *Curr. Opin. Neurology* 15 (5), 539–544. doi:10.1097/00019052-200210000-00004

O'Leary, T. S., Snyder, J., Sadayappan, S., Day, S. M., and Previs, M. J. (2019). MYBPC3 Truncation Mutations Enhance Actomyosin Contractile Mechanics in Human Hypertrophic Cardiomyopathy. *J. Mol. Cell. Cardiol.* 127, 165–173. doi:10.1016/j.yjmcc.2018.12.003

Ono, Y., and Sorimachi, H. (2012). Calpains - an Elaborate Proteolytic System. *Biochimica Biophysica Acta (BBA) - Proteins Proteomics* 1824 (1), 224–236. doi:10.1016/j.bbapap.2011.08.005

Opitz, C. A., Leake, M. C., Makarenko, I., Benes, V., and Linke, W. A. (2004). Developmentally Regulated Switching of Titin Size Alters Myofibrillar Stiffness in the Perinatal Heart. *Circulation Res.* 94 (7), 967–975. doi:10.1161/01.RES.0000124301.48193.E1

Palmio, J., Evilä, A., Chapon, F., Tasca, G., Xiang, F., Brådvik, B., et al. (2014). Hereditary Myopathy with Early Respiratory Failure: Occurrence in Various Populations. *J. Neurology, Neurosurg. Psychiatry* 85 (3), 345–353. doi:10.1136/jnnp-2013-304965

Perera, S., Holt, M. R., Mankoo, B. S., and Gautel, M. (2011). Developmental Regulation of MURF Ubiquitin Ligases and Autophagy Proteins Nbr1, p62/SQSTM1 and LC3 during Cardiac Myofibril Assembly and Turnover. *Dev. Biol.* 351 (1), 46–61. doi:10.1016/j.ydbio.2010.12.024

Pfeffer, G., Barresi, R., Wilson, I. J., Hardy, S. A., Griffin, H., Hudson, J., et al. (2014). Titin Founder Mutation Is a Common Cause of Myofibrillar Myopathy with Early Respiratory Failure. *J. Neurology, Neurosurg. Psychiatry* 85 (3), 331–338. doi:10.1136/jnnp-2012-304728

Plutzky, J. (2011). Macrovascular Effects and Safety Issues of Therapies for Type 2 Diabetes. *Am. J. Cardiol.* 108 (3 Suppl. l), 25b–32b. doi:10.1016/j.amjcard.2011.03.014

Polge, C., Heng, A. E., Jarzaguet, M., Ventadour, S., Claustre, A. s., Combaret, L., et al. (2011). Muscle Actin Is Polyubiquitinylated *In Vitro* and *In Vivo* and Targeted for Breakdown by the E3 Ligase MuRF1. *FASEB J.* 25 (11), 3790–3802. doi:10.1096/fj.11-180968

Portbury, A. L., Willis, M. S., and Patterson, C. (2011). Tearin' up My Heart: Proteolysis in the Cardiac Sarcomere. *J. Biol. Chem.* 286 (12), 9929–9934. doi:10.1074/jbc.R110.170571

Powell, S. R., Samuel, S. M., Wang, P., Divald, A., Thirunavukkarasu, M., Koneru, S., et al. (2008). Upregulation of Myocardial 11S-Activated Proteasome in Experimental Hyperglycemia. *J. Mol. Cell. Cardiol.* 44 (3), 618–621. doi:10.1016/j.yjmcc.2007.12.009

Powell, S. R., Wang, P., Katzeff, H., Shringarpure, R., Teoh, C., Khaliulin, I., et al. (2005). Oxidized and Ubiquitinated Proteins May Predict Recovery of Postischemic Cardiac Function: Essential Role of the Proteasome. *Antioxidants Redox Signal.* 7 (5-6), 538–546. doi:10.1089/ars.2005.7.538

Prado, L. G., Makarenko, I., Andresen, C., Krüger, M., Opitz, C. A., and Linke, W. A. (2005). Isoform Diversity of Giant Proteins in Relation to Passive and Active Contractile Properties of Rabbit Skeletal Muscles. *J. Gen. Physiol.* 126 (5), 461–480. doi:10.1085/jgp.200509364

Prochniewicz, E., Lowe, D. A., Spakowicz, D. J., Higgins, L., O'Conor, K., Thompson, L. V., et al. (2008). Functional, Structural, and Chemical Changes in Myosin Associated with Hydrogen Peroxide Treatment of Skeletal Muscle Fibers. *Am. J. Physiology-Cell Physiology* 294 (2), C613–C626. doi:10.1152/ajpcell.00232.2007

Qian, J., Ren, X., Wang, X., Zhang, P., Jones, W. K., Molkentin, J. D., et al. (2009). Blockade of Hsp20 Phosphorylation Exacerbates Cardiac Ischemia/reperfusion Injury by Suppressed Autophagy and Increased Cell Death. *Circulation Res.* 105 (12), 1223–1231. doi:10.1161/circresaha.109.200378

Queisser, M. A., Yao, D., Geisler, S., Hammes, H.-P., Lochnit, G., Schleicher, E. D., et al. (2010). Hyperglycemia Impairs Proteasome Function by Methylglyoxal. *Diabetes* 59 (3), 670–678. doi:10.2337/db08-1565

Qun Gao, C., Sawicki, G., Suarez-Pinzon, W. L., Csont, T., Wozniak, M., Ferdinandy, P., et al. (2003). Matrix Metalloproteinase-2 Mediates Cytokine-Induced Myocardial Contractile Dysfunction. *Cardiovasc. Res.* 57 (2), 426–433. doi:10.1016/s0008-6363(02)00719-8

Ranek, M. J., Oeing, C., Sanchez-Hodge, R., Kokkonen-Simon, K. M., Dillard, D., Aslam, M. I., et al. (2020). CHIP Phosphorylation by Protein Kinase G Enhances Protein Quality Control and Attenuates Cardiac Ischemic Injury. *Nat. Commun.* 11 (1), 5237. doi:10.1038/s41467-020-18980-x

Ravikumar, B., Sarkar, S., Davies, J. E., Futter, M., Garcia-Arencibia, M., Green-Thompson, Z. W., et al. (2010). Regulation of Mammalian Autophagy in Physiology and Pathophysiology. *Physiol. Rev.* 90 (4), 1383–1435. doi:10.1152/physrev.00030.2009

Raynaud, F., Fernandez, E., Coulis, G., Aubry, L., Vignon, X., Bleimling, N., et al. (2005). Calpain 1-titin Interactions Concentrate Calpain 1 in the Z-Band Edges and in the N2-Line Region within the Skeletal Myofibril. *FEBS J.* 272 (10), 2578–2590. doi:10.1111/j.1742-4658.2005.04683.x

Rees, M., Nikoopour, R., Fukuzawa, A., Kho, A. L., Fernandez-Garcia, M. A., Wraige, E., et al. (2021). Making Sense of Missense Variants in TTN-Related Congenital Myopathies. *Acta Neuropathol.* 141 (3), 431–453. doi:10.1007/s00401-020-02257-0

Rivas-Pardo, J. A., Eckels, E. C., Popa, I., Kosuri, P., Linke, W. A., and Fernández, J. M. (2016). Work Done by Titin Protein Folding Assists Muscle Contraction. *Cell Rep.* 14 (6), 1339–1347. doi:10.1016/j.celrep.2016.01.025

Roberts, A. M., Ware, J. S., Herman, D. S., Schafer, S., Baksi, J., Bick, A. G., et al. (2015). Integrated Allelic, Transcriptional, and Phenomic Dissection of the Cardiac Effects of Titin Truncations in Health and Disease. *Sci. Transl. Med.* 7 (270), 270ra276. doi:10.1126/scitranslmed.3010134

Robertson, A. S., Majchrzak, M. J., Smith, C. M., Gagnon, R. C., Devidze, N., Banks, G. B., et al. (2017). Dramatic Elevation in Urinary Amino Terminal Titin Fragment Excretion Quantified by Immunoassay in Duchenne Muscular

Dystrophy Patients and in Dystrophin Deficient Rodents. *Neuromuscul. Disord.* 27 (7), 635–645. doi:10.1016/j.nmd.2017.05.009

Rudolph, F., Hüttemeister, J., da Silva Lopes, K., Jüttner, R., Yu, L., Bergmann, N., et al. (2019). Resolving Titin's Lifecycle and the Spatial Organization of Protein Turnover in Mouse Cardiomyocytes. *Proc. Natl. Acad. Sci. U.S.A.* 116 (50), 25126–25136. doi:10.1073/pnas.1904385116

Ryder, S., Leadley, R. M., Armstrong, N., Westwood, M., de Kock, S., Butt, T., et al. (2017). The Burden, Epidemiology, Costs and Treatment for Duchenne Muscular Dystrophy: an Evidence Review. *Orphanet J. Rare Dis.* 12 (1), 79. doi:10.1186/s13023-017-0631-3

Salcan, S., Bongardt, S., Monteiro Barbosa, D., Efimov, I. R., Rassaf, T., Krüger, M., et al. (2020). Elastic Titin Properties and Protein Quality Control in the Aging Heart. *Biochimica Biophysica Acta (BBA) - Mol. Cell Res.* 1867 (3), 118532. doi:10.1016/j.bbamcr.2019.118532

Sanbe, A., Daicho, T., Mizutani, R., Endo, T., Miyauchi, N., Yamauchi, J., et al. (2009). Protective Effect of Geranylgeranylacetone via Enhancement of HSPB8 Induction in Desmin-Related Cardiomyopathy. *PLoS One* 4 (4), e5351. doi:10.1371/journal.pone.0005351

Sanbe, A., Yamauchi, J., Miyamoto, Y., Fujiwara, Y., Murabe, M., and Tanoue, A. (2007). Interruption of CryAB-Amyloid Oligomer Formation by HSP22. *J. Biol. Chem.* 282 (1), 555–563. doi:10.1074/jbc.M605481200

Savarese, M., Sarparanta, J., Vihola, A., Udd, B., and Hackman, P. (2016). Increasing Role of Titin Mutations in Neuromuscular Disorders. *Jnd* 3, 293–308. doi:10.3233/JND-160158

Sawicki, G., Leon, H., Sawicka, J., Sariahmetoglu, M., Schulze, C. J., Scott, P. G., et al. (2005). Degradation of Myosin Light Chain in Isolated Rat Hearts Subjected to Ischemia-Reperfusion Injury: a New Intracellular Target for Matrix Metalloproteinase-2. *Circulation* 112 (4), 544–552. doi:10.1161/circulationaha.104.531616

Schafer, S., de Marvao, A., Adami, E., Fiedler, L. R., Ng, B., Khin, E., et al. (2017). Titin-truncating Variants Affect Heart Function in Disease Cohorts and the General Population. *Nat. Genet.* 49 (1), 46–53. doi:10.1038/ng.3719

Schiaffino, S., Dyar, K. A., Ciciliot, S., Blaauw, B., and Sandri, M. (2013). Mechanisms Regulating Skeletal Muscle Growth and Atrophy. *Febs J.* 280 (17), 4294–4314. doi:10.1111/febs.12253

Schlossarek, S., and Carrier, L. (2011). The Ubiquitin-Proteasome System in Cardiomyopathies. *Curr. Opin. Cardiol.* 26 (3), 190–195. doi:10.1097/HCO.0b013e32834598fe

Sciarretta, S., Boppana, V. S., Umapathi, M., Frati, G., and Sadoshima, J. (2015). Boosting Autophagy in the Diabetic Heart: a Translational Perspective. *Cardiovasc Diagn Ther.* 5 (5), 394–402. doi:10.3978/j.issn.2223-3652.2015.07.02

Sciarretta, S., Maejima, Y., Zablocki, D., and Sadoshima, J. (2018). The Role of Autophagy in the Heart. *Annu. Rev. Physiol.* 80, 1–26. doi:10.1146/annurev-physiol-021317-121427

Sciarretta, S., Zhai, P., Shao, D., Maejima, Y., Robbins, J., Volpe, M., et al. (2012). Rheb Is a Critical Regulator of Autophagy during Myocardial Ischemia: Pathophysiological Implications in Obesity and Metabolic Syndrome. *Circulation* 125 (9), 1134–1146. doi:10.1161/circulationaha.111.078212

Scruggs, S. B., Ping, P., and Zong, C. (2011). Heterogeneous Cardiac Proteasomes: Mandated by Diverse Substrates? *Physiology* 26 (2), 106–114. doi:10.1152/physiol.00039.2010

Shaid, S., Brandts, C. H., Serve, H., and Dikic, I. (2012). Ubiquitination and Selective Autophagy. *Cell Death Differ.* 20, 21–30. doi:10.1038/cdd.2012.72

Shi, B., Ma, M., Zheng, Y., Pan, Y., and Lin, X. (2019). mTOR and Beclin1: Two Key Autophagy-related Molecules and Their Roles in Myocardial Ischemia/reperfusion Injury. *J. Cell. Physiology* 234 (8), 12562–12568. doi:10.1002/jcp.28125

Shirakabe, A., Ikeda, Y., Sciarretta, S., Zablocki, D. K., and Sadoshima, J. (2016). Aging and Autophagy in the Heart. *Circ. Res.* 118 (10), 1563–1576. doi:10.1161/CIRCRESAHA.116.307474

Smith, D. A., Carland, C. R., Guo, Y., and Bernstein, S. I. (2014). Getting Folded: Chaperone Proteins in Muscle Development, Maintenance and Disease. *Anat. Rec.* 297 (9), 1637–1649. doi:10.1002/ar.22980

Sorimachi, H., Freiburg, A., Kolmerer, B., Ishiura, S., Stier, G., Gregorio, C. C., et al. (1997). Tissue-specific Expression and α-actinin Binding Properties of the Z-Disc Titin: Implications for the Nature of Vertebrate Z-Discs. *J. Mol. Biol.* 270 (5), 688–695. doi:10.1006/jmbi.1997.1145

Sorimachi, H., and Ono, Y. (2012). Regulation and Physiological Roles of the Calpain System in Muscular Disorders. *Cardiovasc. Res.* 96 (1), 11–22. doi:10.1093/cvr/cvs157

Steinberg, S. F. (2013). Oxidative Stress and Sarcomeric Proteins. *Circ. Res.* 112 (2), 393–405. doi:10.1161/circresaha.111.300496

Sun, Y. (2009). Myocardial Repair/remodelling Following Infarction: Roles of Local Factors. *Cardiovasc. Res.* 81 (3), 482–490. doi:10.1093/cvr/cvn333

Sung, M. M., Schulz, C. G., Wang, W., Sawicki, G., Bautista-López, N. L., and Schulz, R. (2007). Matrix Metalloproteinase-2 Degrades the Cytoskeletal Protein α-actinin in Peroxynitrite Mediated Myocardial Injury. *J. Mol. Cell. Cardiol.* 43 (4), 429–436. doi:10.1016/j.yjmcc.2007.07.055

Swatek, K. N., and Komander, D. (2016). Ubiquitin Modifications. *Cell Res.* 26 (4), 399–422. doi:10.1038/cr.2016.39

Tasca, G., and Udd, B. (2018). Hereditary Myopathy with Early Respiratory Failure (HMERF): Still Rare, but Common Enough. *Neuromuscul. Disord.* 28 (3), 268–276. doi:10.1016/j.nmd.2017.12.002

Thomson, K. L., Ormondroyd, E., Harper, A. R., Dent, T., McGuire, K., Baksi, J., et al. (2019). Analysis of 51 Proposed Hypertrophic Cardiomyopathy Genes from Genome Sequencing Data in Sarcomere Negative Cases Has Negligible Diagnostic Yield. *Genet. Med.* 21 (7), 1576–1584. doi:10.1038/s41436-018-0375-z

Thrower, J. S., Hoffman, L., Rechsteiner, M., and Pickart, C. M. (2000). Recognition of the Polyubiquitin Proteolytic Signal. *EMBO J.* 19 (1), 94–102. doi:10.1093/emboj/19.1.94

Tomaru, U., Takahashi, S., Ishizu, A., Miyatake, Y., Gohda, A., Suzuki, S., et al. (2012). Decreased Proteasomal Activity Causes Age-Related Phenotypes and Promotes the Development of Metabolic Abnormalities. *Am. J. Pathology* 180 (3), 963–972. doi:10.1016/j.ajpath.2011.11.012

Tskhovrebova, L., and Trinick, J. (2004). Properties of Titin Immunoglobulin and Fibronectin-3 Domains. *J. Biol. Chem.* 279 (45), 46351–46354. doi:10.1074/jbc.R400023200

Tskhovrebova, L., and Trinick, J. (2010). Roles of Titin in the Structure and Elasticity of the Sarcomere. *J. Biomed. Biotechnol.* 2010, 7. doi:10.1155/2010/612482

Udd, B., Vihola, A., Sarparanta, J., Richard, I., and Hackman, P. (2005). Titinopathies and Extension of the M-Line Mutation Phenotype beyond Distal Myopathy and LGMD2J. *Neurology* 64 (4), 636–642. doi:10.1212/01.wnl.0000151853.50144.82

Ulbricht, A., Arndt, V., and Höhfeld, J. (2013). Chaperone-assisted Proteostasis Is Essential for Mechanotransduction in Mammalian Cells. *Commun. Integr. Biol.* 6 (4), e24925. doi:10.4161/cib.24925

Unger, A., Beckendorf, L., Böhme, P., Kley, R., von Frieling-Salewsky, M., Lochmüller, H., et al. (2017). Translocation of Molecular Chaperones to the Titin Springs Is Common in Skeletal Myopathy Patients and Affects Sarcomere Function. *Acta Neuropathol. Commun.* 5 (1), 72. doi:10.1186/s40478-017-0474-0

Usui, S., Maejima, Y., Pain, J., Hong, C., Cho, J., Park, J. Y., et al. (2011). Endogenous Muscle Atrophy F-Box Mediates Pressure Overload-Induced Cardiac Hypertrophy through Regulation of Nuclear Factor-Kb. *Circ. Res.* 109 (2), 161–171. doi:10.1161/circresaha.110.238717

van Heerebeek, L., Hamdani, N., Falcão-Pires, I., Leite-Moreira, A. F., Begieneman, M. P. V., Bronzwaer, J. G. F., et al. (2012). Low Myocardial Protein Kinase G Activity in Heart Failure with Preserved Ejection Fraction. *Circulation* 126 (7), 830–839. doi:10.1161/circulationaha.111.076075

Vander Heide, R. S. (2002). Increased Expression of HSP27 Protects Canine Myocytes from Simulated Ischemia-Reperfusion Injury. *Am. J. Physiology-Heart Circulatory Physiology* 282 (3), H935–H941. doi:10.1152/ajpheart.00660.2001

Verma, R., Aravind, L., Oania, R., McDonald, W. H., Yates, J. R., 3rd, Koonin, E. V., et al. (2002). Role of Rpn11 Metalloprotease in Deubiquitination and Degradation by the 26 S Proteasome. *Science* 298 (5593), 611–615. doi:10.1126/science.1075898

Vos, M. J., Hageman, J., Carra, S., and Kampinga, H. H. (2008). Structural and Functional Diversities between Members of the Human HSPB, HSPH, HSPA, and DNAJ Chaperone Families. *Biochemistry* 47 (27), 7001–7011. doi:10.1021/bi800639z

Wagner, S. A., Beli, P., Weinert, B. T., Schölz, C., Kelstrup, C. D., Young, C., et al. (2012). Proteomic Analyses Reveal Divergent Ubiquitylation Site Patterns in Murine Tissues. *Mol. Cell. Proteomics* 11 (12), 1578–1585. doi:10.1074/mcp.M112.017905

Wang, W., Schulze, C. J., Suarez-Pinzon, W. L., Dyck, J. R. B., Sawicki, G., and Schulz, R. (2002). Intracellular Action of Matrix Metalloproteinase-2 Accounts for Acute Myocardial Ischemia and Reperfusion Injury. *Circulation* 106 (12), 1543–1549. doi:10.1161/01.cir.0000028818.33488.7b

Wang, X., Li, J., Zheng, H., Su, H., and Powell, S. R. (2011). Proteasome Functional Insufficiency in Cardiac Pathogenesis. *Am. J. Physiology-Heart Circulatory Physiology* 301 (6), H2207–H2219. doi:10.1152/ajpheart.00714.2011

Wang, Z. V., and Hill, J. A. (2015). Protein Quality Control and Metabolism: Bidirectional Control in the Heart. *Cell Metab.* 21 (2), 215–226. doi:10.1016/j.cmet.2015.01.016

Watanabe, K., Nair, P., Labeit, D., Kellermayer, M. S. Z., Greaser, M., Labeit, S., et al. (2002). Molecular Mechanics of Cardiac Titin's PEVK and N2B Spring Elements. *J. Biol. Chem.* 277 (13), 11549–11558. doi:10.1074/jbc.M200356200

Webster, K. A., Discher, D. J., Hernandez, O. M., Yamashita, K., and Bishopric, N. H. (2000). A Glycolytic Pathway to Apoptosis of Hypoxic Cardiac Myocytes. Molecular Pathways of Increased Acid Production. *Adv. Exp. Med. Biol.* 475, 161–175. doi:10.1007/0-306-46825-5_16

Willis, M. S., and Patterson, C. (2010). Hold Me Tight: Role of the Heat Shock Protein Family of Chaperones in Cardiac Disease. *Circulation* 122 (17), 1740–1751. doi:10.1161/circulationaha.110.942250

Willis, M. S., Schisler, J. C., Portbury, A. L., and Patterson, C. (2008). Build it Up-Tear it Down: Protein Quality Control in the Cardiac Sarcomere. *Cardiovasc. Res.* 81 (3), 439–448. doi:10.1093/cvr/cvn289

Witt, C. C., Burkart, C., Labeit, D., McNabb, M., Wu, Y., Granzier, H., et al. (2006). Nebulin Regulates Thin Filament Length, Contractility, and Z-Disk Structure *In Vivo*. *Embo J.* 25 (16), 3843–3855. doi:10.1038/sj.emboj.7601242

Witt, S. H., Granzier, H., Witt, C. C., and Labeit, S. (2005). MURF-1 and MURF-2 Target a Specific Subset of Myofibrillar Proteins Redundantly: towards Understanding MURF-dependent Muscle Ubiquitination. *J. Mol. Biol.* 350 (4), 713–722. doi:10.1016/j.jmb.2005.05.021

Wu, Y., Peng, J., Campbell, K. B., Labeit, S., and Granzier, H. (2007). Hypothyroidism Leads to Increased Collagen-Based Stiffness and Re-expression of Large Cardiac Titin Isoforms with High Compliance. *J. Mol. Cell. Cardiol.* 42 (1), 186–195. doi:10.1016/j.yjmcc.2006.09.017

Xu, X., Kobayashi, S., Chen, K., Timm, D., Volden, P., Huang, Y., et al. (2013). Diminished Autophagy Limits Cardiac Injury in Mouse Models of Type 1 Diabetes. *J. Biol. Chem.* 288 (25), 18077–18092. doi:10.1074/jbc.M113.474650

Yamasaki, R., Wu, Y., McNabb, M., Greaser, M., Labeit, S., and Granzier, H. (2002). Protein Kinase A Phosphorylates Titin's Cardiac-specific N2B Domain and Reduces Passive Tension in Rat Cardiac Myocytes. *Circulation Res.* 90 (11), 1181–1188. doi:10.1161/01.res.0000021115.24712.99

Yao, T., and Cohen, R. E. (2002). A Cryptic Protease Couples Deubiquitination and Degradation by the Proteasome. *Nature* 419 (6905), 403–407. doi:10.1038/nature01071

Zaunbrecher, R. J., Abel, A. N., Beussman, K., Leonard, A., von Frieling-Salewsky, M., Fields, P. A., et al. (2019). Cronos Titin Is Expressed in Human Cardiomyocytes and Necessary for Normal Sarcomere Function. *Circulation* 140 (20), 1647–1660. doi:10.1161/circulationaha.119.039521

Zhang, M., Windheim, M., Roe, S. M., Peggie, M., Cohen, P., Prodromou, C., et al. (2005). Chaperoned Ubiquitylation-Crystal Structures of the CHIP U Box E3 Ubiquitin Ligase and a CHIP-Ubc13-Uev1a Complex. *Mol. Cell* 20 (4), 525–538. doi:10.1016/j.molcel.2005.09.023

Zhu, C., Yin, Z., Tan, B., and Guo, W. (2017). Insulin Regulates Titin Pre-mRNA Splicing through the PI3K-Akt-mTOR Kinase axis in a RBM20-dependent Manner. *Biochimica Biophysica Acta (BBA) - Mol. Basis Dis.* 1863 (9), 2363–2371. doi:10.1016/j.bbadis.2017.06.023

Zou, J., Tran, D., Baalbaki, M., Tang, L. F., Poon, A., Pelonero, A., et al. (2015). An Internal Promoter Underlies the Difference in Disease Severity between N- and C-Terminal Truncation Mutations of Titin in Zebrafish. *eLife* 4, e09406. doi:10.7554/eLife.09406

Zou, P., Pinotsis, N., Lange, S., Song, Y.-H., Popov, A., Mavridis, I., et al. (2006). Palindromic Assembly of the Giant Muscle Protein Titin in the Sarcomeric Z-Disk. *Nature* 439 (7073), 229–233. doi:10.1038/nature04343

Conflict of Interest: The authors declare that the research was conducted in the absence of any commercial or financial relationships that could be construed as a potential conflict of interest.

Publisher's Note: All claims expressed in this article are solely those of the authors and do not necessarily represent those of their affiliated organizations, or those of the publisher, the editors and the reviewers. Any product that may be evaluated in this article, or claim that may be made by its manufacturer, is not guaranteed or endorsed by the publisher.

frontiers | Frontiers in Physiology

TYPE Original Research
PUBLISHED 23 August 2022
DOI 10.3389/fphys.2022.947206

OPEN ACCESS

EDITED BY
Jose Renato Pinto,
Florida State University, United States

REVIEWED BY
Michael Greenberg,
Washington University in St. Louis, United States
Weikang Ma,
Illinois Institute of Technology, United States

*CORRESPONDENCE
Norio Fukuda,
noriof@jikei.ac.jp

SPECIALTY SECTION
This article was submitted to Striated Muscle Physiology, a section of the journal Frontiers in Physiology

RECEIVED 18 May 2022
ACCEPTED 04 July 2022
PUBLISHED 23 August 2022

CITATION
Nakanishi T, Oyama K, Tanaka H, Kobirumaki-Shimozawa F, Ishii S, Terui T, Ishiwata S and Fukuda N (2022), Effects of omecamtiv mecarbil on the contractile properties of skinned porcine left atrial and ventricular muscles.
Front. Physiol. 13:947206.
doi: 10.3389/fphys.2022.947206

Effects of omecamtiv mecarbil on the contractile properties of skinned porcine left atrial and ventricular muscles

Tomohiro Nakanishi[1,2], Kotaro Oyama[1,3], Hiroyuki Tanaka[4], Fuyu Kobirumaki-Shimozawa[1], Shuya Ishii[3], Takako Terui[2], Shin'ichi Ishiwata[5] and Norio Fukuda[1]*

[1]Department of Cell Physiology, The Jikei University School of Medicine, Tokyo, Japan, [2]Department of Anesthesiology, The Jikei University School of Medicine, Tokyo, Japan, [3]Quantum Beam Science Research Directorate, National Institutes for Quantum Science and Technology, Gunma, Japan, [4]Laboratory of Marine Biotechnology and Microbiology, Hokkaido University, Hakodate, Japan, [5]Department of Physics, Faculty of Science and Engineering, Waseda University, Tokyo, Japan

Omecamtiv mecarbil (OM) is a novel inotropic agent for heart failure with systolic dysfunction. OM prolongs the actomyosin attachment duration, which enhances thin filament cooperative activation and accordingly promotes the binding of neighboring myosin to actin. In the present study, we investigated the effects of OM on the steady-state contractile properties in skinned porcine left ventricular (PLV) and atrial (PLA) muscles. OM increased Ca^{2+} sensitivity in a concentration-dependent manner in PLV, by left shifting the mid-point (pCa_{50}) of the force-pCa curve (ΔpCa_{50}) by ~0.16 and ~0.33 pCa units at 0.5 and 1.0 μM, respectively. The Ca^{2+}-sensitizing effect was likewise observed in PLA, but less pronounced with ΔpCa_{50} values of ~0.08 and ~0.22 pCa units at 0.5 and 1.0 μM, respectively. The Ca^{2+}-sensitizing effect of OM (1.0 μM) was attenuated under enhanced thin filament cooperative activation in both PLV and PLA; this attenuation occurred directly via treatment with fast skeletal troponin (ΔpCa_{50}: ~0.16 and ~0.10 pCa units in PLV and PLA, respectively) and indirectly by increasing the number of strongly bound cross-bridges in the presence of 3 mM MgADP (ΔpCa_{50}: ~0.21 and ~0.08 pCa units in PLV and PLA, respectively). It is likely that this attenuation of the Ca^{2+}-sensitizing effect of OM is due to a decrease in the number of "recruitable" cross-bridges that can potentially produce active force. When cross-bridge detachment was accelerated in the presence of 20 mM inorganic phosphate, the Ca^{2+}-sensitizing effect of OM (1.0 μM) was markedly decreased in both types of preparations (ΔpCa_{50}: ~0.09 and ~0.03 pCa units in PLV and PLA, respectively). The present findings suggest that the positive inotropy of

Abbreviations: BDM, 2,3-butanedione 2-monoxime; CP, phosphocreatine; CPK, creatine phosphokinase; DRX, disordered-relaxed state; DTT, dithiothreitol; HF, heart failure; HFrEF, heart failure with reduced ejection fraction; MyBP-C, myosin-binding protein C; OM, omecamtiv mecarbil; Pi, inorganic phosphate; PKA, protein kinase A; PLA, porcine left atrial muscle; PLV, porcine left ventricular muscle; SL, sarcomere length; SRX, super-relaxed state; sTn, fast skeletal troponin complex.

OM is more markedly exerted in the ventricle than in the atrium, which results from the strongly bound cross-bridge-dependent allosteric activation of thin filaments.

KEYWORDS

Ca^{2+} sensitivity, contractility, myocardium, sarcomere, thin filament

Introduction

Heart failure (HF) is a syndrome characterized by symptoms or signs caused by structural or functional abnormalities of the heart, which results in reduced cardiac output (Metra and Teerlink, 2017). The complex clinical syndrome of HF with reduced ejection fraction (HFrEF) requires specifically established medications, such as angiotensin receptor-neprilysin inhibitors, angiotensin-converting enzyme inhibitors, angiotensin receptor blockers, β-blockers, loop diuretics, aldosterone antagonists, hydralazine/isosorbide dinitrate, ivabradine [I_f (funny current) channel blocker], and sodium-glucose cotransporter 2 inhibitors (Maddox et al., 2021; McDonagh et al., 2021). In contrast, traditional positive inotropic drugs are known to cause untoward effects (Teerlink et al., 2009); these drugs increase the intracellular Ca^{2+} concentration in myocardial cells, and can cause arrhythmias (Francis et al., 2014).

Omecamtiv mecarbil (OM) was developed as a first-in-class "myosin activator" for the treatment of heart failure in patients with HFrEF (Malik and Morgan, 2011). Several lines of evidence indicate that OM is effective in the treatment of HF by improving cardiac function (Shen et al., 2010; Malik et al., 2011; Teerlink et al., 2016). A recent study in heart failure patients showed that those that were treated with OM had a lower incidence of a composite event of HF hospitalization or death than in those who received placebo (Teerlink et al., 2021). It was originally considered that OM increases cardiac contractility by prolonging the duration of ejection with no influence on the intracellular Ca^{2+} concentration, and that the augmented contractility is the result of the increased transition rate of the OM-bound myosin into the strongly bound, force-generating state (Malik et al., 2011; Nagy et al., 2015). Consistent with this view, Mamidi et al. (2015) proposed that OM lowers the cross-bridge detachment rate, and the resultant strongly bound cross-bridges proceed to activate thin filaments (i.e., thin filament "*on-off*" equilibrium shifting from the "*off*" state towards the "*on*" state; cf. Kobirumaki-Shimozawa et al., 2014). It has likewise been shown that OM increases the release rate of inorganic phosphate (Pi) during the actomyosin ATPase cycle (Liu et al., 2015), promoting the formation of strongly bound cross-bridges, with no change in the ADP dissociation rate (Winkelmann et al., 2015). Subsequently, Rohde et al. (2017) provided evidence that OM stabilizes the pre-powerstroke of myosin; therefore, the compound suppresses myosin's working stroke and prolongs the time of myosin binding to actin (see Woody et al., 2018 for details). Taken together, these findings support the above interpretation that the compound's inotropic effect is primarily coupled with cooperative thin filament activation as a result of OM-bound cross-bridges. It can therefore be summarized that OM primarily exerts its positive inotropy as follows: it binds to myosin, increasing the number of strongly bound cross-bridges, and these cross-bridges cooperatively activate thin filaments, thereby recruiting OM-free "recruitable" cross-bridges that can potentially generate active force upon attachment to actin (Lindqvist et al., 2019; Governali et al., 2020; Snoberger et al., 2021) (see Terui et al., 2008, Terui et al., 2010; Kobirumaki-Shimozawa et al., 2014 for "recruitable" cross-bridges).

In porcine hearts, ventricular muscle contains ~20% α- and ~80% β-myosin, and atrial muscle ~90% α- and ~10% β-myosin (Shchepkin et al., 2020). Shchepkin et al. (2020) likewise showed that OM prolongs the actomyosin attachment duration in ventricular and atrial myosin, with a higher sensitivity in ventricular myosin. However, it has not been investigated whether the cardiotonic effect of OM is greater in the ventricle than in the atrium. In the present study, we investigated the effects of OM in the clinically relevant concentration range (i.e., 0.5 and 1.0 μM; see Teerlink et al., 2011, 2016) on steady-state contractile properties in skinned porcine left ventricular (PLV) and atrial (PLA) muscles. We found that OM increased Ca^{2+} sensitivity by a greater magnitude in PLV than in PLA, and that the Ca^{2+}-sensitizing effect of OM was less pronounced under enhanced thin filament cooperative activation. Mechanistic implications are discussed based on the thin filament "*on-off*" regulation and the recently proposed thick filament regulation. Likewise, we discuss the clinical relevance of the present findings focusing on the possible effects of OM on HFrEF.

Materials and methods

All muscle mechanical experiments were performed at The Jikei University School of Medicine in accordance with the guidelines outlined by the university's Institutional Animal Care and Use Committee. Troponin (Tn) extraction was performed at Hokkaido University. All experiments performed in the present study conform to the Guidelines for Proper Conduct of Animal Experiments of the Science Council of Japan (2006).

Preparations of skinned muscles

Skinned porcine ventricular (PLV) and atrial (PLA) muscles were prepared based on previously described procedures (Terui et al., 2008, 2010; Matsuba et al., 2009). In brief, porcine hearts (animals, ~1.0 years) were obtained at a local slaughterhouse. Muscle strips (1–2 mm in diameter and ~10 mm in length) were dissected from the left ventricle and atrium (as performed on bovine hearts; see Fukuda et al., 2003; 2005a), and were skinned in relaxing solution [5 mM MgATP, 40 mM BES, 1 mM Mg^{2+}, 10 mM EGTA, 1 mM dithiothreitol (DTT), 15 mM phosphocreatine (CP), 15 U/ml creatine phosphokinase (CPK), and 180 mM ionic strength (adjusted by K-propionate), pH 7.0, containing 1% (wt/vol) Triton X-100 and 10 mM 2,3-butanedione 2-monoxime (BDM)] overnight at ~3°C (Terui et al., 2008, 2010; Matsuba et al., 2009). Muscles were stored for up to 3 weeks at −20°C in relaxing solution containing 50% (vol/vol) glycerol. All solutions contained protease inhibitors (0.5 mM PMSF, 0.04 mM leupeptin and 0.01 mM E64) to avoid protein degradation (as in Fukuda et al., 2003, 2005a,b; Terui et al., 2008, 2010; Matsuba et al., 2009).

Skinned muscle mechanics: Force-pCa protocol

Isometric force was measured using our previously described procedure with PLV (Terui et al., 2008, 2010; Matsuba et al., 2009). Experiments were all conducted at the relatively low temperature of 15°C to minimize rundowns of active force during the time required to perform force-pCa protocols (cf. Fukuda et al., 2003, 2005b). In brief, small thin preparations (~100 μm in diameter and ~2 mm in length) were dissected from the PLV and PLA strips for isometric force measurement. Sarcomere length (SL) was measured by laser diffraction during relaxation (as in Fukuda et al., 2003, 2005a,b; Terui et al., 2008, 2010; Matsuba et al., 2009; Inoue et al., 2013), and set at 2.1 μm prior to contraction at each pCa. Passive force was not detected at this SL in either PLV or PLA. pCa was obtained by adjusting the ratio of Ca/EGTA (Fukuda et al., 2003, 2005b; Terui et al., 2008, 2010; Matsuba et al., 2009; Inoue et al., 2013). OM was purchased from ChemScene LLC (Monmouth Junction, NJ, United States). OM was initially dissolved in DMSO, and diluted with individual solutions. The final concentration of DMSO of 0.1% had no effect on Ca^{2+} sensitivity or maximal Ca^{2+}-activated force (cf. Fukuda et al., 2000; Terui et al., 2010).

For both PLV and PLA, the muscle preparation was first immersed in high-EGTA (10 mM) relaxing solution. Just before contraction, the preparation was immersed in low-EGTA (0.5 mM) relaxing solution to avoid slowing of contraction and the ensuing damage on sarcomere structures (Terui et al., 2008, 2010; Matsuba et al., 2009; Inoue et al., 2013). The preparation was first activated at pCa 4.5 to obtain maximal Ca^{2+}-activated force, followed by relaxation. The preparation was then activated at various pCa's (from high to low pCa, and lastly at pCa 4.5) to construct the force-pCa curve (i.e., force-pCa protocol). The effect of OM was tested at 0.5 and 1.0 μM, in this order.

Force-pCa curves were fitted to the Hill equation, and the value of the midpoint of the force-pCa curve (i.e., pCa_{50}) was used as an index of Ca^{2+} sensitivity (as in Fukuda et al., 2003, 2005b; Terui et al., 2008, 2010; Matsuba et al., 2009; Inoue et al., 2013; Kobirumaki-Shimozawa et al., 2014). We likewise obtained the Hill coefficient (n_H). Active forces at submaximal Ca^{2+} levels were normalized to maximal force (pCa 4.5) obtained at the beginning or the end of the force-pCa protocol (the rundown in active force during the protocol was less than 10% under all conditions tested). The OM-induced increase in Ca^{2+} sensitivity was quantified by the difference in pCa_{50} obtained in the absence and presence of OM, and expressed as ΔpCa_{50} (in pCa units).

Measurement of MgADP-induced contraction

Ca^{2+}-independent, MgADP-induced active force (ADP-contraction) was measured in PLV and PLA as described previously by us (Fukuda et al., 1998), but at the lower temperature of 15°C. In brief, isometric force was measured in solutions containing 2 mM MgATP, 10 mM MOPS, 2 mM Mg^{2+}, 2 mM EGTA, 1 mM DTT, and 150 mM ionic strength (adjusted by K-propionate), pH 7.0. In order to inhibit the rephosphorylation of ADP to ATP by myokinase (Lienhard and Secemski, 1973; Fukuda et al., 1996, 1998), 0.1 mM P^1,P^5-di(adenosine-5′)pentaphosphate was added. The maximal concentration of MgADP was set at 20 mM for both PLV and PLA, and submaximal active forces were measured at 0.5, 1, 2 and 3 mM and at 1, 3, 5, 8, 10, and 15 mM for PLV and PLA, respectively. Active forces at submaximal Ca^{2+} levels were normalized to maximal force obtained at the beginning or the end of the force-MgADP protocol (the rundown in active force during the protocol was less than 10% under all conditions tested).

Treatment with protein kinase A

Protein kinase A (PKA) treatment was performed for PLV and PLA based on our previously published protocol (Fukuda et al., 2005a; Matsuba et al., 2009; Inoue et al., 2013). In brief, after the force-pCa protocol was performed in the absence of OM, the preparation was incubated for 50 min at room temperature in relaxing solution containing purified PKA (catalytic subunit

from bovine heart; Sigma-Aldrich Co., St. Louis, MO, United States) at a concentration of 1 U/μl. We previously reported that this protocol effectively phosphorylates TnI and myosin-binding protein C (MyBP-C) in skinned myocardial preparations (Inoue et al., 2013). Then, the force-pCa protocol was repeated two times, in the absence and presence of 1.0 μM OM in this order.

Treatment with the Tn complex from rabbit fast skeletal muscle

Tn exchange was performed for PLV and PLA based on our previously published procedure (Terui et al., 2008, 2010; Matsuba et al., 2009; Inoue et al., 2013). In brief, the fast skeletal Tn complex (sTn) was extracted from rabbit fast skeletal muscles (based on Ebashi et al., 1971; Eisenberg and Kielley, 1974). sTn extraction was performed at Hokkaido University, and approved by the Animal Care and Use Committee of Hokkaido University (#09-0134). sTn was transported to The Jikei University School of Medicine by air, and stored at −80°C before use. After the force-pCa protocol was performed in the absence of OM, the preparation was bathed in rigor solution (10 mM BES, 150 mM K-propionate, 2.5 mM EGTA, and 5 mM $MgCl_2$, pH 7.0) containing 2 mg/ml sTn and 80 mM BDM for 60 min at 25°C. Then, the preparation was washed with normal relaxing solution at 15°C for 10 min with gentle agitation to remove excess sTn. We reported that Tn subunits are almost completely replaced by those from rabbit fast skeletal muscle in skinned cardiac preparations with a diameter of ~100 μm (Terui et al., 2008; Matsuba et al., 2009; Inoue et al., 2013). The force-pCa protocol was repeated two times, in the absence and presence of 1.0 μM OM in this order.

Force-pCa protocol in the presence of MgADP or inorganic phosphate

In both PLV and PLA, after the force-pCa protocol was performed, the same procedure in the presence of 3 mM MgADP or 20 mM Pi was repeated (see Terui et al., 2010 for details). Subsequently, the force-pCa protocol was performed with 1.0 μM OM in the presence of 3 mM MgADP or 20 mM Pi. Only when MgADP was present, 0.1 mM P^1,P^5-di(adenosine-5′) pentaphosphate was added to both activating and relaxing solutions, with no CP-CPK to maintain the ADP/ATP ratio (see above).

Statistics

Significant difference was assigned using paired or unpaired Student's *t* test, or Tukey-Kramer test, as appropriate. As part of the statistical processing, we used EZR (Kanda, 2013), which is a graphical user interface for R (version 4.1.2: The R Foundation for Statistical Computing, Vienna, Austria). Data were expressed as means ± SEM, with *n* representing the number of muscles. Statistical significance was assumed to be $p < 0.05$, $p < 0.01$ and $p < 0.001$. "n.s." indicates $p > 0.05$ (not significant).

Results

Effects of OM on Ca^{2+} sensitivity in PLV and PLA

First, we investigated the effects of OM on Ca^{2+} sensitivity in PLV and PLA under the condition with no perturbation (SL 2.1 μm; see **Materials and Methods**). We tested these effects in a paired manner, i.e., one skinned muscle preparation, either PLV or PLA, at no OM, and then at 0.5 and 1.0 μM in this order. In PLV, under the control condition without OM, isometric force started to rise at pCa 6.0 (8%), and became 32% and 76% at pCa 5.75 and 5.5, respectively (Figure 1A: percentages compared to maximal force). OM increased submaximal forces; i.e., the force levels were 28% and 62%, respectively, at pCa 6.0 and 5.75 in the presence of 0.5 μM OM, and 49% and 79%, respectively, in the presence of 1.0 μM OM. Figure 1B shows force-pCa curves in the absence and presence of OM (Table 1). The mid-point of the force-pCa curve (pCa_{50}) was 5.67 ± 0.01 in the absence of OM, which was slightly greater than that obtained in our previous reports using PLV at SL 1.9 μm (Terui et al., 2008, 2010; Matsuba et al., 2009); presumably this was coupled with the SL-dependent increase in Ca^{2+} sensitivity (see Kobirumaki-Shimozawa et al., 2014 and references therein). OM increased Ca^{2+} sensitivity in a concentration-dependent manner, left shifting pCa_{50} by 0.16 ± 0.01 and 0.33 ± 0.01 pCa units (ΔpCa_{50}) at 0.5 and 1.0 μM ($p < 0.001$), respectively (Table 1). Maximal force was not significantly affected by either concentration of OM in PLV (Table 1).

In PLA, under the control condition without OM, active force increased in a manner similar to that in PLV, i.e., 32% and 74% at pCa 5.75 and 5.5, respectively (Figure 1C: percentages compared to maximal force). OM increased submaximal forces; i.e., the force levels were 16% and 42%, respectively, at pCa 6.0 and 5.75 in the presence of 0.5 μM

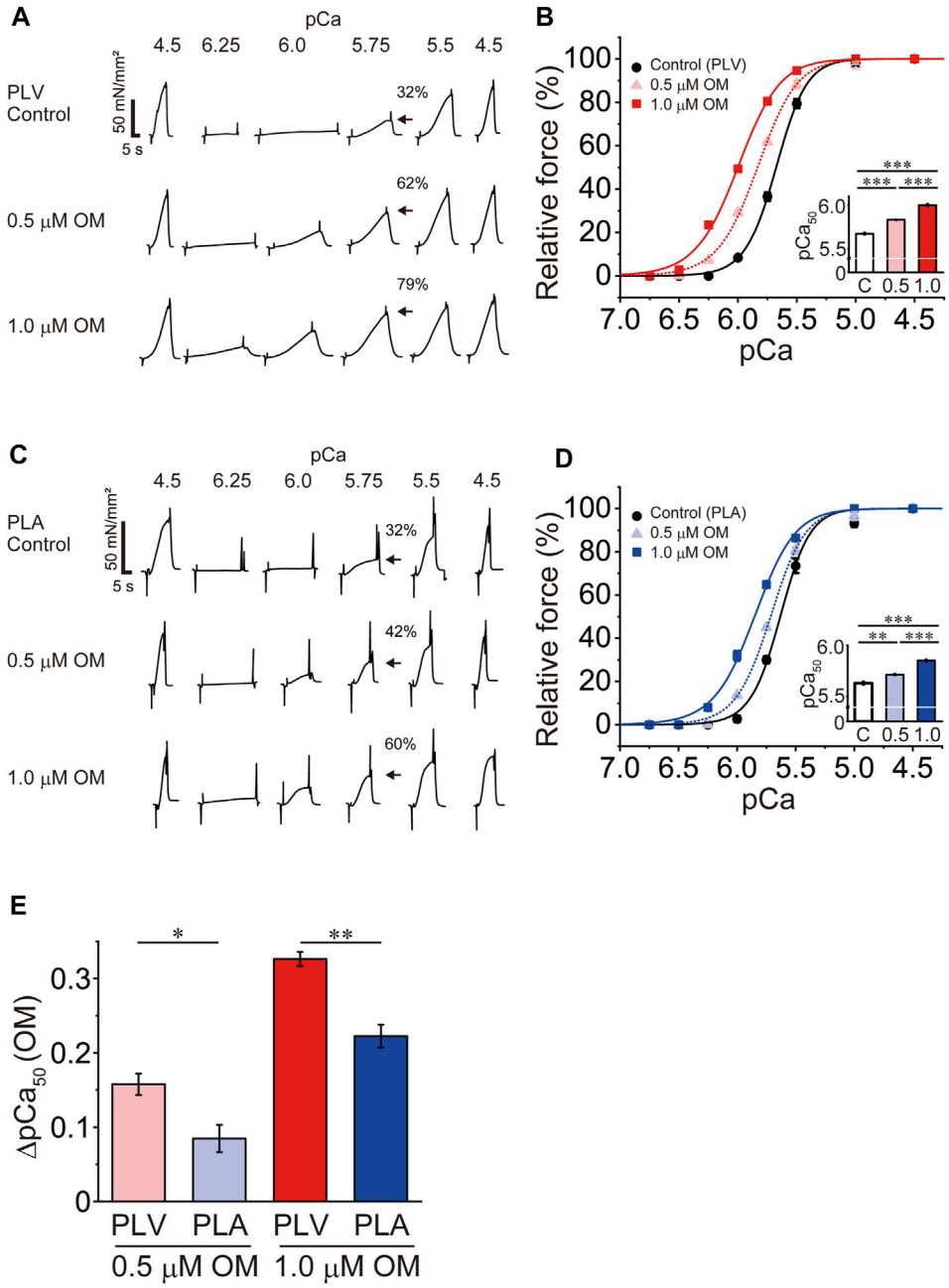

FIGURE 1
Effects of OM on Ca^{2+} sensitivity in PLV and PLA. **(A)** Typical chart recording showing force-pCa protocols in PLV in the absence and presence of OM at 0.5 and 1.0 μM (in this order). Arrows indicate the percentage of active force at pCa 5.75 compared with the maximum obtained at the end of experiment (pCa 4.5). Note that OM increased submaximal force (i.e., at pCa 6.25, 6.0, 5.75 and 5.5). SL was set at 2.1 μm. Control, without OM. **(B)** Force-pCa curves showing the effects of OM at 0.5 and 1.0 μM on Ca^{2+} sensitivity in PLV. Black circles and solid lines, control (without OM); light red triangles and dotted lines, 0.5 μM OM; red squares and solid lines, 1.0 μM OM. Inset, pCa_{50} values in the absence and presence of OM. C, control (without OM); 0.5, 0.5 μM OM; 1.0, 1.0 μM OM. ***$p < 0.001$ (Tukey-Kramer test). $n = 6$ for all groups. **(C)** Same as in **(A)** for PLA in the absence and presence of OM at 0.5 and 1.0 μM (in this order). Arrows indicate the percentage at pCa 5.75 compared with the maximum obtained at the end of experiment (pCa 4.5). Note that OM increased submaximal force (i.e., at pCa 6.25, 6.0, 5.75 and 5.5) [as in PLV; see **(A)**]. SL was set at 2.1 μm. Control, without OM. **(D)** Same as in **(B)** for PLA showing the effects of OM at 0.5 and 1.0 μM on Ca^{2+} sensitivity. Black circles and solid lines, control (without OM); light blue triangles and dotted lines, 0.5 μM OM; blue squares and solid lines, 1.0 μM OM. Inset, pCa_{50} values in the absence and presence of OM. C, control (without OM); 0.5, 0.5 μM OM; 1.0, 1.0 μM OM. **$p < 0.01$; ***$p < 0.001$ (Tukey-Kramer test). $n = 5$ for all groups. **(E)** Graph comparing the Ca^{2+}-sensitizing effect of OM (ΔpCa_{50}) between PLV and PLA at 0.5 and 1.0 μM. At both concentrations, ΔpCa_{50} was greater for PLV than PLA. *$p < 0.05$; **$p < 0.01$ (unpaired Student's t test).

TABLE 1 Summary of the effects of OM on maximal force, Ca^{2+} sensitivity and n_H in PLV and PLA.

	Maximal force (mN/mm^2)	pCa_{50}	ΔpCa_{50}	n_H	*n*
PLV	62.4 ± 1.9	5.67 ± 0.01		3.33 ± 0.12	6
PLV (0.5 μM OM)	66.4 ± 1.7	5.83 ± 0.003***	0.16 ± 0.01	2.53 ± 0.09	6
PLV (1.0 μM OM)	70.1 ± 2.7	6.00 ± 0.01***, ###	0.33 ± 0.01###	2.42 ± 0.07	6
PLA	40.9 ± 0.9†††	5.63 ± 0.02		3.38 ± 0.22	5
PLA (0.5 μM OM)	48.1 ± 1.6*	5.71 ± 0.01**	0.08 ± 0.02†	2.90 ± 0.13	5
PLA (1.0 μM OM)	48.9 ± 1.9*	5.85 ± 0.01***, ###	0.22 ± 0.02###, ††	2.50 ± 0.11	5

Maximal force was obtained by activating muscle at pCa 4.5 prior to or at the end of construction of the force-pCa curve. ΔpCa_{50}, shift of pCa_{50} upon application of OM. *n*, number of experiments. The effects of OM were tested at 0.5 and 1.0 μM, in this order. *, vs. control (without OM) (Tukey-Kramer test); #, vs. 0.5 μM OM (pCa_{50}, Tukey-Kramer test; ΔpCa_{50}, paired Student's *t* test); †, vs. PLV (unpaired Student's *t* test). Single, double and triple symbols denote significant difference at $p < 0.05$, 0.01 and 0.001, respectively.

TABLE 2 Summary of the effects of OM on maximal force, Ca^{2+} sensitivity and n_H in PLV and PLA following PKA treatment.

	Maximal force (mN/mm^2)	pCa_{50}	ΔpCa_{50}	n_H	*n*
PLV	60.7 ± 2.6	5.65 ± 0.02		2.61 ± 0.12	6
PLV (PKA)	75.8 ± 5.2	5.53 ± 0.01***	−0.12 ± 0.02	2.86 ± 0.15	6
PLV (PKA + 1.0 μM OM)	90.4 ± 4.0**	5.79 ± 0.02***, ###	0.26 ± 0.01♭♭	2.47 ± 0.12	6
PLA	40.8 ± 0.9	5.60 ± 0.01		3.76 ± 0.11	5
PLA (PKA)	52.1 ± 3.1*	5.54 ± 0.01**	−0.06 ± 0.01†	3.45 ± 0.26	5
PLA (PKA + 1.0 μM OM)	53.2 ± 3.0*	5.66 ± 0.01**, ###	0.13 ± 0.02†††, ♭♭	2.70 ± 0.12	5

Maximal force was obtained by activating muscle at pCa 4.5 prior to or at the end of construction of the force-pCa curve. ΔpCa_{50}, shift of pCa_{50} upon PKA treatment (PKA) or 1.0 μM OM application following PKA treatment. *n*, number of experiments. *, vs. control (without OM) (Tukey-Kramer test); #, vs. PKA treatment without OM (Tukey-Kramer test); †, vs. PLV (unpaired Student's *t* test); ♭, vs. 1.0 μM OM in Table 1 (unpaired Student's *t* test). Single, double and triple symbols denote significant difference at $p < 0.05$, 0.01 and 0.001, respectively.

OM, and 37% and 60%, respectively, in the presence of 1.0 μM OM. Figure 1D shows force-pCa curves in the absence and presence of OM (Table 1). OM increased Ca^{2+} sensitivity by left shifting pCa_{50} in a concentration-dependent manner; however, the magnitude was less than that in PLV, i.e., ΔpCa_{50} 0.08 ± 0.02 and 0.22 ± 0.02 pCa units at 0.5 and 1.0 μM OM ($p < 0.001$), respectively (Table 1). Unlike in PLV, OM significantly increased maximal force in PLA by ~20% at both concentrations ($p < 0.05$; Table 1).

Figure 1E compares the ΔpCa_{50} values in PLV vs. PLA at 0.5 and 1.0 μM. The compound's Ca^{2+}-sensitizing effect was significantly more pronounced in PLV than in PLA at both concentrations. It can therefore be said that OM increases Ca^{2+} sensitivity in a concentration-dependent manner in both PLV and PLA, with the effect more pronounced in PLV.

Effects of OM on Ca^{2+} sensitivity in PLV and PLA following PKA treatment

PKA treatment decreases Ca^{2+} sensitivity in cardiac muscle, due to phosphorylation of TnI and the ensuing reduction of the TnC-TnI interaction (see Solaro and Rarick, 1998; Matsuba et al., 2009; Inoue et al., 2013 and references therein). It has likewise been reported that PKA phosphorylates MyBP-C and accelerates cross-bridge cycling (Jeacocke and England, 1980; Harris et al., 2002; Tong et al., 2008). Considering that the mammalian heart is constantly under the influence of β-adrenergic stimulation, we next investigated whether or not the Ca^{2+}-sensitizing effect of OM is altered in PLV and PLA following PKA treatment. Consistent with our previous study (Matsuba et al., 2009), PKA decreased Ca^{2+} sensitivity in PLV by right shifting pCa_{50} by 0.12 ± 0.02 pCa units (Figure 2A; Table 2). OM at 1.0 μM increased Ca^{2+} sensitivity following PKA treatment by 0.26 ± 0.01 pCa units. The magnitude of increase in Ca^{2+} sensitivity was ~20% ($p < 0.01$) less than that obtained with no PKA treatment (Tables 1, 2). In PLA, PKA decreased Ca^{2+} sensitivity by right shifting pCa_{50} by 0.06 ± 0.01 pCa units, i.e., ~50% less compared with PLV (Figure 2B; Table 2). As found in PLV, OM at 1.0 μM increased Ca^{2+} sensitivity following PKA treatment by 0.13 ± 0.02 pCa units, i.e., ~43% ($p < 0.01$) less than that obtained with no PKA treatment (Tables 1, 2). Following PKA treatment, therefore, OM increases Ca^{2+} sensitivity in both PLV and PLA, with a greater increase in PLV (Figure 2C); compared with no PKA treatment, however, the effect is less in both

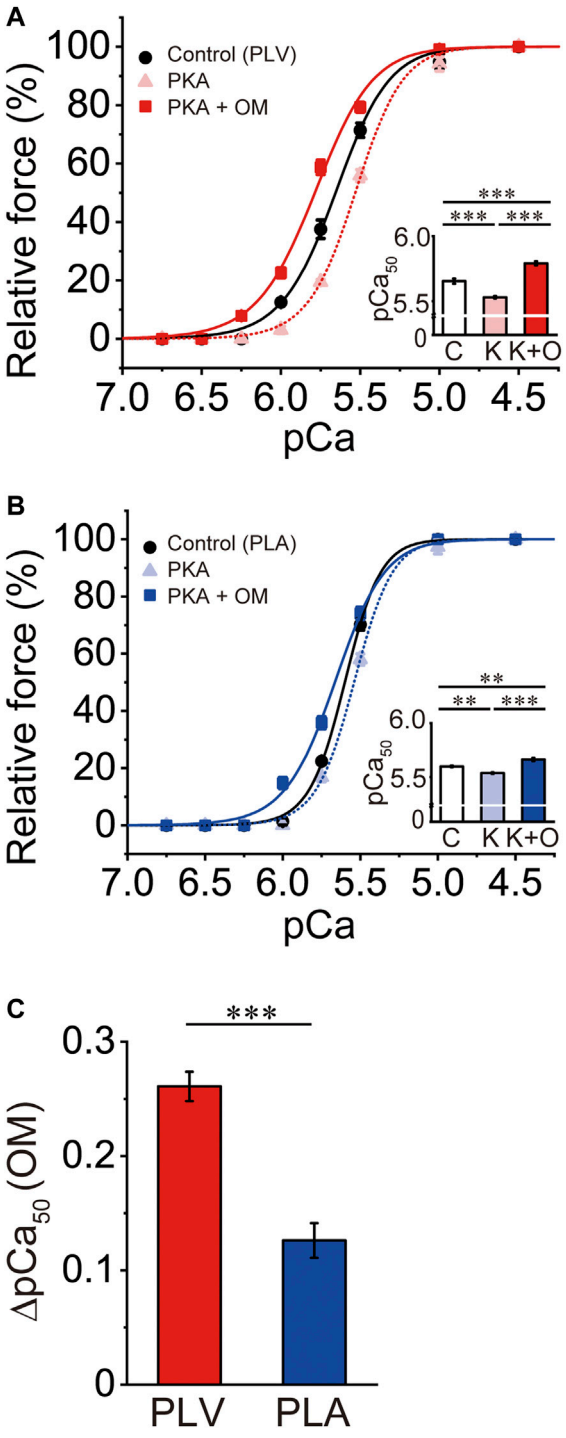

FIGURE 2
Effects of OM on Ca^{2+} sensitivity in PLV and PLA following PKA treatment. **(A)** Force-pCa curves showing the effect of 1.0 μM OM on Ca^{2+} sensitivity following PKA treatment in PLV. Black circles and solid lines, control (before PKA treatment); light red triangles and dotted lines, after PKA treatment; red squares and solid lines, 1.0 μM OM after PKA treatment. Inset, pCa_{50} values under varying conditions. C, control (without OM); K, PKA treatment; K + O, 1.0 μM OM after PKA treatment. ***$p < 0.001$ (Tukey-Kramer test). $n = 6$ for all groups. **(B)** Same as in **(A)** for PLA showing the effect of 1.0 μM OM on Ca^{2+} sensitivity following PKA treatment. Black circles and solid lines, control (before PKA treatment); light blue triangles and dotted lines, after PKA treatment; blue squares and solid lines, 1.0 μM OM after PKA treatment. Inset, pCa_{50} values under varying conditions. C, control (without OM); K, PKA treatment; K + O, 1.0 μM OM after PKA treatment. **$p < 0.01$; ***$p < 0.001$ (Tukey-Kramer test). $n = 5$ for all groups. **(C)** Graph comparing the Ca^{2+}-sensitizing effect of 1.0 μM OM (ΔpCa_{50}) following PKA treatment between PLV and PLA. ***$p < 0.001$ (unpaired Student's t test).

preparations. OM did not significantly alter maximal force in PLV or PLA following PKA treatment (Table 2).

Effects of OM on ADP-contraction in PLV and PLA

We previously reported that increasing the MgADP concentration generates active force in the absence of Ca^{2+} (+ATP and +EGTA); this is a phenomenon known as ADP-induced contraction or "ADP-contraction" which occurs via thin filament cooperative activation by the strongly bound, actomyosin-ADP complex (see e.g., Shimizu et al., 1992; Fukuda et al., 1996, 1998). To confirm whether or not OM increases active force by modulating the processes downstream of Ca^{2+}-binding to TnC in the cross-bridge cycle, we investigated the effects of OM on ADP-contraction in PLV and PLA.

In PLV, ADP-induced active force increased in a concentration-dependent manner, i.e., 9.1% ± 1.5%, 27.4% ± 2.2% and 61.4% ± 3.2% at 1, 2 and 3 mM MgADP (compared to the maximum at 20 mM MgADP), respectively, in the presence of 2 mM MgATP (Figure 3A). This is similar to our earlier finding using bovine left ventricular muscle (Fukuda et al., 1998), but slightly less sensitive to MgADP, due presumably to a decrease in the apparent binding affinity for MgADP at the lower temperature of 15°C in the present study compared to 25°C in Fukuda et al. (1998). OM at 1.0 μM significantly augmented submaximal forces of ADP-contraction, resulting in 15.6% ± 1.5%, 45.4% ± 2.3% and 72.7% ± 2.5% at 1, 2 and 3 mM MgADP. In PLA, MgADP sensitivity was markedly less than that in PLV; submaximal forces were 11.4% ± 2.1%, 33.1% ± 3.6%, 53.0% ± 5.8% and 74.9% ± 4.6% at 5, 8, 10, and 15 mM MgADP, respectively (compared to the maximum at 20 mM MgADP) (Figure 3B). Unlike in PLV, submaximal forces were not significantly affected by 1.0 μM OM at all MgADP concentrations tested. Therefore, OM enhanced Ca^{2+}-independent, strongly bound cross-bridge-dependent contraction in PLV, but not in PLA. It should likewise be noted that OM significantly decreased maximal force of ADP-contraction at 20 mM in PLV (by ~23%), but not in PLA (Figure 3C).

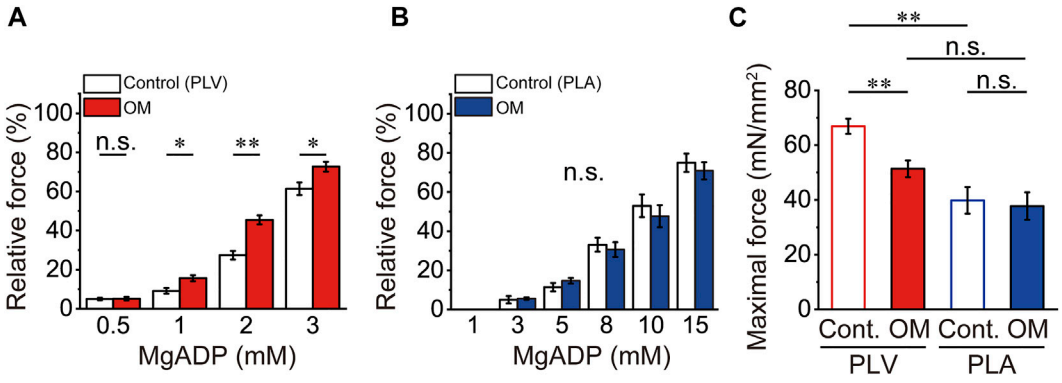

FIGURE 3
Effects of OM on ADP-contraction in PLV and PLA. **(A)** Graph showing the effect of 1.0 μM OM on Ca^{2+}-independent active force in PLV upon increasing the MgADP concentration at 2 mM MgATP. Note that submaximal forces at 1, 2, and 3 mM MgADP were increased in the presence of 1.0 μM OM. *$p < 0.05$; **$p < 0.01$ (unpaired Student's t test). Submaximal forces were normalized compared with that at 20 mM MgADP with or without OM [see **(C)**]. White and red, in the absence (Control) and presence of OM. $n = 5$ for both groups. **(B)** Same as in **(A)** for PLA. Unlike in PLV, submaximal forces were unaffected by 1.0 μM OM. Submaximal forces were normalized compared with that at 20 mM MgADP with or without OM [see **(C)**]. White and blue, in the absence (Control) and presence of OM. $n = 5$ for both groups. **(C)** Comparison of maximal force values at 20 mM MgADP with and without 1.0 μM OM in PLV (red) and PLA (blue). Maximal force was obtained by activating muscle at 20 mM MgADP prior to investigation of submaximal forces. **$p < 0.01$ (unpaired Student's t test).

Effects of OM on Ca^{2+} sensitivity in PLV and PLA under enhanced activation condition

We previously reported that sTn treatment enhances thin filament cooperative activation and accordingly increases Ca^{2+} sensitivity in PLV (Terui et al., 2008, 2010). We then investigated the Ca^{2+}-sensitizing effect of OM under a condition where thin filament cooperative activation is enhanced following sTn treatment. Consistent with our previous results (Terui et al., 2008, 2010), sTn treatment increased Ca^{2+} sensitivity in PLV by left shifting pCa_{50} by 0.14 ± 0.03 pCa units (Figure 4A; Table 3). OM at 1.0 μM further increased Ca^{2+} sensitivity, but ΔpCa_{50} was only 0.16 ± 0.02 pCa units ($p < 0.001$ compared with the value under the control condition; i.e., 0.33 ± 0.01 pCa units in Figure 1B). In PLA, sTn treatment increased Ca^{2+} sensitivity by left shifting pCa_{50} by 0.10 ± 0.02 pCa units (Figure 4B; Table 3). As in the PLV finding, ΔpCa_{50} was less following sTn reconstitution with a value of 0.10 ± 0.01 pCa units when compared with that under the control condition (0.22 ± 0.02 pCa units in Figure 1D; $p < 0.001$).

MgADP is known to augment myocardial contraction by increasing Ca^{2+} sensitivity via formation of strongly bound cross-bridges (actomyosin-ADP complex) and the ensuing enhancement of thin filament cooperative activation (see e.g., Fukuda et al., 1998, 2000; Terui et al., 2010). We then investigated whether or not the Ca^{2+}-sensitizing effect of OM is diminished in the presence of MgADP in PLV and PLA, as with sTn treatment. Consistent with our previous results (Terui et al., 2010), 3 mM MgADP increased Ca^{2+} sensitivity in PLV by left shifting pCa_{50} by 0.24 ± 0.03 pCa units (Figure 4C; Table 3). Ca^{2+} sensitivity was further increased by 1.0 μM OM, but ΔpCa_{50} was significantly ($p < 0.05$) less with 0.21 ± 0.03 pCa units when compared with that under the control condition (i.e., 0.33 ± 0.01 pCa units in Figure 1B). In PLA, 3 mM MgADP increased Ca^{2+} sensitivity by left shifting pCa_{50} by 0.06 ± 0.01 pCa units, significantly less than that in PLV (Figure 4D; Table 3). As in the PLV finding, the Ca^{2+}-sensitizing effect of OM was significantly ($p < 0.001$) less in the presence of MgADP with ΔpCa_{50} 0.08 ± 0.01 pCa units [compared with the value (0.22 ± 0.02 pCa units) under the control condition; cf. Figure 1D].

The Ca^{2+} sensitization by sTn treatment vs. 3 mM MgADP application in PLV and PLA (expressed in ΔpCa_{50}) is compared in Figure 4E. We found that ΔpCa_{50} was statistically insignificant between sTn treatment and MgADP application in PLV and PLA, suggesting that a similar magnitude of thin filament cooperative activation is attained by the two different procedures in both types of preparations (cf. Terui et al., 2010; Kobirumaki-Shimozawa et al., 2014). The magnitude of the OM-induced increase in Ca^{2+} sensitivity (ΔpCa_{50}) was likewise insignificant following sTn treatment and in the presence of 3 mM MgADP in both PLV and PLA (Figure 4F). The greater Ca^{2+}-sensitizing effect of OM in PLV than in PLA was retained in the presence of 3 mM MgADP; however, the effect between PLV and PLA was insignificant following sTn treatment (Figure 4F). OM did not affect maximal force following sTn treatment or MgADP application in both PLV and PLA (Table 3).

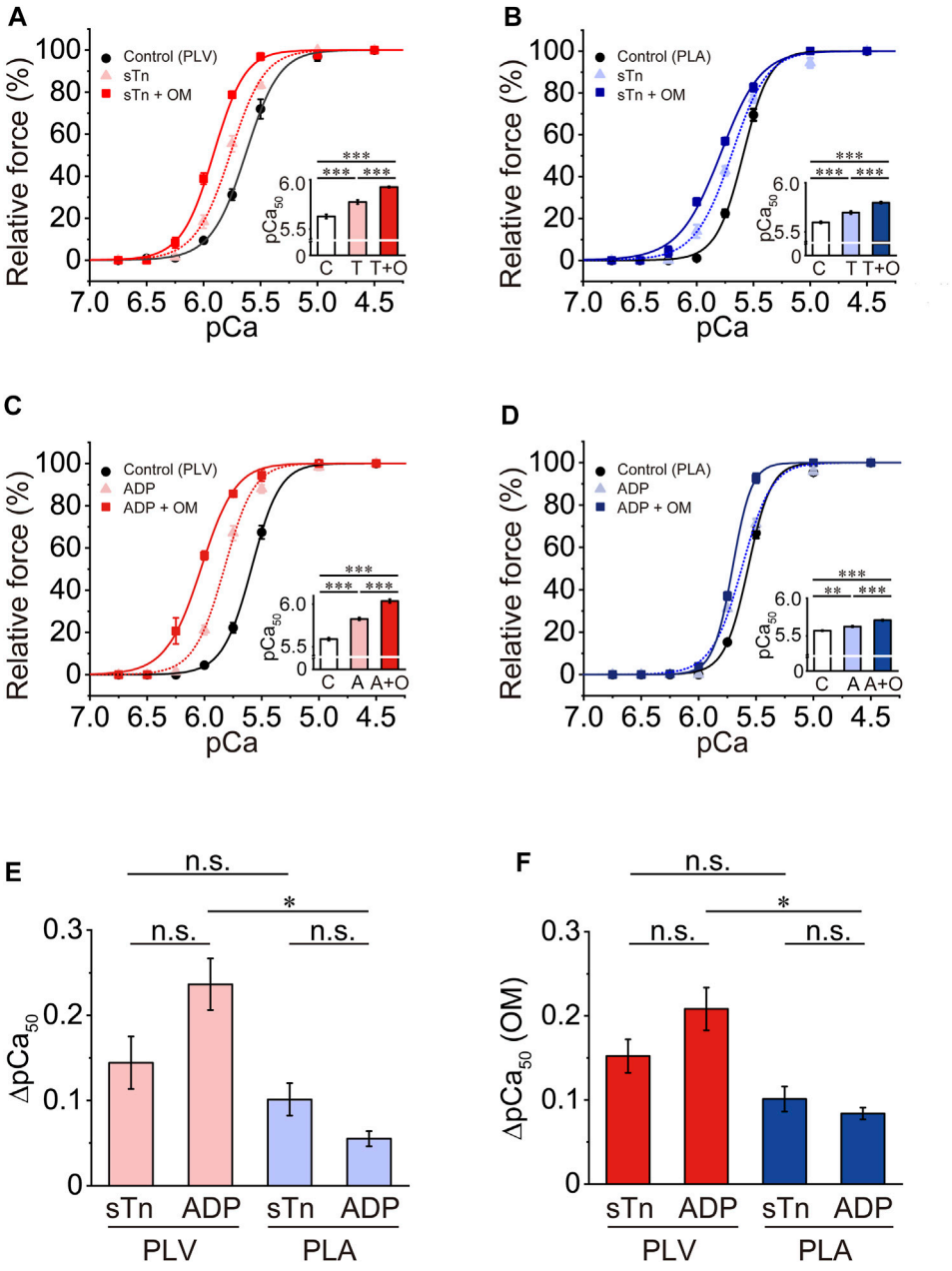

FIGURE 4
Effects of OM on Ca^{2+} sensitivity in PLV and PLA under enhanced activation condition. **(A)** Force-pCa curves showing the effect of 1.0 μM OM on Ca^{2+} sensitivity in PLV following sTn treatment. Black circles and solid lines, control (before sTn treatment); light red triangles and dotted lines, after sTn treatment; red squares and solid lines, 1.0 μM OM after sTn treatment. Inset, pCa_{50} values indicating Ca^{2+} sensitivity under varying conditions. C, control (without OM); T, sTn treatment; T + O, 1.0 μM OM after sTn treatment. ***$p < 0.001$ (Tukey-Kramer test). $n = 6$ for all groups. **(B)** Same as in **(A)** for PLA showing the effect of 1.0 μM OM on Ca^{2+} sensitivity following sTn treatment. Black circles and solid lines, control (before sTn treatment); light blue triangles and dotted lines, after sTn treatment; blue squares and solid lines, 1.0 μM OM after sTn treatment. Inset, pCa_{50} values under varying conditions. C, control (without OM); T, sTn treatment; T + O, 1.0 μM OM after sTn treatment. ***$p < 0.001$ (Tukey-Kramer test). $n = 5$ for all groups. **(C)** Force-pCa curves showing the effect of 1.0 μM OM on Ca^{2+} sensitivity in PLV following 3 mM MgADP application. Black circles and solid lines, control (before MgADP application); light red triangles and dotted lines, after MgADP application; red squares and solid lines, 1.0 μM OM after MgADP application. Inset, pCa_{50} values under varying conditions. C, control (without OM); A, MgADP application; A + O, 1.0 μM OM after MgADP application. ***$p < 0.001$ (Tukey-Kramer test). $n = 4$ for all groups. **(D)** Same as in **(A)** for PLA showing the effect of 1.0 μM OM on Ca^{2+} sensitivity following 3 mM MgADP application. Black circles and solid lines, control (before MgADP application); light blue triangles and dotted lines, after MgADP application; blue squares and solid lines, 1.0 μM OM after MgADP application. Inset, pCa_{50} under varying conditions. C, control (without OM); A, MgADP application; A + O, 1.0 μM OM after MgADP application. **$p < 0.01$; ***$p < 0.001$ (Tukey-Kramer test). $n = 5$ for all groups. **(E)** Graph showing the increased Ca^{2+} sensitivity (ΔpCa_{50}) following sTn treatment (sTn) vs. MgADP application (ADP) in PLV and PLA. *$p < 0.05$ (unpaired Student's t test). Data obtained from **(A–D)**. **(F)** Graph showing the Ca^{2+}-sensitizing effect of 1.0 μM OM [ΔpCa_{50} (OM)] following sTn treatment (sTn) vs. MgADP application (ADP) in PLV and PLA. *$p < 0.05$ (unpaired Student's t test). Data obtained from **(A–D)**.

TABLE 3 Summary of the effects of OM on maximal force, Ca^{2+} sensitivity and n_H in PLV and PLA under enhanced activation condition.

	Maximal force (mN/mm^2)	pCa_{50}	ΔpCa_{50}	n_H	*n*
PLV	60.9 ± 1.5	5.63 ± 0.02		3.10 ± 0.32	6
PLV (sTn)	70.5 ± 3.9	5.77 ± 0.02***	0.14 ± 0.03	3.01 ± 0.19	6
PLV (sTn + 1.0 μM OM)	77.3 ± 6.1	5.93 ± 0.01***, ###	0.16 ± 0.02♭♭♭	3.37 ± 0.30	6
PLA	44.1 ± 0.9	5.60 ± 0.01		3.77 ± 0.28	5
PLA (sTn)	57.8 ± 3.8*	5.70 ± 0.02***	0.10 ± 0.02	2.73 ± 0.15	5
PLA (sTn + 1.0 μM OM)	58.0 ± 3.2*	5.80 ± 0.01***, ###	0.10 ± 0.01♭♭♭	2.43 ± 0.15	5
PLV	62.1 ± 2.0	5.59 ± 0.02		3.49 ± 0.11	4
PLV (ADP)	91.5 ± 5.6*	5.83 ± 0.02***	0.24 ± 0.03	3.39 ± 0.21	4
PLV (ADP + 1.0 μM OM)	94.5 ± 5.6**	6.04 ± 0.02***, ‡‡‡	0.21 ± 0.03♭	2.89 ± 0.18	4
PLA	41.8 ± 1.6	5.57 ± 0.01		4.23 ± 0.25	5
PLA (ADP)	53.3 ± 3.6	5.62 ± 0.01**	0.06 ± 0.01†	3.36 ± 0.20	5
PLA (ADP + 1.0 μM OM)	61.2 ± 2.7**	5.71 ± 0.01***, ‡‡‡	0.08 ± 0.01†, ♭♭♭	6.10 ± 1.10	5

Maximal force was obtained by activating muscle at pCa 4.5 prior to or at the end of construction of the force-pCa curve. ΔpCa_{50}, shift of pCa_{50} upon sTn treatment (sTn), 3 mM MgADP application (ADP) or 1.0 μM OM application after sTn treatment or MgADP application. *n*, number of experiments. *, vs. control (no sTn treatment or MgADP application) (Tukey-Kramer test); #, vs. sTn treatment (without OM) (Tukey-Kramer test); ‡, vs. MgADP application (without OM) (Tukey-Kramer test); †, vs. PLV (unpaired Student's *t* test); ♭, vs. 1.0 μM OM in Table 1 (unpaired Student's *t* test). Single, double and triple symbols denote significant difference at $p < 0.05$, 0.01 and 0.001, respectively.

TABLE 4 Summary of the effects of OM on maximal force, Ca^{2+} sensitivity and n_H in PLV and PLA under depressed activation condition.

	Maximal force (mN/mm^2)	pCa_{50}	ΔpCa_{50}	n_H	*n*
PLV	63.8 ± 1.8	5.63 ± 0.01		4.10 ± 0.30	5
PLV (Pi)	40.3 ± 3.2***	5.39 ± 0.03***	-0.24 ± 0.04	3.66 ± 0.32	5
PLV (Pi + 1.0 μM OM)	50.0 ± 2.9*	5.48 ± 0.003***, #	0.09 ± 0.03♭♭	4.26 ± 0.28	5
PLA	39.9 ± 0.8	5.59 ± 0.01		5.59 ± 0.35	5
PLA (Pi)	20.8 ± 0.3***	5.49 ± 0.01***	-0.10 ± 0.01†	4.22 ± 0.36	5
PLA (Pi + 1.0 μM OM)	27.3 ± 0.8***, ###	5.52 ± 0.01**	0.03 ± 0.01♭♭♭	5.53 ± 0.96	5

Maximal force was obtained by activating muscle at pCa 4.5 prior to or at the end of construction of the force-pCa curve. ΔpCa_{50}, shift of pCa_{50} upon 20 mM Pi application (Pi) or 1.0 μM OM application after Pi application. *n*, number of experiments. *, vs. control (without OM) (Tukey-Kramer test); #, vs. Pi application without OM (Tukey-Kramer test); †, vs. PLV (unpaired Student's *t* test); ♭, vs. 1.0 μM OM in Table 1 (unpaired Student's *t* test). Single, double and triple symbols denote significant difference at $p < 0.05$, 0.01 and 0.001, respectively.

Effects of OM on Ca^{2+} sensitivity in PLV and PLA under depressed activation condition

Pi decreases Ca^{2+} sensitivity in cardiac muscle, by accelerating the detachment of bound cross-bridges (see e.g., Fukuda et al., 1996, 1998; Terui et al., 2010). Finally, we investigated whether or not the Ca^{2+}-sensitizing effect of OM is altered in PLV and PLA under the depressed condition in the presence of 20 mM Pi. Consistent with our previous results (Terui et al., 2010), 20 mM Pi decreased Ca^{2+} sensitivity in PLV by right shifting pCa_{50} by 0.24 ± 0.04 pCa units (Figure 5A; Table 4). OM at 1.0 μM increased Ca^{2+} sensitivity by 0.09 ± 0.03 pCa units, which was markedly smaller than that obtained under the control condition (i.e., $p < 0.01$ compared with 0.33 ± 0.01 pCa units obtained under the control condition in Figure 1B). In PLA, 20 mM Pi decreased Ca^{2+} sensitivity by right shifting pCa_{50} by 0.10 ± 0.01 pCa units (Figure 5B; Table 4). As in the PLV finding, ΔpCa_{50} in PLA was less in the presence of Pi with merely 0.03 ± 0.01 pCa units ($p < 0.001$ compared with 0.22 ± 0.02 pCa units obtained under the control condition in Figure 1D). The difference between PLV and PLA in the Ca^{2+}-sensitizing effect of OM in the presence of Pi was insignificant ($p > 0.05$) (Figure 5C). It should be noted in the presence of Pi that maximal force was significantly augmented by OM in PLA, but not in PLV (Table 4).

Discussion

The findings of the present study are four-fold: 1) OM at clinically relevant concentrations increased submaximal forces in

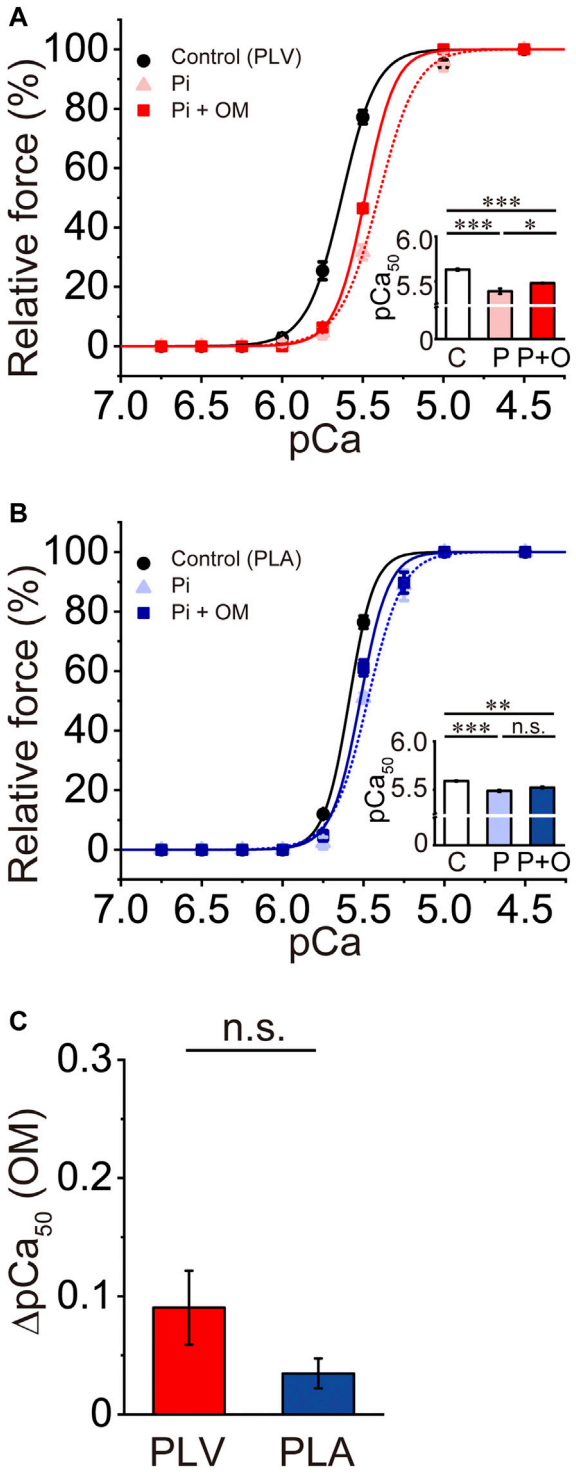

FIGURE 5
Effects of OM on Ca^{2+} sensitivity in PLV and PLA under depressed activation condition. **(A)** Force-pCa curves showing the effect of 1.0 μM OM on Ca^{2+} sensitivity in PLV following 20 mM Pi application. Black circles and solid lines, control (before Pi application); light red triangles and dotted lines, after Pi application; red squares and solid lines, 1.0 μM OM after Pi application. Inset, pCa_{50} values indicating Ca^{2+} sensitivity under

(*Continued*)

FIGURE 5 | varying conditions. C, control (without OM); P, Pi; P + O, 1.0 μM OM after Pi application. *$p < 0.05$; ***$p < 0.001$ (Tukey-Kramer test). $n = 5$ for all groups. **(B)** Same as in **(A)** showing the effect of 1.0 μM OM on Ca^{2+} sensitivity in PLA following 20 mM Pi application. Black circles and solid lines, control (before Pi application); light blue triangles and dotted lines, after Pi application; blue squares and solid lines, 1.0 μM OM after Pi application. Inset, pCa_{50} values indicating Ca^{2+} sensitivity under varying conditions. C, control (without OM); P, Pi; P + O, 1.0 μM OM after Pi application. ***$p < 0.001$ (Tukey-Kramer test). $n = 5$ for all groups. **(C)** Graph comparing the Ca^{2+}-sensitizing effect of 1.0 μM OM (ΔpCa_{50}) between PLV and PLA following 20 mM Pi application.

a concentration-dependent manner in PLV and PLA, with a greater magnitude in PLV, 2) OM augmented Ca^{2+}-independent, strongly bound cross-bridge-dependent submaximal forces in PLV, but not in PLA, 3) OM's Ca^{2+}-sensitizing effect was attenuated in both PLV and PLA upon enhanced thin filament cooperative activation, directly by sTn treatment and indirectly by MgADP application, and 4) Pi markedly decreased the Ca^{2+}-sensitizing effect of OM.

First, OM increased Ca^{2+} sensitivity at 0.5 and 1.0 μM in a concentration-dependent manner in PLV (Figure 1). The magnitude of the increase in Ca^{2+} sensitivity is largely consistent with the findings of previous reports by others using ventricular muscles of various animal species [i.e., rat (Nagy et al., 2015; Kieu et al., 2019), mouse (Mamidi et al., 2015; Utter et al., 2015), guinea pig (Gollapudi et al., 2017) and human (Mamidi et al., 2017)]. Notably, Mamidi et al. (2017) showed that OM at 0.5 and 1.0 μM enhances active force at submaximal Ca^{2+} levels in a concentration-dependent manner in skinned human left ventricular muscle. To the knowledge of the authors, the present study is the first to demonstrate that OM increases Ca^{2+} sensitivity in atrial muscle (PLA) (Figure 1). Considering the previous report by Shchepkin et al. (2020) which demonstrated that OM prolongs the actomyosin attachment duration in ventricular and atrial myosin, with a higher sensitivity in ventricular myosin, the differential Ca^{2+}-sensitizing effect of OM in PLV vs. PLA is likely to reflect the varying sensitivity of OM in the prolongation of the actomyosin attachment duration. Given the possible mechanism of action of OM in that it allosterically promotes the formation of force-generating cross-bridges via thin filament cooperative activation (see **Introduction**), the following mechanism can likewise be proposed to account for the differential effect of OM in PLV vs. PLA: namely, the actomyosin attachment duration in the presence of OM is longer for ventricular than atrial myosin in the porcine heart (at 0.5 and 1.0 μM; see Shchepkin et al., 2020), presumably because the attachment duration is intrinsically longer for the former than the latter. It is therefore likely that in PLV, the thin filament "*on-off*" equilibrium is more easily shifted towards the "*on*" state by OM-bound cross-bridges, and, accordingly, a substantial number of force-generating

cross-bridges are formed (i.e., causing increased Ca^{2+} sensitivity). This scenario may be supported by the result that maximal force was significantly higher in PLV than in PLA (by ~1.5-fold; Table 1) (see a similar tendency on ventricular vs. atrial muscles from bovine hearts; Fukuda et al., 2003). And maximal force was increased by ~20% upon application of OM at 0.5 and 1.0 μM in PLA, but not in PLV (Table 1), reflecting, presumably, the transition of "recruitable" cross-bridges to force-generating cross-bridges via enhanced thin filament cooperative activation. Indeed, it is widely regarded that in both cardiac and skeletal muscles, Ca^{2+} alone cannot fully activate thin filaments; it is the strongly bound cross-bridges, such as rigor cross-bridges (e.g., Bremel and Weber, 1972), *N*-ethylmaleimide-treated myosin subfragment 1 (e.g., Nagashima and Asakura, 1982) and the actomyosin-ADP complex (e.g., Cooke and Pate, 1985; Shimizu et al., 1992; Fukuda et al., 1998), that augment maximal force, cooperatively with Ca^{2+}.

In mammals, the heart is consistently under the influence of β-adrenergic stimulation *in vivo*. As discussed in our earlier papers (e.g., Matsuba et al., 2009; Kobirumaki-Shimozawa et al., 2014), a decrease in the Ca^{2+}-binding affinity to TnC following PKA-dependent phosphorylation of TnI results from the reduced TnC-TnI interaction. We found that OM increased Ca^{2+} sensitivity in both PLV and PLA following PKA treatment, but the effect was significantly less pronounced in both preparations compared with no PKA treatment (by ~20% and ~43% in PLV and PLA, respectively; cf. Figure 1) (Figure 2). Because OM directly binds to myosin (e.g., Winkelmann et al., 2015), it is unlikely that the attenuation of the effect of OM is coupled with a decrease in the Ca^{2+}-binding affinity of TnC. It is important that PKA phosphorylates MyBP-C (e.g., Jeacocke and England, 1980) and titin (e.g., Yamasaki et al., 2002; Fukuda et al., 2005a), other than TnI; phosphorylation of MyBP-C may loosen its constraint on the thick filament backbone and allow myosin heads to interact with thin filaments (Colson et al., 2008; Kensler et al., 2017; McNamara et al., 2019). Therefore, OM's effect may be blunted in both PLV and PLA following PKA treatment because fewer myosin heads would be recruited to thin filaments due to a change in the thick filament-based regulation (see below). Because various types of kinases operate in living myocardium (as discussed in Matsuba et al., 2009), future studies need to be systematically conducted to investigate whether and how these kinases affect the Ca^{2+}-sensitizing effect of OM.

OM at 1.0 μM increased MgADP-induced submaximal forces in PLV, but not in PLA (+ATP and +EGTA; Figure 3). The finding in PLV supports the notion that OM apparently increases Ca^{2+} sensitivity in normal Ca^{2+}-dependent contraction, independent from Ca^{2+}-binding to TnC (see previous papers by others; e.g., Malik et al., 2011). There could be two reasons for the absence of the effect of OM in PLA. First, the binding affinity of OM for PLA is too low to augment submaximal forces of ADP-contraction. Second, while the OM-myosin complex effectively activates thin filaments and promotes the binding of neighboring myosin in PLV during ADP-contraction, this allosteric effect would be less in PLA due to the short attachment duration of atrial myosin. The effectiveness of MgADP in the generation of active force in ADP-contraction was consistently markedly less pronounced in PLA than in PLV (Figure 3), indicating a lesser magnitude of the effect of strongly bound cross-bridges in PLA "turning on" thin filaments. It is to be noted that OM decreased maximal force of ADP-contraction in PLV but not in PLA (Figure 3). It can be considered that due to the long attachment duration of ventricular myosin, the application of OM in the bathing solution containing 20 mM MgADP excessively promotes the formation of the non-force producing, actomyosin-ADP complex (i.e., AM.ADP2 in Fukuda et al., 1998), similar to the characteristics of rigor cross-bridges, and thereby decreases the number of force-generating, working cross-bridges.

We previously reported that the magnitude of the shift of pCa_{50} following sTn treatment depends on SL in PLV; it becomes less pronounced as SL is elongated (i.e., ~0.23 and ~0.12 pCa units at SL 1.9 and 2.3 μm, respectively; Terui et al., 2008). Given, therefore, that throughout the present study SL was set at 2.1 μm in both PLV and PLA, we consider that the present sTn treatment suitably increased Ca^{2+} sensitivity in both types of preparation via enhanced thin filament cooperative activation (Figure 4; cf. Terui et al., 2008). Similarly, we previously reported that pCa_{50} was shifted leftward in a SL-dependent manner in PLV upon application of 3 mM MgADP, by ~0.26 and ~0.13 pCa units at SL 1.9 and 2.3 μm, respectively (Terui et al., 2010). As with the case for sTn treatment, this is because the number of "recruitable" cross-bridges is decreased at a longer SL, resulting in the attenuation of further formation of force-generating cross-bridges via thin filament cooperative activation by strongly bound cross-bridges (i.e., actomyosin-ADP complex; see Fukuda et al., 1998, 2000). We therefore consider that the present finding on the MgADP-induced increase in Ca^{2+} sensitivity in PLV obtained at SL 2.1 μm (i.e., 0.24 ± 0.03 pCa units) is consistent with our previous data (Figure 4; cf. Terui et al., 2010). It should be noted that, despite the same concentration of 3 mM used, the effect of MgADP was markedly less in PLA with a leftward shift magnitude of only 0.06 ± 0.01 pCa units. We consider that the differential effect of MgADP on the leftward shift of pCa_{50} between PLV and PLA results from a difference in the apparent binding affinity of MgADP to ventricular myosin vs. atrial myosin. It has indeed been reported that the equilibrium constant of the ADP-release during the cross-bridge cycling is

higher for atrial myosin than ventricular myosin (Wang et al., 2013; Walklate et al., 2021), thereby decreasing the apparent affinity of exogenously added MgADP.

Here, we discuss the possible mechanisms by which the Ca^{2+}-sensitizing effect of OM was attenuated in PLV and PLA following sTn treatment and in the presence of MgADP. It should be noted that despite different approaches used, both sTn treatment and MgADP application enhance thin filament cooperative activation, as reflected by increased Ca^{2+} sensitivity, the former and latter of which act in a direct and indirect manner, respectively (see Terui et al., 2010). Recent studies have proposed a possible primary mechanism of the cardiotonic action of OM based on the prolongation of the actomyosin attachment duration and the ensuing enhancement of thin filament cooperative activation (see **Introduction**). In the present study, the magnitude of the leftward shift of pCa_{50} between sTn treatment and MgADP application was insignificant (Figure 4), suggesting that a similar magnitude of enhanced thin filament cooperative activation was attained. Likewise, the Ca^{2+}-sensitizing effect of OM was insignificant between the two procedures in both PLV and PLA (Figure 4). These findings suggest that the number of "recruitable" cross-bridges is decreased by a similar magnitude following sTn treatment and MgADP application, thereby attenuating the effect of OM to recruit neighboring myosin into the force-generating state via enhancement of thin filament cooperative activation.

The depressant effect of Pi on the OM-induced increase in Ca^{2+} sensitivity was evident in both PLV and PLA (Figure 5). The present finding on PLV is consistent with our previous result in that pCa_{50} was shifted rightward in a SL-dependent manner, by ~0.27 and ~0.20 pCa units at SL 1.9 and 2.3 μm, respectively (cf. Terui et al., 2010). We found in the present study that the Ca^{2+}-sensitizing effect of OM was markedly decreased in the presence of 20 mM Pi in both PLV and PLA (Figure 5). It has been reported that Pi binds to the actomyosin-ADP complex after the power stroke in the cross-bridge cycle and causes reversal of the stroke (Woody et al., 2019), and accordingly, Ca^{2+} sensitivity is apparently decreased (see Fukuda et al., 1998 and references therein). We therefore consider that although the number of "recruitable" cross-bridges is increased in the presence of Pi (Terui et al., 2010), regardless of the type of preparation (PLV or PLA), due to the acceleration of detachment of OM-bound myosin from thin filaments, thin filament cooperative activation is depressed; consequently, the number of cross-bridges recruited to thin filaments will be limited. Nevertheless, the cardiotonic action of OM was seen under this depressed condition to increase maximal force in PLA (Table 4), which was not the case under enhanced thin filament activation conditions, regardless of the type of preparations (Table 3).

It should be noted that the Ca^{2+}-sensitizing effects of OM may be coupled with a change in the thick filament state, independent of the thin filament "*on-off*" regulation. Stewart et al. (2010) discovered a myosin state in skinned rabbit psoas muscle fibers that has an extremely slow ATP turnover rate. This unique relaxed state has come to be widely known as the "super-relaxed state" (SRX) (see reviews and references therein: e.g., Cooke, 2011; McNamara et al., 2015; Irving, 2017; Spudich, 2019; Craig and Padrón, 2022). SRX is reportedly in equilibrium with the disordered-relaxed state (DRX) in which myosin heads are in closer proximity to thin filaments (e.g., Anderson et al., 2018; Gollapudi et al., 2021; Yuan et al., 2022), and ready to produce force. A decrease in the number of myosin molecules in SRX would increase the proportion of the heads available to form force-generating cross-bridges (e.g., Schmid and Toepfer, 2021). It is possible that mechanical stress on thick filaments, presumably via myosin binding to thin filaments, shifts the SRX-DRX equilibrium towards DRX (Linari et al., 2015). It is considered that SRX is a biochemical and presumably a structural state, in which myosin heads interact with, and are folded back on, the thick filament backbone, and are consequently unavailable for binding thin filaments (e.g., Hooijman et al., 2011; Alamo et al., 2016). Hooijman et al. (2011) reported that in cardiac muscle, a significant proportion of myosin in thick filaments is in SRX, and these myosin molecules in SRX are rather modulatory, providing more graded recruitment of the heads and the ensuing active force production, compared with skeletal muscle. Therefore, OM may modulate the thick filament structure and thereby destabilize SRX, resulting in an increase in the number of myosin heads that can readily bind to thin filaments and produce active force in a graded manner (Kampourakis et al., 2018). We consider that this thick filament-based mechanism may at least in part account for the observed Ca^{2+}-sensitizing effects of OM in both PLV and PLA (Figure 1). It is likewise possible that OM's effect is synergistically brought about via the thick filament-based regulation and the ensuing thin filament "*on-off*" regulation (Spudich, 2019; Nag and Trivedi, 2021). Namely, myosin in the pre-pre-powerstroke state, a state similar to SRX, is stabilized by OM, but not sufficiently compliant to fit into the folded-back thick-filament state and therefore it is able to bind to actin. Ca^{2+} sensitivity would consequently be increased via formation of myosin in the pre-pre-powerstroke state and the ensuing thin filament cooperative activation, as well as by a reduction in the number of myosin heads in the folded-back state.

Likewise, it is important to discuss the possible contribution of the thick filament-based SRX-DRX regulation to the attenuation of the Ca^{2+}-sensitizing effect of OM. First, PKA-dependent phosphorylation of cardiac MyBP-C has been reported to shift the SRX-DRX equilibrium to DRX (McNamara et al., 2019; Harris, 2021). Therefore, fewer cross-bridges would be recruited by OM when MyBP-C is phosphorylated, resulting in the attenuation

of OM's Ca^{2+}-sensitizing effect in both PLV and PLA (Figure 2). Along this line, it is possible that MgADP shifts the SRX-DRX equilibrium to DRX, via structural changes in thick filaments (see Nag and Trivedi, 2021 and references therein), reduces the number of "recruitable" cross-bridges, and thereby attenuates OM's effect (Figure 4). Future studies are needed from the perspective of thick filaments by using various techniques to determine whether and how OM's effect varies in ventricular and atrial muscles under various perturbations.

Ovejero et al. (2022), by taking advantage of X-ray diffraction, reported that upon a decrease in temperature from 39°C to 7°C, myosin heads leave the helical folded state of thick filaments, and the periodicity of the thick filament backbone increases in intact rat ventricular trabeculae. They likewise demonstrated that myosin filament structure and motor conformation of intact trabeculae at 39°C are largely preserved in skinned trabeculae at 27°C or above in the presence of osmotic compression. However, when active force levels are high at high temperatures (e.g., 27°C), or at longer sarcomere length, rundowns easily occur during force measurements in mechanical experimentations with skinned muscle preparations, which would lead to an underestimation of maximal active force and could therefore impact the deduced Ca^{2+} sensitivity (as discussed in Fukuda et al., 2005b). The results of the present study obtained at a low temperature of 15°C might therefore lead to an underestimation of the Ca^{2+}-sensitizing effect of OM because of a loss of cross-bridges in SRX in the relaxing condition that can potentially be activated by OM and form into force-generating cross-bridges.

Finally, we discuss the clinical relevance obtained from the present findings. First, OM increased Ca^{2+} sensitivity at clinically relevant concentrations in PLV and PLA, with the effect more pronounced in PLV. Careful studies are needed to investigate whether OM increases ventricular contraction to a greater magnitude than atrial contraction *in vivo*, especially in patients with HFrEF, thereby effectively increasing cardiac output without causing congestion. Second, the greater Ca^{2+}-sensitizing effect in PLV was retained following PKA treatment, suggesting that OM may be a useful cardiotonic compound under the various PKA-dependent phosphorylation states of myofibrillar proteins. Third, given that OM's Ca^{2+}-sensitizing effect became diminished following sTn treatment in both types of preparations, its cardiotonic effect may be less in patients with HFrEF associated with Tn mutations. Fourth and finally, the marked attenuation of OM's Ca^{2+}-sensitizing effect in the presence of Pi in both PLV and PLA suggests that the compound's cardiotonic effect may be limited in the ischemic heart or under hypoxia. Future basic and clinical studies are warranted to systematically investigate whether and how the inotropic effect of OM is altered in the ventricle and atrium under various disease conditions of the heart.

Data availability statement

The raw data supporting the conclusions of this article will be made available by the authors, without undue reservation.

Ethics statement

The animal study was reviewed and approved by the Animal Care and Use Committee of Hokkaido University.

Author contributions

TN, KO, FK-S, TT, and NF designed the research; TN and HT performed experiments; TN, KO, and NF analyzed data; TN, KO, SI, S'II, and NF interpreted the data; TN, KO, FK-S, S'II, and NF drafted the manuscript. All authors have approved the final draft of the manuscript, and their contributions qualify them as authors.

Funding

This work was supported by JSPS KAKENHI Grant Numbers 15H04677 (to NF), 20H03421 (to NF), 21K19929 (to NF), 21K06789 (to FK-S) and 21K08981 (to TT). This study was also supported by The Naito Foundation (to FK-S).

Acknowledgments

We thank Naoko Tomizawa and Michiyo Murata (The Jikei University School of Medicine) for technical assistance.

Conflict of interest

The authors declare that the research was conducted in the absence of any commercial or financial relationships that could be construed as a potential conflict of interest.

Publisher's note

References

Alamo, L., Qi, D., Wriggers, W., Pinto, A., Zhu, J., Bilbao, A., et al. (2016). Conserved intramolecular interactions maintain myosin interacting-heads motifs explaining tarantula muscle super-relaxed state structural basis. *J. Mol. Biol.* 428, 1142–1164. doi:10.1016/j.jmb.2016.01.027

Anderson, R. L., Trivedi, D. V., Sarkar, S. S., Henze, M., Ma, W., Gong, H., et al. (2018). Deciphering the super relaxed state of human β-cardiac myosin and the mode of action of mavacamten from myosin molecules to muscle fibers. *Proc. Natl. Acad. Sci. U. S. A.* 115, E8143-E8152. doi:10.1073/pnas.1809540115

Bremel, R. D., and Weber, A. (1972). Cooperation within actin filament in vertebrate skeletal muscle. *Nat. New Biol.* 238, 97–101. doi:10.1038/newbio238097a0

Colson, B. A., Bekyarova, T., Locher, M. R., Fitzsimons, D. P., Irving, T. C., Moss, R. L., et al. (2008). Protein kinase A-mediated phosphorylation of cMyBP-C increases proximity of myosin heads to actin in resting myocardium. *Circ. Res.* 103, 244–251. doi:10.1161/CIRCRESAHA.108.178996

Cooke, R., and Pate, E. (1985). The effects of ADP and phosphate on the contraction of muscle fibers. *Biophys. J.* 48, 789–798. doi:10.1016/S0006-3495(85)83837-6

Cooke, R. (2011). The role of the myosin ATPase activity in adaptive thermogenesis by skeletal muscle. *Biophys. Rev.* 3, 33–45. doi:10.1007/s12551-011-0044-9

Craig, R., and Padrón, R. (2022). Structural basis of the super- and hyper-relaxed states of myosin II. *J. Gen. Physiol.* 154, e202113012. doi:10.1085/jgp.202113012

Ebashi, S., Wakabayashi, T., and Ebashi, F. (1971). Troponin and its components. *J. Biochem.* 69, 441–445. doi:10.1093/oxfordjournals.jbchem.a129486

Eisenberg, E., and Kielley, W. W. (1974). Troponin-Tropomyosin complex. *J. Biol. Chem.* 249, 4742–4748. doi:10.1016/S0021-9258(19)42382-X

Francis, G. S., Bartos, J. A., and Adatya, S. (2014). Inotropes. *J. Am. Coll. Cardiol.* 63, 2069–2078. doi:10.1016/j.jacc.2014.01.016

Fukuda, N., Fujita, H., Fujita, T., and Ishiwata, S. (1996). Spontaneous tension oscillation in skinned bovine cardiac muscle. *Pflügers Arch.* 433, 1–8. doi:10.1007/s004240050241

Fukuda, N., Fujita, H., Fujita, T., and Ishiwata, S. (1998). Regulatory roles of MgADP and calcium in tension development of skinned cardiac muscle. *J. Muscle Res. Cell. Motil.* 19, 909–921. doi:10.1023/a:1005437517287

Fukuda, N., Kajiwara, H., Ishiwata, S., and Kurihara, S. (2000). Effects of MgADP on length dependence of tension generation in skinned rat cardiac muscle. *Circ. Res.* 86, E1–E6. doi:10.1161/01.res.86.1.e1

Fukuda, N., Wu, Y., Farman, G., Irving, T. C., and Granzier, H. (2003). Titin isoform variance and length dependence of activation in skinned bovine cardiac muscle. *J. Physiol.* 553, 147–154. doi:10.1113/jphysiol.2003.049759

Fukuda, N., Wu, Y., Nair, P., and Granzier, H. L. (2005a). Phosphorylation of titin modulates passive stiffness of cardiac muscle in a titin isoform-dependent manner. *J. Gen. Physiol.* 125, 257–271. doi:10.1085/jgp.200409177

Fukuda, N., Wu, Y., Farman, G., Irving, T. C., and Granzier, H. (2005b). Titin-based modulation of active tension and interfilament lattice spacing in skinned rat cardiac muscle. *Pflügers Arch.* 449, 449–457. doi:10.1007/s00424-004-1354-6

Gollapudi, S. K., Reda, S. M., and Chandra, M. (2017). Omecamtiv mecarbil abolishes length-mediated increase in Guinea pig cardiac myofiber Ca^{2+} sensitivity. *Biophys. J.* 113, 880–888. doi:10.1016/j.bpj.2017.07.002

Gollapudi, S. K., Yu, M., Gan, Q. F., and Nag, S. (2021). Synthetic thick filaments: a new avenue for better understanding the myosin super-relaxed state in healthy, diseased, and mavacamten-treated cardiac systems. *J. Biol. Chem.* 296, 100114. doi:10.1074/jbc.RA120.016506

Governali, S., Caremani, M., Gallart, C., Pertici, I., Stienen, G., Piazzesi, G., et al. (2020). Orthophosphate increases the efficiency of slow muscle-myosin isoform in the presence of omecamtiv mecarbil. *Nat. Commun.* 11, 3405. doi:10.1038/s41467-020-17143-2

Harris, S. P., Bartley, C. R., Hacker, T. A., McDonald, K. S., Douglas, P. S., Greaser, M. L., et al. (2002). Hypertrophic cardiomyopathy in cardiac myosin binding protein-C knockout mice. *Circ. Res.* 90, 594–601. doi:10.1161/01.res.0000012222.70819.64

Harris, S. P. (2021). Making waves: a proposed new role for myosin-binding protein C in regulating oscillatory contractions in vertebrate striated muscle. *J. Gen. Physiol.* 153, e202012729. doi:10.1085/jgp.202012729

Hooijman, P., Stewart, M. A., and Cooke, R. (2011). A new state of cardiac myosin with very slow ATP turnover: a potential cardioprotective mechanism in the heart. *Biophys. J.* 100, 1969–1976. doi:10.1016/j.bpj.2011.02.061

Inoue, T., Kobirumaki-Shimozawa, F., Kagemoto, T., Fujii, T., Terui, T., Kusakari, Y., et al. (2013). Depressed Frank-Starling mechanism in the left ventricular muscle of the knock-in mouse model of dilated cardiomyopathy with troponin T deletion mutation ΔK210. *J. Mol. Cell. Cardiol.* 63, 69–78. doi:10.1016/j.yjmcc.2013.07.001

Irving, M. (2017). Regulation of contraction by the thick filaments in skeletal muscle. *Biophys. J.* 113, 2579–2594. doi:10.1016/j.bpj.2017.09.037

Jeacocke, S. A., and England, P. J. (1980). Phosphorylation of a myofibrillar protein of Mr 150 000 in perfused rat heart, and the tentative indentification of this as C-protein. *FEBS Lett.* 122, 129–132. doi:10.1016/0014-5793(80)80418-2

Kampourakis, T., Zhang, X., Sun, Y. B., and Irving, M. (2018). Omecamtiv mercabil and blebbistatin modulate cardiac contractility by perturbing the regulatory state of the myosin filament. *J. Physiol.* 596, 31–46. doi:10.1113/JP275050

Kanda, Y. (2013). Investigation of the freely available easy-to-use software "EZR" for medical statistics. *Bone Marrow Transpl.* 48, 452–458. doi:10.1038/bmt.2012.244

Kensler, R. W., Craig, R., and Moss, R. L. (2017). Phosphorylation of cardiac myosin binding protein C releases myosin heads from the surface of cardiac thick filaments. *Proc. Natl. Acad. Sci. U. S. A.* 114, E1355-E1364. doi:10.1073/pnas.1614020114

Kieu, T. T., Awinda, P. O., and Tanner, B. C. W. (2019). Omecamtiv mecarbil slows myosin kinetics in skinned rat myocardium at physiological temperature. *Biophys. J.* 116, 2149–2160. doi:10.1016/j.bpj.2019.04.020

Kobirumaki-Shimozawa, F., Inoue, T., Shintani, S. A., Oyama, K., Terui, T., Minamisawa, S., et al. (2014). Cardiac thin filament regulation and the Frank-Starling mechanism. *J. Physiol. Sci.* 64, 221–232. doi:10.1007/s12576-014-0314-y

Lienhard, G. E., and Secemski, I. I. (1973). P^1, P^5-Di(adenosine-5') pentaphosphate, a potent multisubstrate inhibitor of adenylate kinase. *J. Biol. Chem.* 248, 1121–1123. doi:10.1016/S0021-9258(19)44380-9

Linari, M., Brunello, E., Reconditi, M., Fusi, L., Caremani, M., Narayanan, T., et al. (2015). Force generation by skeletal muscle is controlled by mechanosensing in myosin filaments. *Nature* 528, 276–279. doi:10.1038/nature15727

Lindqvist, J., Lee, E. J., Karimi, E., Kolb, J., and Granzier, H. (2019). Omecamtiv mecarbil lowers the contractile deficit in a mouse model of nebulin-based nemaline myopathy. *PLoS ONE* 14, e0224467. doi:10.1371/journal.pone.0224467

Liu, Y., White, H. D., Belknap, B., Winkelmann, D. A., and Forgacs, E. (2015). Omecamtiv mecarbil modulates the kinetic and motile properties of porcine β-cardiac myosin. *Biochemistry* 54, 1963–1975. doi:10.1021/bi5015166

Maddox, T. M., Januzzi, J. L., Allen, L. A., Breathett, K., Butler, J., Davis, L. L., et al. (2021). 2021 update to the 2017 ACC expert consensus decision pathway for optimization of heart failure treatment: Answers to 10 pivotal issues about heart failure with reduced ejection fraction: a report of the American college of cardiology solution set oversight committee. *J. Am. Coll. Cardiol.* 77, 772–810. doi:10.1016/j.jacc.2020.11.022

Malik, F. I., Hartman, J. J., Elias, K. A., Morgan, B. P., Rodriguez, H., Brejc, K., et al. (2011). Cardiac myosin activation: A potential therapeutic approach for systolic heart failure. *Science* 331, 1439–1443. doi:10.1126/science.1200113

Malik, F. I., and Morgan, B. P. (2011). Cardiac myosin activation part 1: from concept to clinic. *J. Mol. Cell. Cardiol.* 51, 454–461. doi:10.1016/j.yjmcc.2011.05.006

Mamidi, R., Gresham, K. S., Li, A., dos Remedios, C. G., and Stelzer, J. E. (2015). Molecular effects of the myosin activator omecamtiv mecarbil on contractile properties of skinned myocardium lacking cardiac myosin binding protein-C. *J. Mol. Cell. Cardiol.* 85, 262–272. doi:10.1016/j.yjmcc.2015.06.011

Mamidi, R., Li, J., Gresham, K. S., Verma, S., Doh, C. Y., Li, A., et al. (2017). Dose-dependent effects of the myosin activator omecamtiv mecarbil on cross-bridge behavior and force generation in failing human myocardium. *Circ. Heart Fail.* 10, e00425. doi:10.1161/CIRCHEARTFAILURE.117.004257

Matsuba, D., Terui, T., O-Uchi, J., Tanaka, H., Ojima, T., Ohtsuki, I., et al. (2009). Protein kinase A-dependent modulation of Ca^{2+} sensitivity in cardiac and fast skeletal muscles after reconstitution with cardiac troponin. *J. Gen. Physiol.* 133, 571–581. doi:10.1085/jgp.200910206

McDonagh, T. A., Metra, M., Adamo, M., Gardner, R. S., Baumbach, A., Böhm, M., et al. (2021). 2021 ESC Guidelines for the diagnosis and treatment of acute and chronic heart failure. *Eur. Heart J.* 42, 3599–3726. doi:10.1093/eurheartj/ehab368

McNamara, J. W., Li, A., Dos Remedios, C. G., and Cooke, R. (2015). The role of super-relaxed myosin in skeletal and cardiac muscle. *Biophys. Rev.* 7, 5–14. doi:10.1007/s12551-014-0151-5

McNamara, J. W., Singh, R. R., and Sadayappan, S. (2019). Cardiac myosin binding protein-C phosphorylation regulates the super-relaxed state of myosin. *Proc. Natl. Acad. Sci. U. S. A.* 116, 11731–11736. doi:10.1073/pnas.1821660116

Metra, M., and Teerlink, J. R. (2017). Heart failure. *Lancet* 390, 1981–1995. doi:10.1016/S0140-6736(17)31071-1

Nag, S., and Trivedi, D. V. (2021). To lie or not to lie: Super-relaxing with myosins. *Elife* 10, e63703. doi:10.7554/eLife.63703

Nagashima, H., and Asakura, S. (1982). Studies on co-operative properties of tropomyosin-actin and tropomyosin-troponin-actin complexes by the use of N-ethylmaleimide-treated and untreated species of myosin subfragment 1. *J. Mol. Biol.* 155, 409. doi:10.1016/0022-2836(82)90479-x

Nagy, L., Kovács, A., Bódi, B., Pásztor, E. T., Fülöp, G. Á., Tóth, A., et al. (2015). The novel cardiac myosin activator omecamtiv mecarbil increases the calcium sensitivity of force production in isolated cardiomyocytes and skeletal muscle fibres of the rat. *Br. J. Pharmacol.* 172, 4506–4518. doi:10.1111/bph.13235

Ovejero, J. G., Fusi, L., Park-Holohan, S. J., Ghisleni, A., Narayanan, T., Irving, M., et al. (2022). Cooling intact and demembranated trabeculae from rat heart releases myosin motors from their inhibited conformation. *J. Gen. Physiol.* 154, e202113029. doi:10.1085/jgp.202113029

Rohde, J. A., Thomas, D. D., and Muretta, J. M. (2017). Heart failure drug changes the mechanoenzymology of the cardiac myosin powerstroke. *Proc. Natl. Acad. Sci. U. S. A.* 114, E1796-E1804. doi:10.1073/pnas.1611698114

Schmid, M., and Toepfer, C. N. (2021). Cardiac myosin super relaxation (SRX): A perspective on fundamental biology, human disease and therapeutics. *Biol. Open* 10, bio057646. doi:10.1242/bio.057646

Shchepkin, D. V., Nabiev, S. R., Nikitina, L. V., Kochurova, A. M., Berg, V. Y., Bershitsky, S. Y., et al. (2020). Myosin from the ventricle is more sensitive to omecamtiv mecarbil than myosin from the atrium. *Biochem. Biophys. Res. Commun.* 528, 658–663. doi:10.1016/j.bbrc.2020.05.108

Shen, Y. T., Malik, F. I., Zhao, X., Depre, C., Dhar, S. K., Abarzúa, P., et al. (2010). Improvement of cardiac function by a cardiac myosin activator in conscious dogs with systolic heart failure. *Circ. Heart Fail.* 3, 522–527. doi:10.1161/CIRCHEARTFAILURE.109.930321

Shimizu, H., Fujita, T., and Ishiwata, S. (1992). Regulation of tension development by MgADP and Pi without Ca^{2+}. role in spontaneous tension oscillation of skeletal muscle. *Biophys. J.* 61, 1087–1098. doi:10.1016/S0006-3495(92)81918-5

Snoberger, A., Barua, B., Atherton, J. L., Shuman, H., Forgacs, E., Goldman, Y. E., et al. (2021). Myosin with hypertrophic cardiac mutation R712L has a decreased working stroke which is rescued by omecamtiv mecarbil. *Elife* 10, e63691. doi:10.7554/eLife.63691

Solaro, R. J., and Rarick, H. M. (1998). Troponin and tropomyosin: Proteins that switch on and tune in the activity of cardiac myofilaments. *Circ. Res.* 83, 471–480. doi:10.1161/01.res.83.5.471

Spudich, J. A. (2019). Three perspectives on the molecular basis of hypercontractility caused by hypertrophic cardiomyopathy mutations. *Pflugers Arch.* 471, 701–717. doi:10.1007/s00424-019-02259-2

Stewart, M. A., Franks-Skiba, K., Chen, S., and Cooke, R. (2010). Myosin ATP turnover rate is a mechanism involved in thermogenesis in resting skeletal muscle fibers. *Proc. Natl. Acad. Sci. U. S. A.* 107, 430–435. doi:10.1073/pnas.0909468107

Teerlink, J. R., Clarke, C. P., Saikali, K. G., Lee, J. H., Chen, M. M., Escandon, R. D., et al. (2011). Dose-dependent augmentation of cardiac systolic function with the selective cardiac myosin activator, omecamtiv mecarbil: a first-in-man study. *Lancet* 378, 667–675. doi:10.1016/S0140-67361161219-1

Teerlink, J. R., Diaz, R., Felker, G. M., McMurray, J. J. V., Metra, M., Solomon, S. D., et al. (2021). Cardiac myosin activation with omecamtiv mecarbil in systolic heart failure. *N. Engl. J. Med.* 384, 105–116. doi:10.1056/NEJMoa2025797

Teerlink, J. R., Felker, G. M., McMurray, J. J. V., Solomon, S. D., Adams, K. F., Cleland, J. G. F., et al. (2016). Chronic oral study of myosin activation to increase contractility in heart failure (COSMIC-HF): a phase 2, pharmacokinetic, randomised, placebo-controlled trial. *Lancet* 388, 2895–2903. doi:10.1016/S0140-6736(16)32049-9

Teerlink, J. R., Metra, M., Zacà, V., Sabbah, H. N., Cotter, G., Gheorghiade, M., et al. (2009). Agents with inotropic properties for the management of acute heart failure syndromes. traditional agents and beyond. *Heart fail. Rev.* 14, 243–253. doi:10.1007/s10741-009-9153-y

Terui, T., Shimamoto, Y., Yamane, M., Kobirumaki, F., Ohtsuki, I., Ishiwata, S., et al. (2010). Regulatory mechanism of length-dependent activation in skinned porcine ventricular muscle: role of thin filament cooperative activation in the frank-starling relation. *J. Gen. Physiol.* 136, 469–482. doi:10.1085/jgp.201010502

Terui, T., Sodnomtseren, M., Matsuba, D., Udaka, J., Ishiwata, S., Ohtsuki, I., et al. (2008). Troponin and titin coordinately regulate length-dependent activation in skinned porcine ventricular muscle. *J. Gen. Physiol.* 131, 275–283. doi:10.1085/jgp.200709895

Tong, C. W., Stelzer, J. E., Greaser, M. L., Powers, P. A., and Moss, R. L. (2008). Acceleration of crossbridge kinetics by protein kinase a phosphorylation of cardiac myosin binding protein C modulates cardiac function. *Circ. Res.* 103, 974–982. doi:10.1161/CIRCRESAHA.108.177683

Utter, M. S., Ryba, D. M., Li, B. H., Wolska, B. M., and Solaro, R. J. (2015). Omecamtiv mecarbil, a cardiac myosin activator, increases Ca^{2+} sensitivity in myofilaments with a dilated cardiomyopathy mutant tropomyosin E54K. *J. Cardiovasc. Pharmacol.* 66, 347–353. doi:10.1097/FJC.0000000000000286

Walklate, J., Ferrantini, C., Johnson, C. A., Tesi, C., Poggesi, C., Geeves, M. A., et al. (2021). Alpha and beta myosin isoforms and human atrial and ventricular contraction. *Cell. Mol. Life Sci.* 78, 7309–7337. doi:10.1007/s00018-021-03971-y

Wang, Y., Tanner, B. C. W., Lombardo, A. T., Tremble, S. M., Maughan, D. W., VanBuren, P., et al. (2013). Cardiac myosin isoforms exhibit differential rates of MgADP release and MgATP binding detected by myocardial viscoelasticity. *J. Mol. Cell. Cardiol.* 54, 1–8. doi:10.1016/j.yjmcc.2012.10.010

Winkelmann, D. A., Forgacs, E., Miller, M. T., and Stock, A. M. (2015). Structural basis for drug-induced allosteric changes to human β-cardiac myosin motor activity. *Nat. Commun.* 6, 7974. doi:10.1038/ncomms8974

Woody, M. S., Greenberg, M. J., Barua, B., Winkelmann, D. A., Goldman, Y. E., Ostap, E. M., et al. (2018). Positive cardiac inotrope omecamtiv mecarbil activates muscle despite suppressing the myosin working stroke. *Nat. Commun.* 9, 3838. doi:10.1038/s41467-018-06193-2

Woody, M. S., Winkelmann, D. A., Capitanio, M., Ostap, E. M., and Goldman, Y. E. (2019). Single molecule mechanics resolves the earliest events in force generation by cardiac myosin. *Elife* 8, e49266. doi:10.7554/eLife.49266

Yamasaki, R., Wu, Y., McNabb, M., Greaser, M., Labeit, S., Granzier, H., et al. (2002). Protein kinase a phosphorylates titin's cardiac-specific N2B domain and reduces passive tension in rat cardiac myocytes. *Circ. Res.* 90, 1181–1188. doi:10.1161/01.res.0000021115.24712.99

Yuan, C. C., Kazmierczak, K., Liang, J., Ma, W., Irving, T. C., Szczesna-Cordary, D., et al. (2022). Molecular basis of force-pCa relation in MYL2 cardiomyopathy mice: role of the super-relaxed state of myosin. *Proc. Natl. Acad. Sci. U. S. A.* 119, e2110328119. doi:10.1073/pnas.2110328119

frontiers | Frontiers in Physiology

TYPE Original Research
PUBLISHED 02 September 2022
DOI 10.3389/fphys.2022.926422

OPEN ACCESS

EDITED BY
Henk Granzier,
University of Arizona, United States

REVIEWED BY
Jeffrey Fredberg,
Harvard University, United States
Julio Altamirano,
Tecnológico de Monterrey, Mexico
Andrey K. Tsaturyan,
Lomonosov Moscow State University, Russia

*CORRESPONDENCE
Ralph Knöll,
ralph0611@gmail.com

SPECIALTY SECTION
This article was submitted to Striated Muscle Physiology, a section of the journal Frontiers in Physiology

RECEIVED 22 April 2022
ACCEPTED 25 July 2022
PUBLISHED 02 September 2022

CITATION
Haftbaradaran Esfahani P, Westergren J, Lindfors L and Knöll R (2022), Frequency-dependent signaling in cardiac myocytes.
Front. Physiol. 13:926422.
doi: 10.3389/fphys.2022.926422

Frequency-dependent signaling in cardiac myocytes

Payam Haftbaradaran Esfahani[1], Jan Westergren[2], Lennart Lindfors[3] and Ralph Knöll[4,5]*

[1]Department of Medicine Huddinge, Karolinska Institutet, Huddinge, Sweden, [2]Wendelsbergs beräkningskemi AB, Mölnlycke, Sweden, [3]Advanced Drug Delivery, Pharmaceutical Sciences, BioPharmaceuticals R&D, AstraZeneca, Mölndal, Sweden, [4]Department of Medicine, Integrated Cardio Metabolic Centre (ICMC), Heart and Vascular Theme, Karolinska Institute, Stockholm, Sweden, [5]Bioscience Cardiovascular, Research and Early Development, Cardiovascular, Renal and Metabolism (CVRM), BioPharmaceuticals R&D, AstraZeneca, Mölndal, Sweden

Background: Recent experimental data support the view that signaling activity at the membrane depends on its geometric parameters such as surface area and curvature. However, a mathematical, biophysical concept linking shape to receptor signaling is missing. The membranes of cardiomyocytes are constantly reshaped due to cycles of contraction and relaxation. According to constant-volume behavior of cardiomyocyte contraction, the length shortening is compensated by Z-disc myofilament lattice expansion and dynamic deformation of membrane between two adjacent Z-discs. Both morphological changes are strongly dependent on the frequency of contraction. Here, we developed the hypothesis that dynamic geometry of cardiomyocytes could be important for their plasticity and signaling. This effect may depend on the frequency of the beating heart and may represent a novel concept to explain how changes in frequency affect cardiac signaling.

Methods: This hypothesis is almost impossible to answer with experiments, as the *in-vitro* cardiomyocytes are almost two-dimensional and flattened rather than being in their real *in-vivo* shape. Therefore, we designed a COMSOL multiphysics program to mathematically model the dynamic geometry of a human cardiomyocyte and explore whether the beating frequency can modulate membrane signal transduction. Src kinase is an important component of cardiac mechanotransduction. We first presented that Src mainly localizes at costameres. Then, the frequency-dependent signaling effect was studied mathematically by numerical simulation of Src-mediated PDGFR signaling pathway. The reaction-convection-diffusion partial differential equation was formulated to simulate PDGFR pathway in a contracting sarcomeric disc for a range of frequencies from 1 to 4 Hz. Results: Simulations exhibits higher concentration of phospho-Src when a cardiomyocyte beats with higher rates. The calculated phospho-Src concentration at 4, 2, and 1 Hz beat rates, comparing to 0 Hz, was 21.5%, 9.4%, and 4.7% higher, respectively.

Conclusion: Here we provide mathematical evidence for a novel concept in biology. Cell shape directly translates into signaling, an effect of importance particularly for the myocardium, where cells continuously reshape their membranes. The concept of locality of surface-to-volume ratios is demonstrated to lead to changes in membrane-mediated signaling and may

help to explain the remarkable plasticity of the myocardium in response to biomechanical stress.

KEYWORDS

cell geometry, contraction frequency, cardiac myocyte, cardiomyocyte, sarcomere, signaling, mathematical modeling, simulation

Introduction

Cells are constantly exposed to mechanical stress by forces that are generated by gravity, organ motion, blood flow, extracellular cell-to-cell and cell-to-matrix interactions, and intracellular traction. These mechanical forces have been shown to influence a broad spectrum of cellular behaviors, from proliferation and differentiation to transcriptional responses and gene expression.

Mechanotransduction is a fundamental biological process, by which cells sense mechanical stimuli, integrate them, and convert them into biochemical signals, inducing downstream cellular responses (Martino et al., 2018). Because biomechanical force can be transmitted through the cytoskeleton, microtubules, and actin stress fibers, its propagation time is much shorter than the diffusion of molecules in signaling pathways. This means that the cells respond rapidly to their dynamic environment. Defective mechanotransduction has been associated with numerous diseases from all fields of medicine, including cardiology, dermatology, gastroenterology, nephrology, neurology, oncology, ophthalmology, orthopedics, pediatrics, pulmonary medicine, reproductive medicine, and urology. Abnormal mechanotransduction can be caused by alterations in, or malfunctions of, one or more of the entities involved in the force sensing and conversion process, namely, the extracellular matrix (ECM), cell surface receptors, the cell cytoskeleton, and the various molecules associated with the signaling cascade that occurs in the cytoplasm or nucleus.

Signaling activity at the membranes depends on global cell geometry parameters, such as the cellular aspect ratio (Haftbaradaran Esfahani et al., 2019), size (Nowak et al., 2021), membrane surface area, and membrane curvature (Haftbaradaran Esfahani and Knoll, 2020b). A recent paper by Rangamani et al. (2013) has presented a "curvature-dependent mechanism of transient receptor activity enhancement," but its relevance for biology and medicine remains unclear. The authors showed how the enhancement of kinase activity in downstream signaling pathways could be mediated by transient enhancement of receptor activity, following increased ligand binding in the curved plasma membrane areas of elliptic cells with increasing eccentricity. They demonstrated that information contained in the cell's shape could be transformed into measurably different MAPK phosphorylation levels in the nucleus. Matter exchange by lateral diffusion, between areas of high and low curvature at the plasma membrane, will eventually equilibrate the ligand-induced inhomogeneity of receptor activity. However, when fission of membrane areas with high curvature occurs, this matter exchange cannot take place. This could lead to stabilization of the enhanced interaction with cytoplasmic effectors at the membrane interface of the endocytosed vesicle.

It has been well documented that the effects of global cell geometry influence signaling activity and differentiation (Haftbaradaran Esfahani and Knoll, 2020b), but the local effects are still poorly understood. Cells use various local membrane curves to perform cellular functions, such as filopodia to form adhesions, endosomes for intracellular signaling, and caveolae to moderate membrane tension. Invagination or protrusion of local membranes has been shown to respond differently to stimulus, by increasing cell eccentricity. This is due to the transient assembly of the activated receptors in microdomains with higher curvature. This transient inhomogeneity in the distribution of activated receptors arises from a local imbalance between reactions and the diffusion of soluble ligands and receptors in the plane of the membrane (Rangamani et al., 2013).

When protrusion occurs, there is higher accessibility to external ligands, since the reactive volume to surface ratio is higher for ligand-receptor binding. On the other hand, when invagination occurs, the volume to surface ratio for the ligand-receptor binding is limited, although the release of the intracellular receptor-bound signaling molecule is easier.

It has recently been shown by Lou et al. (2018) that curvature sensing proteins were engaged upon manipulating the membrane by nanostructures. In addition to membrane curvatures, they showed that gene expression was dysregulated after nano-structural deformation of nuclear envelope. In another study, Elliott et al. (2015) investigated the closed loop relation between regulation of myosin II and fluctuation of local membrane curvature in endothelial cells.

In heart, cardiac myocytes (CMs) beats with cycles of contraction and relaxation. In each beating cycle, sarcomeres, the contractile unit of CM between two adjacent Z-discs, shorten and elongate. Since the cytosol is incompressible, the cytosol is isovolumetric and the cell volume is constant during a cycle of contraction-relaxation. Therefore, when the sarcomere shortens, the Z-disc lattice spacing expands. Correspondingly, when the sarcomere relaxes (i.e., elongates), the Z-disc lattice spacing compresses [for a review please see (Knoll et al., 2011)]. In the transverse sections, Z-discs show two distinct structural states: the "small square" form and the "basket weave" form. In the classical studies of fixed muscle tissues, it has been proposed that the small square and the basket-weave forms

represent the relaxed and the active contracted states, respectively (Williams et al., 2013; Malingen et al., 2020), but this view has recently been challenged (Oda and Yanagisawa, 2020; Burbaum et al., 2021). Interestingly, it has been shown that in the contracted state, the lattice was not expanded that much, leading to a decrease in Z-line lattice volume (Irving et al., 2000; Toh et al., 2006). Thus, the membrane needs to be stretched (Kamkin et al., 2000; Samarel, 2005) to sustain the normally constant cytosolic volume during contraction by pushing the cytosol towards the cell membrane (Malingen and Daniel, 2020; Cass et al., 2021; Powers et al., 2021).

Since the cell volume is constant, the periodic relative motion of neighboring Z-discs leads to the advection of cytosol molecules. Moreover, the curvature of CM membrane fluctuates periodically with a constraint to isovolumetric cytosol (Knoll, 2015). Accordingly, we developed the hypothesis that dynamic geometry of CMs could be important for CM plasticity and signaling. This effect may depend on the frequency of the beating heart and may represent a novel concept to explain how changes in frequency affect cardiac signaling. This hypothesis is almost impossible to answer with experiments, as the *in-vitro* cultured CMs are nearly two-dimensional and flattened rather than being in their real *in-vivo* shape. Moreover, it is very demanding to prove the hypothesis by culturing adult human CMs for several days, transduce and pace them (Wright et al., 2020). Therefore, comprehensive mathematical models are critical for predicting geometry-dependent cellular signaling. These models could be implemented on platforms that have been specifically designed for modeling cell biological systems, such as VCell (virtual cell) software or on general multi-physics platforms like COMSOL Multiphysics.

In our case, we designed a COMSOL program (COMSOL, 2021) to mathematically model and numerically simulate the dynamic geometry of CM and explore whether the frequency of contraction can modulate membrane signal transduction.

Src kinase is an important component of cardiac mechanotransduction (Schlaepfer and Hunter, 1996; de Cavanagh et al., 2009). In this paper, we first presented that Src kinase mainly localizes at costameres, a crucial site for CM survival and growth (Samarel, 2005). In addition, costameres have substantial roles in mechanically-induced signaling in CMs (Martino et al., 2018). It has been previously demonstrated that Platelet-Derived Growth Factor (PDGF) induces Src activation (Thomas and Brugge, 1997; Rangamani et al., 2013; Lu et al., 2017; Fan et al., 2022). We visualized the spatio-temporal activation characteristics of Src kinase upon PDGF stimulation, by introducing a fluorescent Src activation biosensor into the cultured neonatal rat CMs (NRCMs). The Src biosensor, named KRas-Src, works based on the FRET technique to report Src activation (Liu et al., 2014). We introduced the KRas-Src FRET reporter into the NRCMs through adenoviral delivery. We then stimulate the NRCMs by PDGF and acquire the FRET images using a confocal microscope at 5 s and 5, 10, and 20 min after PDGF treatment. The FRET image analyses were performed afterwards to measure the spatio-temporal Src activity in NRCMs.

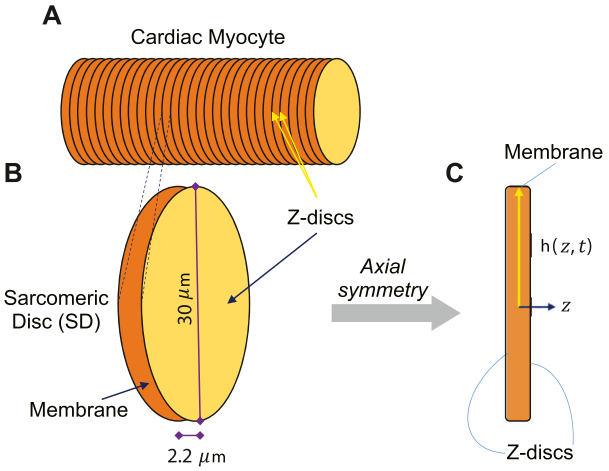

FIGURE 1
(A) The adult human CM was assumed to have cylindrical shape, consisting of several symmetric Sarcomeric Discs (SDs). **(B)** One contracting SD of an adult human CM was assumed to be disk-shaped with 30 μm diameter and 2.2 μm thickness in relaxed state. **(C)** One SD was presumed to have axial symmetry to simplify the simulations to two-dimensional longitudinal section.

We call each bunch of laterally-registered sarcomeres as a "Sarcomeric Disc" (SD) (see Figures 1A,B) and assume signaling is the same for all SDs. Therefore, we mathematically modeled a SD and investigated our central hypothesis by simulating the effect of frequency of contraction on the activation of Src kinase through PDGF signaling in the COMSOL-modeled SD of an adult human CM. In order to monitor the concentration of activated Src at different locations in the SD at different times, transport of all the included substances in combination with reactions were simulated numerically.

To create a dynamic multiphysics model of membrane signaling, we assumed that a CM is like a cylinder, consisting of several symmetric SDs. Since SDs are similar repeating units, we can simply model this membrane signaling at the membrane of one SD instead of modeling a whole CM. During a contraction-relaxation cycle of an adult human CM, the sarcomere length (SL) is shortened from 2.2 μm at the relaxed state to 1.6 μm at the contracted state, widening the Z-disc radially. Although, the SL-lattice spacing relationship has been investigated in *in-vivo* (Toh et al., 2006) and *in-vitro* (Irving et al., 2000) animal models, the amount of lattice expansion in an *in-vivo* adult human CM has not been studied yet. However, if one assumes a similar relationship, this would

indicate that Z-disc lattice of a SD would be expanded about 2 μm at the contracted state in an *in-vivo* adult human CM.

Materials and methods

Src activation biosensor

We used the FRET technique to monitor the activity of Src kinase experimentally. The FRET-based Src activation biosensor (Wang et al., 2005) consists of ECFP (Enhanced Cyan Fluorescent Protein) and YPet, an improved version of YFP (Yellow Fluorescent Protein), linked together by the SH2 domain (from c-Src), a flexible linker and the Src-specific substrate peptide, derived from c-Src substrate p130Cas. The KRas-Src biosensor was constructed by fusing 14 KRas-prenylation sequences (KKKKKKSKTKCVIM) to the C-termini of Src biosensor (Pan et al., 2019). The donor:acceptor (ECFP:YPet) stoichiometry is fixed to 1:1. The activity of Src kinase causes a conformational change which modifies the distance between donor and acceptor, resulting a FRET change. When Src is at the resting state, the conformation of the Src construct is such that ECFP and YPet are juxtaposed, leading to a high FRET. When Src is active, it phosphorylates the substrate domain at tyrosine sites; therefore, the Src reporter is unfolded, inducing the separation of ECFP and YPet, reducing the FRET emission. To increase the delivery efficiency of KRas-Src biosensor, we used an E1-defective adenoviral vector of KRas-Src FRET reporter.

Cell isolation, cell culture and adenoviral transduction

NRCMs were isolated and purified as previously described (Haftbaradaran Esfahani and Knoll, 2020a). Hearts were rapidly excised from two-day-old Sprague-Dawley rats and tissue samples were collected from the dorsal of the apex of the left ventricle. NRCMs were isolated from the tissue using the Neonatal Heart Dissociation Kit (Miltenyi Biotec, Bergisch Gladbach, Germany). Isolated cells were resuspended in DMEM:M199 (4:1), supplemented with 10% horse serum, 5% fetal bovine serum and 1% penicillin/streptomycin (10,000 U/ml) (Thermo Fisher Scientific, Waltham, MA, United States). The suspension was pre-plated for 2 h in 10 cm^2 uncoated cell culture flasks (Nunc, Thermo Fisher Scientific) to remove the fibroblast and endothelial cells, by allowing non-CMs to attach to the surface of the culture flask. Enriched NRCMs were seeded at a density of 7 × 10^3 cells/mm^2 on 35 mm MatTek glass bottom dishes (Part No. P35G-1.5), pre-coated with 2 μg/cm^2 fibronectin. 24 h after plating, the plating medium were replaced with serum-free maintenance medium. Then, the cultured NRCMs were incubated at 37°C with 10 MOI KRas-Src adenovirus for 48 h.

FRET imaging of Src activity

After 72 h in culture, we carried out the FRET imaging of Src activity upon PDGF stimulation of serum-starved NRCMs. To avoid autofluorescence of the culture medium containing phenol red, maintenance medium was washed and replaced with 1 ml HBSS (Hank's Balanced Salt Solution), supplemented with 20 mM HEPES and 2 g.l-1 D-glucose. Then, we placed the culture dish on the stage of a Leica SP5 inverted confocal microscope. We saved the coordinate of a well-transduced, spontaneously contracting NRCM. However, the frequency of contraction should be less than 0.25 Hz to assure the bias from contraction is negligible. Then, we immediately treated NRCMs with 30 ng/ml PDGF. In a temperature-controlled imaging chamber, the selected NRCMs were imaged with a 63X/1.4 oil-immersion objective. Fluorophores were excited with a 457 nm laser. The ECFP and FRET channels were recorded simultaneously at 5 s and 5, 10, and 20 min after PDGF treatment and the fluorescence intensity ratios for ECFP/FRET were plotted as a function of time.

Image processing and FRET analysis

To quantify the spatio-temporal FRET changes of the Src reporter, we used two-channel ratiometric approach (i.e., ECFP/FRET ratio) for time series analysis. Therefore, we acquired a pair of ECFP and FRET images for each time course (i.e., 5 s, 5, 10 and 20 min) of the experiment. The intensity values of the acquired images range from 0 to 255. The image processing procedure for FRET analysis was performed using Fiji ImageJ (Schindelin et al., 2012). We first deducted the image noise average from all pixels of the image. Then, we subtracted the background, surrounding the cell of interest from both ECFP and FRET images. We analyzed Src kinase activity upon PDGF stimulation solely at costameres, since we found that Src kinase mainly concentrated at the costameres in CMs (i.e., pixels belong to costameres have higher fluorescence intensity). Additionally, by just considering the costameres, the bias from cytosolic autofluorescence is reduced drastically. Then, we generated a binary mask by using an intensity threshold of 90 on FRET images, since we found that most of the costamere pixels could be picked out by this threshold. As some pixels which do not belong to costameres could pass the threshold, we used a median filter, called "Despeckle," on the binary thresholding mask to remove these undesired pixels. Despeckle replaces each pixel with the median value of its 3 × 3 surrounding pixels. We then performed the "AND" operation of the tailored binary mask and the original image to generate the masked image. We calculated the FRET ratio of each time course by dividing the masked ECFP image by masked FRET image, pixel by pixel. The obtained FRET ratios of time series were finally normalized by the value of the first time course (i.e., at t = 5 s).

Mathematical model for membrane and intracellular gradients in a beating sarcomeric disc

The adult human CM was assumed to have cylindrical shape, consisting of several symmetric SDs (Figure 1A). Since sarcomeres are similar repeating units, we modeled one contracting SD (Figure 1B). We presumed axial symmetry of one SD to simplify the simulations to two-dimensional longitudinal section (Figure 1C).

The shape of the SD changes with time when the Z-discs are moved towards each other to contract the sarcomere and consequently the entire cell. As the SD shortens and in order to maintain the constant intracellular volume, the Z-discs expand to a bigger diameter and the cell membrane stretches. We let the model to compute the amount of membrane stretch at each time point, constrained to isovolumetric cytosol. The SD radius is a function of the z coordinate and time and is denoted $h(z,t)$ (Figure 1C). The time dependence is modelled as a cosine function with T being the period of the contraction.

$$h(z,t) = 15\ \mu\text{m} + \left(2\ \mu\text{m} + 0.985\ \mu\text{m} \cdot \left(1 - \left|\frac{z}{z_0(t)}\right|^3\right)\right) \cdot \frac{1 - cos\frac{2\pi t}{T}}{2} \quad (1)$$

Note that the location of the Z-discs varies with time. The maximum radius is found at $z = 0$ and the minimum radius at the Z-discs where $z = \pm z_0(t)$.

$$z_0(t) = 1.1\ \mu\text{m} - 0.3\ \mu\text{m} \cdot \frac{1 - cos\frac{2\pi t}{T}}{2} \quad (2)$$

The shape change of the SD is shown in (Figure 2). As a simplification, there are no organelles or other obstacles inside the sarcomere, so the cytosol can flow freely. The shape change causes cytosol flow back and forth towards the cell membrane. Given the membrane shape changes in Eq. 2, the velocity field $\vec{u}$ of the cytosol was calculated using Navier-Stokes equations. No-slip boundary conditions are applied. Thus the velocity of the cytosol at the domain wall are zero relative to the surface. The stretching of the Z-discs was uniform in radial direction.

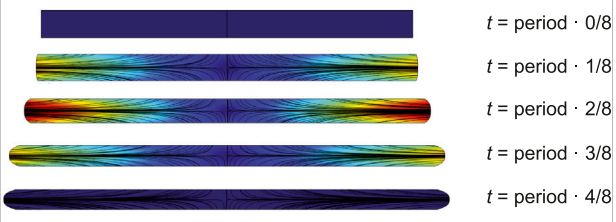

FIGURE 2
Dynamic evolution of SD geometry at 0, $\frac{1}{8}$, $\frac{1}{4}$, $\frac{3}{8}$, $\frac{1}{2}$ of each contraction period. The black contours represent velocity fields of cytosol. The color code shows the magnitude of velocity from dark blue, equals to 0, to dark red as maximum value.

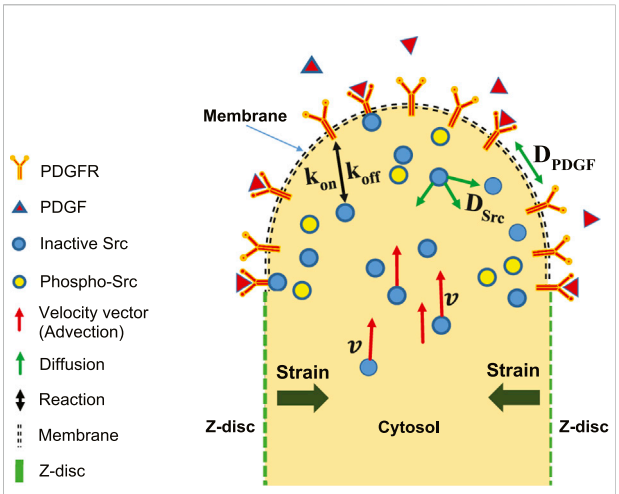

FIGURE 3
Schematic of reaction-diffusion-advection model in the upper half of two-dimensional longitudinal section of one SD. Shortening of SD causes strain. Extracellular PDGF can bind to membrane receptors, PDGFR. The intracellular inactive form of Src can bind to PDGFR. The inactive and activated forms of Src are free to diffuse in any direction, whereas *PDGFR* is limited to diffuse along the membrane plane, with the diffusion coefficients of D_{Src} and D_{PDGFR} respectively. The concentration of inactive and activated Src vary due to diffusion and reaction, but also vary due to advection (shown by velocity vector field v). Advection is a consequence of strain, which is due to SD contraction.

The finite-element mesh was generated to divide the model into small elements, over which the Navier-Stokes equations were solved. The velocity field of cytosol at different times is shown in (Figure 2).

The motion of the different substances in the cytosol is governed by diffusion and advection according to the diffusion-advection equation

$$\frac{\partial c}{\partial t} = D\Delta c - \nabla \cdot \left(\vec{u}c\right) \quad (3)$$

where c is the concentration of a specific substance, D is its diffusivity and $\vec{u}$ is the time-dependent velocity field of cytosol. The Δ is the Laplace operator and ∇ is the Del operator. The membrane receptors are free to move at the membrane by two-dimensional diffusion,

$$\frac{\partial c_{2D}}{\partial t} = D_{2D}\Delta c_{2D} \quad (4)$$

where c_{2D} is the concentration with respect to the area and D_{2D} is a two-dimensional diffusivity. The boundary constraint at the membrane—Z-disc interface is $\partial c/\partial z = 0$ for all substances. In addition, it is assumed that there is no resultant cytosolic flow through the Z-disc during the contraction-relaxation period.

TABLE 1 Reactions and kinetic parameters for modeling Src activation upon PDGF stimulation (Rangamani et al., 2013).

Name	Reaction	Reaction type	Kinetic parameters
PDGF binds PDGF-Receptor	PDGF + PDGFR ↔ PDGF-PDGFR	Binding	K_{on} = 1 μM^{-1}s^{-1} K_{off} = 0.01 s^{-1}
Src phosphorylation	Src + PDGF-PDGFR ↔ Phospho-Src	Enzymatic	K_M = 1 μM K_{cat} = 0.1 s^{-1}
Src inactivation	Phospho-Src + Csk-active ↔ Src	Inactivation	K_M = 1.5 μM K_{cat} = 0.3 s^{-1}
Csk activation	Csk → Csk-active	Activation	K_f = 0.001 s^{-1}

TABLE 2 Initial concentrations for modeling Src activation upon PDGF stimulation (Rangamani et al., 2013).

Name	Initial concentration	Compartment
PDGF	30 ng/ml	Extracellular space
PDGF Receptor	250 molecules.μm-2	Membrane
Src	1 μM	Cytoplasm
Csk	0.1 μM	Cytoplasm

Reactions that take place in the cytosol only add an extra reaction term to Eq. 3.

$$\frac{\partial c}{\partial t} = D\Delta c - \nabla \cdot \left(\vec{u}c\right) + R \tag{5}$$

and analogously for reactions that take place in the membrane only, an extra term is added to Eq. 4.

$$\frac{\partial c_{2D}}{\partial t} = D_{2D}\Delta c_{2D} + R_{2D} \tag{6}$$

Reactions involving substances both in the membrane and in the cytosol are written as a flux from the membrane (production) or towards the membrane (consumption). Thus, these reactions are described by boundary conditions where the normal flux towards the membrane is

$$F = \vec{n} \cdot (D\nabla c) \tag{7}$$

where $\vec{n}$ is the normal vector from the membrane into the SD. This flux equals the reaction rate, i.e., $F = R_{2D}$. For the rest of the boundaries, i.e., the Z-discs, the transport of the all substances are zero. The differential equations are solved with the Finite Element Method (FEM) using the software COMSOL. The time-dependent solver used is the Backward Differentiation Formula (BDF).

A schematic of reaction-diffusion-advection system for the concentration of Src, is shown in (Figure 3). The lists of reactions and kinetic parameters of the simulated PDGF signaling are reported in Table 1 and Appendix 1. Moreover, the initial concentrations and diffusion coefficients of the molecules interacting in simulated PDGF signaling are provided in Tables 2, 3. In addition, it is presented in Table 3 whether 2D or 3D equations were applied to each molecules. In our numerical model, extracellular PDGF binds PDGF receptor (PDGFR), forming PDGF-PDGFR complex which reacts with inactive form of Src in cytosol and activates Src.

Results

Experimental exploration of spatio-temporal activation of Src in neonatal rat CMs

We first studied the spatio-temporal activation of Src kinase upon PDGF stimulation in NRCMs. Src kinase is normally present in its inactive conformation. Upon PDGF treatment of CMs, the extracellular PDGF binds to the membrane-bound receptor, PDGFR, and activates it. The activated transmembrane PDGFR phosphorylates (i.e., activates) the intracellular inactive-Src by recruiting PTP (Protein Tyrosine Phosphatase). The activated Src (phospho-Src) can again be inactivated by a non-receptor tyrosine kinase Csk (C-terminal Src Kinase) (Matsuoka et al., 2004; Okada, 2012).

As described in the Methods section, we studied the characteristics of Src activation in NRCMs using ECFP/FRET ratiometric analysis. Since ECFP is very prone to bleaching, it has to be exposed by the least possible laser exposure in order that we can neglect photobleaching in FRET analysis. Therefore, the intensities of ECFP and FRET channels were recorded at four time courses that are 0+, 5, 10, and 20 min after PDGF treatment.

ECFP and FRET images of some NRCMs were shown in (Figure 4A). The figure illustrates the highest fluorescence intensities emitted from costamere sites, suggesting that Src kinase is mainly localized at the costameres in CMs. Although, lower fluorescence was detected from other regions of the cell, we analyzed Src kinase activity solely at costameres, according to importance of the costameres in CM signaling. In addition, the autofluorescence bias is predominant when analyzing lower fluorescence signal, detected from non-costamere regions.

TABLE 3 Diffusion coefficient, compartment and dimension of equation that applied to the molecules, interacting in the PDGF signaling (Rangamani et al., 2013).

Name	Diffusion coefficient ($\mu m^2/s$)	Compartment	Dimension of equation
Csk	10	Cytoplasm	3D
Csk-active	10	Cytoplasm	3D
Src	10	Cytoplasm	3D
Phospho-Src	1	Cytoplasm	3D
PDGF	1	Extracellular space	N/A
PDGFR	0.041	Membrane	2D
PDGF-PDGFR	0.041	Membrane	2D

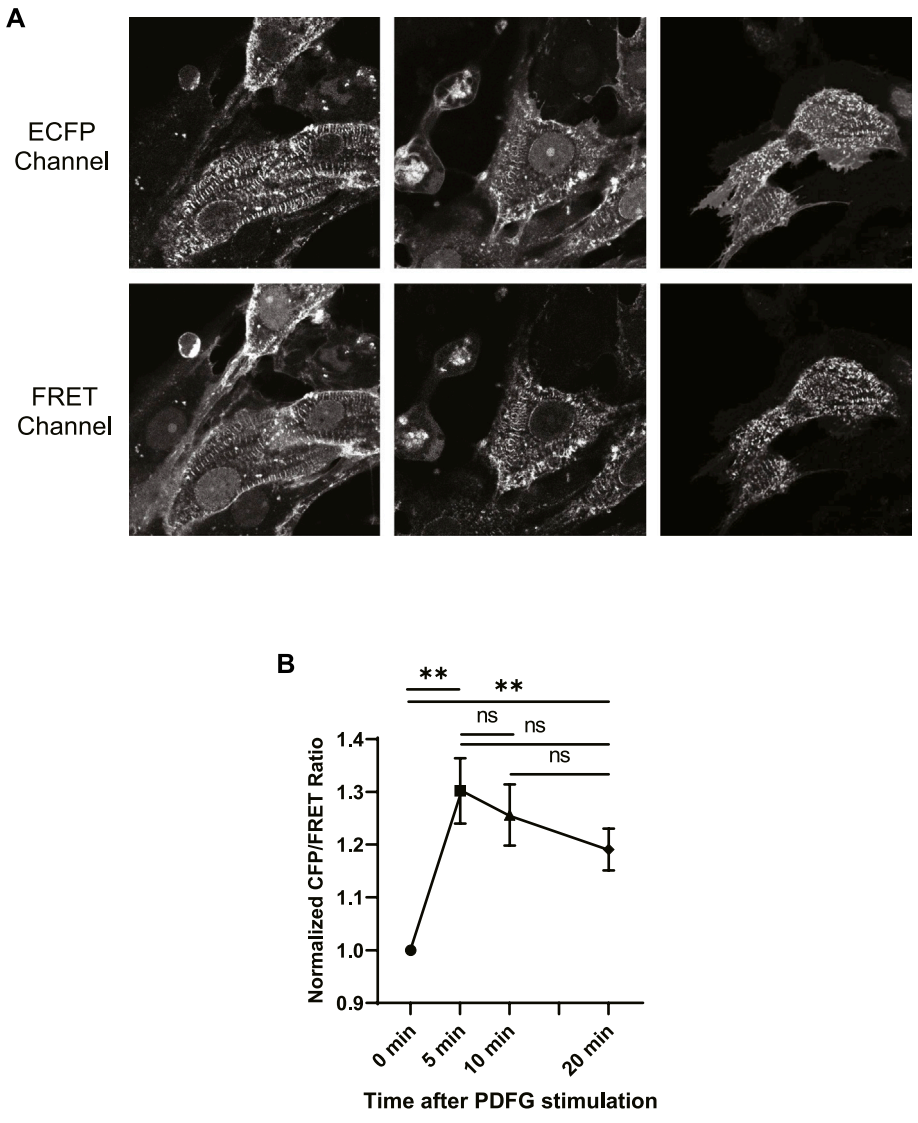

FIGURE 4
(A) Fluorescent signal images of ECFP and FRET emission channels acquired from three ECFP-YPet transduced NRCMs at t = 0+ of PDGF stimulation. **(B)** Normalized ECFP/FRET intensity ratios at t = 0+, 5, 10 and 20 min after PDGF treatment. Although, the ECFP/FRET values of time points t = 5, 10, and 20 min were not significantly different (unpaired two-tailed t-test), compared to each other, the ECFP/FRET values of these time points were significantly higher, compared to t = 0+. The ECFP/FRET measurement was performed at the costameres pixels, using the approach described in the materials and methods section.

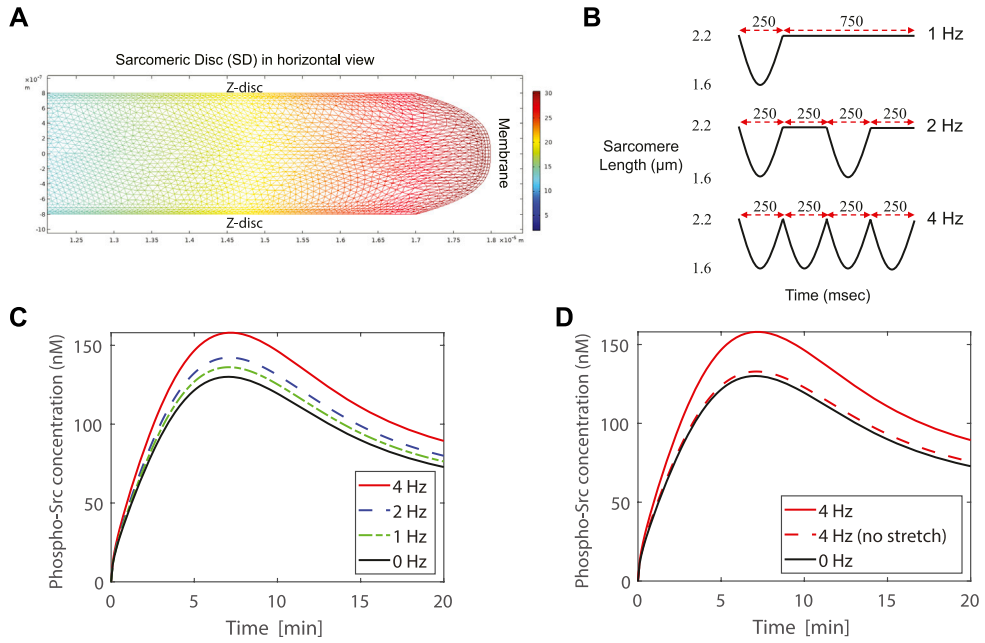

FIGURE 5
(A) The concentration of phospho-Src in the cytosol of one SD in the 4 Hz case at 25 s after PDGF stimulation. The SD is shown in horizontal view. **(B)** Contraction profiles of the modeled SD for 1, 2, and 4 Hz contraction frequency. **(C)** Simulation of a contracting SD, by modeling the lattice expansion together with membrane stretch, exhibits higher concentration of phospho-Src when SD beats with higher rates. Simulations show 21.5%, 9.4%, and 4.7% higher concentration of phospho-Src, respectively at 4, 2, and 1 Hz contraction frequencies, comparing to 0 Hz. **(D)** The dashed-red curve represents a case in which the lattice expansion completely compensates the cytosol displacement and there is no membrane stretch. In this case the peak value of the phospho-Src concentration is only 2.2% higher than the peak value of the 0 Hz case. Simulations demonstrate that membrane stretch has higher impact than lattice expansion in increasing the phospho-Src concentration. The lattice expansion with membrane stretch study are presented in dashed curves. The solid curves show the lattice expansion without membrane stretch.

We then calculated the fluorescence intensity ratios of ECFP/FRET for each time course and plotted the normalized ratio as a function of time in (Figure 4B). Although, the ECFP/FRET values of time points t = 5, 10 and 20 min were not significantly different (unpaired two-tailed t-test), compared to each other, the ECFP/FRET values of these time points were significantly higher, compared to t = 0+. This indicates Src activation upon PDGF stimulation, consistent with previous reports in different cell types (Thomas and Brugge, 1997; Rangamani et al., 2013; Fan et al., 2022). The ECFP/FRET measurement was performed at the costameres pixels, using the approach described in the materials and methods section. Accordingly, we probed costamere to mathematically examine our hypothesis.

Mathematical examination of the hypothesis

Frequency-dependent Src activation in adult human cardiac myocytes

Different frequencies of heart beating and various patterns of contraction and relaxation are common in almost all heart diseases. Variations in pattern of CM beating lead to dynamic geometry of SDs. Accordingly, we hypothesized that changes in the contraction frequency of CM lead to dynamic geometry of SDs. The dynamic geometry of SD generates concentration gradient for membrane and intracellular molecules, which modulate membrane signal transduction. As it is almost impossible to examine our hypothesis using *in-vivo* and *in-vitro* systems, we mathematically simulate Src-mediated PDGF signaling by a finite-element COMSOL model, as described in methods section.

In a simulation, first one cycle of motion is simulated using computational fluid dynamics with moving boundaries. As a result, the velocity field of the cytosol is obtained during this cycle. In a second step, this motion is repeatedly coupled with the transport of the substances both in the cytosol and in the membrane. The changes in concentration due to chemical reactions throughout the cell are simultaneously calculated. As an example, the concentration of phospho-Src in the cytosol of one SD in the 4 Hz case at 25 s after PDGF stimulation is shown in (Figure 5A). The further from the membrane, the lower the concentration.

The contraction-relaxation profiles of the modeled SD are represented in (Figure 5B) for 1, 2, and 4 Hz contraction frequencies. The case of 0 Hz is also drawn as a reference

curve. The FRET microscopy (Figure 4A), in combination with our hypothesis, allowed us to focus on the Src activity at costameres, specifically. As demonstrated in (Figure 4A), Src kinase is mainly localized at the costameres in CMs. Therefore, in the modeled SD, we probed the evolution of phospho-Src concentration underneath the membrane at the costamere site (Figure 5C). All four curves show almost similar trajectories to our experimental results (Figure 4B). Simulations exhibit higher concentration of phospho-Src when sarcomere beats with higher rates. The maximum concentration of phospho-Src at 4, 2, and 1 Hz contraction frequencies, was 21.5%, 9.4%, and 4.7% higher, respectively, comparing to 0 Hz.

To distinguish the impact of membrane stretch from the impact of lattice expansion, we compared the reported SD model with an unrealistic model in which we assumed that the membrane is not elastic and cannot be stretched. This causes the Z-line lattice to be expanded more, to sustain the cytosolic volume constant. At the 4 Hz contraction of this assumed case, the peak value of the phospho-Src concentration was just 2.2% higher than the peak value of the 0 Hz case (Figure 5D). Thus, the membrane stretch has higher impact than lattice expansion in increasing the phospho-Src concentration.

Discussion

The idea of cell shape having effects on cell physiology and pathology is probably not new and dates back to at least 1880s and 1890s, when Pflüger, Driesch and Hertwig reported about the manipulation of amphibian and invertebrate embryos and found that the regulation of mitotic orientations play a role in embryonic patterning (Pflüger, 1884; Driesch, 1891; Hertwig, 1893). This work eventually culminated in Hertwig's Rule: the mitotic spindle bisects the cell perpendicular to its longest axis [for a recent review: (Cadart et al., 2014)].

In contrast, frequency dependent signaling has been proposed and detected in neurons [for a review (Ito and Schuman, 2008)]. While frequency dependent changes in calcium transients in cardiomyocytes are well known (Sipido et al., 1998), with calcium being an important intracellular mediator of contraction, frequency dependent effects on cell signaling did not receive much attention. Inspired by the work of Rangamani et al. and Kuo et al., we developed the concept of frequency dependent signaling in cardiomyocytes [please see for review: (Haftbaradaran Esfahani and Knoll, 2020b)].

Here we elaborate and provide mathematical evidence for the existence of a novel concept in physiology, namely that membrane shape translates into biochemical signaling, as suggested by a previous report (Rangamani et al., 2013), where cell signaling has been put in the context of membrane shape. Convex membranes foster ligand/receptor interaction and hence are expected to increase signaling, as long as the ligand remains extracellular. Elongated, elliptical cells are expected to increase their signaling activity *via* decreasing local membrane to volume ratios.

Our data whereby an increase in frequency increases the activation of Src kinase and where we show that Src kinase also plays an essential role in cardiomyocyte signaling provides evidence for the existence of membrane curvature related molecular mechanisms and that this mechanism displays relevance in biology and medicine.

The myocardium, where contracting myocytes periodically elongate and minimize non-cardiac cells such as cardiac fibroblasts and hence increase their sensitivity to receptor mediated effects, can lead to hypertrophy of these cells.

The situation in cardiac myocytes probably is more complex: cycles of contraction and relaxation will expose and de-expose costameres and the connecting membranes to the surrounding extracellular fluid and hence activate and de-activate this type of signaling (for example integrin mediated signaling such as Src kinase, focal adhesion kinase and integrin linked kinase) (Knoll et al., 2007). The membrane parts between costameres probably are bulging outwards which will increase membrane to cytosol ratios and hence increase signaling.

The frequency of beating hearts is expected to initiate very specific types of hypertrophic or atrophic signaling and as such affect cardiac metabolism, depending on whether costamere or membrane related signaling overweighs (Dixon and Spinale, 2009). This will also give rise to the differentiation of different types of cardiac hypertrophy initiated *via* different signal transduction cascades. For example, very low frequencies likely foster the development of different types of heart failure than very high frequencies (Alboni et al., 2001).

The development of heart failure in other models, such as the ones whereby an increase in cardiac preload or volume stretches cardiac myocytes and non-cardiac myocytes, and which cause eccentric hypertrophy, probably can be better explained by using the concept of local membrane in-homogeneities.

Every hypertrophy will lead to a decrease of surface to volume ratios but membrane ligand/receptor mediated signaling activity can be modified *via* frequency and hence cell shape. In the heart this is expected to lead to modifications of costamere related hypertrophic or atrophic stimuli. Thus hypertrophy can be regarded as part of a negative feedback loop aimed to equilibrate various membrane-mediated signaling pathways. The effects of local membrane in-homogeneities offer a novel molecular mechanism to explain various types of cardiac hypertrophy, which so far largely has been seen as a response to normalize wall stress.

Limitations

Although the concept of locality of surface to volume ratios is attractive, it is still very general and to a large extent based on theoretical considerations which depend on specific reaction kinetics and diffusion probabilities, and which may differ from receptor to receptor, ligand to ligand and cell-type to cell-type. In addition, we primarily focused on Src kinase signaling, but did not take into consideration hundreds of other signal transduction cascades affecting cell survival or performance. Moreover, calcium is well known to be linked to the frequency of the beating cardiomyocyte and hence should be analyzed in the context of signaling as well.

Moreover, for reasons of simplicity, we assumed membrane changes underlie sinusoidal functions but in reality, this type of movement is very unlikely to occur in CMs.

Additional experimental proof is needed, particularly in the cardiovascular system. Nevertheless, this effect could be important for the heart.

Summary

Mechanosensation, mechanotransduction and mechano-conversion are fundamental processes and are present in every living cell. These effects are particularly significant in dynamic cells such as cardiomyocytes and dynamic organs such as hearts. The addition of membrane curvature—and hence frequency-dependent, dynamic processes which differentially affect signaling and hence connect various types of information processing to cellular phenotypes is completely new and provides novel opportunities for basic science, translational medicine, drug development and therapy.

Data availability statement

The raw data supporting the conclusion of this article will be made available by the authors, without undue reservation.

Ethics statement

The animal study was reviewed and approved by the Karolinska Institutet.

Author contributions

PH contributed to the study design, contributed to the mathematical and COMSOL modeling, performed the FRET experiment and co-wrote the manuscript. JW contributed to the mathematical modeling, designed the COMSOL model and co-wrote the manuscript. LL contributed to the study design and the mathematical modeling. RK designed the study and co-wrote the manuscript.

Funding

RK is supported by grants from AstraZeneca, Leducq Transatlantic Network of Excellence (FLQ13CVD04), the German Research Foundation (Kn 448/10-2), Berlin Institutes of Health and Hjärt och Lungfonden in Sweden.

Conflict of interest

Author JW was employed by the company Wendelsbergs beräkningskemi AB. Authors LL and RK were employed by the company AstraZeneca.

The remaining author declares that the research was conducted in the absence of any commercial or financial relationships that could be construed as a potential conflict of interest.

Publisher's note

References

Alboni, P., Scarfo, S., and Fuca, G. (2001). Development of heart failure in bradycardic sick sinus syndrome. *Ital. Heart J.* 2 (1), 9–12.

Burbaum, L., Schneider, J., Scholze, S., Bottcher, R. T., Baumeister, W., Schwille, P., et al. (2021). Molecular-scale visualization of sarcomere contraction within native cardiomyocytes. *Nat. Commun.* 12 (1), 4086. doi:10.1038/s41467-021-24049-0

Cadart, C., Zlotek-Zlotkiewicz, E., Le Berre, M., Piel, M., and Matthews, H. K. (2014). Exploring the function of cell shape and size during mitosis. *Dev. Cell.* 29 (2), 159–169. doi:10.1016/j.devcel.2014.04.009

Cass, J. A., Williams, C. D., Irving, T. C., Lauga, E., Malingen, S., Daniel, T. L., et al. (2021). A mechanism for sarcomere breathing: Volume change and advective flow within the myofilament lattice. *Biophys. J.* 120 (18), 4079–4090. doi:10.1016/j.bpj.2021.08.006

COMSOL, (2021) *COMSOL Multiphysics® v. 5.6.* Stockholm, Sweden: COMSOL AB.

de Cavanagh, E. M. V., Ferder, M., Inserra, F., and Ferder, L. (2009). Angiotensin II, mitochondria, cytoskeletal, and extracellular matrix connections: An integrating viewpoint. *Am. J. Physiol. Heart Circ. Physiol.* 296 (3), H550–H558. doi:10.1152/ajpheart.01176.2008

Dixon, J. A., and Spinale, F. G. (2009). Large animal models of heart failure A critical link in the translation of basic science to clinical practice. *Circ. Heart Fail.* 2 (3), 262–271. doi:10.1161/CIRCHEARTFAILURE.108.814459

Driesch, H. (1891). Entwicklungsmechanische Studien. I. Der Werth der beiden ersten Furchungszellen in der Echinoderm-Entwicklung. Experimentelle Erzeugung von Theil- und Doppelbildungen. II. Ueber die Beziehungen des Lichtes zur ersten Etappe der thierischen Formbildung. *Z. für Wiss. Zool.* 1, 160–184.

Elliott, H., Fischer, R. S., Myers, K. A., Desai, R. A., Gao, L., Chen, C. S., et al. (2015). Myosin II controls cellular branching morphogenesis and migration in three dimensions by minimizing cell-surface curvature. *Nat. Cell. Biol.* 17 (2), 137–147. doi:10.1038/ncb3092

Fan, S. Y., Wang, C., Huang, K., and Liang, M. L. (2022). Myricanol inhibits platelet derived growth factor-BB-induced vascular smooth muscle cells proliferation and migration *in vitro* and intimal hyperplasia *in vivo* by targeting the platelet-derived growth factor receptor-beta and NF-kappa B signaling. *Front. Physiol.* 12, 790345. doi:10.3389/fphys.2021.790345

Haftbaradaran Esfahani, P., ElBeck, Z., Sagasser, S., Li, X., Hossain, M. B., Talukdar, H. A., et al. (2019). Cell shape determines gene expression: Cardiomyocyte morphotypic transcriptomes. *Basic Res. Cardiol.* 115 (1), 7. doi:10.1007/s00395-019-0765-7

Haftbaradaran Esfahani, P., and Knoll, R. (2020a). An approach to study shape-dependent transcriptomics at a single cell level. *J. Vis. Exp.* 165, 1–15. doi:10.3791/61577

Haftbaradaran Esfahani, P., and Knoll, R. (2020b). Cell shape: Effects on gene expression and signaling. *Biophys. Rev.* 12 (4), 895–901. doi:10.1007/s12551-020-00722-4

Hertwig, O. (1893). Ueber den Werth der ersten Furchungszellen für die Organbildung des Embryo Experimentelle Studien am Frosch-und Tritonei. *Arch. F. Mikrosk. Anat.* 42 (4), 662–807. doi:10.1007/bf02976796

Irving, T. C., Konhilas, J., Perry, D., Fischetti, R., and De Tombe, P. P. (2000). Myofilament lattice spacing as a function of sarcomere length in isolated rat myocardium. *Am. J. Physiol. Heart Circ. Physiol.* 279 (5), H2568–H2573. doi:10.1152/ajpheart.2000.279.5.H2568

Ito, H. T., and Schuman, E. M. (2008). Frequency-dependent signal transmission and modulation by neuromodulators. *Front. Neurosci.* 2 (1), 138–144. doi:10.3389/neuro.01.027.2008

Kamkin, A., Kiseleva, I., and Isenberg, G. (2000). Stretch-activated currents in ventricular myocytes: Amplitude and arrhythmogenic effects increase with hypertrophy. *Cardiovasc. Res.* 48 (3), 409–420. doi:10.1016/s0008-6363(00)00208-x

Knoll, R. (2015). A role for membrane shape and information processing in cardiac physiology. *Pflugers Arch.* 467 (1), 167–173. doi:10.1007/s00424-014-1575-2

Knoll, R., Buyandelger, B., and Lab, M. (2011). The sarcomeric Z-disc and Z-discopathies. *J. Biomed. Biotechnol.* 2011, 569628. doi:10.1155/2011/569628

Knoll, R., Postel, R., Wang, J. M., Kratzner, R., Hennecke, G., Vacaru, A. M., et al. (2007). Laminin-alpha4 and integrin-linked kinase mutations cause human cardiomyopathy via simultaneous defects in cardiomyocytes and endothelial cells. *Circulation* 116 (5), 515–525. doi:10.1161/CIRCULATIONAHA.107.689984

Liu, B., Lu, S. Y., Hu, Y. L., Liao, X. L., Ouyang, M. X., and Wang, Y. X. (2014). RhoA and membrane fluidity mediates the spatially polarized Src/FAK activation in response to shear stress. *Sci. Rep.* 4, 7008. doi:10.1038/srep07008

Lou, H. Y., Zhao, W., Zeng, Y., and Cui, B. (2018). The role of membrane curvature in nanoscale topography-induced intracellular signaling. *Acc. Chem. Res.* 51 (5), 1046–1053. doi:10.1021/acs.accounts.7b00594

Lu, Y. Y., Zhao, X. K., Yu, L., Qi, F., Zhai, B., Gao, C. Q., et al. (2017). Interaction of Src and alpha-V integrin regulates fibroblast migration and modulates lung fibrosis in A preclinical model of lung fibrosis. *Sci. Rep.* 7, 46357. doi:10.1038/srep46357

Malingen, S. A., Asencio, A. M., Cass, J. A., Ma, W., Irving, T. C., and Daniel, T. L. (2020). *In vivo* X-ray diffraction and simultaneous EMG reveal the time course of myofilament lattice dilation and filament stretch. *J. Exp. Biol.* 223, jeb224188. doi:10.1242/jeb.224188

Malingen, S. A., and Daniel, T. L. (2020). *The kinematics and mechanics of muscle's myofilament lattice*. Seattle: University of Washington Libraries.

Martino, F., Perestrelo, A. R., Vinarsky, V., Pagliari, S., and Forte, G. (2018). Cellular mechanotransduction: From tension to function. *Front. Physiol.* 9, 824. doi:10.3389/fphys.2018.00824

Matsuoka, H., Nada, S., and Okada, M. (2004). Mechanism of Csk-mediated down-regulation of Src family tyrosine kinases in epidermal growth factor signaling. *J. Biol. Chem.* 279 (7), 5975–5983. doi:10.1074/jbc.M311278200

Nowak, M. B., Veeraraghavan, R., Poelzing, S., and Weinberg, S. H. (2021). Cellular size, gap junctions, and sodium channel properties govern developmental changes in cardiac conduction. *Front. Physiol.* 12, 731025. doi:10.3389/fphys.2021.731025

Oda, T., and Yanagisawa, H. (2020). Cryo-electron tomography of cardiac myofibrils reveals a 3D lattice spring within the Z-discs. *Commun. Biol.* 3 (1), 585. doi:10.1038/s42003-020-01321-5

Okada, M. (2012). Regulation of the Src family kinases by Csk. *Int. J. Biol. Sci.* 8 (10), 1385–1397. doi:10.7150/ijbs.5141

Pan, Y. J., Lu, S. Y., Lei, L., Lamberto, I., Wang, Y., Pasquale, E. B., et al. (2019). Genetically encoded FRET biosensor for visualizing EphA4 activity in different compartments of the plasma membrane. *ACS Sens.* 4 (2), 294–300. doi:10.1021/acssensors.8b00465

Pflüger, E. (1884). Ueber die Einwirkung der Schwerkraft und anderer Bedingungen auf die Richtung der Zelltheilung. *Pfluger Arch.* 34 (1), 607–616. doi:10.1007/bf01612880

Powers, J. D., Malingen, S. A., Regnier, M., and Daniel, T. L. (2021). The sliding filament theory since andrew huxley: Multiscale and multidisciplinary muscle research. *Annu. Rev. Biophys.* 50, 373–400. doi:10.1146/annurev-biophys-110320-062613

Rangamani, P., Lipshtat, A., Azeloglu, E. U., Calizo, R. C., Hu, M., Ghassemi, S., et al. (2013). Decoding information in cell shape. *Cell.* 154 (6), 1356–1369. doi:10.1016/j.cell.2013.08.026

Samarel, A. M. (2005). Costameres, focal adhesions, and cardiomyocyte mechanotransduction. *Am. J. Physiol. Heart Circ. Physiol.* 289 (6), H2291–H2301. doi:10.1152/ajpheart.00749.2005

Schindelin, J., Arganda-Carreras, I., Frise, E., Kaynig, V., Longair, M., Pietzsch, T., et al. (2012). Fiji: An open-source platform for biological-image analysis. *Nat. Methods* 9 (7), 676–682. doi:10.1038/nmeth.2019

Schlaepfer, D. D., and Hunter, T. (1996). Signal transduction from the extracellular matrix - a role for the focal adhesion protein-tyrosine kinase FAK. *Cell. Struct. Funct.* 21 (5), 445–450. doi:10.1247/csf.21.445

Sipido, K. R., Stankovicova, T., Flameng, W., Vanhaecke, J., and Verdonck, F. (1998). Frequency dependence of Ca2+ release from the sarcoplasmic reticulum in human ventricular myocytes from end-stage heart failure. *Cardiovasc. Res.* 37 (2), 478–488. doi:10.1016/s0008-6363(97)00280-0

Thomas, S. M., and Brugge, J. S. (1997). Cellular functions regulated by Src family kinases. *Annu. Rev. Cell. Dev. Biol.* 13, 513–609. doi:10.1146/annurev.cellbio.13.1.513

Toh, R., Shinohara, M., Takaya, T., Yamashita, T., Masuda, S., Kawashima, S., et al. (2006). An X-ray diffraction study on mouse cardiac cross-bridge function *in vivo*: Effects of adrenergic {beta}-stimulation. *Biophys. J.* 90 (5), 1723–1728. doi:10.1529/biophysj.105.074062

Wang, Y. X., Botvinick, E. L., Zhao, Y. H., Berns, M. W., Usami, S., Tsien, R. Y., et al. (2005). Visualizing the mechanical activation of Src. *Nature* 434 (7036), 1040–1045. doi:10.1038/nature03469

Williams, C. D., Salcedo, M. K., Irving, T. C., Regnier, M., and Daniel, T. L. (2013). The length-tension curve in muscle depends on lattice spacing. *Proc. Biol. Sci.* 280 (1766), 20130697. doi:10.1098/rspb.2013.0697

Wright, P. T., Tsui, S. E. F., Francis, A. J., MacLeod, K. T., and Marston, S. B. (2020). Approaches to high-throughput analysis of cardiomyocyte contractility. *Front. Physiol.* 11, 1–19. doi:10.3389/fphys.2020.00612

10.3389/fphys.2022.926422

Appendix 1 List of reactions

PDGF binds PDGFR

Name	Description	Expression	Units
J	Reaction rate	$K_{on}.c_{PDGF}.c_{PDGFR} - K_{off}.c_{PDGF-PDGFR}$	molecules.$\mu m^{-2} \cdot s^{-1}$
K_{on}	Forward rate constant	1	$\mu M^{-1} \cdot s^{-1}$
K_{off}	Reverse rate constant	0.01	s^{-1}
$c_{PDGF-PDGFR}$	PDGF-PDGFR complex concentration	Variable	molecules $\cdot \mu m^{-2}$

Src association with PDGF-PDGFR complex

Name	Description	Expression	Units
J	Reaction rate	$K_f.c_{PDGF-PDGFR}.c_{Src} - K_r.c_{PDGF-PDGFR-Src}$	molecules $\cdot \mu m^{-2} \cdot s^{-1}$
K_f	Forward rate constant	1	$\mu M^{-1} \cdot s^{-1}$
K_r	Reverse rate constant	0.1	s^{-1}
$c_{PDGF-PDGFR-Src}$	PDGF-PDGFR-Src complex concentration	variable	molecules $\cdot \mu m^{-2}$

Src activation (phosphorylation)

Name	Description	Expression	Units
J	Reaction rate	$\frac{V_{max} \cdot c_{PDGF-PDGFR-Src}}{K_m + c_{PDGF-PDGFR-Src}}$	molecules $\cdot \mu m^{-2} \cdot s^{-1}$
V_{max}	Maximum reaction rate	$K_{cat} \cdot PTP$	molecules $\cdot \mu m^{-2} \cdot s^{-1}$
K_{cat}	Reaction constant	9	molecules $\cdot \mu m^{-2} \cdot \mu M^{-1} \cdot s^{-1}$
PTP	Species concentration	0.1	μM
K_m	Km (1/2 max)	0.1	molecules $\cdot \mu m^{-2}$
$c_{PDGF-PDGFR-Src}$	PDGF-PDGFR-Src complex concentration	Variable	molecules $\cdot \mu m^{-2}$

Src dephosphorylation in cytosol

Name	Description	Expression	Units
J	Reaction rate	$\frac{V_{max} \cdot c_{Phospho-Src}}{K_m + c_{Phospho-Src}}$	$\mu M \cdot s^{-1}$
V_{max}	Maximum reaction rate	$0.3 \cdot Csk - active$	$\mu M \cdot s^{-1}$
K_m	Km (1/2 max)	1.5	μM
$c_{Phospho-Src}$	Phospho-Src concentration	Variable	μM

frontiers | Frontiers in Physiology

TYPE Original Research
PUBLISHED 12 September 2022
DOI 10.3389/fphys.2022.980662

OPEN ACCESS

EDITED BY
Sachio Morimoto,
International University of Health and Welfare (IUHW), Japan

REVIEWED BY
Kenneth Scott Campbell,
University of Kentucky, United States
J-P Jin,
Wayne State University, United States

*CORRESPONDENCE
Bradley M. Palmer,
bmpalmer@uvm.edu

SPECIALTY SECTION
This article was submitted to Striated Muscle Physiology, a section of the journal Frontiers in Physiology

RECEIVED 28 June 2022
ACCEPTED 17 August 2022
PUBLISHED 12 September 2022

CITATION
Wakefield JI, Bell SP and Palmer BM (2022), Inorganic phosphate accelerates cardiac myofilament relaxation in response to lengthening.
Front. Physiol. 13:980662.
doi: 10.3389/fphys.2022.980662

Inorganic phosphate accelerates cardiac myofilament relaxation in response to lengthening

Jane I. Wakefield[1], Stephen P. Bell[2] and Bradley M. Palmer[3]*

[1]Department of Biology, University of Vermont, Burlington, VT, United States, [2]Department of Medicine, Larner College of Medicine, University of Vermont, Burlington, VT, United States, [3]Department of Molecular Physiology and Biophysics, Larner College of Medicine, University of Vermont, Burlington, VT, United States

Myocardial relaxation in late systole is enhanced by increasing velocities of lengthening. Given that inorganic phosphate (Pi) can rebind to the force-producing myosin enzyme prior to MgADP release and hasten crossbridge detachment, we hypothesized that myocardial relaxation in late systole would be further enhanced by lengthening in the presence of Pi. Wistar rat left ventricular papillary muscles were attached to platinum clips, placed between a force transducer and a length motor at room temperature, and bathed in Krebs solution with 1.8 mM Ca^{2+} and varying Pi of 0, 1, 2, and 5 mM. Tension transients were elicited by electrical stimulation at 1 Hz. Peak tension was significantly enhanced by Pi: 0.593 ± 0.088 mN mm^{-2} at 0 mM Pi and 0.817 ± 0.159 mN mm^{-2} at 5 mM Pi (mean ± SEM, $p < 0.01$ by ANCOVA). All temporal characteristics of the force transient were significantly shortened with increasing Pi, e.g., time-to-50% recovery was shortened from 305 ± 14 ms at 0 mM Pi to 256 ± 10 ms at 5 mM Pi ($p < 0.01$). A 1% lengthening stretch with varying duration of 10–200 ms was applied at time-to-50% recovery during the descending phase of the force transient. Matching lengthening stretches were also applied when the muscle was not stimulated, thus providing a control for the passive viscoelastic response. After subtracting the passive from the active force response, the resulting myofilament response demonstrated features of faster myofilament relaxation in response to the stretch. For example, time-to-70% relaxation with 100 ms lengthening duration was shortened by 8.8 ± 6.8 ms at 0 Pi, 19.6 ± 4.8* ms at 1 mM Pi, 31.0 ± 5.6* ms at 2 Pi, and 25.6 ± 5.3* ms at 5 mM Pi (*$p < 0.01$ compared to no change). Using skinned myocardium, half maximally calcium-activated myofilaments underwent a 1% quick stretch, and the tension response was subjected to analysis for sensitivity of myosin detachment rate to stretch, g_1, at various Pi concentrations. The parameter g_1 was enhanced from 15.39 ± 0.35 at 0 Pi to 22.74 ± 1.31 s^{-1}/nm at 8 Pi ($p < 0.01$). Our findings suggest that increasing Pi at the myofilaments enhances lengthening-induced relaxation by elevating the sensitivity of myosin crossbridge detachment due to lengthening and thus speed the transition from late-systole to early-diastole.

KEYWORDS

cardiac, myosin, crossbridge, phosphate, diastole

Introduction

The duration of the isovolumic relaxation phase of the cardiac cycle depends upon the rate at which LV contractile force subsides during the transition from late-systole to early-diastole. The decline of intracellular Ca^{2+} is an important contributor to this transition, because Ca^{2+} decline deactivates the thin filament and inhibits the formation of new force-producing myosin crossbridges (Bers, 2002). The detachment rate of myosin crossbridges is another important component. A faster rate of crossbridge detachment translates to faster LV relaxation (Kass et al., 2004). Under normal physiological conditions, which includes saturating MgATP concentrations, further enhancing of crossbridge detachment rate can be achieved via post-translational modification of key myofilament proteins, such as by phosphorylation of myosin binding protein-C (Stelzer et al., 2006).

Using force-clamp experiments, Chung et al. (2017) showed that stretching the myocardium at end-systole also enhances the rate of LV myocardial relaxation. This enhancement of LV relaxation by stretch was greatest with the fastest rates of stretch, which suggests that myosin crossbridge detachment is sensitive to stretch. This and similar findings at the whole heart level (Zile et al., 2015) are relevant to the clinical treatment of heart failure with preserved ejected fraction (Dunlay et al., 2017), as they support the idea that myocardial stretch can enhance LV relaxation during the transition from late-systole to early-diastole.

Knowing that Pi can facilitate myosin detachment due to stretch at the molecular level (Dantzig et al., 1992; Smith and Geeves, 1995), we hypothesized that stretch-induced myocardial relaxation would be enhanced by increasing Pi concentrations. In the current study, we examined isometric excitable myocardium over various extracellular Pi concentrations and imposed a lengthening stretch in late-systole to demonstrate the effects of Pi in hastening the transition to early-diastole.

Methods

Solutions

Chemicals and reagents were obtained from Sigma-Aldrich Corp. (St. Louis, MO) unless otherwise noted. Krebs-Ringer Pi-free bathing solution concentrations (mmol/L) were 115 NaCl, 4.5 KCl, 1.8 $CaCl_2$, 1 $MgCl_2$, 25 $NaHCO_3$, 10 glucose, pH 7.35–7.40. Pi-containing bathing solutions (1, 2, and 5 mM), which cover the physiological range of 0.8–1.3 mM extracellular Pi (Manghat et al., 2014; Jacquillet and Unwin, 2019), were produced by replacing the same concentrations of NaCl with NaH_2PO_4. Propranolol was included in all bathing solutions at 1 μM.

Relaxing solution: pCa 8.0, 5 EGTA, 5 MgATP, 1 Mg^{2+}, 35 phosphocreatine (PCr), 300 U/ml creatine kinase (CK), ionic strength 200, pH 7.0; activating solution: same as relaxing with pCa 4.0 and 0–8 mM Pi; skinning solution: same as relaxing without CK, with 1% Triton-X100 wt/vol, 30 mM 2,3-butanedione 2-monoxime (BDM), 10 uL/ml E-64, 1.25 uL/ml Phenylmethylsulfonyl fluoride (PMSF), 1 tablet/10 ml PhosSTOP phosphatase inhibitor cocktail and 50% glycerol wt/vol; storage solution: same as skinning without Triton-X100. The pH of all solutions was adjusted at the temperature used.

Animal model

All procedures were reviewed and approved by the Institutional Animal Care and Use Committee of The University of Vermont Larner College of Medicine and complied with the *Guide for the Use and Care of Laboratory Animals* published by the National Institutes of Health. Adult female Wistar rats aged 4–5 months were acquired from Charles River. Animals were anesthetized with 2%–4% isoflurane and hearts removed.

Excitable papillary muscle

Hearts were submerged immediately into a Ca^{2+}-free Krebs-Ringer + 30 mM BDM solution bubbled with 95%O_2-5%CO_2 to pH 7.35–7.40 and maintained at 4°C. The large blood vessels, atria, and valves were removed from the base of the ventricles. The right ventricle free wall was removed, and an incision made from the base to the apex along the interventricular septum, therefore exposing the anterior and posterior papillary muscles. Both papillary muscles were excised, trimmed to 0.8–1.4 mm diameter, placed between two platinum omega-shaped clips, and tied with 6-O suture (Selby et al., 2011; Runte et al., 2017). Relative fiber dimensions of top width and side width were measured for later calculation of cross-sectional area.

Clipped muscle was placed between a force transducer (TR6S, Myotronic, Heidelberg, Germany) and voice coil length motor with ±2.5 mm travel (V-522, Physik Instrumente, Auburn, MA) part of a small intact muscle chamber (IonOptix, Westwood, MA) maintained at room temperature. A biphasic electrical stimulus of 1.5 × threshold voltage and 5 ms pulse width was passed through the muscle *via* the platinum hooks on which the clips rested.

Muscles were slowly stretched to an optimal length that achieved maximal peak force. Muscle length (ML) was then measured between sutures and cross-sectional area calculated from the measured major diameter and inferred minor diameter. Force (F) transients were recorded in response to electrical stimuli and were stabilized for 5 min prior to characterizing the transient with peak force, $+dF/dt_{max}$, $-dF/dt_{min}$, time to peak, time to 50% peak, and times to 40%, 50%, 60%, 70% and 80%

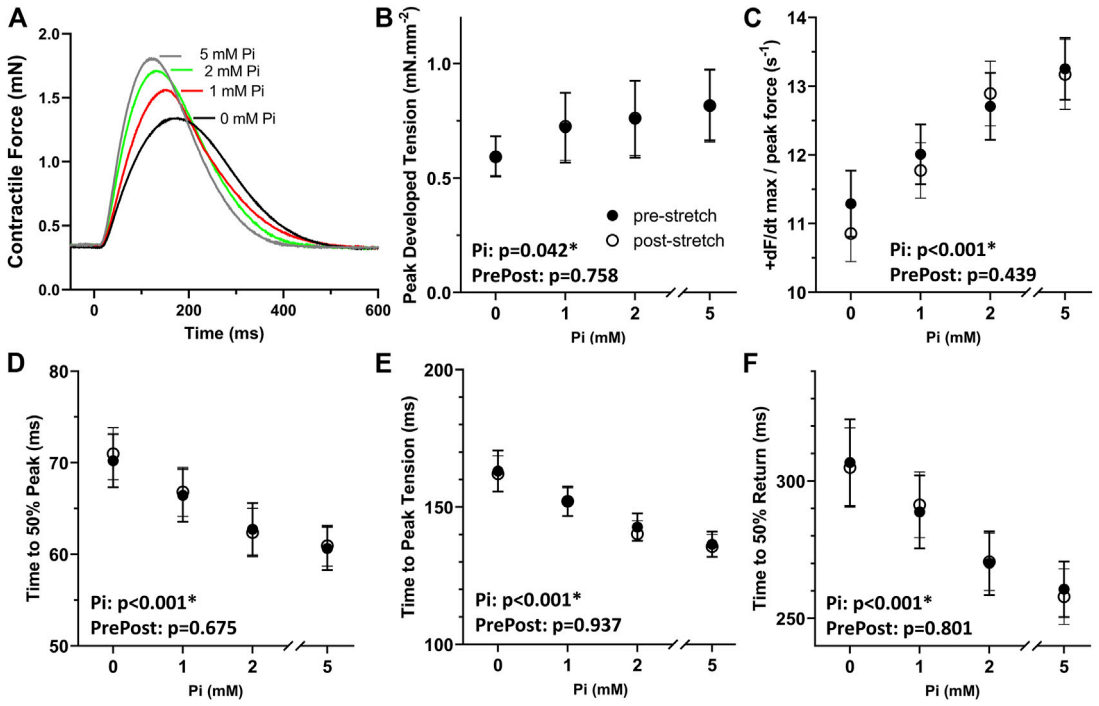

FIGURE 1
Effects of extracellular Pi on isometric myocardial force transients. **(A)** Examples of isometric force transients recorded at 0, 1, 2, and 5 mM extracellular Pi demonstrate a Pi-induced enhancement of systolic and diastolic function. **(B)** Developed peak tension was enhanced with increasing Pi. **(C)** Maximum rate of force increase normalized to peak force was also enhanced with increasing Pi. **(D,E)** Temporal characteristics of systolic function, time to 50% peak and time to peak, were shortened significantly by increasing Pi. **(F)** Time to 50% return was significantly shortened by increasing Pi thus indicating Pi-enhanced diastolic function. n = 8 rat papillary muscles.

recovery to baseline. Tension (P) was calculated by normalizing force to cross-sectional area.

Length changes were applied at time to 50% recovery and followed the shape of a raised cosine: 0.5 × Amp × [1 − cos (πt/T)], where Amp = ending extent of stretch calculated as 1% muscle length, t = time, and T = lengthening period ranging from 10 to 200 ms. The stretch was held for 240–50 ms, and the muscle then shortened over 50 ms back to the original muscle length. The lengthening protocol was also applied when the electrical stimulus was absent, which served as a measure of the force response of the passive components, i.e., excluding myofilaments. The force response to the stretch attributable to active myofilaments was calculated as active response minus passive response.

Demembranated papillary muscle

A portion of papillary muscle not used in excitable strip experiments were demembranated overnight at 4°C in skinning solution then stored at −20°C in storage solution. Strips were trimmed to 150–220 µm diameter before attaching aluminum T-clips and then mounted between a piezoelectric motor (P841.60, Physik Instrumente, Auburn, MA) and a strain gauge (AE801, Kronex, Walnut Creek, CA), lowered into a 30 µl droplet of relaxing solution maintained at room temperature, and stretched to 2.2 µm sarcomere length (IonOptix, Westwood, MA).

Muscles were maximally activated with pCa 5 and then approximately half-maximally activated with pCa 5.75. Force responses were recorded after step length changes of 1% resting muscle length (ML) during exposure to 0, 2, 4, and 8 mM Pi, which covers the physiological range of cytosolic Pi 4–8 mM (Tian et al., 1997; Valkovič et al., 2019). The stress response at pCa 8, $P_8(t)$, was subtracted from the stress response at pCa 5.75, $P_{5.75}(t)$, and the result was used as the response of the myofilaments. Analysis of this myofilament-dependent stress response, $P_m(t)$, resulted in values for peak tension of phase 1 (P_1), minimum tension of phase 2 (P_2), maximum redeveloped tension of phase 3 (P_3), and rates of force release (k_{rel}) and force redevelopment (k_{redev}) (Palmer et al., 2020).

Modeling stretch-induced relaxation

The myofilament-dependent stress response, $P_m(t)$, was further subjected to a non-linear, least-squares fit to the

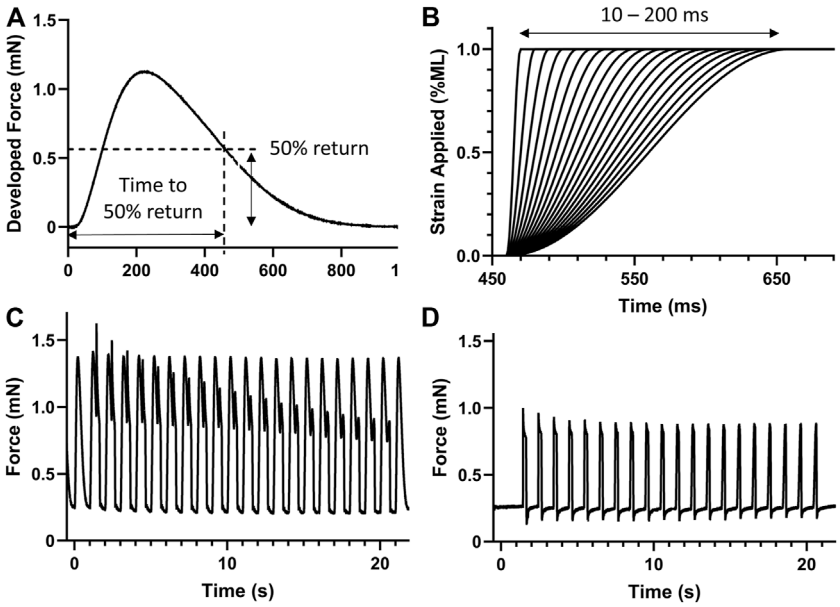

FIGURE 2
Stretch protocol. **(A)** The time to 50% return was noted for the isometric force transient. **(B)** A series of 20 stretches from 10 to 200 ms in duration were generated to apply a 1% strain on the muscle at the time of 50% return, i.e., 461 ms in this case. **(C)** Example stretch protocol applied to stimulated isometric force transients. **(D)** The same stretch protocol was also applied without stimulation to record the expected force response of passive components. n = 8 rat papillary muscles.

following equation, which describes the mechanical consequences of enhanced myosin crossbridge detachment in a two-state model of myosin kinetics when the half sarcomere undergoes strain, ε, due to a quick stretch (Palmer et al., 2020):

$$P_m(t) = \varepsilon G_P t^{-k_p} - \underbrace{\varepsilon L_{hs}\left[\frac{N_{hs}F_{uni}}{CSA}\right]\frac{g_1\bar{A}_0}{f_0}\left(e^{-g_0 t} - e^{-(f_0+g_0)t}\right)}_{R} + \underbrace{\varepsilon L_{hs}\left[\frac{N_{hs}k_{stiff}}{CSA}\right]\bar{A}_0\, e^{-g_0 t}}_{D} \quad (1)$$

The meanings of the terms and parameters are comprehensively explained in Palmer et al. (2020). Briefly, the first term of Eq. 1 refers to the passive power-law relaxation that characterizes the slow decline in stress that occurs after the active force generating mechanisms have completed their response. The second term describes the transient drop in isometric force that results from the temporarily enhanced detachment rate caused by the stretch. Because this second term is modeled to arise from the reversal of the myosin power-stroke caused by stretch, we will refer to the magnitude of this term as R for reversal. The third term describes the transient elevation in stress that results from those crossbridges that are initially stretched by the length change but eventually detach with a rate constant of g_0. We will refer to the magnitude of this term as D for drag.

The parameters in Eq. 1 are defined as follows: G_p and k_p refer to the magnitude and time characteristic, respectively, of the passive power-law relaxation, L_{hs} = length of half sarcomere such that εL_{hs} is the length change in nm applied to the myosin crossbridges, N_{hs} = total number of available myosin crossbridges within a half sarcomere of the muscle under investigation, F_{uni} = unitary force generated by a single crossbridge in pN, k_{stiff} = stiffness of a single attached crossbridge in pN/nm, CSA = cross-sectional area in mm^2, g_1 = the change in the myosin crossbridge detachment rate that occurs with strain on the crossbridge in units of s^{-1}/nm, $\bar{A}_0$ = stead-state fraction of myosin crossbridges attached, f_0 = rate of myosin crossbridge attachment, and g_0 = rate of myosin crossbridge detachment under steady-state conditions. It should be noted that, as written, the conventional rates k_{rel} and k_{redev} are related to the attachment and detachment rates of a model presented in Eq. 1 as $k_{rel} = (f_0 + g_0)$ and $k_{redev} = g_0$.

The constant g_1 refers to the enhancement of myosin crossbridge detachment rate caused by stretch and therefore was used as an index of stretch-induced relaxation. The magnitudes of the second and third terms in Eq. 1, R and D, were used to estimate g_1 as follows:

$$g_1 = \frac{R}{D} f_0 \left[\frac{k_{stiff}}{F_{uni}}\right] \quad (2)$$

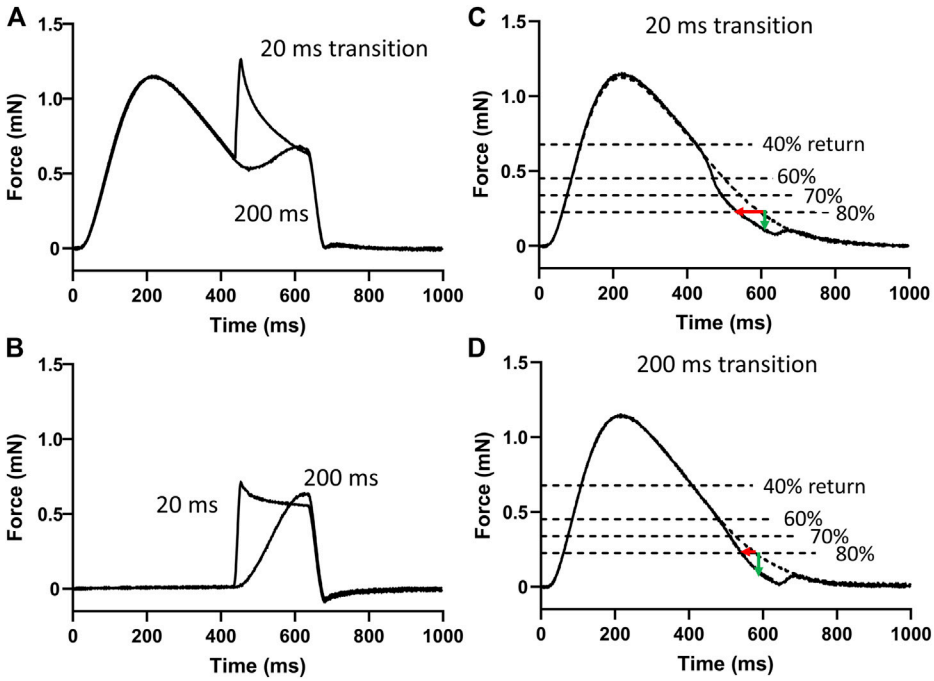

FIGURE 3
Analysis of myofilament response to stretch. **(A)** Two of the 20 force responses recorded during stimulation are overlayed here and represent the force responses of the myofilaments and the passive components during the 20 and 200 ms stretches. **(B)** The corresponding two force responses recorded without stimulation represent the passive components. These responses without stimulation were subtracted from those with stimulation to provide the myofilament response to stretch. **(C)** An example myofilament response to a 20 ms duration stretch to 1% muscle length. Times to 40%, 60%, 70%, and 80% return were detected. The effects of stretch on shortening of these times (red arrow) and on the loss of force at these times (green arrow) relative to the pre-stretch transient were detected. **(D)** An example myofilament response to a 200 ms duration stretch to 1% muscle length.

The values for R, D, and f_0 were estimated from the fit of Eq. 1 to the data. The unitary force F_{uni} is related to the crossbridge stiffness k_{stiff} by the myosin power stroke unitary displacement d_{uni} as $F_{uni} = k_{stiff}\, d_{uni}$, where d_{uni} is ~10 nm (Tyska and Warshaw, 2002). We estimated the ratio k_{stiff}/F_{uni} with a constant value of 0.1 nm^{-1}.

Statistical analysis

Statistical analyses to demonstrate the Pi-sensitivity of parameters describing stimulated isometric force transients was performed using ANCOVA with the Pi condition used as the covariate. Differences in isometric force parameters prior to and post the stretch protocol were examined by paired t-test.

Analysis to demonstrate duration-sensitivity of parameters affected by the stretch protocol was performed using ANCOVA with 20 transition durations (10–200 ms duration) and four Pi conditions (0, 1, 2, and 5 mM Pi) used as covariates. The effects of transition duration were demonstrated by duration main effects and of extracellular Pi by Pi main effects, and the differential Pi-sensitivity of transition durations were tested with Duration × Pi interactions. Statistical analyses to demonstrate the Pi-sensitivity of parameters describing the force response to a quick stretch was performed by ANCOVA with four Pi conditions (0, 2, 4, and 8 mM Pi) used as covariates. Statistical significance was reported at $p < 0.05$ and $p < 0.01$ levels.

Results

Isometric force transients

Increasing extracellular Pi led to enhanced systolic and diastolic function in isometric rat papillary muscle (Figure 1A). Pi-enhanced systolic function was observed as higher developed peak tension, faster rate of contraction normalized to developed peak, shorter time to 50% peak, and shorter time to peak (Figures 1B–E) detected by ANCOVA. Enhanced diastolic function was reflected in a shorter time to peak and shorter time to 50% return (Figures 1E,F), which were significantly affected by Pi.

The results in Figures 1B–F also demonstrate that the stretching protocol, which is described in the next section, did

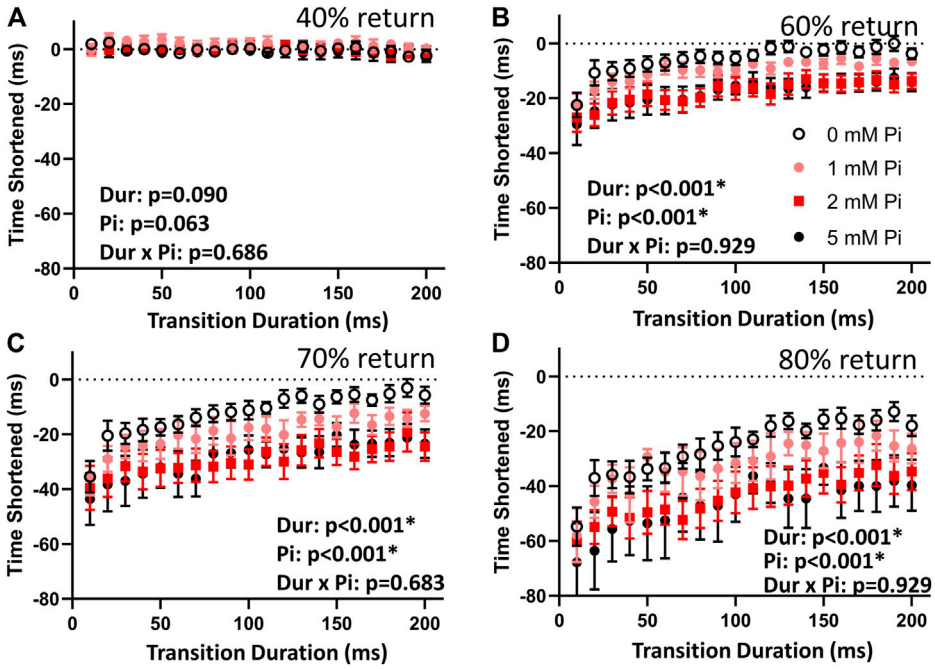

FIGURE 4
Effects of stretch on times to return. **(A)** The time to 40% return was not affected by lengthening imposed at time to 50% return. This result indicates that the stimulated transients were repeatable and comparable throughout the lengthening protocol by this measure. **(B)** When no extracellular Pi was available (0 mM Pi), the time to 60% return was abbreviated by those 1% stretches imposed over less than 110 ms. Faster stretches resulted in shorter times to 60% return, as indicated by the highly significant duration (Dur) main effect. This abbreviation was amplified with increasing extracellular Pi as indicated by a highly significant Pi main effect. **(C)** With no extracellular Pi, the time to 70% return was abbreviated by stretches imposed over less than 170 ms. This effect was amplified by extracellular Pi. **(D)** The time to 80% return was also abbreviated by all stretches under all conditions but was especially abbreviated by faster stretches and increasing extracellular Pi.

not appreciably affect the isometric force transients. Transient parameters recorded after the stretch, i.e., post-stretch, were not different compared to pre-stretch parameters as demonstrated by non-significant ANCOVA.

Stretch protocol

After establishing at least 5 min steady state contractile dynamics at each Pi condition, the time to 50% return was noted (Figure 2A). A series of 20 stretches from 10 to 200 ms in duration was then applied at the time to 50% return (Figure 2B). The strain of each stress was 1% muscle length and followed a smooth half-cosine transition. The 20 stretched transients, including a pre- and post-stretch transient, are shown in Figure 2C. The same stretch protocol was applied without stimulation to provide the response of the passive components of the muscle (Figure 2D).

Two example force transients recorded with 20 and 200 ms stretch responses are shown overlayed in Figure 3A. Responses such as these was considered due to the force-producing myofilaments plus the passive components of the myocardium. The corresponding stretch responses without stimulated transients are shown in Figure 3B and was considered due to passive components only. The passive responses were subtracted from the myofilament plus passive responses to produce the myofilament only responses. Figures 3C,D illustrate examples of the responses to 20 and 200 ms duration stretches, respectively.

The times to 40%, 60%, 70%, and 80% returns in these myofilament-only responses were detected and compared to the same time points recorded in the pre-stretch isometric force transient (dashed line in Figures 3C,D). The differences in these time points were used to demonstrate the effects of stretch and extracellular Pi on enhancing relaxation during the transition from late-systole to early-diastole.

Effects of Pi on stretch response in late-systole

The difference in times to 40% return were not affected by stretch or by Pi (Figure 4A). This result demonstrates that the stimulated isometric force transients up to the point of time to 50% return were consistent in their dynamics.

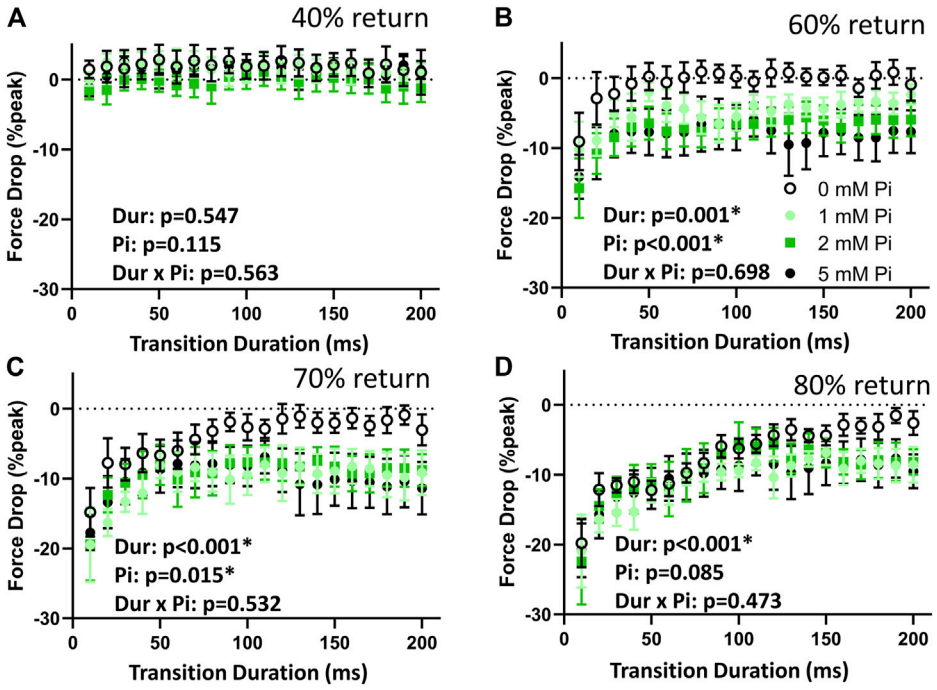

FIGURE 5
Effects of stretch on force drop. **(A)** The force drop at the 40% return time point was not affected by the lengthening protocol at any Pi concentration. The stimulated transients were therefore not affected by lengthening by this measure. **(B)** When no extracellular Pi (0 mM Pi) was available, the drop in force at 60% return timepoint was significant with the 10 ms stretch but was not significant for the more prolonged stretches. This dependence on duration (Dur) was highly significant. The drop in force at the 60% return timepoint was significantly enhanced by Pi. **(C)** With no extracellular Pi, force drop at the 70% return timepoint was significant for stretches of 80 ms duration or shorter. Force drop was significant at all stretch durations when extracellular Pi was available. **(D)** Force drop at the 80% return timepoint was significant for stretches of 170 ms or shorter and for all durations when extracellular Pi was available.

The times to 60%, 70%, and 80% return (Figures 4B–D) for the myofilaments-only transients were shortened by stretch. Shortening was greatest with the fastest stretches as indicated by a significant duration main effect ($p < 0.01$) for these variables. Furthermore, increasing extracellular Pi amplified the effects of stretch as indicated by the significant Pi main effect ($p < 0.01$). There was no significant duration × Pi interaction.

The drop in force at time to 40% return was not affected by stretch or by Pi (Figure 5A) demonstrating again the consistency in the transient characteristics throughout the stretch protocol. The drop in force at times to 60%, 70%, and 80% return (Figure 5B–D) were sensitive to stretch duration ($p < 0.01$) and to Pi ($p < 0.01$ for 60% and $p < 0.05$ for 70%, but not significant for 80%). There were no significant duration × Pi interactions for the measured drop in force at these time points.

Effects of Pi on stretch response in skinned myocardium

To demonstrate the Pi-dependent sensitivity of the force-producing myofilaments in response to stretch, we applied a 1% quick stretch (Figure 6A) to approximately half-activated myofilaments at pCa 5.75. Responses were recorded during exposure to 0, 2, 4, and 8 mM Pi (Figure 6B). The response under relaxed conditions at pCa 8 was subtracted from the responses at pCa 5.75 to produce the stretch response attributable to the myofilaments (Figure 6C). The stress response relative to the isometric stress prior to stretch (Figure 6D) represented the Pi-sensitivity of the myofilament-dependent stress response to quick stretch.

The characteristic stresses (P_1, P_2, and P_3) and rates of release and redevelopment (k_{rel} and k_{redev}) are presented in Figures 6E,F, respectively. Increasing concentrations of Pi induced a reduction in P_1 and P_3 ($p < 0.05$) which suggests that fewer myosin crossbridges are formed in the presence of Pi. Increasing Pi also led to enhancement of the rates k_{rel} and k_{redev} ($p < 0.01$ for both rate parameters) as reported previously by others (Straight et al., 2019).

Modeling stretch response in skinned myocardium

The skinned myocardial response to quick stretch permitted use of previous modeling efforts to interpret the effects of Pi on

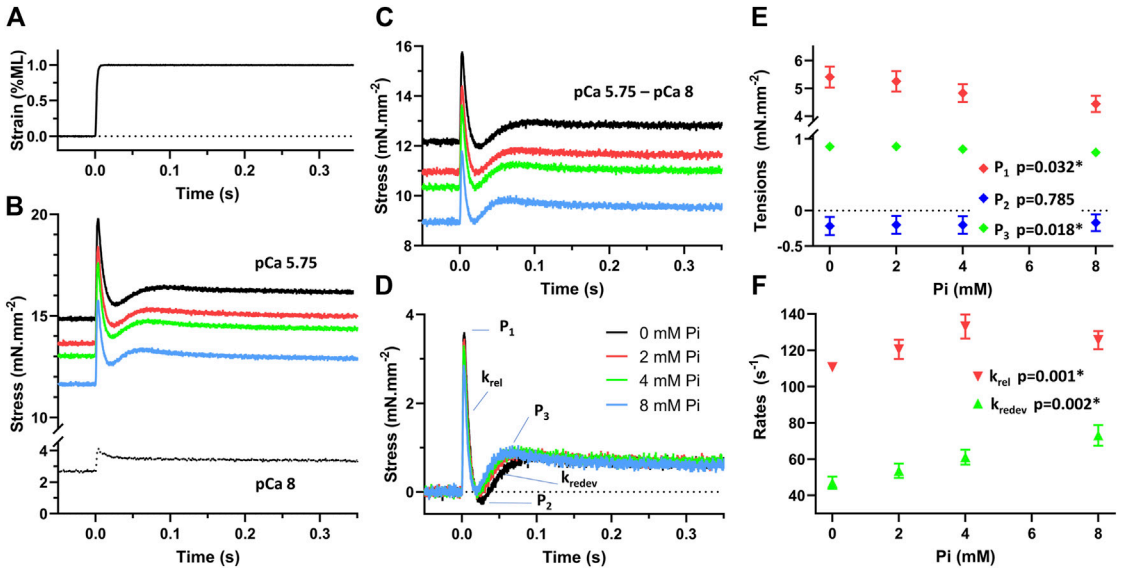

FIGURE 6
Stress response to stretch of demembranated myocardium. **(A)** Muscle was stretched with a quick stretch of 1% muscle length (ML). **(B)** The stress response was recorded under relaxed conditions, pCa 8, and at approximately half-activation, pCa 5.75, with 0, 2, 4, and 8 mM Pi. **(C)** The activated response attributable to the force-producing myofilaments was determined by subtracting the pCa 8 response from the pCa 5.75 responses. **(D)** The stretch response of the myofilaments above the myofilament isometric stress was then determined. This response represents the stress change due to the myofilaments after a quick stretch. **(E)** Peak tension (P_1), lowest tension at nadir (P_2), and recovered tension (P_3) were recorded in response to Pi concentration. P_1 and P_3 were significantly reduced with increasing Pi, $p < 0.05$. P_2 was not found sensitive to Pi. **(F)** Rates of tension release (k_{rel}) and redevelopment (k_{redev}) were significantly enhanced with increasing Pi as indicated by $p < 0.01$.

the stretch-induced detachment rate of myosin. The parameter g_1 represents the change in myosin detachment rate per change in length experienced by the myosin crossbridge while attached. Through the parameters calculated by fitting Eq. 1 to the recorded stress responses, we expected to estimate g_1 using Eq. 2 and then test for its sensitivity to Pi.

An example myofilament-dependent stress response is presented in Figure 7A, and the fit of Eq. 1 to this response demonstrated no more than 3% error relative to the stress at 1 s after the stretch (Palmer et al., 2020). The three terms that make up the model are plotted in Figure 7B. The power-law relaxation term represents the long term elevation in stress that persists after the stretch. The reversal term describes the transient reduction in myofilament-dependent stress and therefore the transient drop in the number of myosin crossbridges producing force. And the drag term is responsible for the initial peak stress immediately after the stretch.

The magnitude for the reversal term, R, was statistically significantly elevated with increasing Pi (Figure 7C, $p < 0.05$), but the relative change was only on the order of 5%–10% across the range of Pi concentrations investigated. The magnitude of the drag term, D, was significantly reduced with increasing Pi (Figure 7C, $p < 0.05$). The ratio R/D, which is required to apply in Eq. 2, was found to be highly significantly enhanced with Pi (Figure 7D, $p < 0.01$).

The myosin attachment rate, f_0, is also necessary for the application of Eq. 2 and calculation of g_1. The value of f_0 was calculated by subtracting k_{redev} from k_{rel}, which according to the model represent ($f_0 + g_0$) and g_0, respectively (Palmer et al., 2020). This attachment rate was not found to be significantly affected by Pi (Figure 7E, $p > 0.05$).

The resulting values for g_1 were found to be significantly enhanced with increasing Pi concentrations (Figure 7F, $p < 0.01$). This result suggests that Pi enhances the increase in myosin detachment rate that occurs with stretch imposed on the crossbridge.

Discussion

This study demonstrated the significance of Pi in stretch-dependent relaxation function of excitable rat myocardium. We confirmed that increasing extracellular Pi enhanced both systolic and diastolic function as reported previously at the whole heart level (Onwochei, 1995; Onwochei et al., 1998). We also found that the rate of relaxation during the transition from late-systole to early-diastole is enhanced by stretch and more so with the higher rates of stretch imposed upon the myocardium, which is consistent with the findings of Chung et al. (2017). The novel result of this study was the demonstration that this increase in

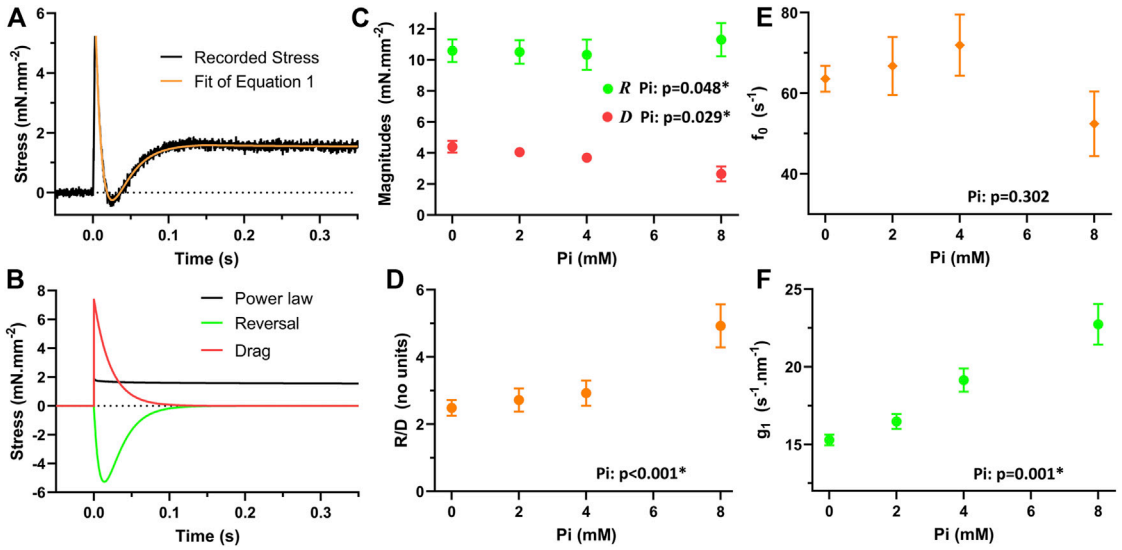

FIGURE 7
Modeled response of myofilaments to quick stretch. **(A)** Eq. 1 was fit to the myofilament response to a quick stretch. **(B)** The three terms of Eq. 1 demonstrate how each term contributes to the response. Power-law relaxation term constitutes the resultant "stretch activated" stress. The reversal term is responsible for the transient drop in the stress. The drag term constitutes the initial brief rise in stress after the stretch. **(C)** The magnitudes of the reversal and drag terms were sensitive to Pi. The magnitude of reversal, *R*, was significantly enhanced with increasing Pi, $p < 0.05$. The magnitude of drag, *D*, was significantly reduced with increasing Pi, $p < 0.05$. **(D)** The ratio of *R/D* was significantly enhanced with increasing Pi, $p < 0.01$. **(E)** According to Eq. 1, the attachment rate, f_0, can be determined by subtracting the k_{redev}, equivalent to g_0 in the model, from k_{rel}, equivalent to $f_0 + g_0$ in the model. This attachment rate was not found to be significantly influenced by Pi. **(F)** The sensitivity of the detachment rate to stretch, g_1 in the model and calculated using Eq. 2, was found to be significantly enhanced with increasing Pi, $p < 0.01$.

relaxation rate by stretch is further enhanced by the presence of Pi. Using skinned myocardium, we were able to demonstrate that Pi enhances the stretch sensitivity of the myosin crossbridge detachment rate, thus providing the underlying mechanism by which stretch enhances relaxation rate at the whole heart (Zile et al., 2015) and myocardial levels (Chung et al., 2017, present work).

The rate of myosin detachment is typically dictated by the rate of MgADP release, which occurs as the myosin crossbridge produces force (Tyska and Warshaw, 2002; Nyitrai and Geeves, 2004). Importantly, the rate of MgADP release is slowed by a resistive load, i.e., an external force that resists the force produce by the crossbridge, which would be experienced by any force-producing myosin being pulled back as would occur during muscle relengthening (Smith and Geeves, 1995; Nyitrai and Geeves, 2004; Veigel et al., 2005; Kad et al., 2007; Liu et al., 2018). If the rate of MgADP release is slowed by lengthening, then the myosin crossbridge lifetime would be prolonged and relaxation would be hindered. The results of the current study and of others (Zile et al., 2015; Chung et al., 2017) do not reflect a slowing of MgADP release from the myosin crossbridge due to sarcomere lengthening. It appears that some other mechanism or some other set of enzymatic steps independent of MgADP release hasten myosin detachment when the sarcomere is lengthened.

One alternative enzymatic pathway to myosin crossbridge force cessation is *via* rebinding of Pi thus prompting reversal of the myosin power stroke (Dantzig et al., 1992; Smith and Geeves, 1995; Woody et al., 2019) or crossbridge detachment (Debold et al., 2013). Cytosolic Pi concentration is expected in the range 2–8 mM in cardiac muscle (Tian et al., 1997; Valkovič et al., 2019). This range of Pi concentrations is known to enhance myosin kinetics and the frequency characteristics of dynamic stiffness of demembranated cardiac muscle (Kawai et al., 2016) as well as skeletal muscle (Ranatunga, 1999). The possibility of reversal of the myosin power stroke is consistent with the findings of reduced Pi release rate during muscle lengthening (Mansfield et al., 2012) in demembranated cardiac muscle. The specific mechanism affected by Pi in excitable myocardial contractile-relaxation function is difficult to study directly, in part because monitoring cytosolic Pi while also measuring myocardial function is not yet technically feasible.

Using demembranated myocardium and applying previous modeling results (Palmer et al., 2020), we were able to demonstrate that Pi enhanced the sensitivity of the rate of myosin crossbridge detachment to stretch of the crossbridge as reflected in the parameter g_1. We were able to estimate g_1 after fitting Eq. 1 to the recorded stress response to a quick stretch and applying the resulting parameter values according to Eq. 2. The current set of results lends some credibility to the model as the

expected enhancement of myosin detachment rate by Pi was demonstrated for the relevant model parameters, i.e., R, D, and g_1.

Limitations

While the demembranated myocardium preparation provided some insights into the effects of Pi on cardiac myosin, it did not mimic the results found with excitable muscle. Specifically, the stretch response in the activated demembranated myocardium was significantly greater in magnitude than that of the relaxed demembranated myocardium. The stretch response of the myofilaments was therefore positively valued even if reduced with increasing Pi. In the excitable muscle, on the other hand, stretches applied during the stimulated tension transient were lower than those under relaxed conditions. The stretch response of the myofilaments was negatively valued.

One difference between the two preparations is the activation status of the thin filament. The thin filament is deactivated during the imposed stretch in the excitable myocardium and activated during stretch in the demembranated myocardium. It appears that the enhancement of relaxation function observed with stretch and further enhanced by Pi reflects the consequences of Pi on myosin detachment and most evident when attachment of myosin crossbridges is inhibited.

Another difference between the two preparations is the presence of Ca^{2+}-regulatory mechanisms in the excitable myocardium. Currently, we are not aware of and do not expect any influence of extracellular Pi on Ca^{2+} handling. Because cytosolic Pi is controlled through the Na^+/Pi cotransporter Pit2 (Jobbagy et al., 1999), any elevation in cytosolic Pi would be expected to be accompanied by an elevation in cytosolic Na^+, which would diminish sodium-calcium exchanger (NCX) activity and raise intracellular Ca^{2+} (Bers, 2002). This hypothetical scenario represents an attractive explanation for the enhanced systolic function with increasing extracellular Pi, but it would be contrary to the enhanced diastolic function also observed with extracellular Pi. We would also not attribute the Pi-enhancement of isometric contraction to an increase in calcium-sensitivity of the myofilaments, because Pi is known to reduce the calcium-sensitivity of myofilament force production (Kentish, 1986; Millar and Homsher, 1990).

We would instead attribute the Pi-enhancement of isometric contraction to the enhanced velocity of contraction that accompanies increasing Pi despite the reduction in crossbridge number (Tesi et al., 2000; Hinken and McDonald, 2004). The enhanced velocity of contraction with increasing Pi would have to make up for the loss of isometric force with increasing Pi. At this point, this is conjecture, and further studies into the mechanism underlying enhanced systolic function by extracellular Pi are warranted.

One final limitation to the current study is the lack of control for sarcomere length in the excitable myocardium. It is notoriously difficult to visualize and control for sarcomere length in myocardial preparations greater than 0.2 mm in diameter, but we would expect the sarcomere length of the excitable myocardium to be near the top of the force-length relatation between 2.1 and 2.3 μm (ter Keurs et al., 1980). In addition, the preparation was held isometric. Working myocardium would be expected to shorten during systole and sarcomere lengths at end-systole would be less than 1.9 μm (Gordon and Pollack, 1980). The effects of Pi on lengthening-induced relaxation, as we have examined in the current work, may be most relevant at these shorter sarcomere lengths.

Conclusion

Our findings suggest that Pi enhances the stretch-dependent increase in cardiac myosin crossbridge detachment rate. Importantly, we found that this effect of Pi is most prominent with faster stretches, which is consistent with the findings of previously investigators (Chung et al., 2017). While these findings were observed by adjusting extracellular Pi, they are reflective of cytosolic Pi maintained by the Na^+/Pi cotransporter Pit2, whose activity can be influenced by certain isoforms of protein kinase-C (Onwochei, 1995; Onwochei et al., 1998; Jobbagy et al., 1999). The modulation of cytosolic Pi *via* protein kinase control of Pit2 activity therefore represents a possible pathway for adjusting myocardial relaxation function.

Data availability statement

The raw data supporting the conclusion of this article will be made available by the authors, without undue reservation.

Ethics statement

The animal study was reviewed and approved by the Institutional Animal Care and Use Committee of the University of Vermont Larner College of Medicine.

Author contributions

All authors contributed to conception and design of the study. JW and SB acquired the data and performed primary analyses. BP performed statistical analyses. JW wrote the first draft of the manuscript. JW and BP additional versions of the

manuscript. All authors contributed to manuscript revision, read, and approved the submitted version.

Funding

This work was supported by National Institutes of Health (R44HL137603, BP) and by National Science Foundation (1660908, BP).

Conflict of interest

Author BP was employed by the company IonOptix, LLC.

The remaining authors declare that the research was conducted in the absence of any commercial or financial relationships that could be construed as a potential conflict of interest.

Publisher's note

All claims expressed in this article are solely those of the authors and do not necessarily represent those of their affiliated organizations, or those of the publisher, the editors and the reviewers. Any product that may be evaluated in this article, or claim that may be made by its manufacturer, is not guaranteed or endorsed by the publisher.

References

Bers, D. M. (2002). Cardiac excitation-contraction coupling. *Nature* 415 (6868), 198–205. doi:10.1038/415198a

Chung, C. S., Hoopes, C. W., and Campbell, K. S. (2017). Myocardial relaxation is accelerated by fast stretch, not reduced afterload. *J. Mol. Cell. Cardiol.* 103, 65–73. doi:10.1016/j.yjmcc.2017.01.004

Dantzig, J. A., Goldman, Y. E., Millar, N. C., Lacktis, J., and Homsher, E. (1992). Reversal of the cross-bridge force-generating transition by photogeneration of phosphate in rabbit psoas muscle fibres. *J. Physiol.* 451, 247–278. doi:10.1113/jphysiol.1992.sp019163

Debold, E. P., Walcott, S., Woodward, M., and Turner, M. A. (2013). Direct observation of phosphate inhibiting the force-generating capacity of a miniensemble of Myosin molecules. *Biophys. J.* 105 (10), 2374–2384. doi:10.1016/j.bpj.2013.09.046

Dunlay, S. M., Roger, V. L., and Redfield, M. M. (2017). Epidemiology of heart failure with preserved ejection fraction. *Nat. Rev. Cardiol.* 14 (10), 591–602. doi:10.1038/nrcardio.2017.65

Gordon, A. M., and Pollack, G. H. (1980). Effects of calcium on the sarcomere length-tension relation in rat cardiac muscle. Implications for the Frank-Starling mechanism. *Circ. Res.* 47 (4), 610–619. doi:10.1161/01.res.47.4.610

Hinken, A. C., and McDonald, K. S. (2004). Inorganic phosphate speeds loaded shortening in rat skinned cardiac myocytes. *Am. J. Physiol. Cell Physiol.* 287 (2), C500–C507. doi:10.1152/ajpcell.00049.2004

Jacquillet, G., and Unwin, R. J. (2019). Physiological regulation of phosphate by vitamin D, parathyroid hormone (PTH) and phosphate (Pi). *Pflugers Arch.* 471 (1), 83–98. doi:10.1007/s00424-018-2231-z

Jobbagy, Z., Olah, Z., Petrovics, G., Eiden, M. V., Leverett, B. D., Dean, N. M., et al. (1999). Up-regulation of the Pit-2 phosphate transporter/retrovirus receptor by protein kinase C epsilon. *J. Biol. Chem.* 274 (11), 7067–7071. doi:10.1074/jbc.274.11.7067

Kad, N. M., Patlak, J. B., Fagnant, P. M., Trybus, K. M., and Warshaw, D. M. (2007). Mutation of a conserved glycine in the SH1-SH2 helix affects the load-dependent kinetics of myosin. *Biophys. J.* 92 (5), 1623–1631. doi:10.1529/biophysj.106.097618

Kass, D. A., Bronzwaer, J. G., and Paulus, W. J. (2004). What mechanisms underlie diastolic dysfunction in heart failure? *Circ. Res.* 94 (12), 1533–1542. doi:10.1161/01.RES.0000129254.25507.d6

Kawai, M., Karam, T. S., Michael, J. J., Wang, L., and Chandra, M. (2016). Comparison of elementary steps of the cross-bridge cycle in rat papillary muscle fibers expressing α- and β-myosin heavy chain with sinusoidal analysis. *J. Muscle Res. Cell Motil.* 37 (6), 203–214. doi:10.1007/s10974-016-9456-2

Kentish, J. C. (1986). The effects of inorganic phosphate and creatine phosphate on force production in skinned muscles from rat ventricle. *J. Physiol.* 370, 585–604. doi:10.1113/jphysiol.1986.sp015952

Liu, C., Kawana, M., Song, D., Ruppel, K. M., and Spudich, J. A. (2018). Controlling load-dependent kinetics of β-cardiac myosin at the single-molecule level. *Nat. Struct. Mol. Biol.* 25 (6), 505–514. doi:10.1038/s41594-018-0069-x

Manghat, P., Sodi, R., and Swaminathan, R. (2014). Phosphate homeostasis and disorders. *Ann. Clin. Biochem.* 51, 631–656. doi:10.1177/0004563214521399

Mansfield, C., West, T. G., Curtin, N. A., and Ferenczi, M. A. (2012). Stretch of contracting cardiac muscle abruptly decreases the rate of phosphate release at high and low calcium. *J. Biol. Chem.* 287 (31), 25696–25705. doi:10.1074/jbc.M112.373498

Millar, N. C., and Homsher, E. (1990). The effect of phosphate and calcium on force generation in glycerinated rabbit skeletal muscle fibers. A steady-state and transient kinetic study. *J. Biol. Chem.* 265 (33), 20234–20240. doi:10.1016/s0021-9258(17)30494-5

Nyitrai, M., and Geeves, M. A. (2004). Adenosine diphosphate and strain sensitivity in myosin motors. *Philos. Trans. R. Soc. Lond. B Biol. Sci.* 359 (1452), 1867–1877. doi:10.1098/rstb.2004.1560

Onwochei, M. O., Ofori, A. O., and Agodoa, I. L. (1998). Interaction between Na+/phosphate-cotransporter and the adrenoceptors in myocardial depression. *J. Cardiovasc. Pharmacol.* 31 (1), 10–17. doi:10.1097/00005344-199801000-00002

Onwochei, M. O. (1995). Role of Na+/phosphate-cotransporter in myocardial contractile responses to alpha 1-agonist. *J. Cardiovasc. Pharmacol.* 25 (5), 833–839. doi:10.1097/00005344-199505000-00021

Palmer, B. M., Swank, D. M., Miller, M. S., Tanner, B. C. W., Meyer, M., and LeWinter, M. M. (2020). Enhancing diastolic function by strain-dependent detachment of cardiac myosin crossbridges. *J. Gen. Physiol.* 152 (4), e201912484. doi:10.1085/jgp.201912484

Ranatunga, K. W. (1999). Effects of inorganic phosphate on endothermic force generation in muscle. *Proc. Biol. Sci.* 266 (1426), 1381–1385. doi:10.1098/rspb.1999.0791

Runte, K. E., Bell, S. P., Selby, D. E., Häußler, T. N., Ashikaga, T., LeWinter, M. M., et al. (2017). Relaxation and the role of calcium in isolated contracting myocardium from patients with hypertensive heart disease and heart failure with preserved ejection fraction. *Circ. Heart Fail.* 10 (8), e004311. doi:10.1161/CIRCHEARTFAILURE.117.004311

Selby, D. E., Palmer, B. M., LeWinter, M. M., and Meyer, M. (2011). Tachycardia-induced diastolic dysfunction and resting tone in myocardium from patients with a normal ejection fraction. *J. Am. Coll. Cardiol.* 58 (2), 147–154. doi:10.1016/j.jacc.2010.10.069

Smith, D. A., and Geeves, M. A. (1995). Strain-dependent cross-bridge cycle for muscle. II. Steady-state behavior. *Biophys. J.* 69 (2), 538–552. doi:10.1016/S0006-3495(95)79927-1

Stelzer, J. E., Patel, J. R., and Moss, R. L. (2006). Protein kinase A-mediated acceleration of the stretch activation response in murine skinned myocardium is eliminated by ablation of cMyBP-C. *Circ. Res.* 99, 884–890. doi:10.1161/01.RES.0000245191.34690.66

Straight, C. R., Bell, K. M., Slosberg, J. N., Miller, M. S., and Swank, D. M. (2019). A myosin-based mechanism for stretch activation and its possible role revealed by varying phosphate concentration in fast and slow mouse skeletal muscle fibers. *Am. J. Physiol. Cell Physiol.* 317 (6), C1143–C1152. doi:10.1152/ajpcell.00206.2019

ter Keurs, H. E., Rijnsburger, W. H., van Heuningen, R., and Nagelsmit, M. J. (1980). Tension development and sarcomere length in rat cardiac trabeculae.

Evidence of length-dependent activation. *Circ. Res.* 46 (5), 703–714. doi:10.1161/01.res.46.5.703

Tesi, C., Colomo, F., Nencini, S., Piroddi, N., and Poggesi, C. (2000). The effect of inorganic phosphate on force generation in single myofibrils from rabbit skeletal muscle. *Biophys. J.* 78 (6), 3081–3092. doi:10.1016/S0006-3495(00)76845-7

Tian, R., Christe, M. E., Spindler, M., Hopkins, J. C., Halow, J. M., Camacho, S. A., et al. (1997). Role of MgADP in the development of diastolic dysfunction in the intact beating rat heart. *J. Clin. Invest.* 99 (4), 745–751. doi:10.1172/JCI119220

Tyska, M. J., and Warshaw, D. M. (2002). The myosin power stroke. *Cell Motil. Cytoskelet.* 51 (1), 1–15. doi:10.1002/cm.10014

Valkovič, L., Clarke, W. T., Schmid, A. I., Raman, B., Ellis, J., Watkins, H., et al. (2019). Measuring inorganic phosphate and intracellular pH in the healthy and hypertrophic cardiomyopathy hearts by *in vivo* 7T ^{31}P-cardiovascular magnetic resonance spectroscopy. *J. Cardiovasc. Magn. Reson.* 21 (1), 19. doi:10.1186/s12968-019-0529-4

Veigel, C., Schmitz, S., Wang, F., and Sellers, J. R. (2005). Load-dependent kinetics of myosin-V can explain its high processivity. *Nat. Cell Biol.* 7 (9), 861–869. doi:10.1038/ncb1287

Woody, M. S., Winkelmann, D. A., Capitanio, M., Ostap, E. M., and Goldman, Y. E. (2019). Single molecule mechanics resolves the earliest events in force generation by cardiac myosin. *Elife* 8, e49266. doi:10.7554/eLife.49266

Zile, M. R., Baicu, C. F., Ikonomidis, J. S., Stroud, R. E., Nietert, P. J., Bradshaw, A. D., et al. (2015). Myocardial stiffness in patients with heart failure and a preserved ejection fraction: Contributions of collagen and titin. *Circulation* 131 (14), 1247–1259. doi:10.1161/CIRCULATIONAHA.114.013215

frontiers | Frontiers in Physiology

TYPE Review
PUBLISHED 26 September 2022
DOI 10.3389/fphys.2022.975076

OPEN ACCESS

EDITED BY
Shin'Ichi Ishiwata,
Waseda University, Japan

REVIEWED BY
Yale Goldman,
University of Pennsylvania, United States
Charles Redwood,
University of Oxford, United Kingdom
Thomas Charles Irving,
Illinois Institute of Technology,
United States

*CORRESPONDENCE
Kathleen M. Ruppel,
kruppel@stanford.edu

SPECIALTY SECTION
This article was submitted to Striated Muscle Physiology,
a section of the journal
Frontiers in Physiology

RECEIVED 21 June 2022
ACCEPTED 22 August 2022
PUBLISHED 26 September 2022

CITATION
Kawana M, Spudich JA and Ruppel KM (2022), Hypertrophic cardiomyopathy: Mutations to mechanisms to therapies. *Front. Physiol.* 13:975076.
doi: 10.3389/fphys.2022.975076

Hypertrophic cardiomyopathy: Mutations to mechanisms to therapies

Masataka Kawana[1,2], James A. Spudich[1] and Kathleen M. Ruppel[1]*

[1]Department of Biochemistry, Stanford University School of Medicine, Stanford, CA, United States, [2]Department of Medicine, Division of Cardiovascular Medicine, Stanford University School of Medicine, Stanford, CA, United States

Hypertrophic cardiomyopathy (HCM) affects more than 1 in 500 people in the general population with an extensive burden of morbidity in the form of arrhythmia, heart failure, and sudden death. More than 25 years since the discovery of the genetic underpinnings of HCM, the field has unveiled significant insights into the primary effects of these genetic mutations, especially for the myosin heavy chain gene, which is one of the most commonly mutated genes. Our group has studied the molecular effects of HCM mutations on human β-cardiac myosin heavy chain using state-of-the-art biochemical and biophysical tools for the past 10 years, combining insights from clinical genetics and structural analyses of cardiac myosin. The overarching hypothesis is that HCM-causing mutations in sarcomere proteins cause hypercontractility at the sarcomere level, and we have shown that an increase in the number of myosin molecules available for interaction with actin is a primary driver. Recently, two pharmaceutical companies have developed small molecule inhibitors of human cardiac myosin to counteract the molecular consequences of HCM pathogenesis. One of these inhibitors (mavacamten) has recently been approved by the FDA after completing a successful phase III trial in HCM patients, and the other (aficamten) is currently being evaluated in a phase III trial. Myosin inhibitors will be the first class of medication used to treat HCM that has both robust clinical trial evidence of efficacy and that targets the fundamental mechanism of HCM pathogenesis. The success of myosin inhibitors in HCM opens the door to finding other new drugs that target the sarcomere directly, as we learn more about the genetics and fundamental mechanisms of this disease.

KEYWORDS

myosin, hypertrophic cardiomyopathy, super relaxed state, mavacamten, omecamtiv mercarbil

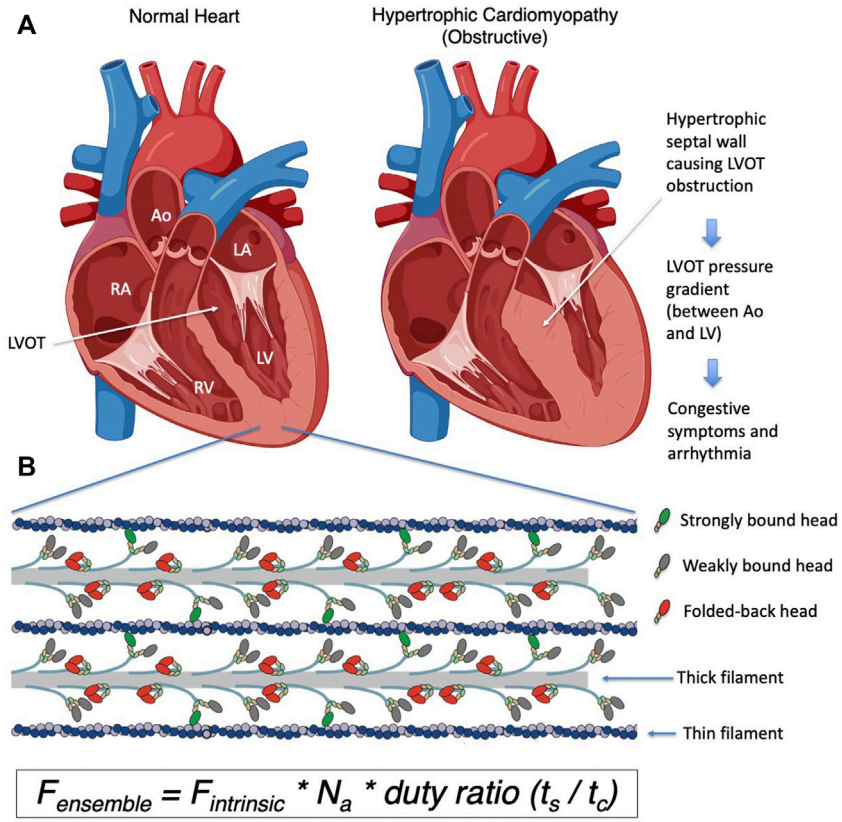

FIGURE 1
(A) Schematic representation of a normal heart and a heart with obstructive hypertrophic cardiomyopathy. The obstruction to blood flow occurs when the septal hypertrophy impedes blood flow from the left ventricular cavity to the aorta *via* the left ventricular outflow tract or LVOT, and a pressure gradient from the left ventricle to the aorta occurs. **(B)** A closeup schematic drawing of a sarcomere, showing the myosin containing thick filaments interdigitating with the actin containing thin filaments. The myosin heads highlighted in red are folded back onto the thick filament and are unavailable to interact with actin. Myosin heads bound to actin are shown in green, and heads that are released from the thick filament but not bound to actin are shown in grey. The number of available myosin heads (N_a) is the sum of green and grey heads within each sarcomere. The duty ratio is defined as the proportion of the total cycle time (t_c) an available myosin head spends strongly bound to actin (t_s). This ratio (t_s/t_c) determines the proportion of available heads that are strongly bound to actin in the sarcomere during systole. LA, left atrium; LV, left ventricle; RA, right atrium; RV, right ventricle; Ao, aorta; LVOT, left ventricular outflow tract. Figure 1A was created using BioRender.

Introduction

Hypertrophic cardiomyopathy (HCM) is the most common form of inherited heart disease, affecting more than 1 in 500 people in the general population (Semsarian et al., 2015). It is characterized by left ventricular hypertrophy (LVH) without an alternative etiology such as aortic stenosis or systemic hypertension, loss of left ventricular cavity size, and is associated with significant comorbidities including heart failure and arrhythmia. The earliest manifestation of the disease is impaired diastolic function and generally hypercontractile left ventricular systolic function by echocardiography. Except for the rare early-onset cases, left ventricular wall thickness is typically normal at first and becomes thicker during adolescence and early adulthood. As wall thickness increases, the size of the LV cavity decreases, and diastolic dysfunction also progresses (Figure 1A). The clinical manifestations are driven by increased pressure in the ventricle from these alterations in the systolic and diastolic function that are fundamentally based on increased myosin-actin crossbridge formation. The increase in left ventricular and atrial pressures leads to elevated pulmonary pressure and congestion which are hallmarks of congestive heart failure, along with an increased risk of both ventricular and atrial arrhythmias. Moreover, patients are at higher risk of sudden cardiac death due to ventricular arrhythmias that are thought to be due to an increased burden of myocardial fibrosis in the hypertrophied ventricle (Seidman and Seidman, 2001).

Until recently, the fundamental mechanism underlying these pathophysiological changes was poorly understood, and hence the available therapies for HCM rely on targeting the secondary physiological changes seen at the organ level. Betablockers and

calcium channel blockers are used to suppress the observed hyperdynamic systolic function and arrhythmias. While these agents have been used for decades, there is only anecdotal evidence to support their use in HCM patients and they are often poorly tolerated in young patients. When the LVH primarily involves the septum and obstructs blood flow into the left ventricular outflow tract (LVOT) (Figure 1A), the pressure in the LV further increases, leading to worsening symptoms. Mechanical solutions to this obstruction include either surgically resecting the myocardial tissue that is obstructing the flow (myectomy) or injecting alcohol into the coronary artery that supplies the septum to induce a controlled myocardial infarction to remove excess tissue (alcohol septal ablation). These procedures are invasive and require technical expertise in performing adequate reduction of the obstruction. Hence, a medical therapy that targets the fundamental pathogenesis of HCM and can inhibit and potentially reverse the hypertrophic process, especially hypertrophy that causes the obstruction, has been desired for many decades.

The contractility of the heart is central to cardiovascular physiology and is determined by loading conditions (i.e. preload and afterload) and intrinsic properties of the contractile apparatus of the cardiac myocyte. The sarcomere–comprised of interdigitating myosin-containing thick filaments and actin-containing thin filaments–is the fundamental unit of the contractile apparatus (Figure 1B). Myosin is the motor protein that uses the energy produced by hydrolysis of ATP to undergo a power stroke when bound to actin to create force and sarcomere shortening, which is the basis of cardiac contraction. Other proteins in the sarcomere, such as cardiac myosin binding protein C (MyBP-C) and titin, modulate the effect and efficiency of this actin-myosin interaction in response to physiological stimulation and pharmacological intervention. As discussed below, many genetic variants in sarcomere proteins are known to cause hypertrophic and dilated cardiomyopathies, suggesting that subtle changes in sarcomere function can lead to a significant change in myocardial morphology and function. Thus, understanding the mechanism of disease pathogenesis requires a molecular analysis of this actin-myosin interaction.

In this review, we summarize our current understanding of the molecular basis of contractility, our strategy for assessing molecular determinants of contractility, progress in understanding the effect of mutations in cardiac myosin that cause hypertrophic cardiomyopathy, and the recent development of novel sarcomere modulators. Given the space limitation and the importance of using human proteins (described below) in assessing the mechanism of HCM, this review focuses primarily on studies that utilized a reconstituted system of expressed and purified human proteins, as well as some studies of human-induced pluripotent stem cell-derived cardiomyocytes (hiPSC-CM).

Understanding the ensemble force of the sarcomere

Biochemical and biophysical determinants of myosin function

We begin by defining the molecular determinants of contractility. By the mid-20th century, biochemists and physiologists had determined the basic components of the contractile elements of muscle to be myosin and actin (Huxley and Hanson, 1959), as well as regulatory units of actomyosin crossbridge interactions including tropomyosin and the troponin complex. Myosin is a hexamer comprised of two heavy chains and two pairs of light chains. The heavy chains form a coiled-coil rod to form an elongated tail, and globular heads which interact with actin. Myosin and myosin binding protein C (MyBP-C) comprise the major components of the thick filament, whereas actin, troponin and tropomyosin form regulated thin filaments (RTF) (Bailey et al., 1946). Hugh Huxley provided compelling evidence for a sliding filament model of muscle contraction based on observations of thin and thick filaments by electron microscopy and on X-ray diffraction patterns in the 1950s, and further proposed a swinging cross-bridge hypothesis of muscle contraction in 1969 (Huxley, 1969), which has been supported over the years as we have learned details of how myosin works as a molecular motor.

Myosin is the first protein to be identified as a mechanoenzyme–an enzyme that uses the chemical energy from hydrolysis of ATP and converts it to mechanical movement–in this case the displacement of actin filaments within the sarcomere (Figure 2A). Upon ATP binding, myosin detaches from actin and hydrolyzes the bound ATP to ADP*Pi, which remain bound to the active site. With this binding and hydrolysis, the motor exhibits significant structural changes from a post-stroke to a pre-powerstroke (PPS) state. Myosin in the PPS state then binds to actin, which triggers release of the Pi associated with a major part of the power stroke. ADP is then released, accompanied by a small further stroke to complete the power stroke. This post-stroke state myosin is released from actin when ATP binds to the nucleotide binding pocket.

We focus experimentally on key parameters of the above described chemomechanical cycle as follows: First, in cardiac myocytes where ATP concentration is saturating and the myosin motor has a low duty ratio (described below), the rate-limiting step of the whole cycle is the phosphate release rate (k_{cat}), and the inverse of k_{cat} equals the total cycle time (t_c) of the whole reaction cycle. Within this cycle, particular interest is paid to how long the myosin stays strongly bound to actin (the duration is termed the strongly bound state time, or t_s). The ratio of t_s and t_c ($= t_s/t_c$) is termed the "duty ratio" of the actin-myosin interaction in the sarcomere (Figure 2A). N_a is the number of myosin heads that are accessible to interact with actin, and this is related to the conformation of myosin in the thick filament (Figure 2B). The

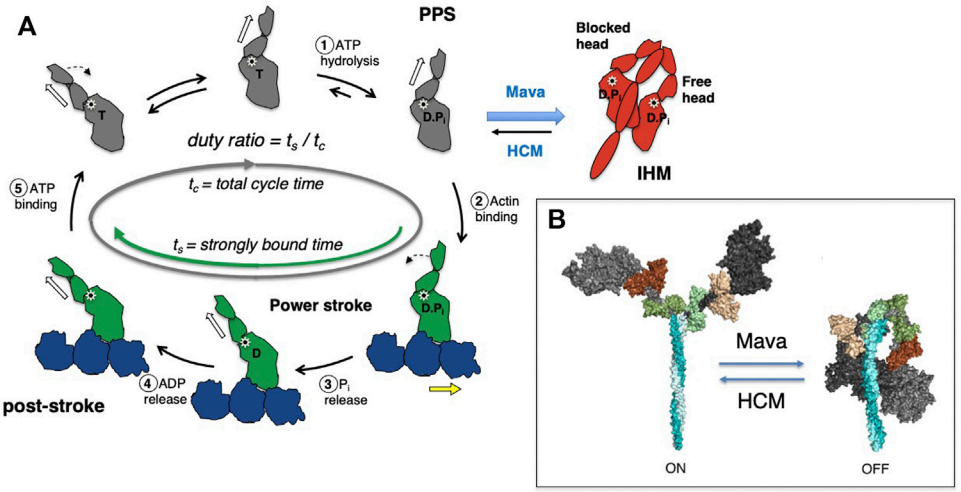

FIGURE 2
(A) Chemomechanical cycle of myosin interacting with actin. Only one head (S1 motor) is being depicted in the cycle for clarity. *1)* S1 hydrolyzes ATP to ADP and phosphate (Pi), which remain bound in the active site, stabilizing the pre-powerstroke state (PPS, white arrow is tilted to the right). *2)* The PPS S1-ADP-Pi binds strongly (grey to green) to actin (blue). *3)* Pi is released while S1 is bound to actin and the lever arm swings to the left (black dashed arrow) about a fulcrum point (black star), moving the actin filament to the right (yellow arrow) with respect to the myosin thick filament (power stroke). *4)* ADP release allows a further small stroke to the poststroke position (white arrow to the left) and frees the active site for binding of ATP. *5)* ATP binds and weakens the interaction of S1 and actin, releasing S1 from the actin filament. S1 undergoes a recovery stroke to the PPS state (dotted arrow; white arrow moves from the left to the right). S1 in the pre-powerstroke configuration can be pulled into the folded IHM state (red). Mavacamten (Mava) affects the equilibrium of these heads as shown, and stabilizes the IHM form, whereas HCM mutations destabilize the IHM in many cases and shift more myosin into the cycle. In the cycle, weakly bound and detached S1 motors are shown in gray, and strongly bound motors are shown in green. **(B)** Structural homology models of cardiac myosin showing the effect of HCM mutations shifting the equilibrium toward the open state (ON), and mavacamten treatment shifting the equilibrium toward the folded state (OFF).

power stroke produced by the myosin produces force against the actin filament and displaces the actin filament. The distance by which actin is displaced by the myosin power stroke is termed stroke size (d), and the force generated by an individual myosin power stroke is termed intrinsic force ($F_{intrinsic}$). These parameters are related to the physical properties of the myosin motor (Uyeda et al., 1990). As every myosin head acts as an independent force generator, we define the net contractile force of the sarcomere, or ensemble force ($F_{ensemble}$, Figure 1B), using the above fundamental parameters of actin-myosin crossbridge formation as follows (Spudich, 2014):

$$F_{ensemble} = F_{intrinsic} * N_a * \text{duty ratio}$$
$$= F_{intrinsic} * N_a * t_S/t_C$$

Various experimental methods have been developed to study each parameter in detail. First, biochemical and structural analysis of the actin-myosin ATPase cycle has been vital to our understanding of sarcomere function (De La Cruz and Ostap, 2004; Sweeney and Houdusse, 2010; Walklate et al., 2016). Measurements of the rate and equilibrium constants of each step in the cycle, including actin-myosin binding and dissociation, ATP binding, ATP hydrolysis, phosphate release, and ADP release and binding have been extensively performed (*see* review by De La Cruz and Ostap (De La Cruz and Michael Ostap, 2009)). As the rate-limiting step of the cardiac myosin cycle is the release of phosphate from the actin-myosin-ADP*Pi complex, its ATPase activity is determined by an actin-activated ATPase assay measuring the rate of phosphate release (De La Cruz and Michael Ostap, 2009; Sommese et al., 2013a; Nag et al., 2015; Adhikari et al., 2016; Kawana et al., 2017). To interrogate the biophysical aspects of the actin-myosin interaction, *in vitro* motility assays were developed by Kron and Spudich (Kron and Spudich, 1986) and Yanagida et al. (Yanagida et al., 1984) in the 1980s. In the Kron and Spudich assay fluorescently-labeled actin filaments are observed sliding over a glass surface coated with myosin (Figure 3A), enabling the visualization of the displacement of actin filaments by the motor protein under a microscope. The velocity of a sliding actin filament is proportional to the distance moved divided by time (Uyeda et al., 1990; Uyeda et al., 1996); in this case the myosin stroke size divided by the time that myosin spends strongly bound to actin. Hence, $v \propto d/t_s$. *In vitro* motility assays have been used to characterize the function of different isoforms of myosin, including the cardiac isoforms (UP et al., 2004; Debold et al., 2007; Lowey et al., 2008). When myosin is the only protein on the surface capable of interacting with actin and bovine serum albumin is used to block non-specific interactions between the actin filament and the surface, the assay is assumed to represent

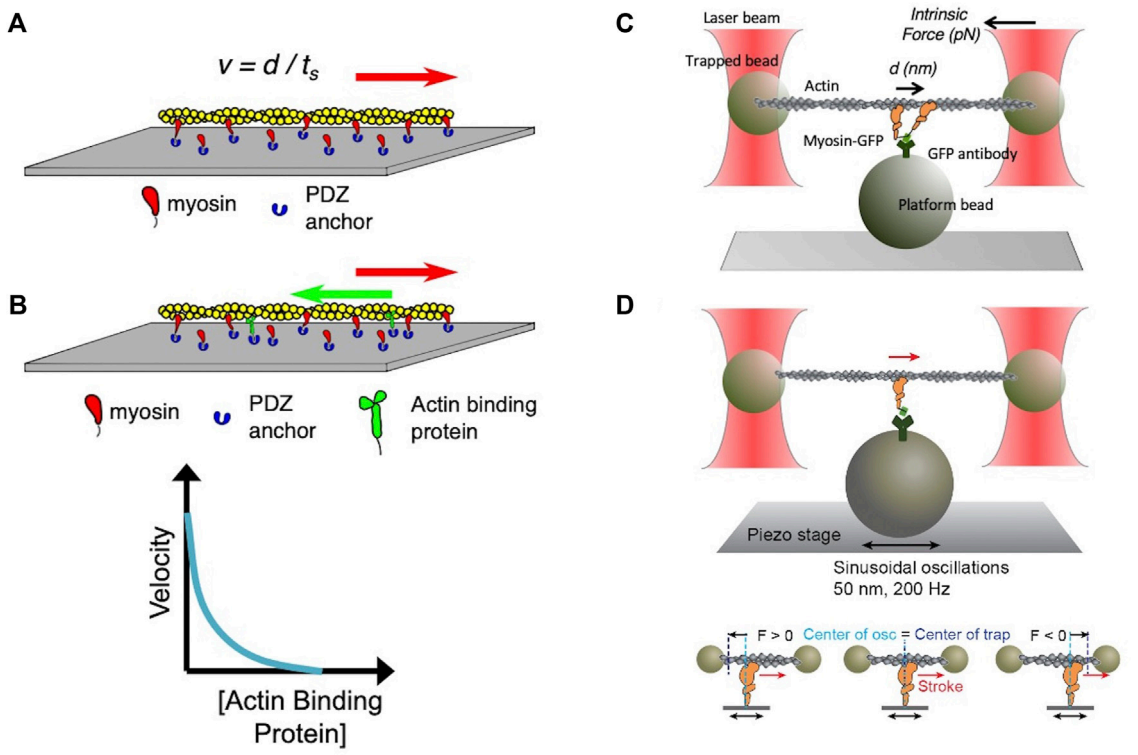

FIGURE 3
(A) Schematic of an *in vitro* motility assay. Myosin is anchored with its C-terminus bound *via* an anchoring peptide to a PDZ protein on a glass surface. Fluorescently labeled actin is added, and in the presence of ATP the actin filament is propelled by the myosin head powerstrokes. The unloaded gliding velocity is proportional to the powerstroke (d) divided by the strongly bound state time (t_s). **(B)** Schematic of a loaded *in vitro* motility assay. Myosin and an actin-binding protein (such as utrophin) are anchored on the surface, and fluorescent actin filaments are added in the presence of ATP. The actin-binding protein impedes (puts a load on) the actin filament movement. The velocity of the gliding filament is plotted against the concentration of the actin-binding protein to obtain a force-velocity curve. **(C)** Schematic of the unloaded single molecule optical trap assay. Two beads coated with neutravidin are trapped by an infrared laser beam, and a biotinylated actin filament is attached at its ends to the two optically trapped beads to form an actin dumbbell. The position of each of the trapped beads is determined accurately by two position-sensitive detectors (PSD) located in the optical path above the trapped beads. Myosin is attached to the platform bead at a very low concentration to ensure only one myosin is attached to the platform bead to measure single molecule behavior. As the myosin interacts with the actin dumbbell, the myosin produces a stroke (the single head is seen to stroke to the right). At low trap force compared to the force produced by the myosin, the distance of the stroke (d) is measured by the displacement of the trapped bead's positions. Intrinsic force is measured by applying an instantaneous counter force by increasing the trap strength to match the myosin force, bringing the beads to the original position. The matching trap force can be read out. **(D)** Schematic of the harmonic force spectroscopy optical trap. Oscillations of the piezo stage on which myosin (orange) is attached in the three-bead optical trap system (top) apply a sinusoidal load (force) to myosin upon attachment to actin (bottom). The time myosin is bound to actin (t_s) is recorded and analyzed against the applied load on the myosin molecule to obtain detachment rates and force sensitivity. Figures adapted from Aksel et al. (Aksel et al., 2015) and Liu et al. (Liu et al., 2018).

an unloaded state of actomyosin interaction. As muscle is always operating under some load *in vivo*, modification of the *in vitro* motility assay was done to simulate more physiological conditions by adding an actin-binding protein on the surface (Greenberg et al., 2010; Greenberg and Moore, 2010; Aksel et al., 2015) to create a "loaded *in vitro* motility assay" (Figure 3B). Further spatial optimization of the *in vitro* motility assay has been carried out using a DNA nanotube scaffold that allows precise spacing of a defined number of myosin motors on a track along which actin filaments can be propelled, more closely mimicking the natural organization of the myosin and actin in the muscle sarcomere (Hariadi et al., 2015).

In the 1990s, Finer et al. (Finer et al., 1994) built a dual-beam laser trap for single-molecule analysis that allowed them to measure fundamental aspects of the actomyosin interaction including the distance by which myosin moves actin during a single ATPase cycle (stroke size d ≈ 10 nm) and the intrinsic force a single myosin exerts on an actin filament ($F_{intrinsic} \approx 5$ pN) (Figure 3C). In the past several decades, the laser trap system has been used by many other laboratories, and it has undergone continuous upgrading to allow increasingly precise measurements of d, $F_{intrinsic}$ and t_s (Sung et al., 2010). Furthermore, the use of dual-beam laser traps with either a high-speed feedback system or harmonic force spectroscopy

(HFS) (Veigel et al., 2003; Veigel et al., 2005; Sung et al., 2015) allowed the measurement of load-dependent changes in myosin function at the single molecule level. In HFS, the durations of binding events between a single myosin and an actin filament under different load forces are measured at ATP concentrations (2 mM) approaching physiological (Figure 3D). The sample stage oscillates sinusoidally so that by the randomness of where myosin initially attaches to actin, a range of mean forces are automatically applied over the course of many binding events (Sung et al., 2015; Vander Roest et al., 2021). This technique has been used to quantify changes in the load-dependent detachment of myosin from actin filaments.

Both the *in vitro* motility assay and the single molecule assay have been used to study a wide variety of muscle and non-muscle myosin motors. However, *in vitro* studies of mutated forms of human striated muscle myosins were limited to biopsy samples due to the difficulty in expressing functional recombinant cardiac or skeletal muscle myosins. With the demonstration that striated muscle motors expressed in a mouse myoblast cell line containing muscle-specific chaperone proteins are fully functional, a new era was ushered in in which recombinant human cardiac myosin (Srikakulam and Winkelmann, 2004; Liu et al., 2008; Resnicow et al., 2010) can be highly purified and studied using these and other assays, as detailed below.

Myosin conformation determines the number of myosin heads functionally accessible to interact with actin in the sarcomere

The above-described enzymatic and biophysical assays have been the main tools used to study the function of myosin as a motor protein. However, while we studied the effects of HCM-causing mutations on β-cardiac myosin motor function as described below, it became apparent that in order to have a full understanding of sarcomere function using the $F_{ensemble}$ calculation, we needed to understand what determines N_a. It was already well understood that the troponin-tropomyosin containing thin filament regulates the interaction between myosin heads and actin by blocking the ability of myosin to bind to the thin filament when Ca^{2+} concentrations are low (i.e. diastole, *see* part 3 below). Over the last several years, it has become increasingly clear that the actomyosin interaction is also regulated at the level of the thick filament.

Structural evidence for thick filament-mediated regulation of N_a was first provided by Wendt and others who determined a cryo-electron microscopic structure of unphosphorylated smooth muscle myosin (Wendt et al., 1999) in which the motor domains are folded-back asymmetrically onto the proximal portion of the coiled-coil tail. This folded-back state of myosin, later termed the "interacting heads motif" or IHM, was postulated to represent a sequestered state of smooth muscle myosin in which the motor domains were positioned such that one or both heads were unavailable to interact with actin. Subsequently, similar folded structures were reported for other myosins including skeletal (Woodhead et al., 2005) and cardiac myosin (Zoghbi et al., 2008), and an electron microscopy study showed that the proximal S2 region of the myosin tail is involved in stabilizing the IHM structure (Lee et al., 2018). When myosin forms the IHM, these myosin heads appear to be sequestered onto the thick filament backbone (Craig and Woodhead, 2006; Brunello et al., 2020), further making them functionally unavailable for actin interaction and thus reducing N_a (red motors in Figures 1B, 2B).

This potential mechanism for switching on/off myosin in muscle and non-muscle cells by IHM formation has been observed in a variety of species (Craig and Woodhead, 2006; Jung et al., 2008; Lowey and Trybus, 2010) and the potential effects of HCM-causing mutations on IHM formation were proposed by Moore, Leinwand and Warshaw (Moore et al., 2012). Given that the folded state of myosin was thought to conserve energy utilization (discussed in more detail below), the dysregulation of structural stability in cardiac myosin was thought to be an attractive explanation for altered energetics seen in HCM patients (Ashrafian et al., 2003; Moore et al., 2012; van der Velden et al., 2018). Our laboratory was the first to test this hypothesis using purified recombinant human β-cardiac myosin containing HCM mutations. It was noted that a relatively flat surface of the myosin motor domain, termed the "myosin mesa," contained highly conserved residues from mouse to human and was enriched for residues mutated in patients with HCM (Spudich, 2015; Homburger et al., 2016). This myosin mesa appeared to work as a docking platform for another protein to bind, thereby sequestering these heads into an inactive state (Spudich, 2015; Homburger et al., 2016). Nag et al. (Nag et al., 2017) tested whether the S2 tail or MyBP-C might act as this sequestering protein. They created recombinant human cardiac HMM constructs with either 25 heptad repeats of the proximal S2 tail (long tail - able to form a structure in which the heads fold back against the tail) or two heptad repeats (short tail - head cannot stably fold back) and showed that the presence of the long tail, but not the short tail, inhibits the actin-activated ATPase activity of the myosin (Nag et al., 2017). They further showed that this inhibition is reduced by phosphorylating the myosin regulatory light chain. They then assessed the binding affinity of the head and tail domain using microscale thermophoresis (MST), which follows the diffusion of a fluorescent probe along a temperature gradient and is used to measure bi-molecular interactions (Wienken et al., 2010; Ponnam and Kampourakis, 2022). This technique has been used to measure binding affinity of protein-protein or protein-small molecule interactions over a broad range of affinities, including K_d values in the double-digit μM range, suitable for characterization of protein interactions in the sarcomere (Nag et al., 2017; Adhikari et al., 2019). Similar to previous analytical centrifugation studies that

assayed the binding between MyBP-C and S2 or the regulatory light chain (RLC) of myosin (Starr and Offer, 1978; Gruen and Gautel, 1999; Harris et al., 2011), Nag et al. (Nag et al., 2017) showed binding between MyBP-C and actin, MyBP-C and a proximal S2 fragment, S1 and S2, and S1 and either full-length MyBP-C or its N-terminal C0-C2 domains. Taken together, this experimental evidence supports the idea that human cardiac myosin exists in an equilibrium between open and sequestered states, where sequestered heads are functionally unavailable to interact with actin. The myosin motor domain can bind its proximal S2 tail leading to a sequestered conformation with decreased actin-activated ATPase activity, and this interaction can be regulated by post-translational modification such as phosphorylation (Trivedi et al., 2018; Nag et al., 2021). Furthermore, the MST data suggests that this equilibrium may also be governed by interactions between myosin and surrounding thick filament proteins.

In parallel with the development of structural evidence for a folded-back closed state of myosin, functional studies were also pointing to the existence of sequestered myosin heads in muscle. Using skinned skeletal muscle fibers, Cooke and his colleagues showed that there are three functional states of myosin in thick filaments, termed active, "disordered relaxed (DRX)" and "super relaxed (SRX)" states that have different ATP turnover lifetimes (Stewart et al., 2010; Cooke, 2011; Hooijman et al., 2011; McNamara et al., 2015). The active cycling state of myosin interacts with the thin filament and has a rapid ATP turnover of <1 s. The DRX state, in which myosin is detached from the actin and cycles ATP at a basal rate, turns over ATP in ~30 s. Lastly, the SRX state has an ATP turnover time 10X slower than the normal basal rate, ~300 s. This SRX state is found in both skeletal (Stewart et al., 2010) and cardiac (Hooijman et al., 2011) muscle; however, there is a key difference between the two. In skeletal muscle, upon activation by Ca^{2+} the SRX state is completely abolished, leading to maximal instantaneous force upon activation. In cardiac muscle, where there is a cyclical flux of Ca^{2+} with each heartbeat, the population of SRX myosin heads remains stable with Ca^{2+} activation. It was postulated that the SRX state in skeletal muscle serves to decrease the energy consumption of resting muscle while allowing rapid recruitment of myosin heads upon muscle activation, whereas the more stable cardiac myosin SRX population likely serves as a reserve pool of sequestered heads which conserves energy expenditure at rest but can be recruited when increased cardiac contractility is required (eg exercise).

In the original experiments done by the Cooke group, the relaxed skinned myofibers were initially incubated with a fluorescent ATP (mant-ATP), followed by a rapid chase with dark ATP (Stewart et al., 2010). The mant-ATP has increased fluorescence when bound to myosin, and a signal decay is observed as mant-ADP gets replaced by dark ATP. This is a single turnover experiment, the rate of which is limited by the phosphate release rate, which is slower than the mant-ADP release rate. The signal decay is fit to a double exponential, and the rate and proportion of the two different populations (DRX and SRX) are obtained. These populations had only been described in skinned striated muscle fibers where other sarcomeric proteins and other ATPase enzymes could potentially affect either the observed proportions or turnover rates. To determine whether these populations could be identified using purified myosin, the Spudich group developed a plate-based assay to study mant-ATP turnover using purified recombinant human cardiac protein (Anderson et al., 2018). Using the same HMM constructs with either 25-hep or 2-hep repeats of the proximal S2 tail, single nucleotide turnover assays of 2-hep HMM showed predominantly the DRX myosin population (~80%) while 25-hep construct showed a majority of the population (60%) in the SRX state (Anderson et al., 2018). As this assay is done using purified myosin only, this observation is consistent with the notion that when the myosin cannot form a folded back (IHM-like) conformation (2-hep HMM), the majority of myosin is in the DRX state, while the myosin construct containing a long tail which presumably can form a folded back state will have a greater proportion of myosin heads in the SRX state. While this observation supports the correlation between the SRX functional state and the IHM structural state, it does not equate the two. Additional experimental perturbations that correlate the SRX and IHM (described below) strengthen the case that there is a causative association. However, it is worth emphasizing that in single turnover experiments the short S1 fragment of myosin, which has no proximal S2 to fold back onto, showed a small (10%) population of molecules in an SRX state, with a low ATP turnover rate (Anderson et al., 2018). As such, the SRX state of myosin cannot be exclusively defined as a folded-back state. Future (technically challenging) experiments combining single molecule FRET and simultaneous visualization of single molecule ATP turnover may provide information about both the structural and enzymatic state of myosin and thus lead to a better understanding of the relationship between SRX and IHM.

Regulation of thick and thin filament activation

The myosin-actin interaction is the fundamental unit of force generation in the sarcomere, and other regulatory proteins modulate this process. MyBP-C is an important sarcomeric thick filament protein which binds to the myosin thick filament through MyBP-C's C-terminal domains and to actin as well as the myosin head domain through MyBP-C's N-terminal domains (Harris, 2021). MyBP-C has long been thought to work as either a "brake" for the sliding filament or an activator of the tropomyosin-troponin, reducing Ca^{2+} sensitivity of force and rates of force development (Flashman et al., 2004; Harris et al., 2011; Harris, 2021). Phosphorylation of MyBP-C by cAMP-dependent protein kinase (PKA) is thought to be a key element in regulating force production of the

sarcomere (Kuster et al., 2012). As discussed earlier, MyBP-C has been known to interact with not just myosin, but also actin (Craig et al., 2014), myosin's regulatory light chain (RLC) (Ratti et al., 2011), S1 without the RLC (Nag et al., 2017) and the proximal part of the S2 tail (Gruen and Gautel, 1999), and is an important determinant of sarcomere function. The thick filament is tied to the Z-disc by titin. Titin is the largest protein known in human cells, contains binding sites for many muscle-associated proteins, and is thought to sense the tension generated by the sarcomere (LeWinter and Granzier, 2013). Titin modulates the stiffness of the muscle, with its extensible I-band region acting as a molecular spring that develops passive force when the sarcomere is stretched during diastolic filling. As discussed later, myosin and MyBP-C comprise the vast majority of mutations responsible for HCM (Maron et al., 2012; Semsarian et al., 2015), while titin is now recognized as the gene most frequently mutated in patients with idiopathic DCM, but is rarely associated with HCM (Herman et al., 2012; LeWinter and Granzier, 2013; McNally et al., 2013).

On the thin filament side, the troponin complex, along with tropomyosin, has been identified to be the key regulator of actin-myosin crossbridge formation. In the heart, this regulatory unit converts increases in cytosolic Ca^{2+} concentration due to cardiac excitation into increased contractility of cardiac muscle by increasing the availability of the actin filament for myosin heads to bind and undergo a power stroke (so-called excitation-contraction coupling) (Kobayashi and Solaro, 2005). Troponin has three subunits, namely TnT, TnC and TnI. TnT interacts with tropomyosin, TnC binds to Ca^{2+} and TnI exerts an inhibitory effect on crossbridge formation by occupying the myosin-binding domain of actin (Parmacek and Solaro, 2004; de Tombe et al., 2010). There is one troponin complex to every seven actin monomers (Parmacek and Solaro, 2004). When Ca^{2+} binds to TnC, the whole troponin complex undergoes a conformational change, releasing TnI from the myosin-binding domain and allowing myosin heads access to the actin filament.

Ca^{2+} is the key regulator of thin filament activity, and its concentration is tightly regulated by Ca^{2+} release and reuptake in the sarcoplasmic reticulum (SR) by ryanodine receptor 2 (RyR2) and the sarco/endoplasmic reticulum-Ca^{2+}-ATPase (SERCA2a), and by various voltage gated Ca^{2+} channels (Bers, 2002; Bers and Guo, 2005). Cytosolic Ca^{2+} concentrations oscillate between ~10^{-7} M in diastole and up to 10^{-5} M during systole (Fearnley et al., 2011), and shift on the order of milliseconds (Bers, 2002), which allows appropriate cellular response to instantaneous changes in load. There is evidence for positive cooperativity in Ca^{2+} binding to TnC, which is part of the length-dependent thin filament activation seen in striated muscle (Bers, 2002; Bers and Guo, 2005; de Tombe et al., 2010). It has also been observed that the rate of force production continues to rise even after Ca^{2+} concentrations reach their peak. This may be ascribed to strong binding of myosin heads to the regulated thin filament, facilitating the movement of tropomyosin on nearby actin monomers away from the myosin binding site on actin, thus allowing the binding of heads in adjacent regions of the thin filament in a cooperative manner (Moss et al., 2004; Moss and Fitzsimons, 2010).

Thin filament activation can be controlled by phosphorylation of TnI, which decreases the affinity of TnC for Ca^{2+} and increases the off rate of Ca^{2+} from TnC (de Tombe et al., 2010). Phosphorylation of Ca^{2+} handling proteins, including phospholamban and RyR2, controls Ca^{2+} homeostasis in the myocyte, and can be disturbed in failing hearts which are under hyper-adrenergic stimulation (Wehrens and Marks, 2004). A recent report also suggests that the structure of the troponin complex in the thin filament is altered by increasing sarcomere length and is the main contributor to the increased Ca^{2+} sensitivity at low Ca^{2+} concentrations that is seen with length-dependent activation (Zhang et al., 2017). In contrast, the bulk of evidence suggests that conformational changes of myosin in the thick filament are responsible for increased force production in length-dependent activation (Zhang et al., 2017). There is also a report by Ait-Mou et al. (Ait-Mou et al., 2016) showing that titin strain mediates length-dependent activation *via* stretching of the sarcomere that causes structural rearrangements within both thick and thin filaments. Length-dependent activation of the sarcomere has been an active area of research for decades, and ongoing studies suggest that it involves important crosstalk between the thin and thick filaments (de Tombe et al., 2010)

Ca^{2+} sensitivity is an intrinsic property of the troponin complex, and it can be assessed, for example, by determining the pCa_{50} (−log [Ca^{2+}] at half-maximal activation) of an enzymatic or motility assay over a range of Ca^{2+} concentrations (Kreutziger et al., 2007). A typical pCa curve involving regulated thin filaments is sigmoidal, with low activity on the left side of the curve at low Ca^{2+} concentrations (i.e. at high pCa value), followed by a steep increase in activity within a physiological Ca^{2+} concentration (pCa of 5–7), and plateauing of activity at high Ca^{2+} concentrations (i.e. at low pCa value). The pCa_{50} is the Ca^{2+} concentration that gives half-maximal activity. If the system is Ca^{2+} sensitized, the sigmoidal curve will shift to the left, and the pCa_{50} will increase (i.e. the system will show half-maximal activity at lower Ca^{2+} concentration). Functional assays incorporating these regulatory proteins that modulate the actin-myosin interaction are therefore extremely useful (Kobayashi and Solaro, 2005; Willott et al., 2010; Tardiff et al., 2011). The actin filament can be assembled with troponin-tropomyosin complexes to form a regulated thin filament *in vitro*, and can be used to perform all the *in vitro* assays used for actin-myosin analysis (Nag et al., 2015; Kawana et al., 2017). By using recombinant protein expression, functional human troponin and tropomyosin containing various disease-causing mutations can be expressed in bacteria (Sommese et al., 2013b; Gupte et al., 2015; Pan et al., 2015). Higher pCa_{50} values are seen in assays using regulated thin filaments comprised of tropomyosin or one of the troponin subunits containing an HCM-causing

mutation, suggesting that the sarcomere is active at lower Ca^{2+} concentration and thus has higher Ca^{2+} sensitivity in these HCM patients (Sommese et al., 2013b; Gupte et al., 2015).

In addition to thin filament activation, there has been growing interest in the mechanism of activation of the thick filament through Ca^{2+} mediated processes (Ma et al., 2022). Ma et al. (Ma et al., 2022) used a small molecule inhibitor of the thin filament that enhances the Ca^{2+} off rate from troponin, and small-angle X-ray diffraction to show that Ca^{2+} progressively moves the myosin heads from an ordered "off" state on the thick filament backbone to a disordered "on" state closer to the thin filament. When reconstituted cardiac synthetic thick filaments were used to assess the SRX population with either a single turnover assay or a basal ATPase activity assay under varying Ca^{2+} concentrations, there was a Ca^{2+}-dependent decrease in SRX proportion and increase in basal activity (Ma et al., 2022). This Ca^{2+}-dependent activation was not seen in purified HMM with varying tail lengths (all lacked the filament-forming light meromyosin: LMM), and it is speculated that the presence of LMM and assembly into bipolar thick filaments is necessary for this property. The authors also tested adding saturating amounts of free Mg^{2+}, which would bind to the Ca^{2+}/Mg^{2+} binding site of RLC, and saw no change in activation suggesting that the RLC motif is not the primary Ca^{2+} transducer responsible for the off-to on-transition in the thick filament (Ma et al., 2022).

Myocytes containing mutated sarcomeric proteins or treated with small molecules that shift the pCa_{50} curve to the left contract at lower Ca^{2+} concentrations and do not fully relax at physiological diastolic Ca^{2+} levels (Fraysse et al., 2012; Marston, 2016). While it is not clear whether the changes seen at the protein level using *in vitro* assays always translate into similar findings at the cell or tissue level, activation of the sarcomere at lower Ca^{2+} levels may have important implications for the pathophysiology of hypertrophic cardiomyopathy, which is characterized by the development of diastolic dysfunction in the early stages of the disease. Ho et al. reported that patients who were carriers of HCM mutations in sarcomere genes, but who were yet to develop significant hypertrophy, still had echocardiographic evidence of diastolic dysfunction as well as increased systolic function (Ho et al., 2002). The diastolic dysfunction in this cohort cannot be attributed to either hypertrophy or to the myocardial fibrosis that typically accompanies it, suggesting that the primary factor driving this early diastolic dysfunction is likely found at the sarcomere level where actin-myosin crossbridges are being formed.

Genetic alteration of $F_{ensemble}$ parameters leads to HCM

We now consider the effect of mutations in sarcomeric proteins that cause cardiovascular disease. Since the discovery of the R403Q mutation in MYH7 as the first HCM-causing mutation by the Seidman group (Geisterfer-Lowrance et al., 1990), it has been well established that HCM is largely a disease of the sarcomere, except for a few phenocopies such as glycogen storage disease and amyloidosis (Seidman et al., 2011). Linkage analysis and candidate gene screening in families and sporadic cases have led to the discovery of disease-causing mutations in genes encoding many other sarcomeric proteins, including MyBP-C, the troponin complex and tropomyosin (Marston, 2011; Moore et al., 2012; Fatkin et al., 2014). Functional characterization of the effects of these HCM mutations has been a long-time challenge in the field, especially for myosin mutations: for example, earlier studies of cardiac myosin purified from human cardiac biopsy samples have shown conflicting results in *in vitro* motility assays (CUDA et al., 1997; Palmiter et al., 2000). Biopsy material suffers from limited availability, typically comes from patients with late stage disease, is a mix of wildtype and mutant protein as virtually all patients are heterozygous for their disease-causing mutations (Helms et al., 2014), and requires careful handling to preserve enzymatic function. Therefore, a number of animal models harboring HCM mutations in their corresponding genes have been generated and studied.

The best-characterized model is the transgenic mouse carrying the R403Q mutation in α-cardiac myosin (Geisterfer-Lowrance et al., 1996), which is the predominant ventricular isoform in small rodents. At age 30-week the mouse recapitulated human HCM pathophysiology and histopathology (Geisterfer-Lowrance et al., 1996; Georgakopoulos et al., 1999). Mutant α-cardiac myosin purified from ventricular tissue showed increased ATPase activity and actin filament gliding velocity by *in vitro* motility assays (Tyska et al., 2000), and increased ensemble force, but no change in intrinsic force (Tyska et al., 2000; Debold et al., 2007). However, seminal work by Susan Lowey and others showed that when the same mutation was introduced into the mouse β-cardiac myosin backbone, there was no significant change seen in actin velocity, and there was a slight decrease in ATPase activity (Lowey et al., 2008). In keeping with the *in vitro* motility results, the ADP release rate was 20% higher for α-cardiac myosin with the R403Q mutation while there was no change with the same mutation in the β-cardiac myosin background (Fatkin et al., 2014). There are over 80 amino acid residue differences between mouse α-cardiac myosin and human β-cardiac myosin (Weiss et al., 1999), and there are considerable functional differences between α- and β-cardiac myosin in ATPase activity and motility (Deacon et al., 2012; Aksel et al., 2015). In other words, while the R403Q mutation in α-cardiac myosin likely shows hypertrophy in mouse models due to increased ATPase activity and ensemble force leading to hypercontractility, the R403Q mutation in human β-cardiac myosin may cause hypertrophy through entirely different changes to myosin biomechanics. Taken together, these observations highlight the difficulty in using mouse models to study disease-causing mutations in MYH7 and the importance of using the appropriate myosin backbone to accurately determine the effects of these mutations on myosin function.

Functional assessment of HCM mutations using purified recombinant human cardiac myosin *in vitro*

For many years there has been a gap in knowledge between the identification of disease-causing mutations and how these mutations lead to the secondary cellular events that cause hypertrophic signaling (Sivaramakrishnan et al., 2009). Model systems such as transgenic mice that recapitulate HCM morphology have been important in understanding the cell biology of hypertrophy, while the exact mechanism of the index signal that triggers the hypertrophic signaling has been lacking. *In vitro* expression of enzymatically active recombinant cardiac myosin had been challenging until an expression system was developed using the C2C12 mouse myoblast cell line (Srikakulam and Winkelmann, 2004; Liu et al., 2008; Resnicow et al., 2010). Using this approach, we and others are now able to obtain highly purified, functional recombinant human β-cardiac myosin with engineered disease-causing mutations.

The overarching hypothesis here is that HCM mutations result in increased power output (Anan et al., 1994) by altering the contractility parameters discussed in part 1 above. As mentioned earlier, power is the product of force and velocity, and is also represented by the area under the curve of the force vs. velocity relationship of muscle contraction. This hypothesis is based on the clinical observation that HCM patients often present with hyperdynamic physiology (Klein et al., 1965; Wilson et al., 1967; Seidman et al., 2019), and the earliest signs of HCM pathology are abnormal diastolic function and supranormal ejection fractions suggestive of a hypercontractile left ventricle (Ho et al., 2002).

The first reported biomechanical analyses of recombinant human β-cardiac myosin containing HCM-causing mutations led to confusing and inconclusive results. The first experiments focused on **R453C** (Sommese et al., 2013a), which is one of the earliest identified mutations known to cause a severe clinical phenotype (Watkins et al., 1992). Similar to prior mouse work (Palmer et al., 2004; Debold et al., 2007), the R453C mutation in human β-cardiac myosin caused a 50% increase in $F_{intrinsic}$, ~30% decrease in both ATPase activity and actin gliding velocity, and thus no significant change in duty ratio (Sommese et al., 2013a). By simple calculations, the overall ensemble force is expected to be increased, and the power output also increased despite a 30% decrease in velocity. This finding was consistent with the hypothesis that an increase in power output leads to HCM. However, in contrast to the steady-state experiments, transient kinetic studies of the R453C mutant protein by Michael Geeves' group revealed that surprisingly few parameters were altered by the mutation, with the exceptions being a 35% reduction in ATP binding to the motor domain and a three-fold slowing of the ATP hydrolysis step/recovery stroke, which could become the rate-limiting step for the ATPase cycle in place of the phosphate release step (Bloemink et al., 2014).

Next, the **R403Q** mutation was rigorously characterized (Nag et al., 2015). When assayed using actin filaments, the R403Q myosin resulted in an ~15% reduction in $F_{intrinsic}$, two-fold reduction in actin-binding affinity, and ~10% increase in unloaded actin gliding velocity compared to wildtype (WT) (Nag et al., 2015). There was no significant change in ATPase activity (= $1/t_c$), step size (d), or ADP release rate (which affects t_s). The loaded *in vitro* motility assay showed characteristics of lower contractility at higher external loads. With RTFs, however, there was no increase in the unloaded velocity of gliding filaments, and an ~30% lower ATPase activity (Nag et al., 2015). In addition to the interesting differences between actin-based vs. RTF-based assays, it was quite surprising to see an overall decrease of contractile parameters with the R403Q mutation.

Further investigations were performed on well-known HCM mutations in the converter region of myosin, which has been known as a hot-spot for HCM mutagenesis (Colegrave and Peckham, 2014; García-Giustiniani et al., 2015; Homburger et al., 2016). We chose three mutations that were known to be severely pathogenic, namely **R719W** (Anan et al., 1994), **R723G** (Enjuto et al., 2000) and **G741R** (Fananapazir et al., 1993). Given that converter movement is coupled to major mechanical changes including the power stroke, as well as biochemical events including load-dependent ADP release, ATP hydrolysis and phosphate release, we expected major alteration in these parameters for these HCM mutations. In contrast to our prediction, we did not see significant increases in either enzymatic or biophysical properties: R719W and R723G resulted in 15–30% reductions in $F_{intrinsic}$ and ~15% increases in velocity, while ATPase activity was unchanged. Loaded *in vitro* motility showed characteristics of a trend toward lower contractility. Meanwhile, G741R did not show significant changes compared to WT in any of the parameters tested. Unlike the R403Q mutation, which sits near the actin-binding domain, there was no difference in the results between actin-based or RTF-based assays.

In summary, the biochemical and biophysical effects of these HCM mutations at the molecular level did not support the clinically observed hypercontractility, leading us to suspect an alternative mechanism as discussed below.

Myosin availability as a primary mechanism for hypercontractility in HCM

As mentioned earlier, a relatively flat surface of the myosin motor domain termed the "myosin mesa" was noted for its high proportion of highly conserved residues across different species. In addition, this surface turned out to be enriched in HCM mutations (Spudich, 2015; Homburger et al., 2016). The myosin

mesa has a cluster of positively charged (predominantly arginine) residues, most of which, when mutated, cause HCM. Homburger and others searched a large HCM patient registry database and mapped the location of mutations in cardiac myosin (Homburger et al., 2016) and found that the myosin mesa, converter domain and proximal S2 tail domain are three hot spots for HCM mutations in the myosin molecule. The converter domain and proximal S2 tail domain have been previously implicated in the stability of the IHM folded back state (Wendt et al., 1999; Blankenfeldt et al., 2006) and the positively-charged myosin mesa is an attractive site for binding other protein surfaces, either intramolecularly or intermolecularly (for example with MyBP-C) (Trivedi et al., 2018). Therefore, it was hypothesized that any mutations in these areas might be expected to weaken either inter- or intra-molecular interactions important for forming the folded back state, thereby pushing the equilibrium to more myosin heads in an "on state" and increasing the number of myosin heads functionally accessible (N_a) for interaction with actin (Trivedi et al., 2018; Spudich, 2019; Nag et al., 2021).

Nag et al. (Nag et al., 2017) first tested this hypothesis by studying three mutations that lie on the myosin mesa surface (**R249Q, H251N** and **R453C**) and one in proximal S2 (**D906G**), which were hypothesized to disrupt head-tail interactions as described above. Strikingly, all four mutants significantly weakened the affinity of proximal S2 for short S1[15,48]. In contrast, three HCM mutations lying outside of these areas (R403Q, D239N and R870H) did not have any effect on proximal S2 binding affinity, as studied using MST (Adhikari et al., 2016; Nag et al., 2017). The four mutations that showed weakened affinity for S2 are predicted to open folded-back heads to become functionally available, hence increasing N_a.

As mentioned above, HMM constructs were developed with both long and short proximal tail domains (Nag et al., 2017) which show differing abilities to form the sequestered state. Utilizing these 2-hep and 25-hep HMM constructs, Adhikari et al. (Adhikari et al., 2019) studied the R249Q and H251N mutations, which are thought to affect residues involved in the S1-S2 interface of the folded-back state, along with the converter domain mutation R719W and a mutation (D382Y), both of which are located at the S1-S1 interface in homology models of folded back β-cardiac myosin. The mant ATP single nucleotide turnover experiment using H251N or R249Q mutant 25-hep HMM resulted in significant decreases (41% and 59%, respectively) in the number of SRX heads as compared to WT. The increase in the DRX/SRX ratio also corresponded to an increase in actin-activated ATPase activity of the mutant 25-hep HMMs, suggesting that the mutations cause more heads to be functionally accessible to actin and thus increased the ensemble enzymatic activity. R719W and D382Y also increased the percentage of DRX heads in the context of 25-HMM constructs, and increased actin-activated ATPase activity (k_{cat}) as well. In particular, the k_{cat} of R719W 25-hep HMM was essentially the same as R719W 2-hep HMM, suggesting that the R719W mutation had a strong effect on opening up the heads of folded-back 25-hep HMM molecules and made these heads accessible for interaction with actin. This significant increase in N_a would likely dominate the minor decreases in $F_{intrinsic}$ and duty ratio parameters measured previously to drive an increase in ensemble force (Kawana et al., 2017). Indeed, all four HCM-causing mutations affecting residues located at putative interfaces in the folded back state appeared to cause an increase in N_a as the primary driver of hypercontractility.

Interestingly, Adhikari et al. (Adhikari et al., 2019) also tested an HCM-causing mutation, I457T, that affects a residue in the transducer region of the motor that is remote from putative head-head or head-tail interfaces. They found that the mutated 25-hep HMM had an SRX/DRX ratio indistinguishable from WT 25-hep HMM in single turnover experiments and a similar ratio of 2-hep:25-hep actin-activated ATPase activity as WT, suggesting that this mutation did not affect N_a. Instead, I457T caused a ~75% increase in the k_{cat} and a greater than 2-fold increase in the *in vitro* sliding velocity compared to WT controls. This mutation illustrates that increases in myosin motor function alone can drive hypercontractility without affecting N_a. However, I457T is unique in not increasing N_a among the >20 HCM-causing mutations we have studied in the context of the 2-hep and 25-hep HMM constructs, and may well be the exception that proves the rule.

Sarkar et al. (Sarkar et al., 2020) studied the **R403Q** and **R663H** mutations using the 2-hep and 25-hep HMM constructs. The R663H mutation is a well-known HCM-causing mutation and the initial clinical report of it showed a strong correlation between the mutation and the development of atrial fibrillation (Gruver et al., 1999). Interestingly, a short S1 construct with the R663H mutation showed no difference compared to WT in terms of ATPase, *in vitro* motility, or single molecule force measurements. There was no difference in the binding affinity of short S1 and proximal S2 between WT and R663H or R403Q using MST, which might be expected given that neither R663 nor R403 are predicted to be in direct contact with proximal S2 in the folded back state. However, when R663H 25-hep and 2-hep HMM were analyzed with single nucleotide turnover and actin-activated ATPase assays, R403Q 25-hep HMM and R663H 25-hep HMM showed significantly higher DRX percentages and higher ATPase activity than WT 25-hep HMM, suggesting that these mutations destabilize the folded back state and provide more myosin heads for interaction with actin. Sarkar et al. (Sarkar et al., 2020) also evaluated the effect of adding the large N-terminal fragment of MyBP-C (C0C7 domain) and showed that binding of the purified C0C7 fragment to WT 25-hep HMM led to an increase in the percentage of myosin heads in the SRX. The R403Q mutation, however, abolished the binding of 25-hep HMM to the C0C7 fragment, and the ratio of SRX/DRX in single turnover assay was similar with or without the addition of C0C7. In contrast, the R663H 25-hep HMM did

bind C0C7 with an affinity similar to that of WT; despite that, the SRX/DRX ratio of R663H 25-hep HMM was unaltered by the presence of C0C7. Taken together, these observations suggest that while MyBP-C can bind to heads that are not in the auto-inhibited SRX state, such binding does not necessarily cause those heads to adopt the SRX state. Therefore, some MYH7 mutations like R663H may increase N_a despite binding to MyBPC, thus escaping this mechanism of thick filament regulation (Sarkar et al., 2020).

Finally, Morck et al. (Morck et al., 2022) reported the effect of five HCM-causing mutations in the myosin lever arm. These included mutations in the pliant region (D778V, L781P, and S782N), the bent region between the light chains (A797T), and the hook joint (F834L). Using the actin-activated ATPase assay, they found that 2-hep HMM with any of these five mutations had a similar k_{cat} to WT 2-hep, while 25-hep HMM containing any of these mutations showed a relative increase in k_{cat} compared to WT 25-hep, demonstrating that these mutations caused more heads to be available to interact with actin. Interestingly, the three pliant region mutations did not lead to a decrease in the SRX population in the single turnover assay, emphasizing that the IHM state and the SRX state cannot always be equated. In this case, it's possible that the autoinhibition of the myosin is disrupted only in the presence of actin. These three mutations also caused a variable impact on duty ratio, ensemble force and power output at the single molecule level. On the other hand, the light chain binding region mutations (A797T and F834L) led to both an increase in k_{cat} of the actin-activated myosin ATPase compared to 25-hep WT HMM and a significantly reduced SRX population in the single turnover assay (and had no effects on basic biomechanical parameters). Specific light chain positioning is likely required to access the folded state, and these mutations may act primarily by disrupting that positioning. The lever arm mutations highlight the importance of assessing all aspects of myosin function using multimodal assay systems.

Early vs. late onset HCM mutations

All of the above MYH7 mutations are observed predominantly in patients with adult-onset HCM. Adhikari et al. (Adhikari et al., 2016) studied mutations that are found predominantly in the pediatric population and thus termed "early-onset" HCM (Kaski et al., 2009). Two mutations were chosen - **H251N** on the "myosin mesa" and **D239N** within the Switch-1 (nucleotide-binding) domain, and both were studied in the context of short S1. Both mutations significantly increased ATPase activity, 24% for H251N and 50% for D239N compared to WT (Adhikari et al., 2016). $F_{intrinsic}$ was increased 46% for H251N and 23% for D239N, and significant increases in actin gliding velocity were seen as well (94% for D239N and 40% for H251N) (Adhikari et al., 2016). Loaded *in vitro* motility assay experiments showed an upward shift in the load-velocity curve suggestive of increased ensemble force compared to WT (Adhikari et al., 2016). These striking changes contrast significantly compared to five mutations seen predominantly in adult patients (R403Q, R663H, R719W, R723G, G741R) and may be the basis for the early-onset, more severe phenotype compared to the more typical adult-onset disease.

However, when Vera et al. (Vera et al., 2019) compared short S1 constructs containing either early (H251N, D382Y, P710R and V763M) or adult onset (R719W, R723G and G741R) HCM mutations by measuring steady-state and transient kinetics, there was no clear difference in the degree of changes in these parameters. There was also no unifying direction of changes in any of the kinetic parameters. The H251N mutation had significant increases in the above parameters, while the other mutations showed only modest changes (Vera et al., 2019). Interestingly, one of the HCM mutations, P710R, shared properties with the DCM-causing mutations (Ujfalusi et al., 2018), including reduced ATPase activity (k_{cat}), lower occupancy of the force holding actin-myosin-ADP state, a lower duty ratio and a more economical use of ATP for both rapid movement and force generation (Ujfalusi et al., 2018).

Given the seemingly inconsistent findings for the kinetics of the P710R myosin, this mutation was studied further (Vander Roest et al., 2021). Using optical trapping with harmonic force spectroscopy (HFS), the single molecule properties of P710R short S1 showed reduced load sensitivity and a decrease in the step size. The velocity of actin filament gliding was also reduced. Based on actin-activated ATPase rates and load-dependent actin detachment rates, it was calculated that P710R reduced the duty ratio especially at higher loads. Similar to the results from the kinetic studies, these findings using the short S1 construct suggested that the P710R mutation should result in hypocontractility. However, when P710R 2-hep HMM and 25-hep HMM were studied using the actin-activated ATPase assay, the P710R mutation did not result in the ~40% decrease in k_{cat} between 2-hep and 25-hep HMM which is seen with the WT constructs. The single turnover assay showed that P710R significantly reduced the proportion of myosin in the SRX state down to 27%, close to the SRX proportion for the 2-hep HMM, which is around 20%. These findings suggest that the P710R mutation results in a significant disruption of the SRX state, leading to more myosin heads functionally available. As for R403Q and R719W, this significant increase in N_a may compensate for the hypocontractile features seen in other assays, resulting in a net increase in ensemble force leading to hypercontractility.

Multiscale effects of HCM mutations

In order to understand which effects (hypercontractile vs. hypocontractile) of the P710R mutation on myosin function predominate in an ensemble, an induced pluripotent

stem cell-derived cardiomyocyte (iPSC-CM) line carrying the P710R mutation in one allele of MYH7 was generated using CRISPR/Cas9 gene editing and the resultant cells were micropatterned on substrates of appropriate physiological stiffness to obtain cardiomyocytes containing well-aligned myofibrils (Ribeiro et al., 2015; Vander Roest et al., 2021). Traction force microscopy showed that the iPSC-CM with P710R β-cardiac myosin had significantly higher contractile force, with increased peak force and contraction time. The transmission electron microscopy image of also showed significantly disrupted myofibril organization when compared to isogenic controls. The cell size was also increased, and ERK and Akt pathways were activated more than in control cells. Further computational modeling integrating the biochemical and biophysical parameters predicted the measured increase in traction forces, highlighting the effect of myosin availability (N_a) as a major molecular determinant of hypercontractility in HCM.

The effect of other HCM mutations in myosin on N_a have also been studied using iPSC-CMs. Toepfer et al. (Toepfer et al., 2019) reported the effect of pathogenic MYH7 variants (R403Q, V606M and R719W), which resulted in decreased SRX fractions and enhanced cardiomyocyte contractility. They also showed that HCM-causing mutations in MYBPC3 (the gene encoding MyBP-C), as well as stepwise loss of MYBPC, resulted in decreases in the SRX population and increases in cardiomyocyte contractility. The effect of MyBP-C loss was attenuated by introducing a DCM variant (F764L) of MYH7 or a myosin inhibitor (MYK-461) (Toepfer et al., 2019). The effect of loss of MyBP-C on myosin function observed in the cellular model highlights the key role MyBP-C plays in the modulation of myosin function and overall sarcomere activity. It is also a proof of principle that a myosin inhibitor is capable of attenuating the overall cellular contractility in HCM due to non-MYH7 variants (Toepfer et al., 2019).

Myosin modulation as a therapeutic tool for treating cardiomyopathy

Myosin inhibitors for HCM

Based on the hypothesis that HCM is fundamentally due to hypercontractile function at the sarcomere level, a small molecule to inhibit myosin activity was developed as a proof of principle to treat HCM. Mavacamten (MYK-461) was developed (Green et al., 2016) and tested in three different HCM mouse models (R403Q (Geisterfer-Lowrance et al., 1996), R453C (Palmer et al., 2004) and R719W (Teekakirikul et al., 2010)). Early treatment of pre-hypertrophic mice with MYK-461 prevented development of hypertrophy, and treatment of older mice with existing hypertrophy reversed the increased wall thickness (Green et al., 2016). The molecular mechanism of mavacamten was reported by Anderson et al. (Anderson et al., 2018). They used negative stain EM to show that mavacamten stabilized a folded back state of 25-hep human β-cardiac HMM, and used the single nucleotide turnover assays to show in parallel that it also increased the fraction of heads in the SRX state (Anderson et al., 2018). The ability of mavacamten treatment to increase the SRX population was also seen in skinned cardiac fibers from an R403Q heterozygous pig model and a biopsy sample from a patient carrying the R663H mutation. At baseline, the skinned cardiac fiber from the R403Q pig had reduced SRX population (16% vs. 26% in WT pig), and mavacamten treatment restored the SRX population up to 30%. In addition, the maximum tension in the skinned pig fiber was reduced after treatment with mavacamten (Anderson et al., 2018). Mavacamten also caused an increase in the ordering of myosin heads along the backbone of the thick filament, as observed by the substantial increase in the myosin-based helical layer line reflections in low-angle X-ray diffraction images (Anderson et al., 2018). Taken together, mavacamten reduced the population of functionally available myosin motors (N_a) in the sarcomere by stabilizing a folded back state of myosin, and the resultant reduction in $F_{ensemble}$ led to prevention and/or reversal of hypertrophy in HCM mouse models. Mavacamten was subsequently tested in a series of clinical trials with HCM patients.

The phase I study was completed and showed good safety and tolerability in healthy volunteers and a small number of patients (Maron et al., 2016). The phase II study was conducted in patients with obstructive HCM who had significant LVOT gradients due to the hypertrophied septum with resultant heart failure symptoms such as exertional dyspnea (Heitner et al., 2019) (*see* Introduction and Figure 1). The mavacamten treatment resulted in a dramatic decrease in LVOT gradient down to the normal range, and after the treatment period concluded, the LVOT gradients returned to pre-treatment baselines (Heitner et al., 2019). In the phase III study of obstructive HCM patient (EXPLORER-HCM), mavacamten showed improvement in the composite endpoint of exercise capacity and symptom severity (using the New York Heart Association (NYHA) functional classification) (Olivotto et al., 2020). This is the first medication for HCM that showed a benefit in a randomized controlled trial. Mavacamten was also studied in a phase II study for non-obstructive HCM patients (MAVERICK-HCM). This trial showed no significant change in the above composite endpoint, while the biomarker for ventricular stretch was significantly reduced (Ho et al., 2020). It is worth noting that the participants in these trials did not necessarily carry MYH7 variants, and thus the effect of mavacamten is exerted by bringing down the net $F_{ensemble}$ which leads to normalization of sarcomere function.

Currently a long-term extension study for EXPLORER-HCM and MAVERICK-HCM participants is under way (MAVA-LTE), to study the long-term effects of this medication (Rader et al., 2021). For the former EXPLORER-HCM participants,

mavacamten showed durable improvement in reduction of LVOT gradients, diastolic function, NT-proBNP (biomarker for ventricular stretch) and NYHA functional class (assessment of subjective symptoms) (Rader et al., 2021). The imaging study of the EXPLORER-HCM participants also showed significant changes in HCM morphology. The MRI study showed reductions in cardiac mass and wall thickness (Saberi et al., 2021), and the echocardiographic analysis also showed improvement in left ventricular diastolic function parameters and left atrial size (Hegde et al., 2021). The participants in these trials have already developed hypertrophy, and thus these imaging studies suggest that the effect of myosin inhibition to reduce hypercontractility at the sarcomere level has a downstream effect on hypertrophic processes resulting in at least partial remodeling of existing hypertrophied myocardium. Based on the result of EXPLORER-HCM, mavacamten was recently approved by the FDA for the treatment of patients with obstructive HCM.

A newer generation myosin inhibitor was developed by Cytokinetics and has been studied in obstructive HCM patients (Chuang et al., 2021). Aficamten has a shorter half-life and less drug interactions than mavacamten. A phase II study was reported last year, and showed significant reductions in LVOT gradient with a return to the pre-treatment baseline when the therapy was stopped (Maron, 2021). Currently, a phase III study is being conducted, mainly focusing on exercise capacity assessed by cardiopulmonary exercise testing.

Myosin activators for systolic heart failure

Although this review is primarily focused on HCM molecular pathophysiology and the pharmacotherapy for HCM that has been developed under the hypothesis that HCM is fundamentally a hyperactive sarcomeric disease, the opposite end of the spectrum - systolic heart failure where the contractile function of the heart is compromised due to various underlying etiologies, is worthy of mention. Malik and others performed a small molecule screen using thin-filament activated ATPase activity of β-cardiac myosin, and developed **omecamtiv mecarbil (OM)** as the first cardiac myosin activator (Malik et al., 2011). OM showed increases in cell length shortening without changing Ca^{2+} transients in isolated rat cardiac myocytes. OM also improved echocardiographic and hemodynamic parameters using a dog heart failure model, primarily through increases in systolic ejection time, without changes in the rate of LV pressure development (dP/dt). Interestingly, OM seems to increase RTF-activated cardiac myosin ATPase activity at lower Ca^{2+} concentrations up to pCa 6, at which point a crossover occurs and at higher concentration it actually reduces the ATPase activity (Malik et al., 2011). Subsequent reports of RTF-activated porcine cardiac myosin ATPase activity (Marston, 2011) and actin-activated human cardiac myosin ATPase activity (Fatkin et al., 2014) both showed decreased ATPase activity at OM concentration of 10 and 100 μM, respectively. From this work, the binding site for OM was speculated to be a cleft in a region where the relay helix and the converter domain converge at the base of the lever arm (Malik et al., 2011).

OM was studied in a series of clinical trials (Cleland et al., 2011; Teerlink et al., 2011; Teerlink et al., 2016a; Teerlink et al., 2016b), and showed increases in systolic ejection time, ejection fraction and stroke volume on echocardiographic assessment (Cleland et al., 2011; Teerlink et al., 2011; Teerlink et al., 2016a). OM recently completed a phase III randomized, double-blind, placebo-controlled clinical trial in 8,000 systolic heart failure patients (Teerlink et al., 2021). The primary endpoint of the study was a composite of cardiovascular death and heart failure hospitalization, and OM met the primary endpoint, though the effect was small (8% relative risk reduction). Interestingly, subgroup analysis showed that the sicker patients (more advanced symptoms or lower LVEF) had more benefits from OM therapy.

There have been many investigations on the exact mechanism of sarcomere activation by OM. Using recombinant human cardiac myosin motor domain fused to GFP, Winkelmann et al. (Winkelmann et al., 2015) reported that OM binds in a narrow cleft that separates the N-terminal 25-K domain from the lower portion of the 50-K domain of the motor domain, which is involved in coupling structural elements that are linked to the rotation of the lever arm into the PPS conformation. Rohde et al. (Rohde et al., 2017) investigated the effect of OM on the kinetics of the myosin powerstroke using a combination of transient time-resolved FRET and transient biochemical assays. By measuring the FRET signal between a fluorescent donor on the RLC domain and fluorescent nucleotide, the group dissected the steps of actin binding, the powerstroke, and phosphate release. They concluded that in the absence of OM, myosin binds to actin, undergoes the powerstroke, and then releases phosphate, which is the rate-limiting step of the ATPase cycle. However, whether phosphate release occurs before or after the stroke is still a matter of debate (Houdusse and Sweeney, 2016; Planelles-Herrero et al., 2017) In the presence of OM, the phosphate release rate is increased; however the overall ATP turnover rate was slowed, owing to even greater slowing of the actin-induced rotation of the myosin light chain binding domain (Rohde et al., 2017). There was no change in ADP release rate from a post-stroke state (Liu et al., 2015), and the rate-limiting step for the steady-state ATPase cycle now became the actin-induced rotation of myosin in the presence of OM. This results in the accumulation of a prolonged actin-bound state of the myosin which might act as a load in the contracting sarcomere (Rohde et al., 2017), but might also serve to induce cooperative binding of more myosin heads to actin by its effect on the tropomyosin-troponin system, thus activating the sarcomere.

A similar conclusion was reached by Swenson et al. (Swenson et al., 2017) using recombinant human cardiac myosin and transient kinetic assays that showed a slow product release pathway, resulting in the accumulation of non-force generating heads (Swenson et al.,

TABLE 1 Summary of the functional effect of HCM mutations in cardiac myosin.

HCM mutation	Intrinsic force ($F_{intrinsic}$)	Velocity (v)	ATPase (k_{cat})	Number of available myosin heads (N_a)	References
Change from wildtype human β-cardiac myosin					
R403Q	↓	↑	↑	↑	Nag et al. (2015), Nag et al. (2017), Sarkar et al. (2020)
R453C	↑	↓	↓	-	Sommese et al. (2013), Nag et al. (2017), Bloemink et al. (2014)
R719W	↓	↑	NC	↑	Kawana et al. (2017), Adhikari et al. (2019)
R723G	↓	↑	NC	-	Kawana et al. (2017)
G741R	NC	NC	NC	-	Kawana et al. (2017)
R663H	NC	NC	NC	↑	Sarkar et al. (2020)
R249Q	-	↓	↓	↑	Nag et al. (2017), Adhikari et al. (2019)
I457T	-	↑	↑	NC	Adhikari et al. (2019)
P710R	-*	↓	↓	↑	Vander Roest et al. (2021), Vera et al. (2019)
V763M	-	↑	NC	-	Vera et al. (2019)
H251N	↑	↑	↑	↑	Adhikari et al. (2016), Nag et al. (2017), Adhikari et al. (2019), Vera et al. (2019)
D239N	↑	↑	↑	↑	Adhikari et al. (2016)
D778V	↓**	↑	↑	↑	Morck et al. (2022)
L781P	NC**	↓	NC	↑	Morck et al. (2022)
S782N	↓**	NC	NC	↑	Morck et al. (2022)
A797T	-	NC	NC	↑	Morck et al. (2022)
F834L	-	NC	NC	↑	Morck et al. (2022)

Summary of HCM mutations that have been studied using purified human β-cardiac myosin heavy chain containing human ventricular cardiac light chains. While $F_{intrinsic}$, v and k_{cat} values showed no consistent trends among the HCM variants, the N_a was increased in all tested variants except one. NC, no change; dash, not determined. * The intrinsic force has not been measured, while optical trapping using harmonic force spectroscopy assay showed reduced step size of the myosin motor and reduced load sensitivity of the actin detachment rate at the single molecule level. ** The intrinsic force has not been measured for this mutation. Optical trapping using harmonic force spectroscopy was used to obtain load-dependent detachment rate, load sensitivity and step size. The average force of the sarcomere was calculated using these parameters.

2017). The accumulation of a state of myosin that undergoes prolonged binding to actin is likely the reason for significant slowing of gliding actin filament velocities in *in vitro* motility assays in previous reports (Aksel et al., 2015; Liu et al., 2015; Winkelmann et al., 2015; Swenson et al., 2017). Liu et al. (Liu et al., 2018) used HFS technology to study the load-dependent detachment of myosin from the actin filament. In the presence of OM, myosin's detachment rate at zero load (k_0), the distance to the transition state (a measure of force sensitivity, δ), and the myosin stroke size were all reduced. Woody et al. (Woody et al., 2018) used a feedback-controlled laser trap and observed a similar effect of OM causing the detachment rate to become independent of both applied load and ATP concentration (Woody et al., 2018). The decrease in detachment rate was manifest as slowing of actin gliding velocity using *in vitro* motility assays (Aksel et al., 2015; Liu et al., 2018) and as reduced cardiomyocyte contractility (Kampourakis et al., 2018). Taken together, these findings suggest that OM binding to myosin results in a myosin head that attaches to the actin filament but does not produce a full functional stroke (Spudich, 2019).

The effect of OM at the cellular and organ level was rather surprising, given that OM appears to inhibit the individual myosin from stroking and hence should reduce contractility (Liu et al., 2018). The activation effect of OM is seen at the whole sarcomere level when only a fraction of the myosin heads are bound to OM. As discussed above, activation of the myocyte is likely due to activation of the thin filament by the OM-bound myosin, which has a prolonged binding to the thin filament, promoting more non-OM-bound myosin heads to interact with actin, leading to myocyte activation (Malik et al., 2011). This is a distinct way of increasing the ensemble force. This type of activation has been seen in HCM mutations affecting thin filament components, including the troponin complex (Sommese et al., 2013b), which resulted in an increase in Ca^{2+} sensitivity and activation of the thin filament at lower [Ca^{2+}]. It is notable that OM had a similar effect on thin filament activation *via* interaction with myosin and not the thin filament components. Overall, the mechanism of OM highlights the complexity of myosin function in the sarcomere and the potential for pharmacological modulation.

Future perspectives and conclusion

The fundamental mechanisms underlying HCM pathogenesis have long been studied using a variety of

approaches, but it is only in the last 10–15 years that the field has advanced to using engineerable human proteins and cells to accurately study the effects of HCM-causing mutations. Using expressed and purified human β-cardiac myosin containing the ventricular human cardiac light chains, extensive work has led to the conclusion that a majority of HCM mutations cause hypercontractility of the heart by shifting myosin molecules from an off-state to an on-state, which results in an increase in N_a, the number of heads functionally available for interacting with actin (Table 1).

In 2018, Robert-Paganin, Auguin and Houdusse (Robert-Paganin et al., 2018) reported important structural data using an optimized quasi-atomic model of the folded back IHM state of bovine cardiac myosin, coupled to in silico analysis of the effects of 178 HCM mutations previously described (Robert-Paganin et al., 2018). They suggested that the formation of the IHM requires that both heads adopt an asymmetric conformation while the two motor domains position the lever arm up as in the PPS state. According to their prediction, a majority of the mutations, about two-thirds, would lead to destabilization of the IHM, increasing N_a. Out of these mutations, roughly half were not located at the interfaces of the IHM (head-head, or head-tail), but are predicted to alter the stability of the PPS conformation that is necessary to form the IHM (Robert-Paganin et al., 2018). The fraction of HCM mutations that are primarily increasing N_a could be higher than this. The homology model is unlikely to fully recapitulate the true human β-cardiac myosin IHM structure, and an actual high-resolution structure has been desperately needed. This structure has now been obtained and reported by Robert-Paganin et al. at the 2022 Gordon Research Conference (Cytoskeletal Motors) meeting. We will soon have the true structural information to properly assess the destabilizing effects of HCM mutations on the IHM off-state. But even with the true human β-cardiac myosin IHM structure, for such an allosteric molecule, it is difficult to predict in silico which mutations will increase N_a. Functional tests described in this review using purified human β-cardiac myosin containing the ventricular human cardiac light chains are required to biochemically assess the effects of any particular HCM mutation (Table 1). Nonetheless, the mesa hypothesis (Spudich, 2015), which states that increasing N_a is a unifying hypothesis for the cause of hypercontractility by HCM mutations, now has a good deal of support experimentally.

The stability of the IHM is likely regulated by other proteins in the sarcomere, including MyBPC. Mutations in MyBPC are known to cause about one-third of genetically defined HCM cases, with many cases thought to be caused by haploinsufficiency due to frameshift, nonsense or splice site mutations that result in premature termination codons (Helms et al., 2020). This fits well with the mesa hypothesis, since a stabilizing effect of MyBP-C on the IHM state would be relieved by loss of some MyBP-C in the sarcomere. There are, however, also MyBP-C missense mutations that cause HCM and their mechanisms of action are not well defined (Harris et al., 2011). Decades of studies on MyBPC has revealed binding interactions with actin to activate the thin filament, and binding to myosin to control myosin head availability through the thick filament (Heling et al., 2020). Its ability to bind to both actin and myosin with similar affinities, and unique spatial localization within the sarcomere makes MyBPC a particularly interesting and challenging molecule to study. Titin is also an important player in sarcomere function and will likely have direct effects on thick filament activity by interacting with MyBP-C and either the HMM portion of the myosin or the LMM core of the thick filament which is involved in the sequestering of myosin heads (Spudich, 2019). It is important to note that, while titin mutations are the most commonly identified genetic etiology of DCM (~30%), it is rarely associated with HCM (Herman et al., 2012; LeWinter and Granzier, 2013). The reason for this skewed phenotypic effect is unclear, and the function of titin requires further investigation.

The recent development of pharmacotherapy with myosin modulators sheds further light on the regulation of sarcomere function (Trivedi et al., 2018; Spudich, 2019; Nag et al., 2021). Increasing the ensemble force of the sarcomere can be achieved through three different mechanisms: *1*) thick filament activation that leads to more myosin heads released and available to bind to actin, *2*) enhanced thin filament activation that allows more myosin heads to bind to actin, which in turn cooperatively opens more myosin binding sites and promotes more crossbridge formation, and *3*) enhanced biochemical/biophysical properties of the myosin motor. It should be noted that these three mechanisms are not mutually exclusive, and in fact there are likely many crossover effects. For example, OM stabilizes the PPS state, which pulls more myosin out of the IHM state, but OM also causes slowing of the actin-induced rotation of the myosin light chain binding domain during the actin-myosin cycle, and this myosin state enters a prolonged actin-bound state that likely activates the RTF by moving tropomyosin away from the myosin binding site on actin (Rohde et al., 2017). Further drug development targeting sarcomere function will require attention to the impact on overall ensemble force from all three mechanisms.

The characterization of the primary effects of HCM mutations on human cardiac myosin has revealed many aspects of sarcomere function that can be altered by a single amino acid change. As discussed above, there is growing evidence that these HCM mutations cause hypercontractility which leads over time to hypertrophy. These effects have been recapitulated at the cellular level, demonstrating the usefulness of induced pluripotent stem cell-derived cardiac myocytes as a system for assessing the effect of mutations in either a patient-derived or isogenic background (Vander Roest et al., 2021). How the increased contractility is perceived by the cardiac myocyte is as yet unclear, and will be critical to understand the mechanism of cellular hypertrophy, myocyte disarray and the

development of fibrosis. Increases in contractility could increase overall ATP utilization, resulting in energy imbalance (Abel and Doenst, 2011; Ashrafian et al., 2011), Ca^{2+} dysregulation and changes in wall tension that can trigger hypertrophic signaling (van Berlo et al., 2013; Davis et al., 2016). Therapeutic interventions to either reduce or augment myosin function hold promise for unmet clinical needs in cardiomyopathy and heart failure of various etiologies, respectively, as shown in the multiple clinical trials described above. Increasingly precise understanding of the alterations in contractility in disease states like HCM will continue to yield more sophisticated therapeutic interventions.

Author contributions

MK wrote the review with guidance and editorial assistance from KR and JS.

Funding

This work was supported by NIH grants 5R01-GM033289, 1R01-HL117138, and 1RM1-GM131981 to JS, and an NIH Career Development Award (1K08HL145020) and an AHA Career Development Award (19CDA34760125) to MK.

Conflict of interest

JS is cofounder and a member of the Scientific Advisory Board of Cytokinetics, Inc., a company developing small molecule therapeutics for treatment of hypertrophic cardiomyopathy and heart failure.

The remaining authors declare that the research was conducted in the absence of any commercial or financial relationships that could be construed as a potential conflict of interest.

Publisher's note

References

Abel, E. D., and Doenst, T. (2011). Mitochondrial adaptations to physiological vs. pathological cardiac hypertrophy. *Cardiovasc. Res.* 90 (2), 234–242. doi:10.1093/cvr/cvr015

Adhikari, A. S., Kooiker, K. B., Sarkar, S. S., Liu, C., Bernstein, D., Spudich, J. A., et al. (2016). Early-onset hypertrophic cardiomyopathy mutations significantly increase the velocity, force, and actin-activated ATPase activity of human β-cardiac myosin. *Cell. Rep.* 17 (11), 2857–2864. doi:10.1016/j.celrep.2016.11.040

Adhikari, A. S., Trivedi, D. V., Sarkar, S. S., Song, D., Kooiker, K. B., Bernstein, D., et al. (2019). β-Cardiac myosin hypertrophic cardiomyopathy mutations release sequestered heads and increase enzymatic activity. *Nat. Commun.* 10 (1), 2685. doi:10.1038/s41467-019-10555-9

Ait-Mou, Y., Hsu, K., Farman, G. P., Kumar, M., Greaser, M. L., Irving, T. C., et al. (2016). Titin strain contributes to the Frank–Starling law of the heart by structural rearrangements of both thin- and thick-filament proteins. *Proc. Natl. Acad. Sci. U. S. A.* 113 (8), 2306–2311. doi:10.1073/pnas.1516732113

Aksel, T., Choe Yu, E., Sutton, S., Ruppel, K. M., and Spudich, J. A. (2015). Ensemble force changes that result from human cardiac myosin mutations and a small-molecule effector. *Cell. Rep.* 11 (6), 910–920. doi:10.1016/j.celrep.2015.04.006

Anan, R., Greve, G., Thierfelder, L., Watkins, H., McKenna, W. J., Solomon, S., et al. (1994). Prognostic implications of novel beta cardiac myosin heavy chain gene mutations that cause familial hypertrophic cardiomyopathy. *J. Clin. Investig.* 93 (1), 280–285. doi:10.1172/JCI116957

Anderson, R. L., Trivedi, D. V., Sarkar, S. S., Henze, M., Ma, W., Gong, H., et al. (2018). Deciphering the super relaxed state of human β-cardiac myosin and the mode of action of mavacamten from myosin molecules to muscle fibers. *Proc. Natl. Acad. Sci. U. S. A.* 115 (35), E8143-E8152. doi:10.1073/pnas.1809540115

Ashrafian, H., McKenna, W. J., and Watkins, H. (2011). "Disease pathways and novel therapeutic targets in hypertrophic cardiomyopathy,". Editor J. Robbins, 109, 86–96. doi:10.1161/CIRCRESAHA.111.242974 *Circ. Res.*1.

Ashrafian, H., Redwood, C., Blair, E., and Watkins, H. (2003). Hypertrophic cardiomyopathy:a paradigm for myocardial energy depletion. *Trends Genet.* 19 (5), 263–268. doi:10.1016/S0168-9525(03)00081-7

Bailey, K., Reiss, M., and Baxter, J. S. (1946). Tropomyosin : A new asymmetric protein component of muscle. *Nature* 157 (3986), 368–369. doi:10.1038/157368a0

Bers, D. M. (2002). Cardiac excitation–contraction coupling. *Nature* 415, 198–205. doi:10.1038/415198a

Bers, D. M., and Guo, T. (2005). Calcium signaling in cardiac ventricular myocytes. *Ann. N. Y. Acad. Sci.* 1047 (1), 86–98. doi:10.1196/annals.1341.008

Blankenfeldt, W., Thoma, N. H., Wray, J. S., Gautel, M., and Schlichting, I. (2006). Crystal structures of human cardiac β-myosin II S2-Δ provide insight into the functional role of the S2 subfragment. *Proc. Natl. Acad. Sci. U. S. A.* 103, 17713–17717. doi:10.1073/pnas.0606741103

Bloemink, M., Deacon, J., Langer, S., Vera, C., Combs, A., Leinwand, L., et al. (2014). The hypertrophic cardiomyopathy myosin mutation R453C alters ATP binding and hydrolysis of human cardiac β-myosin. *J. Biol. Chem.* 289 (8), 5158–5167. doi:10.1074/jbc.M113.511204

Brunello, E., Fusi, L., Ghisleni, A., Park-Holohan, S. J., Ovejero, J. G., Narayanan, T., et al. (2020). Myosin filament-based regulation of the dynamics of contraction in heart muscle. *Proc. Natl. Acad. Sci. U. S. A.* 117 (14), 8177–8186. doi:10.1073/pnas.1920632117

Chuang, C., Collibee, S., Ashcraft, L., Wang, W., Vander Wal, M., Wang, X., et al. (2021). Discovery of aficamten (CK-274), a next-generation cardiac myosin inhibitor for the treatment of hypertrophic cardiomyopathy. *J. Med. Chem.* 64 (19), 14142–14152. doi:10.1021/acs.jmedchem.1c01290

Cleland, J. G., Teerlink, J. R., Senior, R., Nifontov, E. M., Mc Murray, J. J. V., Lang, C. C., et al. (2011). The effects of the cardiac myosin activator, omecamtiv mecarbil, on cardiac function in systolic heart failure: A double-blind, placebo-controlled, crossover, dose-ranging phase 2 trial. *Lancet* 378 (9792), 676–683. doi:10.1016/S0140-6736(11)61126-4

Colegrave, M., and Peckham, M. (2014). Structural implications of β-cardiac myosin heavy chain mutations in human disease: Cardiac myosin mutations and disease. *Anat. Rec.* 297 (9), 1670–1680. doi:10.1002/ar.22973

Cooke, R. (2011). The role of the myosin ATPase activity in adaptive thermogenesis by skeletal muscle. *Biophys. Rev.* 3 (1), 33–45. doi:10.1007/s12551-011-0044-9

Craig, R., Lee, K. H., Mun, J. Y., Torre, I., and Luther, P. K. (2014). Structure, sarcomeric organization, and thin filament binding of cardiac myosin-binding protein-C. *Pflugers Arch.* 466 (3), 425–431. doi:10.1007/s00424-013-1426-6

Craig, R., and Woodhead, J. L. (2006). Structure and function of myosin filaments. *Curr. Opin. Struct. Biol.* 16 (2), 204–212. doi:10.1016/j.sbi.2006.03.006

Cuda, G., Fananapazir, L., Epstein, N. D., and Sellers, J. R. (1997). The in vitro motility activity of β-cardiac myosin depends on the nature of the β-myosin heavy chain gene mutation in hypertrophic cardiomyopathy. *J. Muscle Res. Cell. Motil.* 18 (3), 275–283. doi:10.1023/A:1018613907574

Davis, J., Davis, L. C., Correll, R. N., Makarewich, C. A., Schwanekamp, J. A., Moussavi-Harami, F., et al. (2016). A tension-based model distinguishes hypertrophic versus dilated cardiomyopathy. *Cell.* 165 (5), 1147–1159. doi:10.1016/j.cell.2016.04.002

De La Cruz, E. M., and Michael Ostap, E. (2009)., 455. Elsevier, 157–192. doi:10.1016/S0076-6879(08)04206-7 Chapter 6 kinetic and equilibrium analysis of the myosin ATPase*Methods Enzym.*

De La Cruz, E. M., and Ostap, E. M. (2004). Relating biochemistry and function in the myosin superfamily. *Curr. Opin. Cell. Biol.* 16 (1), 61–67. doi:10.1016/j.ceb.2003.11.011

de Tombe, P. P., Mateja, R. D., Tachampa, K., Mou, Y. A., Farman, G. P., and Irving, T. C. (2010). Myofilament length dependent activation. *J. Mol. Cell. Cardiol.* 48 (5), 851–858. doi:10.1016/j.yjmcc.2009.12.017

Deacon, J. C., Bloemink, M. J., Rezavandi, H., Geeves, M. A., and Leinwand, L. A. (2012). Identification of functional differences between recombinant human α and β cardiac myosin motors. *Cell. Mol. Life Sci.* 69 (13), 2261–2277. doi:10.1007/s00018-012-0927-3

Debold, E. P., Schmitt, J. P., Patlak, J. B., Beck, S. E., Moore, J. R., Seidman, J. G., et al. (2007). Hypertrophic and dilated cardiomyopathy mutations differentially affect the molecular force generation of mouse α-cardiac myosin in the laser trap assay. *Am. J. Physiol. Heart Circ. Physiol.* 293 (1), H284–H291. doi:10.1152/ajpheart.00128.2007

Enjuto, M., Francino, A., Navarro-López, F., Viles, D., Paré, J. C., and Ballesta, A. M. (2000). Malignant hypertrophic cardiomyopathy caused by the Arg723Gly mutation in β -myosin heavy chain gene. *J. Mol. Cell. Cardiol.* 32 (12), 2307–2313. doi:10.1006/jmcc.2000.1260

Fananapazir, L., Dalakas, M. C., CyranF., Cohn, G., and Epstein, N. D. (1993). Missense mutations in the beta-myosin heavy-chain gene cause central core disease in hypertrophic cardiomyopathy. *Proc. Natl. Acad. Sci. U. S. A.* 90, 3993–3997. doi:10.1073/pnas.90.9.3993

Fatkin, D., Seidman, C. E., and Seidman, J. G. (2014). Genetics and disease of ventricular muscle. *Cold Spring Harb. Perspect. Med.* 4 (1), a021063. doi:10.1101/cshperspect.a021063

Fearnley, C. J., Roderick, H. L., and Bootman, M. D. (2011). Calcium signaling in cardiac myocytes. *Cold Spring Harb. Perspect. Biol.* 3 (11), a004242. doi:10.1101/cshperspect.a004242

Finer, J. T., Simmons, R. M., and Spudich, J. A. (1994). Single myosin molecule mechanics: Piconewton forces and nanometre steps. *Nature* 368 (6467), 113–119. doi:10.1038/368113a0

Flashman, E., Redwood, C., Moolman-Smook, J., and Watkins, H. (2004). Cardiac myosin binding protein C: Its role in physiology and disease. *Circ. Res.* 94 (10), 1279–1289. doi:10.1161/01.RES.0000127175.21818.C2

Fraysse, B., Weinberger, F., Bardswell, S. C., Cuello, F., Vignier, N., Geertz, B., et al. (2012). Increased myofilament Ca2+ sensitivity and diastolic dysfunction as early consequences of Mybpc3 mutation in heterozygous knock-in mice. *J. Mol. Cell. Cardiol.* 52 (6), 1299–1307. doi:10.1016/j.yjmcc.2012.03.009

García-Giustiniani, D., Arad, M., Ortíz-Genga, M., Barriales-Villa, R., Fernandez, X., Rodriguez-Garcia, I., et al. (2015). Phenotype and prognostic correlations of the converter region mutations affecting the β myosin heavy chain. *Heart* 101 (13), 1047–1053. doi:10.1136/heartjnl-2014-307205

Geisterfer-Lowrance, A. A. T., Christe, M., Conner, D. A., Ingwall, J. S., Schoen, F. J., Seidman, C. E., et al. (1996). A mouse model of familial hypertrophic cardiomyopathy. *Science* 272 (5262), 731–734. doi:10.1126/science.272.5262.731

Geisterfer-Lowrance, A. A. T., Kass, S., Tanigawa, G., Vosberg, H. P., McKenna, W., Seidman, C. E., et al. (1990). A molecular basis for familial hypertrophic cardiomyopathy: A β cardiac myosin heavy chain gene missense mutation. *Cell.* 62 (5), 999–1006. doi:10.1016/0092-8674(90)90274-I

Georgakopoulos, D., Christe, M. E., Giewat, M., Seidman, C. M., Seidman, J. G., and Kass, D. A. (1999). The pathogenesis of familial hypertrophic cardiomyopathy: Early and evolving effects from an α-cardiac myosin heavy chain missense mutation. *Nat. Med.* 5 (3), 327–330. doi:10.1038/6549

Green, E. M., Wakimoto, H., Anderson, R. L., Evanchik, M. J., Gorham, J. M., Harrison, B. C., et al. (2016). A small-molecule inhibitor of sarcomere contractility suppresses hypertrophic cardiomyopathy in mice. *Science* 351 (6273), 617–621. doi:10.1126/science.aad3456

Greenberg, M. J., Kazmierczak, K., Szczesna-Cordary, D., and Moore, J. R. (2010). Cardiomyopathy-linked myosin regulatory light chain mutations disrupt myosin strain-dependent biochemistry. *Proc. Natl. Acad. Sci. U. S. A.* 107 (40), 17403–17408. doi:10.1073/pnas.1009619107

Greenberg, M. J., and Moore, J. R. (2010). The molecular basis of frictional loads in the in vitro motility assay with applications to the study of the loaded mechanochemistry of molecular motors. *Cytoskeleton* 67 (5), 273–285. doi:10.1002/cm.20441

Gruen, M., and Gautel, M. (1999). Mutations in beta-myosin S2 that cause familial hypertrophic cardiomyopathy (FHC) abolish the interaction with the regulatory domain of myosin-binding protein-C. *J. Mol. Biol.* 286, 933–949. doi:10.1006/jmbi.1998.2522

Gruver, E. J., Fatkin, D., Dodds, G. A., Kisslo, J., Maron, B. J., Seidman, J. G., et al. (1999). Familial hypertrophic cardiomyopathy and atrial fibrillation caused by Arg663His beta–cardiac myosin heavy chain mutation. *Am. J. Cardiol.* 83 (1), 13H-18H–18H. doi:10.1016/S0002-9149(99)00251-9

Gupte, T. M., Haque, F., Gangadharan, B., Sunitha, M. S., Mukherjee, S., Anandhan, S., et al. (2015). Mechanistic heterogeneity in contractile properties of α-tropomyosin (TPM1) mutants associated with inherited cardiomyopathies. *J. Biol. Chem.* 290 (11), 7003–7015. doi:10.1074/jbc.M114.596676

Hariadi, R. F., Sommese, R. F., Adhikari, A. S., Taylor, R. E., Sutton, S., Spudich, J. A., et al. (2015). Mechanical coordination in motor ensembles revealed using engineered artificial myosin filaments. *Nat. Nanotechnol.* 10 (8), 696–700. doi:10.1038/nnano.2015.132

Harris, S. P., Lyons, R. G., and Bezold, K. L. (2011). "In the thick of it: HCM-causing mutations in myosin binding proteins of the thick filament,". Editors J. Robbins, C. Seidman, and H. Watkins, 108, 751–764. doi:10.1161/CIRCRESAHA.110.231670 *Circ. Res.*6.

Harris, S. P. (2021). Making waves: A proposed new role for myosin-binding protein C in regulating oscillatory contractions in vertebrate striated muscle. *J. Gen. Physiol.* 153 (3), e202012729. doi:10.1085/jgp.202012729

Hegde, S. M., Lester, S. J., Solomon, S. D., Michels, M., Elliott, P. M., Nagueh, S. F., et al. (2021). Effect of mavacamten on echocardiographic features in symptomatic patients with obstructive hypertrophic cardiomyopathy. *J. Am. Coll. Cardiol.* 78 (25), 2518–2532. doi:10.1016/j.jacc.2021.09.1381

Heitner, S. B., Jacoby, D., Lester, S. J., Owens, A., Wang, A., Zhang, D., et al. (2019). Mavacamten treatment for obstructive hypertrophic cardiomyopathy: A clinical trial. *Ann. Intern. Med.* 170 (11), 741–748. doi:10.7326/M18-3016

Heling, L. W. H. J., Geeves, M. A., and Kad, N. M. (2020). MyBP-C: One protein to govern them all. *J. Muscle Res. Cell. Motil.* 41 (1), 91–101. doi:10.1007/s10974-019-09567-1

Helms, A. S., Davis, F. M., Coleman, D., Bartolone, S. N., Glazier, A. A., Pagani, F., et al. (2014). Sarcomere mutation-specific expression patterns in human hypertrophic cardiomyopathy. *Circ. Cardiovasc. Genet.* 7 (4), 434–443. doi:10.1161/CIRCGENETICS.113.000448

Helms, A. S., Tang, V. T., O'Leary, T. S., Friedline, S., Wauchope, M., Arora, A., et al. (2020). Effects of MYBPC3 loss-of-function mutations preceding hypertrophic cardiomyopathy. *JCI Insight* 5 (2), e133782. doi:10.1172/jci.insight.133782

Herman, D. S., Lam, L., Taylor, M. R. G., Wang, L., Teekakirikul, P., Christodoulou, D., et al. (2012). Truncations of titin causing dilated cardiomyopathy. *N. Engl. J. Med.* 366 (7), 619–628. doi:10.1056/NEJMoa1110186

Ho, C. Y., Mealiffe, M. E., Bach, R. G., Bhattacharya, M., Choudhury, L., Edelberg, J. M., et al. (2020). Evaluation of mavacamten in symptomatic patients with nonobstructive hypertrophic cardiomyopathy. *J. Am. Coll. Cardiol.* 75 (21), 2649–2660. doi:10.1016/j.jacc.2020.03.064

Ho, C. Y., Sweitzer, N. K., McDonough, B., Maron, B. J., Casey, S. A., Seidman, J. G., et al. (2002). Assessment of diastolic function with Doppler tissue imaging to predict genotype in preclinical hypertrophic cardiomyopathy. *Circulation* 105 (25), 2992–2997. doi:10.1161/01.CIR.0000019070.70491.6D

Homburger, J. R., Green, E. M., Caleshu, C., Sunitha, M. S., Taylor, R. E., Ruppel, K. M., et al. (2016). Multidimensional structure-function relationships in human β-cardiac myosin from population-scale genetic variation. *Proc. Natl. Acad. Sci. U. S. A.* 113 (24), 6701–6706. doi:10.1073/pnas.1606950113

Hooijman, P., Stewart, M. A., and Cooke, R. (2011). A new state of cardiac myosin with very slow ATP turnover: A potential cardioprotective mechanism in the heart. *Biophys. J.* 100 (8), 1969–1976. doi:10.1016/j.bpj.2011.02.061

Houdusse, A., and Sweeney, H. L. (2016). How myosin generates force on actin filaments. *Trends biochem. Sci.* 41 (12), 989–997. doi:10.1016/j.tibs.2016.09.006

Huxley, H. E., and Hanson, J. (1959). The structural basis of the contraction mechanism in striated muscle. *Ann. N. Y. Acad. Sci.* 81 (2), 403–408. doi:10.1111/j.1749-6632.1959.tb49323.x

Huxley, H. E. (1969). The mechanism of muscular contraction. *Science* 164 (3886), 1356–1365. doi:10.1126/science.164.3886.1356

Jung, H. S., Komatsu, S., Ikebe, M., and Craig, R. (2008). "Head–head and head–tail interaction: A general mechanism for switching off myosin II activity in cells,". Editor T. D. Pollard, 19, 3234–3242. doi:10.1091/mbc.e08-02-0206

Kampourakis, T., Zhang, X., Sun, Y. B., and Irving, M. (2018). Omecamtiv mercabil and blebbistatin modulate cardiac contractility by perturbing the regulatory state of the myosin filament. *J. Physiol.* 596 (1), 31–46. doi:10.1113/JP275050

Kaski, J. P., Syrris, P., Esteban, M. T. T., Jenkins, S., Pantazis, A., Deanfield, J. E., et al. (2009). Prevalence of sarcomere protein gene mutations in preadolescent children with hypertrophic cardiomyopathy. *Circ. Cardiovasc. Genet.* 2 (5), 436–441. doi:10.1161/CIRCGENETICS.108.821314

Kawana, M., Sarkar, S. S., Sutton, S., Ruppel, K. M., and Spudich, J. A. (2017). Biophysical properties of human β-cardiac myosin with converter mutations that cause hypertrophic cardiomyopathy. *Sci. Adv.* 3 (2), e1601959. doi:10.1126/sciadv.1601959

Klein, M. D., Lane, F. J., and Gorlin, R. (1965). Effect of left ventricular size and shape upon the hemodynamics of subaortic stenosis. *Am. J. Cardiol.* 15 (6), 773–781. doi:10.1016/0002-9149(65)90379-6

Kobayashi, T., and Solaro, R. J. (2005). CALCIUM, thin filaments, and the integrative biology of cardiac contractility. *Annu. Rev. Physiol.* 67 (1), 39–67. doi:10.1146/annurev.physiol.67.040403.114025

Kreutziger, K. L., Gillis, T. E., Davis, J. P., Tikunova, S. B., and Regnier, M. (2007). Influence of enhanced troponin C Ca $^{2+}$ -binding affinity on cooperative thin filament activation in rabbit skeletal muscle: sTnC Ca $^{2+}$ -binding properties and cooperative thin filament activation. *J. Physiol.* 583 (1), 337–350. doi:10.1113/jphysiol.2007.135426

Kron, S. J., and Spudich, J. A. (1986). Fluorescent actin filaments move on myosin fixed to a glass surface. *Proc. Natl. Acad. Sci. U. S. A.* 83 (17), 6272–6276. doi:10.1073/pnas.83.17.6272

Kuster, D. W. D., Bawazeer, A. C., Zaremba, R., Goebel, M., Boontje, N. M., and van der Velden, J. (2012). Cardiac myosin binding protein C phosphorylation in cardiac disease. *J. Muscle Res. Cell. Motil.* 33 (1), 43–52. doi:10.1007/s10974-011-9280-7

Lee, K. H., Sulbarán, G., Yang, S., Mun, J. Y., Alamo, L., Pinto, A., et al. (2018). Interacting-heads motif has been conserved as a mechanism of myosin II inhibition since before the origin of animals. *Proc. Natl. Acad. Sci. U. S. A.* 115 (9), E1991-E2000. doi:10.1073/pnas.1715247115

LeWinter, M. M., and Granzier, H. L. (2013). Titin is a major human disease gene. *Circulation* 127 (8), 938–944. doi:10.1161/CIRCULATIONAHA.112.139717

Liu, C., Kawana, M., Song, D., Ruppel, K. M., and Spudich, J. A. (2018). Controlling load-dependent kinetics of β-cardiac myosin at the single-molecule level. *Nat. Struct. Mol. Biol.* 25 (6), 505–514. doi:10.1038/s41594-018-0069-x

Liu, L., Srikakulam, R., and Winkelmann, D. A. (2008). Unc45 activates hsp90-dependent folding of the myosin motor domain. *J. Biol. Chem.* 283 (19), 13185–13193. doi:10.1074/jbc.M800757200

Liu, Y., White, H. D., Belknap, B., Winkelmann, D. A., and Forgacs, E. (2015). Omecamtiv mecarbil modulates the kinetic and motile properties of porcine β-cardiac myosin. *Biochemistry* 54 (10), 1963–1975. doi:10.1021/bi5015166

Lowey, S., Lesko, L. M., Rovner, A. S., Hodges, A. R., White, S. L., Low, R. B., et al. (2008). Functional effects of the hypertrophic cardiomyopathy R403Q mutation are different in an α- or β-myosin heavy chain backbone. *J. Biol. Chem.* 283 (29), 20579–20589. doi:10.1074/jbc.M800554200

Lowey, S., and Trybus, K. M. (2010). Common structural motifs for the regulation of divergent class II myosins. *J. Biol. Chem.* 285 (22), 16403–16407. doi:10.1074/jbc.R109.025551

Ma, W., Gong, H., Qi, L., Nag, S., and Irving, T. C. (2022). *Cardiac myosin filaments are directly regulated by calcium*. BioRxiv. doi:10.1101/2022.02.19.481172

Malik, F. I., Hartman, J. J., Elias, K. A., Morgan, B. P., Rodriguez, H., Brejc, K., et al. (2011). Cardiac myosin activation: A potential therapeutic approach for systolic heart failure. *Science* 331 (6023), 1439–1443. doi:10.1126/science.1200113

Maron, B. J., Maron, M. S., and Semsarian, C. (2012). Genetics of hypertrophic cardiomyopathy after 20 years: Clinical perspectives. *J. Am. Coll. Cardiol.* 60 (8), 705–715. doi:10.1016/j.jacc.2012.02.068

Maron, M., Ashley, E., and Blok, T. (2016). Abstract 16842: Obstructive hypertrophic cardiomyopathy: Initial single ascending dose data in healthy volunteers and patients. *Circulation* 134 (1), A16842. doi:10.1161/circ.134.suppl_1.16842

Maron, Martin (2021). "Redwood-HCM: A randomized, double-blind, placebo-controlled, dose-finding trial of the cardiac myosin inhibitor, aficamten," in *Obstructive hypertrophic cardiomyopathy* (Heart Failure Society of America, Annual Scientific Meeting).

Marston, S. B. (2011). How do mutations in contractile proteins cause the primary familial cardiomyopathies? *J. Cardiovasc. Transl. Res.* 4 (3), 245–255. doi:10.1007/s12265-011-9266-2

Marston, S. B. (2016). Why is there a limit to the changes in myofilament Ca2+-sensitivity associated with myopathy causing mutations? *Front. Physiol.* 7, 415. doi:10.3389/fphys.2016.00415

McNally, E. M., Golbus, J. R., and Puckelwartz, M. J. (2013). Genetic mutations and mechanisms in dilated cardiomyopathy. *J. Clin. Investig.* 123 (1), 19–26. doi:10.1172/JCI62862

McNamara, J. W., Li, A., dos Remedios, C. G., and Cooke, R. (2015). The role of super-relaxed myosin in skeletal and cardiac muscle. *Biophys. Rev.* 7 (1), 5–14. doi:10.1007/s12551-014-0151-5

Moore, J. R., Leinwand, L., and Warshaw, D. M. (2012). "Understanding cardiomyopathy phenotypes based on the functional impact of mutations in the myosin motor,". Editors J. Robbins, C. Seidman, and H. Watkins, 111, 375–385. doi:10.1161/CIRCRESAHA.110.223842

Morck, M. M., Bhowmik, D., Pathak, D., Dawood, A., Spudich, J., and Ruppel, K. M. (2022). in *Hypertrophic cardiomyopathy mutations in the pliant and light chain-binding regions of the lever arm of human β-cardiac myosin have divergent effects on myosin function*. Editors J. R. Sellers, A. Akhmanova, J. R. Sellers, and E. M. Ostap (Cambridge, UK: eLife), 11, e76805. doi:10.7554/eLife.76805

Moss, R. L., and Fitzsimons, D. P. (2010). Regulation of contraction in mammalian striated muscles—The plot thick-ens. *J. Gen. Physiol.* 136 (1), 21–27. doi:10.1085/jgp.201010471

Moss, R. L., Razumova, M., and Fitzsimons, D. P. (2004). Myosin crossbridge activation of cardiac thin filaments: Implications for myocardial function in Health and disease. *Circ. Res.* 94 (10), 1290–1300. doi:10.1161/01.RES.0000127125.61647.4F

Nag, S., Sommese, R. F., Ujfalusi, Z., Combs, A., Langer, S., Sutton, S., et al. (2015). Contractility parameters of human β-cardiac myosin with the hypertrophic cardiomyopathy mutation R403Q show loss of motor function. *Sci. Adv.* 1 (9), e1500511. doi:10.1126/sciadv.1500511

Nag, S., and Trivedi, D. V. (2021). in *To lie or not to lie: Super-relaxing with myosins*. Editor S. R. Pfeffer (Cambridge, UK: eLife), 10, e63703. doi:10.7554/eLife.63703

Nag, S., Trivedi, D. V., Sarkar, S. S., Adhikari, A. S., Sunitha, M. S., Sutton, S., et al. (2017). The myosin mesa and the basis of hypercontractility caused by hypertrophic cardiomyopathy mutations. *Nat. Struct. Mol. Biol.* 24 (6), 525–533. doi:10.1038/nsmb.3408

Olivotto, I., Oreziak, A., Barriales-Villa, R., Abraham, T. P., Masri, A., Garcia-Pavia, P., et al. (2020). Mavacamten for treatment of symptomatic obstructive hypertrophic cardiomyopathy (EXPLORER-HCM): A randomised, double-blind, placebo-controlled, phase 3 trial. *Lancet* 396 (10253), 759–769. doi:10.1016/S0140-6736(20)31792-X

Palmer, B. M., Fishbaugher, D. E., Schmitt, J. P., Wang, Y., Alpert, N. R., Seidman, C. E., et al. (2004). Differential cross-bridge kinetics of FHC myosin mutations R403Q and R453C in heterozygous mouse myocardium. *Am. J. Physiol. Heart Circ. Physiol.* 287 (1), H91–H99. doi:10.1152/ajpheart.01015.2003

Palmiter, K. A., Tyska, M. J., Haeberle, J. R., Alpert, N. R., Fananapazir, L., and Warshaw, D. M. (2000). R403Q and L908V mutant beta-cardiac myosin from patients with familial hypertrophic cardiomyopathy exhibit enhanced mechanical performance at the single molecule level. *J. Muscle Res. Cell. Motil.* 21, 609–620. doi:10.1023/a:1005678905119

Pan, S., Sommese, R. F., Sallam, K. I., Nag, S., Sutton, S., Miller, S. M., et al. (2015). Establishing disease causality for a novel gene variant in familial dilated cardiomyopathy using a functional *in-vitro* assay of regulated thin filaments and human cardiac myosin. *BMC Med. Genet.* 16 (1), 97. doi:10.1186/s12881-015-0243-5

Parmacek, M. S., and Solaro, R. J. (2004). Biology of the troponin complex in cardiac myocytes. *Prog. Cardiovasc. Dis.* 47 (3), 159–176. doi:10.1016/j.pcad.2004.07.003

Planelles-Herrero, V. J., Hartman, J. J., Robert-Paganin, J., Malik, F. I., and Houdusse, A. (2017). Mechanistic and structural basis for activation of cardiac myosin force production by omecamtiv mecarbil. *Nat. Commun.* 8 (1), 190. doi:10.1038/s41467-017-00176-5

Ponnam, S., and Kampourakis, T. (2022). Microscale thermophoresis suggests a new model of regulation of cardiac myosin function via interaction with cardiac myosin-binding protein C. *J. Biol. Chem.* 298 (1), 101485. doi:10.1016/j.jbc.2021.101485

Rader, F., Choudhury, L., Saberi, S., Fermin, D., Wheeler, M. T., Abraham, T. P., et al. (2021). Long-term safety of mavacamten in patients with obstructive hypertrophic cardiomyopathy: Interim results of the mava-long term extension (lte) study. *J. Am. Coll. Cardiol.* 77 (1), 532. doi:10.1016/S0735-1097(21)01891-X

Ratti, J., Rostkova, E., Gautel, M., and Pfuhl, M. (2011). Structure and interactions of myosin-binding protein C domain C0. *J. Biol. Chem.* 286 (14), 12650–12658. doi:10.1074/jbc.M110.156646

Resnicow, D. I., Deacon, J. C., Warrick, H. M., Spudich, J. A., and Leinwand, L. A. (2010). Functional diversity among a family of human skeletal muscle myosin motors. *Proc. Natl. Acad. Sci. U. S. A.* 107 (3), 1053–1058. doi:10.1073/pnas.0913527107

Ribeiro, A. J. S., Ang, Y. S., Fu, J. D., Rivas, R. N., Mohamed, T. M. A., Higgs, G. C., et al. (2015). Contractility of single cardiomyocytes differentiated from pluripotent stem cells depends on physiological shape and substrate stiffness. *Proc. Natl. Acad. Sci. U. S. A.* 112 (41), 12705–12710. doi:10.1073/pnas.1508073112

Robert-Paganin, J., Auguin, D., and Houdusse, A. (2018). Hypertrophic cardiomyopathy disease results from disparate impairments of cardiac myosin function and auto-inhibition. *Nat. Commun.* 9 (1), 4019. doi:10.1038/s41467-018-06191-4

Rohde, J. A., Thomas, D. D., and Muretta, J. M. (2017). Heart failure drug changes the mechanoenzymology of the cardiac myosin powerstroke. *Proc. Natl. Acad. Sci. U. S. A.* 114 (10), E1796-E1804. doi:10.1073/pnas.1611698114

Saberi, S., Cardim, N., Yamani, M., Schulz-Menger, J., Li, W., Florea, V., et al. (2021). Mavacamten favorably impacts cardiac structure in obstructive hypertrophic cardiomyopathy: EXPLORER-HCM cardiac magnetic resonance substudy analysis. *Circulation* 143 (6), 606–608. doi:10.1161/CIRCULATIONAHA.120.052359

Sarkar, S. S., Trivedi, D. V., Morck, M. M., Adhikari, A. S., Pasha, S. N., Ruppel, K. M., et al. (2020). The hypertrophic cardiomyopathy mutations R403Q and R663H increase the number of myosin heads available to interact with actin. *Sci. Adv.* 6 (14), eaax0069. doi:10.1126/sciadv.aax0069

Seidman, C. E., and Seidman, J. G. (2019). "Hypertrophic cardiomyopathy," in *The online metabolic and molecular bases of inherited disease*. Editors D. L. Valle, S. Antonarakis, A. Ballabio, A. L. Beaudet, and G. A. Mitchell (McGraw-Hill Education). ommbid.mhmedical.com/content.aspx?aid=1181476540 (Accessed April 1, 2022).

Seidman, C. E., and Seidman, J. G. (2011). "Identifying sarcomere gene mutations in hypertrophic cardiomyopathy: A personal history," in *Circ res*. Editors J. Robbins and H. Watkins, 108, 743–750. doi:10.1161/CIRCRESAHA.110.223834 6

Seidman, J. G., and Seidman, C. E. (2001). The genetic basis for cardiomyopathy: From mutation identification to mechanistic paradigms. *Cell.* 104, 557–567. doi:10.1016/s0092-8674(01)00242-2

Semsarian, C., Ingles, J., Maron, M. S., and Maron, B. J. (2015). New perspectives on the prevalence of hypertrophic cardiomyopathy. *J. Am. Coll. Cardiol.* 65 (12), 1249–1254. doi:10.1016/j.jacc.2015.01.019

Sivaramakrishnan, S., Ashley, E., Leinwand, L., and Spudich, J. A. (2009). Insights into human β-cardiac myosin function from single molecule and single cell studies. *J. Cardiovasc. Transl. Res.* 2 (4), 426–440. doi:10.1007/s12265-009-9129-2

Sommese, R. F., Nag, S., Sutton, S., Miller, S. M., Spudich, J. A., and Ruppel, K. M. (2013). "Effects of troponin T cardiomyopathy mutations on the calcium sensitivity of the regulated thin filament and the actomyosin cross-bridge kinetics of human β-cardiac myosin,". Editor A. Kimura, 8, e83403. doi:10.1371/journal.pone.0083403

Sommese, R. F., Sung, J., Nag, S., Sutton, S., Deacon, J. C., Choe, E., et al. (2013). Molecular consequences of the R453C hypertrophic cardiomyopathy mutation on human β-cardiac myosin motor function. *Proc. Natl. Acad. Sci. U. S. A.* 110 (31), 12607–12612. doi:10.1073/pnas.1309493110

Spudich, J. A. (2014). Hypertrophic and dilated cardiomyopathy: Four decades of basic research on muscle lead to potential therapeutic approaches to these devastating genetic diseases. *Biophys. J.* 106 (6), 1236–1249. doi:10.1016/j.bpj.2014.02.011

Spudich, J. A. (2015). The myosin mesa and a possible unifying hypothesis for the molecular basis of human hypertrophic cardiomyopathy. *Biochem. Soc. Trans.* 43 (1), 64–72. doi:10.1042/BST20140324

Spudich, J. A. (2019). Three perspectives on the molecular basis of hypercontractility caused by hypertrophic cardiomyopathy mutations. *Pflugers Arch.* 471 (5), 701–717. doi:10.1007/s00424-019-02259-2

Srikakulam, R., and Winkelmann, D. A. (2004). Chaperone-mediated folding and assembly of myosin in striated muscle. *J. Cell. Sci.* 117 (4), 641–652. doi:10.1242/jcs.00899

Starr, R., and Offer, G. (1978). The interaction of C-protein with heavy meromyosin and subfragment-2. *Biochem. J.* 171 (3), 813–816. doi:10.1042/bj1710813

Stewart, M. A., Franks-Skiba, K., Chen, S., and Cooke, R. (2010). Myosin ATP turnover rate is a mechanism involved in thermogenesis in resting skeletal muscle fibers. *Proc. Natl. Acad. Sci. U. S. A.* 107 (1), 430–435. doi:10.1073/pnas.0909468107

Sung, J., Nag, S., Mortensen, K. I., Vestergaard, C. L., Sutton, S., Ruppel, K., et al. (2015). Harmonic force spectroscopy measures load-dependent kinetics of individual human β-cardiac myosin molecules. *Nat. Commun.* 6 (1), 7931. doi:10.1038/ncomms8931

Sung, J., Sivaramakrishnan, S., Dunn, A. R., and Spudich, J. A. (2010). "Single-molecule dual-beam optical trap analysis of protein structure and function," in *Methods in enzymology* (Elsevier), 475, 321–375. doi:10.1016/S0076-6879(10)75014-X

Sweeney, H. L., and Houdusse, A. (2010). Structural and functional insights into the myosin motor mechanism. *Annu. Rev. Biophys.* 39 (1), 539–557. doi:10.1146/annurev.biophys.050708.133751

Swenson, A. M., Tang, W., Blair, C. A., Fetrow, C. M., Unrath, W. C., Previs, M. J., et al. (2017). Omecamtiv mecarbil enhances the duty ratio of human β-cardiac myosin resulting in increased calcium sensitivity and slowed force development in cardiac muscle. *J. Biol. Chem.* 292 (9), 3768–3778. doi:10.1074/jbc.M116.748780

Tardiff, J. C. (2011). "Thin filament mutations: Developing an integrative approach to a complex disorder," in *Circ res*. Editors J. Robbins, C. Seidman, and H. Watkins, 108, 765–782. doi:10.1161/CIRCRESAHA.110.2241706

Teekakirikul, P., Eminaga, S., Toka, O., Alcalai, R., Wang, L., Wakimoto, H., et al. (2010). Cardiac fibrosis in mice with hypertrophic cardiomyopathy is mediated by non-myocyte proliferation and requires Tgf-β. *J. Clin. Investig.* 120 (10), 3520–3529. doi:10.1172/JCI42028

Teerlink, J. R., Clarke, C. P., Saikali, K. G., Lee, J. H., Chen, M. M., Escandon, R. D., et al. (2011). Dose-dependent augmentation of cardiac systolic function with the selective cardiac myosin activator, omecamtiv mecarbil: A first-in-man study. *Lancet* 378 (9792), 667–675. doi:10.1016/S0140-6736(11)61219-1

Teerlink, J. R., Diaz, R., Felker, G. M., McMurray, J. J. V., Metra, M., Solomon, S. D., et al. (2021). Cardiac myosin activation with omecamtiv mecarbil in systolic heart failure. *N. Engl. J. Med.* 384 (2), 105–116. doi:10.1056/NEJMoa2025797

Teerlink, J. R., Felker, G. M., McMurray, J. J. V., Ponikowski, P., Metra, M., Filippatos, G. S., et al. (2016). Acute treatment with omecamtiv mecarbil to increase contractility in acute heart failure: The ATOMIC-AHF study. *J. Am. Coll. Cardiol.* 67 (12), 1444–1455. doi:10.1016/j.jacc.2016.01.031

Teerlink, J. R., Felker, G. M., McMurray, J. J. V., Solomon, S. D., Adams, K. F., Cleland, J. G. F., et al. (2016). Chronic oral study of myosin activation to increase contractility in heart failure (COSMIC-HF): A phase 2, pharmacokinetic, randomised, placebo-controlled trial. *Lancet* 388 (10062), 2895–2903. doi:10.1016/S0140-6736(16)32049-9

Toepfer, C. N., Wakimoto, H., Garfinkel, A. C., McDonough, B., Liao, D., Jiang, J., et al. (2019). Hypertrophic cardiomyopathy mutations in *MYBPC3* dysregulate myosin. *Sci. Transl. Med.* 11 (476), eaat1199. doi:10.1126/scitranslmed.aat1199

Trivedi, D. V., Adhikari, A. S., Sarkar, S. S., Ruppel, K. M., and Spudich, J. A. (2018). Hypertrophic cardiomyopathy and the myosin mesa: Viewing an old disease in a new light. *Biophys. Rev.* 10 (1), 27–48. doi:10.1007/s12551-017-0274-6

Tyska, M. J., Hayes, E., Giewat, M., Seidman, C. E., Seidman, J. G., and Warshaw, D. M. (2000). Single-molecule mechanics of R403Q cardiac myosin isolated from the mouse model of familial hypertrophic cardiomyopathy. *Circ. Res.* 86 (7), 737–744. doi:10.1161/01.RES.86.7.737

Ujfalusi, Z., Vera, C. D., Mijailovich, S. M., Svicevic, M., Yu, E. C., Kawana, M., et al. (2018). Dilated cardiomyopathy myosin mutants have reduced force-generating capacity. *J. Biol. Chem.* 293 (23), 9017–9029. doi:10.1074/jbc.RA118.001938

Up, Malmqvist, Aronshtam, A., and Lowey, S. (2004). Cardiac myosin isoforms from different species have unique enzymatic and mechanical properties. *Biochemistry* 43 (47), 15058–15065. doi:10.1021/bi0495329

Uyeda, T. Q., Abramson, P. D., and Spudich, J. A. (1996). The neck region of the myosin motor domain acts as a lever arm to generate movement. *Proc. Natl. Acad. Sci. U. S. A.* 93 (9), 4459–4464. doi:10.1073/pnas.93.9.4459

Uyeda, T. Q. P., Kron, S. J., and Spudich, J. A. (1990). Myosin step size estimation from slow sliding movement of actin over low densities of heavy meromyosin. *J. Mol. Biol.* 214, 699–710. doi:10.1016/0022-2836(90)90287-V

van Berlo, J. H., Maillet, M., and Molkentin, J. D. (2013). Signaling effectors underlying pathologic growth and remodeling of the heart. *J. Clin. Investig.* 123 (1), 37–45. doi:10.1172/JCI62839

van der Velden, J., Tocchetti, C. G., Varricchi, G., Bianco, A., Sequeira, V., Hilfiker-Kleiner, D., et al. (2018). Metabolic changes in hypertrophic cardiomyopathies: Scientific update from the working group of myocardial function of the European society of cardiology. *Cardiovasc. Res.* 114 (10), 1273–1280. doi:10.1093/cvr/cvy147

Vander Roest, A. S., Liu, C., Morck, M. M., Kooiker, K. B., Jung, G., Song, D., et al. (2021). Hypertrophic cardiomyopathy β-cardiac myosin mutation (P710R) leads to hypercontractility by disrupting super relaxed state. *Proc. Natl. Acad. Sci. U. S. A.* 118 (24), e2025030118. doi:10.1073/pnas.2025030118

Veigel, C., Molloy, J. E., Schmitz, S., and Kendrick-Jones, J. (2003). Load-dependent kinetics of force production by smooth muscle myosin measured with optical tweezers. *Nat. Cell. Biol.* 5 (11), 980–986. doi:10.1038/ncb1060

Veigel, C., Schmitz, S., Wang, F., and Sellers, J. R. (2005). Load-dependent kinetics of myosin-V can explain its high processivity. *Nat. Cell. Biol.* 7 (9), 861–869. doi:10.1038/ncb1287

Vera, C. D., Johnson, C. A., Walklate, J., Adhikari, A., Svicevic, M., Mijailovich, S. M., et al. (2019). Myosin motor domains carrying mutations implicated in early or late onset hypertrophic cardiomyopathy have similar properties. *Biophysics*. doi:10.1074/jbc.RA119.010563

Walklate, J., Ujfalusi, Z., and Geeves, M. A. (2016). "Myosin isoforms and the mechanochemical cross-bridge cycle," in *J exp biol*. Editors S. L. Lindstedt and H. H. Hoppeler, 219, 168–174. doi:10.1242/jeb.124594 2

Watkins, H., Rosenzweig, A., Hwang, D. S., Tatjana, L., McKenna, W., Seidman, C. E., et al. (1992). Characteristics and prognostic implications of myosin missense mutations in familial hypertrophic cardiomyopathy. *N. Engl. J. Med.* 326 (17), 1108–1114. doi:10.1056/NEJM199204233261703

Wehrens, X., and Marks, A. (2004). Molecular determinants of altered contractility in heart failure. *Ann. Med.* 36 (1), 70–80. doi:10.1080/17431380410032481

Weiss, A., Schiaffino, S., and Leinwand, L. A. (1999). Comparative sequence analysis of the complete human sarcomeric myosin heavy chain family: Implications for functional diversity. *J. Mol. Biol.* 290, 61–75. doi:10.1006/jmbi.1999.2865

Wendt, T., Taylor, D., Messier, T., Trybus, K. M., and Taylor, K. A. (1999). Visualization of head–head interactions in the inhibited state of smooth muscle myosin. *J. Cell. Biol.* 147 (7), 1385–1390. doi:10.1083/jcb.147.7.1385

Wienken, C. J., Baaske, P., Rothbauer, U., Braun, D., and Duhr, S. (2010). Protein-binding assays in biological liquids using microscale thermophoresis. *Nat. Commun.* 1 (1), 100. doi:10.1038/ncomms1093

Willott, R. H., Gomes, A. V., Chang, A. N., Parvatiyar, M. S., Pinto, J. R., and Potter, J. D. (2010). Mutations in Troponin that cause HCM, DCM AND RCM: What can we learn about thin filament function? *J. Mol. Cell. Cardiol.* 48 (5), 882–892. doi:10.1016/j.yjmcc.2009.10.031

Wilson, W. S., Criley, J. M., and Ross, R. S. (1967). Dynamics of left ventricular emptying in hypertrophic subaortic stenosis: A cineangiographic and hemodynamic study. *Am. Heart J.* 73 (1), 4–16. doi:10.1016/0002-8703(67)90303-1

Winkelmann, D. A., Forgacs, E., Miller, M. T., and Stock, A. M. (2015). Structural basis for drug-induced allosteric changes to human β-cardiac myosin motor activity. *Nat. Commun.* 6 (1), 7974. doi:10.1038/ncomms8974

Woodhead, J. L., Zhao, F. Q., Craig, R., Egelman, E. H., Alamo, L., and Padrón, R. (2005). Atomic model of a myosin filament in the relaxed state. *Nature* 436 (7054), 1195–1199. doi:10.1038/nature03920

Woody, M. S., Greenberg, M. J., Barua, B., Winkelmann, D. A., Goldman, Y. E., and Ostap, E. M. (2018). Positive cardiac inotrope omecamtiv mecarbil activates muscle despite suppressing the myosin working stroke. *Nat. Commun.* 9 (1), 3838. doi:10.1038/s41467-018-06193-2

Yanagida, T., Nakase, M., Nishiyama, K., and Oosawa, F. (1984). Direct observation of motion of single F-actin filaments in the presence of myosin. *Nature* 307 (5946), 58–60. doi:10.1038/307058a0

Zhang, X., Kampourakis, T., Yan, Z., Sevrieva, I., Irving, M., and Sun, Y. B. (2017). Distinct contributions of the thin and thick filaments to length-dependent activation in heart muscle. *eLife* 6, e24081. doi:10.7554/eLife.24081

Zoghbi, M. E., Woodhead, J. L., Moss, R. L., and Craig, R. (2008). Three-dimensional structure of vertebrate cardiac muscle myosin filaments. *Proc. Natl. Acad. Sci. U. S. A.* 105 (7), 2386–2390. doi:10.1073/pnas.0708912105

frontiers | Frontiers in Physiology

TYPE Mini Review
PUBLISHED 24 October 2022
DOI 10.3389/fphys.2022.969314

OPEN ACCESS

EDITED BY
Norio Fukuda,
Jikei University School of Medicine, Japan

REVIEWED BY
Fuyu Kobirumaki-Shimozawa,
The Jikei University School of Medicine, Japan
Eiki Takimoto,
The University of Tokyo Hospital, Japan

*CORRESPONDENCE
Mark T. Ziolo,
Ziolo.1@osu.edu

SPECIALTY SECTION
This article was submitted to Striated Muscle Physiology, a section of the journal Frontiers in Physiology

RECEIVED 14 June 2022
ACCEPTED 05 October 2022
PUBLISHED 24 October 2022

CITATION
Sturgill SL, Shettigar V and Ziolo MT (2022), Antiquated ejection fraction: Basic research applications for speckle tracking echocardiography. *Front. Physiol.* 13:969314. doi: 10.3389/fphys.2022.969314

Antiquated ejection fraction: Basic research applications for speckle tracking echocardiography

Sarah L. Sturgill, Vikram Shettigar and Mark T. Ziolo*

Frick Center for Heart Failure and Arrhythmia, Department of Physiology and Cell Biology, Davis Heart and Lung Research Institute, The Ohio State University, Columbus, OH, United States

For years, ejection fraction has been an essentially ubiquitous measurement for assessing the cardiovascular function of animal models in research labs. Despite technological advances, it remains the top choice among research labs for reporting heart function to this day, and is often overstated in applications. This unfortunately may lead to misinterpretation of data. Clinical approaches have now surpassed research methods, allowing for deeper analysis of the tiers of cardiovascular performance (cardiovascular performance, heart performance, systolic and diastolic function, and contractility). Analysis of each tier is crucial for understanding heart performance, mechanism of action, and disease diagnosis, classification, and progression. This review will elucidate the differences between the tiers of cardiovascular function and discuss the benefits of measuring each tier *via* speckle tracking echocardiography for basic scientists.

KEYWORDS

cardiovascular performance, heart performance, contractility, echocardiography, speckle tracking

1 Introduction

Proper heart function is mandatory for the quintessential operation of the cardiovascular system. Thus, for proper evaluation of cardiovascular performance, all constituents of heart performance (systolic function, diastolic function, and contractility) must be assessed. An increase in metabolic demand from the body (in situations such as exercise) mandates an increase in cardiac output to meet this demand. The heart increases cardiac output *in vivo via* three mechanisms: by the Bowditch effect (i.e., increasing heart rate), Starling's Law of the heart (i.e., increasing end diastolic volume), and through sympathetic (i.e., β-adrenergic) stimulation (Klabunde, 2012). These influences on the heart utilize the cardiac reserve, augmenting systolic and diastolic function. Contractility is a key contributor to systolic function and cardiac reserve. Unfortunately, cardiovascular disease is the leading cause of death in the world and proper evaluation of all aspects of heart performance is crucial in determining the development and progression of heart disease (Tan, 1986). Thus, the *in vivo* assessment of all tiers of cardiovascular performance, including left ventricular systolic and diastolic function and contractility, is significant to understand how well the heart is performing and its role in the development and progression of heart disease.

TABLE 1 Definitions and measurements of the different tiers.

Tier	Definition	Parameter	Methodology
Cardiovascular performance	Determined by how well the pulmonary and peripheral vasculature and the heart are functioning	Mean arterial pressure	Tail cuff, catheter, telemetry
		Ejection fraction	M-mode, speckle tracking
Heart performance	Determined by how the atria and ventricles are functioning, and is determined by systolic and diastolic function	Cardiac output	M-mode, speckle tracking
		Stroke volume	M-mode, speckle tracking
Systolic function	Occurs when the ventricle is contracting, and is determined by heart rate, preload, afterload and contractility	Fractional shortening	M-mode, speckle tracking
		dP/dt_{max}	Intra-ventricular catheterization
Diastolic Function	Occurs when the ventricle is relaxed and filling with blood, and is determined by preload, heart rate and ventricular compliance	Mitral valve filling	Speckle tracking, power doppler, tissue doppler
		Diastolic strain rate	Speckle tracking
		dP/dt_{min}	Intra-ventricular catheterization
Contractility	Innate ability of the heart to eject a SV at a given preload/afterload	dP/dt/EDV	Intra-ventricular catheterization
		Strain	Speckle tracking
		Strain rate	Speckle tracking

1.1 The tiers of cardiovascular performance

The overall health of cardiovascular performance (definition can be found in Table 1) can be deduced by ejection fraction (EF) and mean arterial pressure (MAP) (Eqs 1, 2). Indices of cardiovascular performance are highly dependent upon preload, afterload, and heart rate. Preload is measured by End Diastolic Volume (EDV) and afterload, or the systemic pressure to overcome for the heart to eject blood, is correlated to MAP. A major contributor to poor cardiovascular performance is heart disease (e.g, heart failure, HF).

The performance of the heart is complex and can be broken down into systolic and diastolic function and contractility. Heart performance is a subset of cardiovascular performance, and thus is dependent upon preload, afterload, heart rate, and contractility. Heart performance (definition can be found in Table 1) is measured by cardiac output (CO), which takes into account the electrical and mechanical function, or by stroke volume, which takes into account only the mechanical function (Eqs 3, 4).

Systolic function (definition can be found in Table 1) can be measured by fractional shortening, which is dependent upon preload, afterload, heart rate, and contractility (Eqs 5, 6). Diastolic function (definition can be found in Table 1) can be measured by E/A ratio (measured by Doppler ultrasound) or E'/A' ratio (measured by left ventricular wall velocity), which measures the ratio of early to late ventricular filling *via* mitral valve flow. E/A ratio is dependent upon preload, ventricular compliance, and heart rate.

The definition of contractility is heavily debated. The definition can be as complicated as "the preload, afterload and length-independent intrinsic kinetically controlled, chemo-mechanical processes responsible for the development of force and velocity" (Muir and Hamlin, 2020). For this discussion, contractility is considered an intrinsic property of the cardiomyocyte and is inherently preload-, afterload-, and heart rate-independent. Hence, contractility contributes to systolic function, which, along

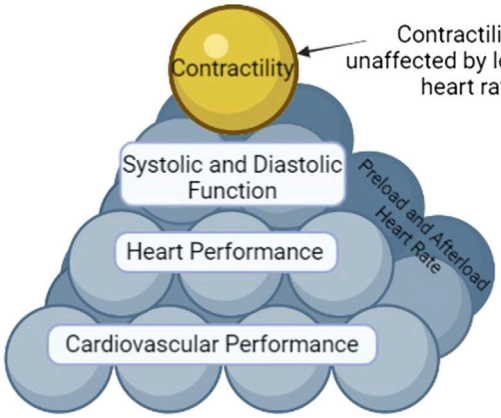

FIGURE 1
The Pyramid of Cardiovascular Performance. Affecting all tiers except for contractility are heart rate and loading parameters (preload and afterload). Cardiovascular performance encompasses the function of all tiers and is thus the bottom of the pyramid. Heart performance is a component of cardiovascular performance. Systolic and diastolic function and contractility are components of heart performance. However, AS contractility is by definition an inherent, load and heart rate independent characteristic of the myocyte, it sits at the top of the pyramid, unaffected by heart rate or load like the other tiers.

with diastolic function, contribute to heart performance, which in turn contributes to cardiovascular performance.

Shown in Figure 1 are the different tiers (or factors) that determine cardiovascular performance. Contractility is on top of the pyramid since it is an independent variable (not affected by load and heart rate independent) (Muir and Hamlin, 2020). Contractility contributes to systolic function. Systolic and diastolic function (both of which are load and heart rate dependent) contribute to heart performance. Heart performance contributes to cardiovascular performance. Proper functioning of each tier is necessary for health. Hence, as each tier is interconnected, to understand cardiovascular performance and to be able to truly understand mechanisms, classifications, and prognosis of disease it is vital that one measures *in vivo* systolic and diastolic function and contractility and not just cardiovascular performance (i.e., EF).

1.1.1 Tiers of cardiovascular performance in the clinics

While there are multiple means to diagnose heart disease in patients (physical exam, blood tests, noninvasive such as cardiac imaging (echocardiography, CT scan, MRI, etc.), stress test, electrocardiogram, and invasive such as angiography and cardiac catheterization), a common choice for diagnosis is echocardiography due to cost and ease. Typically, a special emphasis is placed on EF, which can be calculated through a multitude of techniques ranging in accuracy.

EF can be measured by short or long-axis M-mode, which follows the displacement of the walls of the heart along a user-drawn line, which has user-dependent error and is highly variable. The most accurate method of measuring EF is 3D echocardiography to measure full LV chamber volume at systole and diastole (Lang et al., 2015). Alternatively, the most accurate 2D method to calculate EF is Modified Simpson's method, also known as the Biplane of Discs model recommended by the American Society of Echocardiography (Lang et al., 2015). While this method does allow for an accurate calculation of EF compared to traditional M-mode measurements, it is rarely applied in basic research despite increased accuracy. While EF varies in accuracy of quantification, it still is dependent on loading parameters and heart rate.

EF is antiquated and often misstated as an assessment of systolic function or contractility. This is incorrect as EF is highly preload- and heart rate-dependent and thus cannot be a measure of contractility (Kass et al., 1987). *In vivo* modulators of heart function (Bowditch, Starling's Law, and sympathetic) result in changes to preload, a greater SV, and thus increased CO (Ricci et al., 1979; Sequeira and van der Velden, 2015). These resultant changes in ventricular volume are associated with corresponding changes in EF, since these volumes are used in the calculation of EF (please see Section 5- Equations). For example, with Starling's Law, this is usually associated with a decrease in EF (due to increased EDV even though SV increases), while sympathetic stimulation will increase EF (Mangano et al., 1980; Stratton et al., 1987). Also, changes in EDV (i.e., Starling's Law) will result in changes in left ventricular end diastolic dimension and thus, fractional shortening (FS). There is also a misconception in the field that EF equates to systolic function. For example, a high EF is not necessarily indicative of healthy or superior heart function and must be interpreted in conjunction with SV. A high EF but with low SV (due to low EDV) likely suggests a hypertrophic heart. Preservation or improvement of EF is a common occurrence in models of concentric hypertrophy, and often presents with comorbidities such as hypertension, obesity, diabetes, renal dysfunction, etc (Hieda et al., 2020; Mouton et al., 2020). Conversely, a low EF is not necessarily indicative of worsened heart function, as the heart can remodel both pathologically and physiologically to increase preload. Physiological remodeling through exercise can cause decreased baseline EF, but increased cardiac reserve (Roof et al., 2013). EF is also highly afterload dependent (Kolh et al., 2003). Thus, there may be changes in EF that may not be due to altered heart performance (i.e., hypertension). Further, a normal EF does not preclude changes to heart performance, as there may be corresponding changes to volumes. This can clearly be observed in HF, a syndrome in which the heart cannot pump enough blood to meet the body's requirements. There are two classifications of HF: reduced (HFrEF) or preserved EF (HFpEF). Since EF has been presumed to be a measure of systolic function and/or contractility, HFrEF is also known as systolic HF, while HFpEF is also known as diastolic HF. However, there is both systolic and diastolic dysfunction in both types of HF (Daubert Melissa, 2019; Pfeffer et al., 2019). Thus, cardiologists realized that a better understanding of heart performance (ventricular systolic function, diastolic function, and contractility) was needed for better diagnosis and treatment for cardiac patients as EF is insufficient.

Clinicians have implemented quantitative methods that assess all tiers of cardiovascular function since the early 2000s (Konstam and Abboud, 2017). Since its clinical implementation, speckle tracking echocardiography (STE) has been used on a day-to-day basis, resulting in earlier diagnosis and therefore better treatment options for patients (Pérez et al., 1992; Inaba et al., 2005; Ciarka et al., 2021; Pastore et al., 2021). Clinicians have established proper assessment of the tiers of cardiovascular function in determining their treatment of human patients. This has ultimately improved the understanding of cardiovascular health and treatment.

1.1.2 Tiers of cardiovascular performance in research

Researchers commonly perform standard methods of echocardiography (M-mode measurements) and with good reason. This method remains the simplest and cheapest method to assess cardiovascular function over multiple time points throughout an experiment, allowing for assessment of progression of disease. However, this method falls short of assessing all tiers of cardiovascular performance. Specifically, standard echocardiography

cannot assess diastolic function or cardiac contractility. Researchers often revert to alternative methods of assessing cardiovascular function, such as intra-left ventricular catheterization for pressure-volume analysis (PV loops) (Peterson et al., 2018). Although this method does provide indices for all tiers of cardiovascular performance (cardiovascular performance, heart performance, systolic and diastolic function, and contractility) with the added benefit of decreased load dependence, it is unfortunately a terminal procedure.

Contractility is a difficult, yet necessary index to measure in research settings. There is an abundance of wide-ranging reasons that scientists need to properly measure contractility. Clinicians have learned that in order to determine how the heart is impacted through various treatments, proper characterization of the cardiovascular system at all tiers is essential. Inherently, contractility is an intrinsic property of the myocyte. Excitation-contraction coupling (ECC) is the process by which the cardiac myocyte contracts and changes in myocyte contraction will alter contractility (Bers, 2002). Hence to examine the *in vivo* effects of alterations to ECC proteins (Wang et al., 2012; Nixon et al., 2013; Nixon et al., 2014), signaling pathways targeting ECC proteins (Traynham et al., 2012), etc. as potential therapeutic strategies for heart disease, one should measure contractility to correctly understand the resultant effects on systolic function, diastolic function, heart performance, and cardiovascular performance. Measuring *in vivo* contractility (and the effects of Bowditch, Starling's law, and sympathetic) is also important in helping to ascertain disease mechanisms, testing if new treatment strategies (i.e., drugs, devices, regenerative medicine, etc.) will be beneficial, etc. Another traditional *in vivo* measurement of contractility is performed *via* intra-left ventricular catheterization to measure pressure-volume changes in the heart. Indices such as dP/dt_{max} and dP/dt_{min} (normalized to volume) reflect isovolumetric contraction and relaxation and can be obtained from PV loops (Rhodes et al., 1997). Unfortunately, as previously mentioned, this is a terminal procedure.

Although this review is focused on contractility, with the recent explosion of HFpEF, it is also vitally important to measure diastolic function. Unfortunately M-mode echocardiography, unlike STE, does not provide any measures of diastolic function.

2 Use and interpretation of parameters of cardiovascular function in research

Due to the small heart size and fast heart rate, there are a lack of techniques to measure true parameters of heart performance in mice. Thus researchers, all too frequently, misuse parameters of cardiovascular performance, heart performance, systolic function, diastolic function, and contractility. Often researchers revert to using EF as a measure of systolic function or contractility. Other commonly misused parameters include SV, MAP, CO, and FS (Eqs 2–5) which all are dependent upon contractility, but also on preload, afterload, and heart rate, and thus, cannot be considered indices of contractility (Lipshultz et al., 1994). Contemporary standards in the field compel these measurements to be performed *in vivo* to enhance the reliability, relevance, and translational aspects.

Thus, researchers should explore nonterminal procedures that can properly evaluate of all aspects of heart function. Parameters of cardiovascular performance, heart performance, systolic function, diastolic function, and contractility with their proper corresponding accurate measurement are listed in Table 1. Precise measurements of all tiers individually are needed to fully evaluate cardiovascular function. Technology has advanced to tools in which this can now be performed by using speckle tracking echocardiography. In fact, speckle tracking is already widely used in the clinics. With technological advancement, these tools are now available for measurements in the most commonly used animal model in research: the mouse. Thus, researchers should recognize that EF is an antiquated measurement that poorly assesses heart function because of its reliance on physiological parameters and instead explore speckle tracking echocardiography.

3 Speckle tracking echocardiography

For basic research application, echocardiography has the advantage of longitudinal measurements for changes in heart function over time, rather than being the endpoint of an experiment. Traditional methods of echocardiography acquisition are often performed in M-mode, which traces the movement of the heart walls that occurs on a line drawn through the left ventricle. Besides misusing parameters obtained, this technique also introduces many sources of error and variation between measurements (i.e., the angle of the line drawn, the position of the probe in acquisition, the consistency of the placement by the user between animals, etc.) as well as sources of variation in analysis (Chukwu et al., 2008). Despite being well utilized in clinics, echocardiography has only recently been utilized to the full extent of its capabilities in basic research labs. STE has quantitative capabilities to truly measure systolic and diastolic function and contractility (Marwick et al., 2009; Morris et al., 2012; Oleynikov et al., 2018). STE uses B-mode, which is often the same imaging modality as an M-mode, but records a video clip of the entire heart wall rather than movement along one line. Therefore, as an average measurement, STE provides data points along the entire heart wall rather than only two from M-mode, which increases its accuracy as an indicator of heart function (Wang et al., 2018).

STE has only in recent years infiltrated basic cardiovascular sciences as a means of measuring heart function in research models (de Lucia et al., 2019). STE analysis performed on B-mode images traces the naturally occurring acoustic markers in a cine loop of the heart. Calculated from STE is displacement, velocity, strain, and

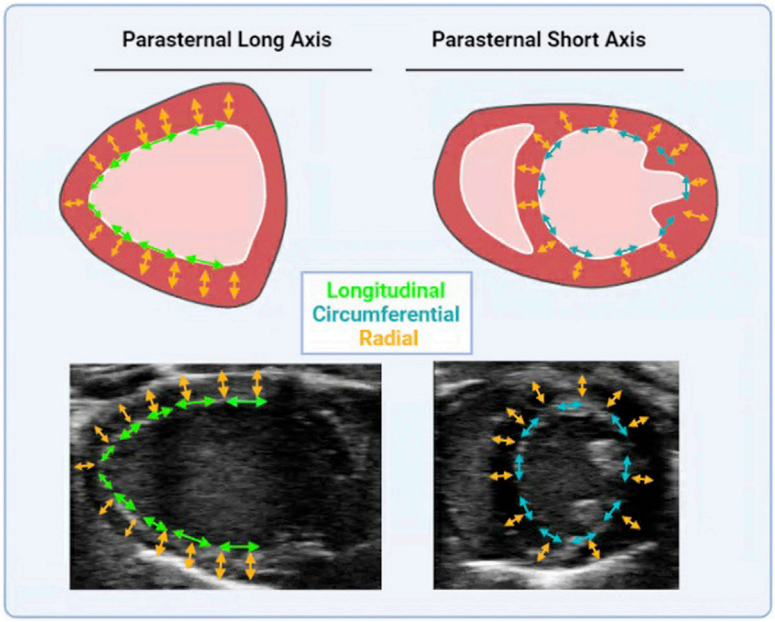

FIGURE 2
Directional vectors of Cardiac Strain. Cardiac strain is measured in parasternal long axis and short axis. Long axis cine loops provide long axis radial (in yellow arrows) and longitudinal strain (in green arrows). Short axis cine loops provide short axis radial (in yellow arrows) and circumferential strain (in red arrows). Cartoon and anatomical views are provided.

strain rate in radial, longitudinal, and circumferential axes (see Figure 2). The axes of cardiac strain are dependent upon directionalities of the vector in the wall movement (Eq. 6). Cardiac strain delineates the deformation of the myocardium from diastole to systole, thus indicating systolic function. Strain rate is the derivative of strain with respect to time, and thus has distinct systolic and diastolic peaks (Eq. 7). Relative to EF, cardiac strain exhibits less load dependence, and strain rate is the least load dependent measurement of cardiac function thus far. Systolic strain is preload and heart rate dependent while systolic and diastolic strain rate have little preload dependence and no heart rate dependence (Sutherland et al., 2004; Hoit, 2011; Salvo et al., 2015). Comparisons between longitudinal, circumferential, and radial strain (and their corresponding strain rates) with EF and pressure-volume derived data reveal that strain and strain rate were weakly associated with load (arterial elastance and EDV). Strain and strain rate are more strongly associated with chamber elastance and contractility as compared to EF, which has a modest correlation with arterial elastance yet no correlation with chamber elastance (Zhang et al., 2014). Other studies have correlated strain and strain rate with pressure-volume loop- derived contractility indices, ESPVR (or End Systolic Elastance- Ees) and diastolic indices, EDPVR, specifically longitudinal strain and strain rate as well as circumferential strain and strain rate (Park et al., 2016). Strain has been shown to be less load dependent than EF, as well as have correlations with previously established indices of load-independent function (Zhang et al., 2014). Thus, unlike the variable effects of Bowditch effect, Starling's Law and sympathetic stimulation on EF (dependent on which effect is larger- the increase in EDV or SV), the Bowditch effect and sympathetic stimulation will increase strain, while there will be little effect of Starling's Law since strain measurements are virtually load-independent (Boettler et al., 2005; Ferferieva et al., 2013). Thus, STE has numerous benefits, with the major benefit being that a truer measurement of the heart performance, systolic function, diastolic function, and contractility. This method gives researchers the ability to fully characterize the heart without performing a fatal procedure and thus introduces the possibility for longitudinal studies. Contrary to all other methods of measuring cardiac function, STE also has the least user-dependent variability for image acquisition (Muraru D et al., 2018).

Monitoring and maintaining a close to physiological heart rate during measurements of heart function is incredibly important for accurate recordings (Lindsey et al., 2018). Variability in heart rate results in inconsistent measurements and difficulty comparing experimental variables. Additionally, an increased heart rate changes functional parameters (i.e., heart rate positively correlates with SV) (Lindsey et al., 2018). The resting physiological heart rate of a mouse averages around 600 BPM and frame rates on most current echocardiography equipment struggle to meet frame rates to obtain accurate measurements. A frame rate of >100 fps is required for speckle tracking analysis which improves with increasing frame rate (D'Hooge et al., 2000). Frame

rates can be improved by reducing image width which decreases scan size and improves tracing (Voigt et al., 2015). Additionally, recent improvements in technology in the basic sciences field (i.e., VevoF2, Visual Sonics) allows for frame rate acquisition of up to 400 fps, making it easier to obtain and analyze speckle tracking echocardiography at higher heart rates.

STE and its subsequent measurements also have the distinct advantage of deciphering early onset of disease, specifically in certain axes of strain. Circumferential strain and strain rate have been shown to be sensitive enough to detect early onset of disease. Strain and strain rate decrease earlier than EF, and thus can be used as earlier indicators of onset of disease. Circumferential strain has also been indicated as an independent predictor of negative outcomes and ventricular remodeling after myocardial infarction (Hung et al., 2010). Longitudinal strain also exhibits similar sensitivity to early onset of disease and is an indicator of negative outcomes after MI. Thus another major advantages of STE in both humans and animal models is the ability to decipher early onset of disease (Pastore et al., 2021).

STE can also elucidate regional functional measurements (Pastore et al., 2021). Regional data is not only unavailable through every other method of analysis, but can provide quantification of models of heart disease, such as myocardial infarction (i.e., infarct size) (Munk et al., 2010). For example, global longitudinal strain has been shown to be more effective at quantifying infarct size compared to standard echocardiographic indices, such as EF and end systolic volume (Munk et al., 2010). STE also provides indices of diastolic function from one data acquisition and analysis, compared to the need for multiple methods of measurement such as Power Doppler and M-mode. STE can measure diastolic strain rate, which has been shown to be advantageous over myocardial velocity and blood flow velocity for assessment of diastolic function (Rivas-Gotz et al., 2003; Wang et al., 2007). Additionally, analysis of diastolic function through STE removes Doppler-associated angulation errors and tethering artifacts of other diastolic measurement techniques (Choudhury A et al., 2017).

In summary, STE is the superior method of *in vivo* analysis of the tiers of heart performance, providing indices that measure not only heart structure, but cardiovascular performance and heart performance. Most importantly, STE is a nonterminal procedure that can provide indices of contractility not previously been accessible to basic research *via* echocardiography.

4 Conclusion

The purpose of the heart is to pump blood to meet the metabolic demands of the body. In order to meet these demands, the heart needs healthy components of all aspects of function, including proper systolic and diastolic function and contractility. Proper evaluation of all the tiers are essential for the determining mechanism of action, the development, and progression of heart disease. A critical hallmark and determining factor of heart disease is a blunted contractility (Houser and Margulies, 2003), which significantly contributes to systolic function, heart performance, and cardiovascular performance. Thus, elucidating all contributing factors to heart function (i.e., systolic and diastolic function and contractility) is significant to understand how well the heart is performing, mechanistic studies, and the possibility to develop heart disease in animal models. STE is an accurate and reliable method to measure all facets of cardiac performance with one all-encompassing measurement. Most importantly, STE is a noninvasive and nonterminal procedure that can be repeated at multiple time points to provide indices of contractility through longitudinal studies.

5 Equations

$$\textit{Ejection Fraction}\,(EF) = \frac{EDV - ESV}{EDV} * 100\% \tag{1}$$

$$\begin{aligned}\textit{Mean Arterial Pressure} &= CO * \textit{Total Peripheral Resistance} \\ &= \frac{2}{3}DBP + \frac{1}{3}SBP\end{aligned} \tag{2}$$

$$\textit{Stroke Volume}\,(SV) = EDV - ESV \tag{3}$$

$$\textit{Cardiac Output}\,(CO) = SV * \textit{Heart Rate} \tag{4}$$

$$\textit{Fractional Shortening}\,(FS) = \frac{(LVIDd - LVIDs)}{LVIDd} * 100\% \tag{5}$$

$$\textit{Cardiac Strain} = \frac{L(t) - L(t_0)}{L(t_0)} * 100\% \tag{6}$$

$$\textit{Cardiac Strain Rate} = \frac{\Delta \frac{L(t) - L(t_0)}{L(t_0)}}{\Delta t} \tag{7}$$

Author contributions

All authors listed have made a substantial, direct, and intellectual contribution to the work and approved it for publication.

Funding

This work was supported by National Institutes of Health Grant R01 AG060542 (MZ) and T32 HL134616 (SS).

Conflict of interest

The authors declare that the research was conducted in the absence of any commercial or financial relationships that could be construed as a potential conflict of interest.

Publisher's note

References

Bers, D. M. (2002). Cardiac excitation-contraction coupling. *Nature* 415, 198–205. doi:10.1038/415198a

Boettler, P., Hartmann, M., Watzl, K., Maroula, E., Schulte-Moenting, J., Knirsch, W., et al. (2005). Heart rate effects on strain and strain rate in healthy children. *J. Am. Soc. Echocardiogr.* 18, 1121–1130. doi:10.1016/j.echo.2005.08.014

Choudhury A, M. R., Malik, V., Kapoor, P. M., and Ramakrishnan, S. (2017). Studying diastology with speckle tracking echocardiography: The essentials. *Ann. Card. Anaesth.* 20, S57–S60. doi:10.4103/0971-9784.197800

Chukwu, E. O., Barasch, E., Mihalatos, D. G., Katz, A., Lachmann, J., Han, J., et al. (2008). Relative importance of errors in left ventricular quantitation by two-dimensional echocardiography: Insights from three-dimensional echocardiography and cardiac magnetic resonance imaging. *J. Am. Soc. Echocardiogr.* 21, 990–997. doi:10.1016/j.echo.2008.07.009

Ciarka, A., Cordeiro, F., Droogne, W., Van Cleemput, J., and Voigt, J. U. (2021). Speckle-tracking-based global longitudinal and circumferential strain detect early signs of antibody-mediated rejection in heart transplant patients. *Eur. Heart J. Cardiovasc. Imaging*, jeab212. doi:10.1093/ehjci/jeab212

D'Hooge, J., HeimdAl, A., JamalF.Kukulski, T., Bijnens, B., RademakersF., et al. (2000). Regional strain and strain rate measurements by cardiac ultrasound: Principles, implementation and limitations. *Eur. J. Echocardiogr.* 1, 154–170. doi:10.1053/euje.2000.0031

Daubert Melissa, A. (2019). Diastolic function in heart failure with reduced ejection fraction. *JACC. Heart Fail.* 7, 818–820. doi:10.1016/j.jchf.2019.06.005

de Lucia, C., Wallner, M., Eaton, D. M., Zhao, H., Houser, S. R., and Koch, W. J. (2019). Echocardiographic strain analysis for the early detection of left ventricular systolic/diastolic dysfunction and dyssynchrony in a mouse model of physiological aging. *J. Gerontol. A Biol. Sci. Med. Sci.* 74, 455–461. doi:10.1093/gerona/gly139

Ferferieva, V., VAn den Bergh, A., Claus, P., Jasaityte, R., La Gerche, A., RademakersF., et al. (2013). Assessment of strain and strain rate by two-dimensional speckle tracking in mice: Comparison with tissue Doppler echocardiography and conductance catheter measurements. *Eur. Heart J. Cardiovasc. Imaging* 14, 765–773. doi:10.1093/ehjci/jes274

Hieda, M., Sarma, S., Hearon, C. M., Dias, K. A., Martinez, J., Samels, M., et al. (2020). Increased myocardial stiffness in patients with high-risk left ventricular hypertrophy: The hallmark of stage-B heart failure with preserved ejection fraction. *Circulation* 141, 115–123. doi:10.1161/circulationaha.119.040332

Hoit, B. D. (2011). Strain and strain rate echocardiography and coronary artery disease. *Circ. Cardiovasc. Imaging* 4, 179–190. doi:10.1161/circimaging.110.959817

Houser, S. R., and Margulies, K. B. (2003). Is depressed myocyte contractility centrally involved in heart failure? *Circ. Res.* 92, 350–358. doi:10.1161/01.RES.0000060027.40275.A6

Hung, C. L., Verma, A., Uno, H., Shin, S. H., Bourgoun, M., Hassanein, A. H., et al. (2010). Longitudinal and circumferential strain rate, left ventricular remodeling, and prognosis after myocardial infarction. *J. Am. Coll. Cardiol.* 56, 1812–1822. doi:10.1016/j.jacc.2010.06.044

Inaba, Y., Yuda, S., Kobayashi, N., Hashimoto, A., Uno, K., Nakata, T., et al. (2005). Strain rate imaging for noninvasive functional quantification of the left atrium: Comparative studies in controls and patients with atrial fibrillation. *J. Am. Soc. Echocardiogr.* 18, 729–736. doi:10.1016/j.echo.2004.12.005

Kass, D. A., Maughan, W. L., Guo, Z. M., Kono, A., Sunagawa, K., and Sagawa, K. (1987). Comparative influence of load versus inotropic states on indexes of ventricular contractility: Experimental and theoretical analysis based on pressure-volume relationships. *Circulation* 76, 1422–1436. doi:10.1161/01.CIR.76.6.1422

Klabunde, R. E. (2012). *Cardiovascular Physiology concepts*. Netherlands: Wolters Kluwer.

Kolh, P., Ghuysen, A., Tchana-Sato, V., D'Orio, V., Gerard, P., Morimont, P., et al. (2003). Effects of increased afterload on left ventricular performance and mechanical efficiency are not baroreflex-mediated. *Eur. J. Cardiothorac. Surg.* 24, 912–919. doi:10.1016/s1010-7940(03)00617-1

Konstam, M. A., and Abboud, F. M. (2017). Ejection fraction: Misunderstood and overrated (changing the paradigm in categorizing heart failure). *Circulation* 135, 717–719. doi:10.1161/circulationaha.116.025795

Lang, R. M., Badano, L. P., Mor-Avi, V., Afilalo, J., Armstrong, A., Ernande, L., et al. (2015). Recommendations for cardiac chamber quantification by echocardiography in adults: An update from the American society of echocardiography and the European association of cardiovascular imaging. *J. Am. Soc. Echocardiogr.* 28, 1–39.e14. doi:10.1016/j.echo.2014.10.003

Lindsey, M. L., Kassiri, Z., Virag, J. A. I., Brás, L. E. d. C., and Scherrer-Crosbie, M. (2018). Guidelines for measuring cardiac physiology in mice. *Am. J. Physiol. Heart Circ. Physiol.* 314, H733–H752. doi:10.1152/ajpheart.00339.2017

Lipshultz, S. E., Orav, E. J., Sanders, S. P., McIntosh, K., and Colan, S. D. (1994). Limitations of fractional shortening as an index of contractility in pediatric patients infected with human immunodeficiency virus. *J. Pediatr.* 125, 563–570. doi:10.1016/s0022-3476(94)70008-7

Mangano, D. T., Dyke, D. C. V., and Ellis, R. J. (1980). The effect of increasing preload on ventricular output and ejection in man. Limitations of the Frank-Starling Mechanism. *Circulation* 62, 535–541. doi:10.1161/01.CIR.62.3.535

Marwick, T. H., Leano, R. L., Brown, J., Sun, J. P., Hoffmann, R., Lysyansky, P., et al. (2009). Myocardial strain measurement with 2-dimensional speckle-tracking echocardiography: Definition of normal range. *JACC. Cardiovasc. Imaging* 2, 80–84. doi:10.1016/j.jcmg.2007.12.007

Morris, D. A., Boldt, L. H., Eichstädt, H., Ozcelik, C., and Haverkamp, W. (2012). Myocardial systolic and diastolic performance derived by 2-dimensional speckle tracking echocardiography in heart failure with normal left ventricular ejection fraction. *Circ. Heart Fail.* 5, 610–620. doi:10.1161/circheartfailure.112.966564

Mouton, A. J., Li, X., Hall, M. E., and Hall, J. E. (2020). Obesity, hypertension, and cardiac dysfunction: Novel roles of immunometabolism in macrophage activation and inflammation. *Circ. Res.* 126, 789–806. doi:10.1161/circresaha.119.312321

Muir, W. W., and Hamlin, R. L. (2020). Myocardial contractility: Historical and contemporary considerations. *Front. Physiol.* 11, 222. doi:10.3389/fphys.2020.00222

Munk, K., Andersen, N. H., Nielsen, S. S., Bibby, B. M., Botker, H. E., Nielsen, T. T., et al. (2010). Global longitudinal strain by speckle tracking for infarct size estimation. *Eur. J. Echocardiogr.* 12, 156–165. doi:10.1093/ejechocard/jeq168

Muraru D, N. A., Rodriguez-Zanella, H., Cherata, D., and Badano, L. (2018). Three-dimensional speckle-tracking echocardiography: Benefits and limitations of integrating myocardial mechanics with three-dimensional imaging. *Cardiovasc. Diagn. Ther.* 8, 101–117. doi:10.21037/cdt.2017.06.0110.21037/cdt.2017.06.01

Nixon, B. R., Liu, B., Scellini, B., Tesi, C., Piroddi, N., Ogut, O., et al. (2013). Tropomyosin Ser-283 pseudo-phosphorylation slows myofibril relaxation. *Arch. Biochem. Biophys.* 535, 30–38. doi:10.1016/j.abb.2012.11.010

Nixon, B. R., Walton, S. D., Zhang, B., Brundage, E. A., Little, S. C., Ziolo, M. T., et al. (2014). Combined troponin I Ser-150 and Ser-23/24 phosphorylation sustains thin filament Ca(2+) sensitivity and accelerates deactivation in an acidic environment. *J. Mol. Cell. Cardiol.* 72, 177–185. doi:10.1016/j.yjmcc.2014.03.010

Oleynikov, V. E., Galimskaya, V. A., Kupriyanova, S. N., and Burko, N. V. (2018). Use of the Speckle tracking method for determining global parameters of heart contractility in healthy individuals. *MethodsX* 5, 125–135. doi:10.1016/j.mex.2018.01.011

Park, J. H., Lee, J. H., Lee, S. Y., Choi, J. O., Shin, M. S., Kim, M. J., et al. (2016). Normal 2-dimensional strain values of the left ventricle: A substudy of the normal echocardiographic measurements in Korean population study. *J. Cardiovasc. Ultrasound* 24, 285–293. doi:10.4250/jcu.2016.24.4.285

Pastore, M. C., Mandoli, G. E., Contorni, F., Cavigli, L., Focardi, M., D'Ascenzi, F., et al. (2021). Speckle tracking echocardiography: Early predictor of diagnosis and prognosis in coronary artery disease. *Biomed. Res. Int.* 2021, 6685378. doi:10.1155/2021/6685378

Pérez, J. E., Waggoner, A. D., Barzilai, B., Melton, H. E., Miller, J. G., and Sobel, B. E. (1992). On-line assessment of ventricular function by automatic boundary detection and ultrasonic backscatter imaging. *J. Am. Coll. Cardiol.* 19, 313–320. doi:10.1016/0735-1097(92)90484-5

Peterson, J. M., Wang, D. J., Shettigar, V., Roof, S. R., Canan, B. D., Bakkar, N., et al. (2018). NF-κB inhibition rescues cardiac function by remodeling calcium genes in a Duchenne muscular dystrophy model. *Nat. Commun.* 9, 3431. doi:10.1038/s41467-018-05910-1

Pfeffer, M. A., Shah, A. M., and Borlaug, B. A. (2019). Heart failure with preserved ejection fraction in perspective. *Circ. Res.* 124, 1598–1617. doi:10.1161/CIRCRESAHA.119.313572

Rhodes, J., Fulton, D. R., Levine, J. C., and Marx, G. R. (1997). Comparison between the mean dP/dt during isovolumetric contraction and other echocardiographic indexes of ventricular systolic function. *Echocardiogr. Mt. Kisco, N.Y.)* 14, 215–222. doi:10.1111/j.1540-8175.1997.tb00713.x

Ricci, D. R., Orlick, A. E., Alderman, E. L., Ingels, N. B., Daughters, G. T., and Stinson, E. B. (1979). Influence of heart rate on left ventricular ejection fraction in human beings. *Am. J. Cardiol.* 44, 447–451. doi:10.1016/0002-9149(79)90395-3

Rivas-Gotz, C., Manolios, M., Thohan, V., and Nagueh, S. F. (2003). Impact of left ventricular ejection fraction on estimation of left ventricular filling pressures using tissue Doppler and flow propagation velocity. *Am. J. Cardiol.* 91, 780–784. doi:10.1016/S0002-9149(02)03433-1

Roof, S. R., Tang, L., Ostler, J. E., Periasamy, M., Gyorke, S., Billman, G. E., et al. (2013). Neuronal nitric oxide synthase is indispensable for the cardiac adaptive effects of exercise. *Basic Res. Cardiol.* 108, 332. doi:10.1007/s00395-013-0332-6

Salvo, G. D., Pergola, V., Fadel, B., Bulbul, Z. A., and Caso, P. (2015). Strain echocardiography and myocardial mechanics: From basics to clinical applications. *J. Cardiovasc. Echogr.* 25, 1–8. doi:10.4103/2211-4122.158415

Sequeira, V., and van der Velden (2015). Historical perspective on heart function: The frank-starling law. *Biophys. Rev.* 7, 421–447. doi:10.1007/s12551-015-0184-4

Stratton, J. R., Pfeifer, M. A., and Halter, J. B. (1987). The hemodynamic effects of sympathetic stimulation combined with parasympathetic blockade in man. *Circulation* 75, 922–929. doi:10.1161/01.cir.75.5.922

Sutherland, G. R., Di Salvo, G., Claus, P., D'Hooge, J., and Bijnens, B. (2004). Strain and strain rate imaging: A new clinical approach to quantifying regional myocardial function. *J. Am. Soc. Echocardiogr.* 17, 788–802. doi:10.1016/j.echo.2004.03.027

Tan, L. B. (1986). Cardiac pumping capability and prognosis in heart failure. *Lancet (London, Engl.* 2, 1360–1363. doi:10.1016/s0140-6736(86)92006-4

Traynham, C. J., Roof, S. R., Wang, H., Prosak, R. A., Tang, L., Viatchenko-Karpinski, S., et al. (2012). Diesterified nitrone rescues nitroso-redox levels and increases myocyte contraction via increased SR Ca(2+) handling. *PLoS One* 7, e52005. doi:10.1371/journal.pone.0052005

Voigt, J. U., Pedrizzetti, G., Lysyansky, P., Marwick, T. H., Houle, H., Baumann, R., et al. (2015). Definitions for a common standard for 2D speckle tracking echocardiography: Consensus document of the EACVI/ASE/industry task force to standardize deformation imaging. *Eur. Heart J. Cardiovasc. Imaging* 16, 1–11. doi:10.1093/ehjci/jeu184

Wang, H., Bonilla, I. M., Huang, X., He, Q., Kohr, M. J., Carnes, C. A., et al. (2012). Prolonged action potential and after depolarizations are not due to changes in potassium currents in NOS3 knockout ventricular myocytes. *J. Signal Transduct.* 2012, 645721–645728. doi:10.1155/2012/645721

Wang, J., Khoury, D. S., Thohan, V., Torre-Amione, G., and Nagueh, S. F. (2007). Global diastolic strain rate for the assessment of left ventricular relaxation and filling pressures. *Circulation* 115, 1376–1383. doi:10.1161/CIRCULATIONAHA.106.662882

Wang, L. W., Kesteven, S. H., Huttner, I. G., Feneley, M. P., and Fatkin, D. (2018). High-frequency echocardiography - transformative clinical and research applications in humans, mice, and zebrafish. *Circ. J.* 82, 620–628. doi:10.1253/circj.CJ-18-0027

Zhang, K. W., French, B., May Khan, A., Plappert, T., Fang, J. C., Sweitzer, N. K., et al. (2014). Strain improves risk prediction beyond ejection fraction in chronic systolic heart failure. *J. Am. Heart Assoc.* 3, e000550. doi:10.1161/jaha.113.000550

Frontiers in Physiology

Understanding how an organism's components work together to maintain a healthy state

The second most-cited physiology journal, promoting a multidisciplinary approach to the physiology of living systems - from the subcellular and molecular domains to the intact organism and its interaction with the environment.

Discover the latest Research Topics

See more →

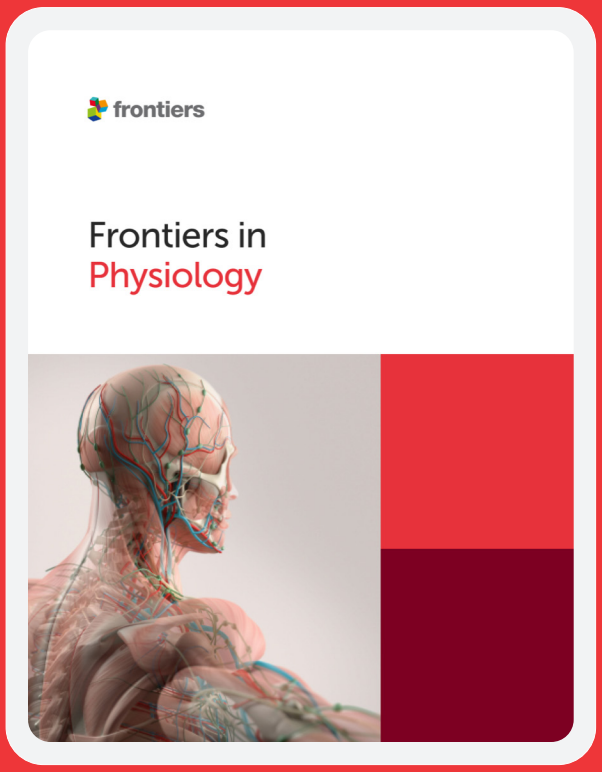

Frontiers

Avenue du Tribunal-Fédéral 34
1005 Lausanne, Switzerland
frontiersin.org

Contact us

+41 (0)21 510 17 00
frontiersin.org/about/contact